Homogenization of Composites With Extended General Interfaces: Comprehensive Review and Unified Modeling

S. Firooz
Institute of Applied Mechanics,
University of Erlangen-Nuremberg,
Egerland Str. 5,
Erlangen 91058, Germany

P. Steinmann
Institute of Applied Mechanics,
University of Erlangen-Nuremberg,
Egerland Str. 5,
Erlangen 91058, Germany;
Glasgow Computational Engineering Centre,
James Watt School of Engineering,
University of Glasgow,
Glasgow G12 8QQ, UK

A. Javili[1]
Department of Mechanical Engineering,
Bilkent University,
Ankara 06800, Turkey
e-mail: ajavili@bilkent.edu.tr

Interphase regions that form in heterogeneous materials through various underlying mechanisms such as poor mechanical or chemical adherence, roughness, and coating, play a crucial role in the response of the medium. A well-established strategy to capture a finite thickness interphase behavior is to replace it with a zero-thickness interface model characterized by its own displacement and/or traction jumps, resulting in different interface models. The contributions to date dealing with interfaces commonly assume that the interface is located in the middle of its corresponding interphase. This paper revisits this assumption and introduces an extended general interface model, wherein a unifying approach to the homogenization of heterogeneous materials embedding interfaces between their constituents is developed within the framework of linear elasticity. Through utilizing a weighted average operator, we demonstrate that the assumption of enforcing the interface to coincide with the midlayer is not required and thereby develop a new class of interfaces where the interface is allowed to take any arbitrary position between its bulk neighbors. The proposed novel interface model can recover any of the classical interface models. Next, via incorporating this extended general interface model into homogenization, we develop bounds and estimates for the overall moduli of fiber-reinforced and particle-reinforced composites as functions of the interface position and properties. Finally, we carry out a comprehensive numerical study to highlight the influence of interface position, stiffness ratio, and interface parameters on the overall properties of composites. The developed interface-enhanced homogenization framework also successfully captures size effects, which are immediately relevant to emerging applications of nanocomposites due to their pronounced interface effects at small scales.
[DOI: 10.1115/1.4051481]

Keywords: homogenization, weighted average, interface position, general interface, cohesive interface, surface elasticity, Gurtin–Murdoch elasticity

1 Introduction

Over the last few decades, composites have been playing a promising role in many engineering applications due to their superb physical and mechanical properties. The overall behavior of a composite mainly depends on its underlying microstructure or more specifically, on orientation, distribution, volume fraction, and the shape of its constituents. The complexity of the microstructure escalates by incorporating interface effects, the interaction of the constituents, and debonding or damage between the constituents. Predicting the overall response of composites is a challenging task. Many micromechanical methods have been developed to determine the overall behavior of composites among which, homogenization has been particularly well-established. A major shortcoming of classical homogenization is that it fails to account for size-dependent material behavior, often referred to as size effects. Size effects in composites are essentially attributed to surface and interface effects due to the pronounced area-to-volume ratio at small scales, for example, in nanocomposites. In addition, to conduct more realistic analyses, various interface models have been developed to incorporate imperfect bonding between the constituents of heterogeneous material. Therefore, it is important to extend the homogenization method to account for interface effects between the constituents of heterogeneous materials, thereby capturing size-dependent effective properties.

Although a plethora of contributions are available in the literature investigating interfaces and the role they play in the overall response of heterogeneous materials, a comprehensive review on this subject is yet missing. This section provides an exhaustive literature review on this subject. The first part provides a brief review of homogenization. This is then followed by a comprehensive review of the contributions incorporating interphases into homogenization. Next, commonly accepted interface models to capture interphases are reviewed. Afterward, the significance of interface position is highlighted giving rise to an *extended general interface model* elaborated in the remainder of the paper. *Any attempt to provide a comprehensive review of this caliber on the subject is a challenging task. We believe that the current structure forms a continuous and rigorous composition.*

1.1 State of the Art Review of Homogenization. Homogenization has proven to be a powerful technique in determining the overall behavior of heterogeneous materials. The main objective of homogenization is to estimate the macroscopic behavior of heterogeneous material from the response of its underlying microstructure, thereby allowing to substitute the heterogeneous material with an equivalent homogeneous medium. There exist extensive contributions to both *analytical* and *computational* homogenization. Hence, only selected representative papers are included here to establish an appropriate context. Table 1 gathers

[1]Corresponding author.
Manuscript received January 14, 2021; final manuscript received June 2, 2021; published online August 3, 2021. Assoc. Editor: Thomas Siegmund.

Table 1 Major analytical and computational contributions on homogenization

Analytical	Voigt [1], Reuss [2], Hill [3–9], Taylor [10], Sachs [11], Bishop and Hill [12], Hashin and shtrikman [13–16], Hashin [17–19], Beran and Molyneux [20], Walpole [21–23], Fan [24], Zimmerman [25], Hashin and Rosen [26,27], Milton, [28], Bornert et al. [29], Nemat-Nasser et al. [30], Aboudi [31], Torquato [32], Milton and Kohn [33], Bisegna and Luciano [34,35], Hori and Nemat-Nasser [36–38], Li and Dunn [39], Gibiansky and Torquato [40], Eshelby [41], Rodin [42], Markenscoff [43], Mura [44], Lubarda and Markenscoff [45], Zohdi and Wriggers [46], Hershey [47], Kroner [48], Budiansky [49], Laws [50], Kerner [51], Christensen and Lo [52], Huang et al. [53], Huang and Hu [54], Benveniste and Berdichevsky [55], Benveniste and Milton [56], Chatzigeorgiou et al. [57], Boucher [58], McLaughlin [59], Norris [60], Mori and Tanaka [61], Pierard et al. [62], Benveniste [63], Luo and Weng [64,65], Weng [66], Qiu and Weng [67], Tandon and Weng [68], Hu and Weng [69], Aboutajeddine and Neale [70], Riccardi and Montheillet [71], Ogden [72], Talbot and Willis [73–75], Willis [76–78], Ponte Castañeda et al. [79], Ponte Castañeda and Willis [80], Suquet [81], De-Botton and Ponte Castañeda [82], Olson [83], Ponte Castañeda [84–89], Ponte Castañeda and Suquet [90], Leroy and Ponte Castañeda [91], Lopez-Pamies and Ponte Castañeda [92], Mura [93], Charalambakis [94], Firooz et al. [95], Mandel [96]
Computational	Tvergaard [97], Smit et al. [98], Bao et al. [99], van der Sluis et al. [100,101], Nemat-Nasser and Hori [102], Miehe [103], Kaczmarczyk et al. [104], Terada et al. [105], Drago and Pindera [106], Irving and Kirkwood [107], Mercer et al. [108], Fritzen and Böhlke [109], Yuan and Tomita [110], Jiang and Cheung [111], Inglis et al. [112], Larsson et al. [113], Glüge [114], Saroukhani et al. [115], Nguyen et al. [116], Drugan and Willis [117], Kanit et al. [118], Gitman et al. [119], Khisaeva and Ostoja-Starzewski [120], Temizer and Zohdi [121], Thomas et al. [122], Temizer et al. [123], Dirrenberger et al. [124], Dai et al. [125], Ostoja-Starzewski [126], Ghosh et al. [127], Ghosh and Moorthy [128,129], Moulinec and Suquet [130], Michel et al. [131], Vinogradov and Milton [132], Lee et al. [133], Monchiet and Bonnet [134], Moulinec and Silva [135], Kabel et al. [136], Kamiński [137], Okada et al. [138], Procházka [139], Renard and Marmonier [140], Takano et al. [141], Feyel and Chaboche [142], Terada and Kikuchi [143], Miehe and Koch [144], Segurado and Llorca [145,146], Miehe and Schröder [147], Feyel [148], Terada et al. [149], Klinge and Hackl [150], Moës [151], Spieler et al. [152], Savvas et al. [153], Patil et al. [154], Lee and Mear [155], Wang and Weng [156], Monette et al. [157], Böhm et al. [158], Ghosh et al. [159], Brockenbrough et al. [160], Kouznetsova et al. [161], Chawla et al. [162], Kanoute et al. [163], Geers et al. [164], Nguyen et al. [165], Saeb et al. [166], Firooz et al. [95], Matouš et al. [167]

the major analytical and computational contributions on homogenization for mechanical problems.

1.1.1 Analytical Homogenization. Pioneering works on *analytical homogenization* were carried out by Voigt [1] and Reuss [2] where they assumed a uniform strain and stress field within the heterogeneous medium resulting in upper and lower bounds on the strain energy [3], respectively. The nonlinear equivalents to Voigt's and Reuss' assumptions are usually referred to as Taylor's [10] and Sachs' [11] bounds, respectively, which were later derived for polycrystals [12]. Although being general and simple, these bounds are very rough estimates and have been improved in the past decades. Using extremum and variational principles, Hashin and Shtrikman [13–15,17], Hill [4–6], Beran and Molyneux [20] and Walpole [21,22] determined more restrictive bounds compared to Voigt and Reuss bounds for the overall bulk and shear modulus of composites. See Fan et al. [24] for bounds on Young's modulus and Zimmerman [25] for bounds on the Poisson ratio.

Two specific branches of analytical homogenization based on variational methods are the composite cylinder assemblage (CCA) [26] and composite sphere assemblage (CSA) [18] suitable to analyze fiber-reinforced and particle-reinforced composites, respectively. While no restriction is considered for the shapes of the heterogeneities in the original variational approach, CCA and CSA require morphological and geometrical information about the microstructure. Using perturbations, Milton and Phan-Thein [28] introduced more geometrical features of the microstructure and improved the accuracy of the Hashin–Shtrikman bounds and Walpole bounds from second-order error to fourth-order error resulting in tighter bounds. Further generalizations of variational principles include accounting for anisotropy [29], periodic microstructures [30,31], random microstructures [32], magnetic permeability [16], piezo-electricity [33–36,39] and thermal expansion [27,40].

A more sophisticated method, compared to variational principles, to examine heterogeneous media was developed by Eshelby [41] where he derived a solution for the stress and strain fields within ellipsoidal inhomogeneities in an infinite matrix subjected to uniform remote tractions. Eshelby assumed that the inhomogeneities are so dilutely distributed that their interactions could be neglected. Investigation of Eshelby's formulation for other inclusion shapes is discussed in Refs. [42–45]. The assumption of neglecting the interactions of inhomogeneities makes Eshelby's model unrealistic for heterogeneous media with a random distribution of inhomogeneities [46]. To overcome this drawback, other methods such as the self-consistent method (SCM) [7,8,23,47–50,76], the generalized self-consistent method (GSCM) [51–57], and the differential method [58–60] have been established. Besides offering implicit formulations that make SCM and GSCM convenient to use, these two methods treat the matrix and the inclusions similarly, and therefore, they can be used for cases with very high concentrations of inclusions. However, the morphology of the inclusions is limited to spheres and short fibers. Parallel to these studies, the Mori–Tanaka method [61] was developed based on the mean-field approximation [62]. This model yields a better and more explicit solution for composite properties where limited information about strain or stress concentrations in the constituents are available [63–65]. Weng [66] studied the connections between the Mori–Tanaka method [61] and the variational theory proposed by Hashin and Shtrikman [15] and Walpole [21,22] and found that Mori–Tanaka equivalent polarization stress and strain in Eshelby's equivalent inclusion equation [41] are essentially those that Hashin and Shtrikman [15] and Walpole [21,22] used to construct their bounds. Also, he reported that the average stress and strain in the matrix in the Mori–Tanaka method are exactly the image stress and strain imposed by Walpole, see also Ref. [67]. Tandon and Weng [68] combined Eshelby's theory and Mori–Tanaka's method to obtain a closed form solution for finite concentrations of ellipsoidal inclusions with a wide range of inclusion aspect ratios. Hori and Nemat-Nasser [37,38], via generalizing the self-consistent scheme and the Mori–Tanaka method, proposed a double-inclusion model in which the interaction between the constituents is taken into account more appropriately. They showed that the self-consistent scheme and the Mori–Tanaka method are special cases of their framework. Further contributions on the double inclusion model include [69,70]. Riccardi and Montheillet [71] compared the

Mori–Tanaka method and the generalized self-consistent scheme and showed that the generalized self-consistent method predicts a stronger dependence on the inclusion aspect ratio.

Extensions of the application of analytical homogenization to nonlinear composites and finite deformation elasticity were studied in the pioneering works of Hill [9] and Ogden [72]. A significant advancement is due to the derivation of nonlinear variational principles by Talbot and Willis [73] based on the original work of Willis [77]. Later, Ponte Castañeda [89] proposed an alternative variational approach in which the properties of a nonlinear composite can be found via the properties of its linear counterpart with the same microstructure. Using the two methods in [73] and [89], improved bounds and estimates were obtained for nonlinear dielectric composites [74,79], two-phase random composites made of nonlinearly viscous phases [80], power-law composites [81], plastic and elastoplastic nonlinear composites [82,83,88] and general classes of nonlinear composites [75,78,84,90]. Ponte Castañeda [85] used second-order Taylor expansion for phase potentials in a nonlinear composite and developed second-order estimates for mechanical properties of such media. Comparing their results with "exact" numerical results, they found that their new method provided more accurate estimates for the effective behavior of nonlinear composites than the presented approaches by Talbot and Willis [73] and Ponte Castañeda [89]. Later, Leroy and Ponte Castañeda [91] demonstrated that such a methodology may violate Hashin–Shtrikman bounds in some special cases. This issue was addressed by Ponte Castañeda [86,87] via proposing an improved form of the second-order method, see also [92]. For further studies on analytical homogenization see the reviews [19,93,94] and the references therein.

1.1.2 Computational Homogenization. *Computational homogenization* proves to be a compelling alternative to analytical homogenization, especially for complex microstructures and nonlinear material behavior. In *computational homogenization*, one of the widely adopted approaches in modeling heterogeneous materials is the unit-cell method. In this method, it is assumed that the constitutive material behavior at the microscale is known, and via solving the boundary value problem and proper averaging throughout the sample, the macroscopic material properties are determined [97–100]. An energy equivalence between the micro- and macro-scales must be imposed, commonly referred to as the Hill–Mandel condition [9,96], to bridge between the scales.

Among many boundary conditions satisfying the Hill–Mandel condition, the canonical ones are (i) linear displacement boundary condition (DBC), (ii) constant traction boundary condition (TBC) and (iii) periodic displacement and antiperiodic traction boundary condition (PBC). It is commonly known that in mechanical problems, the overall material behavior obtained using PBC is bounded by DBC from above and TBC from below [101–104]. Nonetheless, Terada et al. [105] argued that this statement should not imply that the results obtained by PBC are always closest to the exact solution. Also, Drago and Pindera [106] demonstrated that the effective transverse Poisson's ratio obtained by PBC is not necessarily bounded between the Poisson ratios obtained by TBC and DBC. Inspired by the classical Irving–Kirkwood method [107], Mercer et al. [108] developed a broader set of admissible boundary conditions. These boundary conditions filled the gap between the canonical boundary conditions and predict the overall material response more precisely. Aspects of the numerical solution and computational cost associated with various types of boundary conditions are investigated by Fritzen and Böhlke [109]. Further details on the formulation, implementation, and application of appropriate boundary conditions in the context of computational homogenization can be found in Refs. [110–116].

Another important and yet delicate task in the computational homogenization framework is the definition of the representative volume element (RVE). It is widely accepted that the response of the material must be independent of the choice of boundary conditions imposed on the RVE. A proper RVE must be selected such that it contains enough details to sufficiently represent the microstructure and it has to be small enough to fulfill the assumption of scale separation [117–125]. According to Hill [4], an RVE is well defined when it contains enough inclusions and the responses under DBC and TBC coincide. This definition forms the basis of the work of Ostoja-Starzewski [126] to determine the RVE size where he demonstrates that the RVE size greatly depends on the problem type and in particular, the inclusion to matrix stiffness ratio. A similar study has been carried out by Temizer and Zohdi [121] where they report that depending on the mesh resolution of the finite element discretization of the microstructure, different RVE sizes may be obtained.

To perform computational analyses over the RVE, various schemes have been developed such as Voronoi cell finite element scheme [127–129], fast Fourier transform [130–136], boundary element method (BEM) [137–139], finite element method (FEM) [140–145,147–150] and extended finite element method [151–154]. Using these schemes, numerous contributions have investigated the effects of the inclusion shape, distribution, volume fraction, and stiffness on the overall behavior of composites, see for instance, [155–159]. Brockenbrough et al. [160] analyzed the effect of volume fraction, shape, and distribution of particles in a metal-matrix composite and showed that the distribution pattern of the particles has a stronger effect on the overall response compared to their shapes. Kouznetsova et al. [161] examined the influence of the randomness of the microstructure on the macroscopic behavior for a constant volume fraction of voids. They demonstrated that for elastic materials, a microstructure with a random distribution of voids renders more compliant behavior compared to a microstructure with a periodic distribution of voids. Segurado and Llorca [146] investigated the influence of particle clustering in a cubic RVE embedding stiff spherical particles and found that the spatial distribution of particles has an insignificant effect on the effective properties of a composite in the elastic and plastic regimes. On the other hand, Chawla et al. [162] studied the influence of different particle shapes (spherical, ellipsoidal, and angular) on the elastic-plastic behavior of particle-reinforced composites and reported that the shape of the particles may have a considerable impact on the behavior of the composite even for very small strains. For further studies on computational homogenization see the reviews [163–167] and the references therein.

1.2 State of the Art Review of Interphase Models. In heterogeneous materials, it is often assumed that the constituents are perfectly bonded together. The assumption of a perfect bonding between the constituents of a heterogeneous medium is, however, inadequate to describe the mechanical behavior and physical nature of the material. In real heterogeneous materials, processing and other factors such as poor mechanical or chemical adherence, roughness, coating, damage or fracture can lead to imperfect bonding between the constituents [168–177]. The degree of bonding between the constituents and the bond conditions have been examined via experimental methods such as scanning electron microscopy, polarized light microscopy, dynamic mechanical analysis, Rayleigh surface wave measurement, and photoelasticity [178–181]. Imperfections give rise to the formation of a distinct interphase region [182–184] that can significantly influence the behavior of materials [185–193]. Table 2 gathers major analytical and computational contributions on interphases in composite materials.

Since the properties of interphases depend on the manufacturing process, they cannot be directly determined from the bulk material. An efficient way to determine the elastic properties of interphases is to utilize micromechanical models and compare the results with the elastic properties of an equivalent homogeneous medium. Papanicolaou et al. [327,328] introduced the concept of interphase in composites and investigated the thermomechanical properties and volume fraction of an interphase layer for a large group of composites via comparing the experimental data against

Table 2 Major analytical and computational contributions on interphases in composite materials

Analytical	Adams [173], Wang and Jasiuk [184], Walpole [194], Theocaris and Papanicolaou [195], Rosen [196], Lou and Weng [64,65], Benveniste et al. [197,198], Chen et al. [199], Carman et al. [200], Mikata, Taya and Hatta [201–203], Pagano and Tandon [204,205], Duan et al. [206], Sullivan and Hashin [207], Maurer [208], Qiu and Weng [209], Cherkaoui et al. [210,211], Barhdadi et al. [212], El-Mouden et al. [213], Sarvestani [214], Nazarenko et al. [215–217], Seidel and Lagoudas [218], Xu et al. [219–222], Wu et al. [223], Nie and Basaran [224], Lu et al. [225], Shi et al. [226], Marcadon et al. [227], Liu and Sun [228], Deng and Van Vliet [229], Gardner et al. [230–232], Ordónéz-Miranda et al. [233], Pham and Torquato [234], Tong and Jasiuk [235], Chouchaoui and Benzeggagh [236], Guinovart-Díaz [237], Lurie et al. [238], Lebon and Rizzoni [239,240], Papanicolaou et al. [241], Ostaja-Starzewski et al. [242], Sottos et al. [243], Jayaraman et al. [244–246], Mikata [247], Ru [248], Theocaris et al. [249,250], Sideridis [251], Theocaris [252,253], Dasgupta and Bhandarkar [254], Shabana [255], Hervé and Zaoui [256,257], Berbenni, M. Cherkaoui [258], Bonfoh et al. [259], Jasiuk and Kouider [260], Wang and Jasiuk [184], Wu et al. [261], Zhong et al. [262], Xu et al. [263], Lutz and Zimmerman [264–267], Low et al. [268,269], Li [270], Shen et al. [271–273], Sevostianov and Kachanov [274], Jiang et al. [275], Li et al. [276], Hernández-Pérez and Avilés [277], Mahiou and Béakou [278], Kiritsi and Anifantis [279], You et al. [280], Yao et al. [281], Sabiston et al. [282], Sburlati and Cianci [283,284], Rao and Dai [285], Yang et al. [286]
Computational	Broutman and Agarwal [287,288], Tsai et al. [289], Nassehi et al. [290,291], Wu and Dong [292], Tsui et al. [293], Al-Ostaz and Jasiuk [294], Kari et al. [295], Pathan et al. [296], Riaño et al. [297], Chang et al. [298], Gosz et al. [299], Gulrajani et al. [300], Liu et al. [301], Chen and Liu [302], Yao et al. [303], Mogilevskaya and Crouch [304], Wacker et al. [191], Ozmusul and Picu [305], Wang et al. [306], Lagache et al. [307], Pan et al. [308], Hayes et al. [309], Lane et al. [310], Fisher and Brinson [311], Wang et al. [306], Wang et al. [312], Han et al. [313,314], Xu et al. [315] Lee et al. [316], Jiang et al. [317], Sabiston et al. [318], Sokolowski and Kamiński [319–321], Kamiński and Ostrowski [322], Tac and Gürses [323], Cheng et al. [324], Huang et al. [325], Le [326]

the results obtained from the rule of mixture. Chu and Rokhlin [329] presented a method for inverse determination of elastic moduli of carbon interphase in a ceramic-SiC composite. They obtained an analytical expression for the effective transverse shear modulus using the generalized self-consistent method and compared the results against experimentally measured elastic moduli and calculated the properties of the interphase. Their work was extended by Huang and Rokhlin [330] to incorporate graded and multilayered interphases. Rohklin and Huang [331] measured the wave velocity in a SiC fiber composite using low frequency ultrasound to calculate the effective elastic moduli of the material. Using the generalized self-consistent method, they determined the effective elastic moduli, and via an inverse determination method, they calculated the elastic properties of the interphase. A similar study has been carried out by Hashin and Monteiro [332] and Ramesh et al. [333] to obtain the elastic properties of an interfacial transition zone between cement and aggregates in concrete. Meurs et al. [334], via measuring the displacement field around interphase with the aid of scanning electron microscopy and using finite element analysis, presented a mixed numerical-experimental method to characterize the interphase properties in a composite using an iterative estimation procedure. Matzenmiller and Gerlach [335], using the generalized method of cells [336] together with a gradient-based optimization scheme, developed a numerical algorithm for the inverse identification of elastic parameters of interphases in fiber composites, see also [337]. Other examples of experimental methods suitable to identify the properties of interphases include the fiber pull-out method, the fiber fragmentation method, and the fiber microcompression method [338–345].

1.2.1 Analytical Studies. Besides experimental methods, several analytical schemes have been developed to study the effects of interphases on the overall behavior of composites. Considering the interphase as a homogeneous independent phase between the constituents has been the primary idea of accounting for interphase effects in analytical studies and has been widely adopted in the literature.

The first analytical study on homogeneous interphases was carried out by Walpole [194] where he presented a mathematical model to analyze the effects of interphases on local fields in a composite medium with coated inclusions. Assuming that the stresses and strains in the inclusion are similar to those in the absence of the interphase, Walpole has shown that thin interphase around an inclusion considerably influences the elastic fields in the surrounding medium. Theocaris and Papanicolaou [195] developed a methodology based on the work of Rosen [196] to investigate the role of the interphase on the thermomechanical load transfer across the fiber-matrix interphase in a Glass-Resin composite with short fibers. Lou and Weng [64,65] proposed a modified Mori–Tanaka method to determine the elastic fields within the constituents of composites with coated particles and fibers. Applying appropriate strain fields, they obtained the elastic moduli of such composites and observed that all moduli lie within the Hashin–Shtrikman bounds. Similar studies on local fields in composites with interphases were carried out by Benveniste et al. [197] where they employed the Mori–Tanaka method based on the work in Ref. [63] to evaluate both the effective moduli and the local stresses in the constituents of a composite with coated fibers. Their work was later extended in Refs. [198] and [199] to incorporate phase anisotropy. Carman et al. [200] investigated the effect of coatings applied to the fibers in a composite on the stress distribution throughout the medium subjected to transverse loading. They developed an optimization procedure to determine an optimal interphase property that minimizes the composite transverse stress, hence the increase in the material transverse failure resistance. Further studies on stress field analysis have been conducted by Mikata, Taya, and Hatta [201–203] and Pagano and Tandon [204,205] for composites with coated fibers under mechanical, thermal, and thermomechanical loadings. Duan et al. [206] investigated the problem of an arbitrarily oriented spheroidal inclusion surrounded by interphase embedded in an infinite medium and developed a methodology to determine the displacement and stress fields inside and around the inhomogeneity. Besides the analysis of local fields, the determination of the overall moduli of composites has been another interesting subject in analytical studies on homogeneous interphases. Sullivan and Hashin [207] exploited the composite cylinder assemblage and the generalized self-consistent scheme to determine the elastic properties of a fiber composite with an interphase layer surrounding the fibers, see Ref. [208] for a similar study on thermal and electrical problems. Later, Qiu and Weng [209] extended Hashin's methodology in Refs. [18] and [26] and obtained bounds and estimates on the effective properties of coated fibrous- and particulate-composites. They compared their results against the bounds reported by Hashin and Shtrikman [18], Hill [4], and Walpole [23] and observed that all their estimates lie within these bounds.

Cherkaoui et al. [210,211] claimed that the assumption made by Walpole [194] about the elastic fields in the inclusion could lead to a nonrealistic analysis. Via considering the interaction between the inclusions, they developed a new micromechanical model based on Green's function technique and interfacial operators, and then using the self-consistent scheme, they determined the effective properties of composites embedding coated inclusions, see also [212]. Their work was extended to the case of composites with the periodic distribution of coated inclusions by El-Mouden et al. [213].

Analyses of composites containing multiple coated inclusions were carried out by Sarvestani [214] where he determines the effective elastic moduli of particulate-composites based on the extended Eshelby's equivalent inclusion method [346]. Thermoelastic properties of random composites containing anisotropic interphases have been obtained by Nazarenko et al. [216,217]. For further analytical contributions on homogeneous interphases, the reader is referred to the following references studying the generalized self-consistent method [218,219], the Mori–Tanaka method [220,223], the composite sphere assemblage [224], the double/multiple-inclusion model [222,225,226], the equivalent inclusion method [215,227–229], the method of cells [230–232], the differential effective medium approximation [221,233], the strong-contrast expansions [234], the successive iteration method [235] and the asymptotic analysis [236–240].

A more general model to analyze interphases is to consider that the interphase has nonuniform spatial properties. That is, the interphase properties may vary in the domain. Examples of such interphases include graded interphases, multilayered interphases, or nonhomogeneous interphases. A pioneering work on these types of interphases was carried out by Papanicolaou et al. [241]. They extended the works further in Refs. [327] and [328] and investigated the adhesion efficiency between the fiber and matrix in a fiber-reinforced polymer composite via considering inhomogeneous interphase between the components. In view of the heterogeneity of the interphase, the inhomogeneous continuum model should also account for local anisotropy and randomness of the constitutive laws which has been investigated by Ostaja-Starzewski et al. [242] for functionally graded interphases. Sottos et al. [243] studied thermal stresses in the proximity of fiber in a unidirectional fiber composite with a hexagonal arrangement of fibers. In their analysis, the interphase elastic modulus and thermal expansion coefficient were assumed to vary linearly in the radial direction. A few years later, Jayaraman et al. [244–246] extended the work by Benveniste et al. [197] to account for inhomogeneous interphases and investigated the local thermal and mechanical stress fields near the fiber in a unidirectional fiber composite. Mikata [247] used a model based on four concentric circular cylinders for thermomechanical analysis of stress fields in composites with variable interphase properties. Ru [248] considered a circular inclusion embedded in an infinite matrix with multilayered graded interphase and proposed a new method to determine the exact stress fields within the inclusion and the matrix under thermomechanical loadings.

So far, the authors in the aforementioned papers [243–248] have been concerned with the local fields throughout the composite medium. Investigation of the effective properties of composites with inhomogeneous interphases was carried out in the seminal works of Theocaris et al. [249,250]. They proposed a multicylinder model based on the work of Hashin and Rosen [26] to determine the overall properties of fiber composites with variable interphase properties, see Refs. [251] and [253] for similar works by the same authors. The contributions of Theocaris and his coworkers in this area were summarized in a book by Theocaris [252]. Dasgupta and Bhandarkar [254] employed the Mori–Tanaka method and the generalized self-consistent method to determine the overall thermomechanical properties of unidirectional composites with multiply coated cylindrical fibers, see Ref. [255] for ellipsoidal fibers. Hervé and Zaoui [256,257] derived the elastic strain and stress fields in an infinite medium comprised of a multilayered isotropic inclusion embedded in a matrix subjected to uniform stress or strain conditions at infinity. Via considering some of the inclusion layers as multilayer interphase, this model is suited to analyze graded interphases, see Refs. [258] and [259]. Jasiuk and Kouider [260] employed the generalized self-consistent method and composite cylinder assemblage to predict the overall elastic moduli of fiber composites embedding inhomogeneous interphases with variable elastic constants changing in the radial direction. Their work was later extended for particulate-composites by Wang and Jasiuk [184]. They showed that, compared to a uniform interphase, the effect of lacking interphase homogeneity on the overall properties is more significant when the particles are stiffer than the matrix, and the effect is negligible when the matrix is stiffer than the particles, see also [261–263]. Lutz and Zimmerman [264,266,267] obtained closed-form solutions for the effective bulk modulus, shear modulus, conductivity, and diffusivity of particulate-composites with inhomogeneous interphases. In their work they allowed the interphase elastic properties to vary smoothly from the particle to the matrix with a power-law. This methodology was also employed by the same authors to estimate the local elastic properties of concretes considering interfacial transition zones [265].

Composites with rectangular fibers with variable interphase properties have been examined by Low et al. [268,269] where they establish a micromechanical model based on the method of cells to analyze the stress fields and the effective transverse shear properties of such media. The thermoelastic behavior of composites with multiple inclusions with functionally graded interphases was examined by Li [270] and closed-form expressions for effective thermoelastic moduli of such composites were obtained. Shen et al. [271–273] proposed a new energy balance equation and derived a generalized noninteracting solution for the effective properties of particulate-composites. They used a method in which the inclusion/interphase system was replaced by an equivalent inclusion and then extended the solution to account for a random distribution of inclusions. Via testing a broad range of parameters such as inclusion to matrix stiffness ratios or interphase thicknesses, Sevostianov and Kachanov [274] improved Shen's methodology [271–273]. Analysis of composites with the periodic distribution of particles surrounded by inhomogeneous interphases was carried out by Jiang et al. [275] where they exploited the Mori–Tanaka method and developed a micromechanic model to examine the overall properties of such media. Li et al. [276] conducted a comprehensive study to investigate the influence of size, interphase thickness, and inclusion shape on the enhancement mechanism of composites, see [277] for carbon nanotube composites. Further analytical studies on inhomogeneous interphases include [278–286].

1.2.2 Computational Studies. Computational analysis of interphase effects on the overall behavior of heterogeneous materials has been growing rapidly during the last decades. The two main techniques that have been widely adopted to carry out computational studies in this context are the finite element method and the boundary element method.

Broutman and Agarwal [287,288] elaborated on homogeneous interphases embedded in a fiber composite via proposing a three-dimensional finite element solution. They evaluated the stress fields within the constituents, stress concentrations at the interphase, and the overall mechanical properties of the medium and showed that for a composite medium with aligned fibers, interphase can improve the overall medium's toughness. Motivated by the work of Mandell et al. [347], Tsai et al. [289] conducted a comprehensive study on the effects of homogeneous interphase properties on stress and fracture toughness of composites. Developing an axisymmetric finite element method, they determined the shear strength of the composite medium and the relationship between the thickness and shear modulus of the interphase. They concluded that some factors like fiber diameter, fiber Young's modulus, interphase shear strength, and interphase thickness

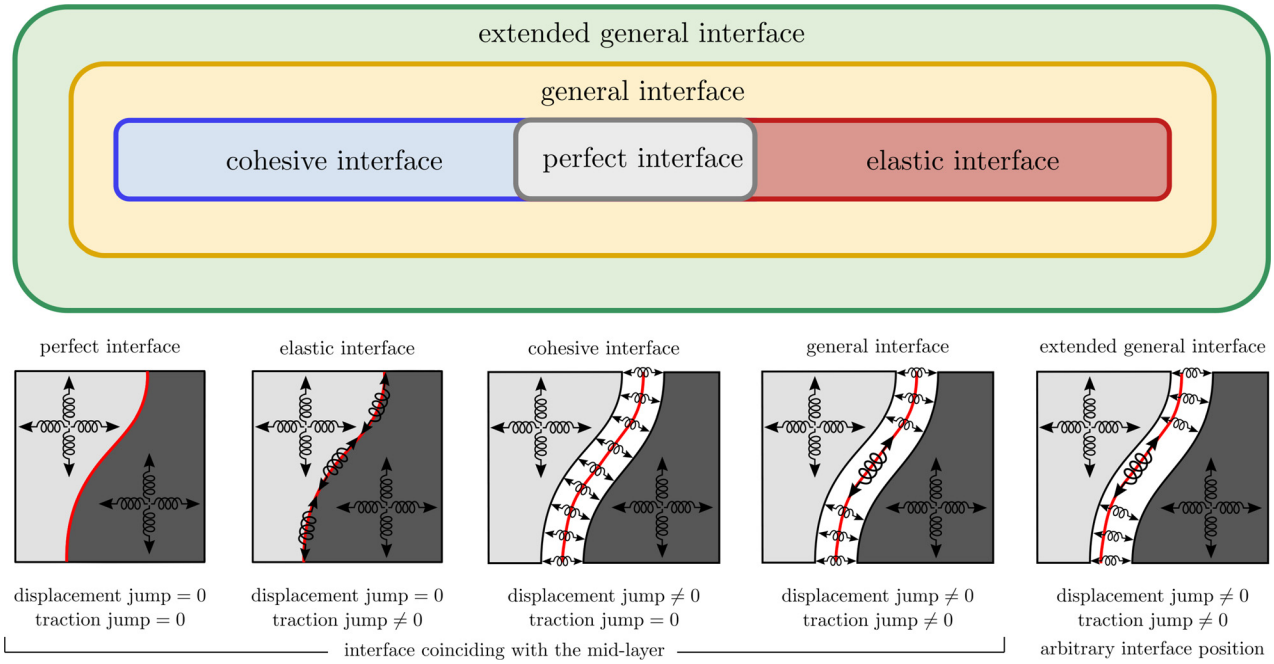

Fig. 1 Classification of the classical interface models together with the extended general interface model

greatly contribute to the toughness of the composite. For further studies on failure analysis of composites with interphases see [348–355]. Finite element analysis on polymer composites with coated fibers was carried out by Nassehi et al. [290,291] where the effects of the interphase on stress distribution around the fibers were examined. Similar analyses have been carried out by Wu and Dong [292] and Tsui et al. [293] for coated particles. The study of interphases in composites with multiple inclusions was initially conducted by Al-Ostaz and Jasiuk [294] where they studied the local stress fields in a composite with coated disk-like inclusions with both random and periodic distribution throughout the medium. They observed that random distribution of the inclusions yields higher stress concentrations than the periodic distribution owing to stress localizations. Later, Kari et al. [295] studied the influence of homogeneous interphase parameters such as stiffness and volume fraction on overall properties of (transversely) randomly distributed unidirectional fiber composites and randomly distributed spherical particle composites. Using finite element analysis, they reported that the overall properties are significantly affected if the interphase is not stiff enough to transmit the load between the constituents. Further computational studies on composites with randomly distributed inclusions with interphases include [296–298].

Gosz et al. [299] are the pioneers of developing the boundary element method to analyze heterogeneous media with interphases. They utilized a variationally coupled finite element and boundary element method to determine the mechanical response of a cell containing fibers and concluded that the transverse strength of composites may be enhanced in the manufacturing process by avoiding the occurrence of isolated fibers or isolated group of fibers in the matrix. Gulrajani et al. [300] employed a direct differentiation approach and the boundary element method to obtain optimal values of interphase parameters that minimize the possibility of failure in a composite. Later, Liu et al. [301] employed the boundary element method to model a unit cell embedding a single fiber surrounded by an interphase layer representing a composite material. They examined the effects of stiffness and thickness of the interphases on the micromechanical behavior of the composites. Later, Chen and Liu [302] extended the work to include multiple cells. Yao et al. [303] incorporated the fast multipole method in a substructuring boundary element method to model fiber composites with homogeneous interphases. Mogilevskaya and Crouch [304] also presented a boundary element method to solve the problem of an infinite, isotropic elastic plane embedding a large number of randomly dispersed circular elastic inclusions surrounded by uniform interphase layers. Via extending the work of Mogilevskaya and Crouch [304], Wang et al. [306] employed a boundary element method to examine radially graded interphases. Computational analysis of inhomogeneous interphases was first carried out by Wacker et al. [191] where they investigated the effects of Young's modulus and the thickness of an interphase layer on the effective properties of fiber composites using the finite element method, see also [305]. For further contributions to computational analyses of composites with interphases, the reader is referred to Refs. [306–315] and [326] for homogeneous and to Refs. [316–321] and [323–325] for inhomogeneous interphases.

1.3 State of the Art Review of Interface Models. A well-established strategy to capture a finite thickness interphase, proposed by Sanchez-Palencia and Pham-Huy [356,357], is to replace the interphase with a zero-thickness interface model characterized by certain field jumps. In elasticity problems, the interfacial field jumps are displacement jump and traction jump. The seminal works of Hashin [358–360] and Benveniste and Miloh [361] have meticulously investigated the correlation between the interphase properties and the field jumps that occur across the interfaces, see Ref. [362] for a related work. As the characteristic length of a medium decreases, the significance of the surface and interface effects become more pronounced, since the area-to-volume ratio is proportional to the inverse of the dimension. Accounting for interfaces results in a size-dependent material response [363–365]. Lack of a physical length-scale and therefore inability to capture size effects has been regarded as one of the major shortcomings of classical homogenization.

This section introduces the most common interface models within the framework of elasticity and elaborates on how these interface models have been taken into account for the analysis of heterogeneous media. Figure 1 categorizes all the classical interface models together with the *extended general interface model* developed in this paper based on the continuity of the

displacement field across the interface, the continuity of traction field across the interface, and the interface position.

1.3.1 Perfect Interface Model. A trivial assumption to analyze the overall behavior of composites is the "perfect condition" at the interface between the constituents such that the displacement and the traction fields across the interface remain continuous, as depicted in Fig. 1. This assumption defines the *perfect interface model*. Hence, other interface models with admissible displacement or the traction discontinuities across the interface, are commonly referred to as imperfect interfaces. Analysis of composite materials with perfect interfaces is, in principle, identical to classical homogenization discussed in detail in Sec. 1.1. By contrast, imperfect interface models, gathered in Table 3, shall be discussed next.

1.3.2 Cohesive Interface Model. The second option is to assume that the traction field is continuous whereas the displacement field experiences a jump across the interface, coaxial to the interface traction, see Fig. 1. This interface model is commonly referred to as the *cohesive (spring-type) interface model*. The cohesive interface model allows one to represent intermediate states between perfect bonding and complete debonding. Pioneering works on cohesive interfaces can be traced back to the 1960s in the works of Barenblatt [366,367] studying finite strength of brittle materials, Dugdale [368] investigating the yield phenomenon at a crack tip and size of the plastic zone, and Jones and Whittier [369] examining elastic wave propagation between two dissimilar planes connected with an elastic bond. The cohesive interface model has experienced a prolific growth and has been extensively employed in studying fracture [641–648], adhesive joints [649–656], delamination [657–662], crack growth [663–668], bond failure [669,670], screw dislocations [671], grain boundaries [672–674], and peeling [675]. There is a myriad of other contributions in the literature investigating these phenomena that are not mentioned to avoid digression. Here, we focus our attention on contributions studying the overall behavior of composites embedding cohesive interfaces within the framework of homogenization from both analytical and computational perspectives.

1.3.2.1 Analytical studies. Mal and Bose [370] conducted the first study on the overall behavior of composites embedding randomly distributed inclusions that were imperfectly bonded to the matrix. They determined the velocity and attenuation of the average harmonic elastic waves propagating through such a medium. Four years later, Theocaris et al. [371] investigated the overall elastic behavior of composites with cohesive interfaces. Analyzing a three-dimensional model including an ellipsoidal inclusion embedded in an infinitely extended matrix, they reported that the

Table 3 Major analytical and computational contributions on interface models

Cohesive interface	Analytical	Barenblatt [366,367], Dugdale [368], Jones and Whittier [369], Mal and Bose [370], Theocaris et al. [371], Benveniste [372], Benveniste and Miloh [373], Aboudi [374,375], Takahashi and Shan and Chou [376,377], Karihaloo and Viswanathan [378,379], Hashin [358–360,380], Lipton and Vernescu [364], Levy [381,382], Qu [383], Gao [384], Lee and Pyo [385], Ju and Chen [386], Esteva and Spanos [387], Othmani et al. [388], Xu et al. [389], Yanase and Ju [390], Hosseini Kordkheili and Toozandehjani [391], Lee et al. [392,393], Qu [394], Tan et al. [395–397], Zhao and Weng [398], Liu et al. [399], Shao et al. [400], Brassart et al. [401], Teng [402], Koyama et al. [403], NafarDastgerdi et al. [404], Duan et al. [405–407], Shen et al. [408,409], Ru and Schiavone [410], Sudak et al. [411], Ru [412,413], Pagano and Tandon [414,415], Teng [416], Sudak and Mioduchowski [417], Sangani and Mo [418], Bigoni et al. [419], Sabina et al. [420], Artioli et al. [421], Sevostianov et al. [422], Ghahremani [423], Mura, Jasuik and Tsuchida [424,425], Mura and Furuhashi [426], Zhong and Meguid [427], Furuhashi et al. [428], Huang et al. [429], Lee et al. [430], Kouris and Mura [431], Benveniste and Aboudi [432], Shibata et al. [433], Devries [434,435], Jasiuk et al. [436,437], Lubarda and Markenscoff [438,439], Königsberger et. al. [440,441], Fritsch et. al. [442], He and Jiang [443], Funn and Dutta [444], Qu et. al. [445], He and Liu [446], Shahidi et. al. [447–450], Eberhardsteiner et. al. [451], Chaboche et. al. [452], Nair et. al. [453], Chen and Li [454]
	Computational	Owen and Lyness [455], Lene and Leguillon [456], Needleman [457], Steif and Hayson [458], Xu and Needleman [459], Bisegna and Luciano [460], Wriggers et al. [461], Würkner et al. [462,463], Zheng et al. [464], Caporale et al. [465], Achenbach and Zhu [466,467], Zhu et al. [468], Fritzen and Leuschner [469,470], Koutsawa [471], Nairn [472], Yeh [473], Camacho and Ortiz [474], de-Andrés et al. [475], Ortiz and Pandolfi [476], Alfano and Crisfield [477], Mi et al. [478], Gasser and Holzapfel [479], Mergheim and Steinmann [480], Hansbo and Hansbo [481,482], van den Bosch et al. [483–485], Vossen et al. [486], Ottosen et al. [487,488], Heitbreder et al. [489,490], Hillerborg et al. [491], Ghosh et al. [492], Wells and Sluys [493], Guo et al. [494], Segurado and Llorca [495], Aghdam and Falahatgar [496], Raghavan and Ghosh [497], Fagerström and Larsson [498], Charlotte et al. [499], Ghosh et al. [500], Aymerich et al. [501], Paggi and Wriggers [502,503], Bouhala et al. [504], Wang et al. [505], Tu and Pindera [506], Pike and Oskay [507], Wu et al. [508], Rezaei et al. [509,510], Bayat et al. [511]
Elastic interface	Analytical	Cammarata [512–515], Shuttlewoth [516], Chen et al. [517], Povstenko [518], Gurtin and Murdoch [519–521], Cahn and Lärché [522], Nix and Gao [523], Gao et al. [524,525], Caillerie [526], Lemrabet and Lions [527], Benveniste and Miloh [361], Rubin and Benveniste [528], Rizzoni et al. [529], Fried and Todres [530], Fried and Gurtin [531], Dingreville and Qu [532,533], Dingreville et al. [534,535], Dumont et al. [536], Sharma et al. [537,538], Yang [539], Sun et al. [540], Duan et al. [406,407,541–543], Huang and Wang [544], Monteiro et al. [545], Huang and Sun [546], He [547], Lim et al. [548], Chen et al. [549,550], Mi and Kouris [551,552], Mi [553], Le-Quang and He [554–556], Mogilevskaya et al. [557–560], Jammes et al. [561], Kushch et al. [562–564], Muskhelishvili [565], Kushch and Sevostianov [566], Benveniste and Miloh [567], Gao et al. [525], Dormieux and Kondo [568,569], Monchiet and Bonnet [134], Brach et al. [570], Kushch [571] Sharma and Wheeler [572], Yang [573], Chen and Dvorak [574], Chen [575], Chen et al. [576], Fischer and Svoboda [577], Brisard et al. [578], Li et al. [579], Dong [580], Javili [581], Javili et al. [582] Nazarenko et al. [583], Chatzigeorgiou et al. [584–586], Dai et al [587] Steigmann and Ogden [588,589], Chhapadia et al. [590], Zemlyanova and Mogilevskaya [591,592], Han et al. [593], Ban and Mi [594], Le [595,596]
	Computational	Tian and Rajapakse [597,598], Yvonnet et al. [599], Dong and Pan [600], Dai et al. [601], Javili et al. [602–604] Koutsawa et al. [605], Chen et al. [606–608], Dong and Pan [600], Dong and Lo [609], Dong and Zhang [610], Zhao et al. [611], Gao et al. [612], Farsad et al. [613], Parvanova et al. [614], Liu et al. [615]
General interface	Analytical	Hashin [616], Benveniste [617–619], Bövik [620], Monchiet and Bonnet [621], Gu and He [622], Gu et al. [623,624], Serpilli et al. [625], Wang and Ye [626], Xu et al. [627], Firooz et al. [628,629], Chatzigeorgiou et al. [630]
	Computational	Gu et al. [631], Javili et al. [632,633], Kaessmair et al. [634], Javili [635], Saeb et al. [636–638], Firooz and Javili [639], Firooz [640]

particle shape does not influence the effective moduli. This statement was later contradicted by Hashin [380]. Benveniste [372] established the fundamental concepts in the theory of composite materials with interfacial displacement discontinuities, see also [432]. Formulating a general theory, Benveniste defined the representative volume averages of the stress and strain fields based on surface integrals via exploiting average stress and strain theorems developed by Hashin [676]. Applying the methodology to composite sphere assemblage, he derived the effective shear modulus of particulate-composites. Similar studies for thermal problems have been done by Benveniste and Miloh [373]. A continuum theory to determine the average behavior of unidirectional fiber composites with admissible interfacial debonding between the constituents was proposed by Aboudi [374]. Following Ref. [375], he defined two parameters representing the interfacial resistance against debonding in normal and tangential directions and developed closed-form expressions for the effective transversely isotropic properties of such composites. A mathematical model to predict the transverse elastic moduli of unidirectional fiber composites with cohesive interfaces was presented by Takahashi, Shan, and Chou [376,377]. To analyze complete debonding, they adopted the cavity formation model [677] and replaced the fiber and surrounding cavities with an imaginary anisotropic inclusion that could only sustain compression. See Refs. [378,379], and [381] for analysis of stress and displacement fields of debonded inclusions in an infinite elastic medium.

At the beginning of the 1990s, Hashin carried out a series of studies on the overall behavior of composites embedding cohesive interfaces [358–360,380] and demonstrated that the cohesive interface model is suitable to represent very thin and compliant interphases. In Refs. [358] and [360], Hashin employed the generalized self-consistent scheme to obtain the thermal and elastic properties of fiber-reinforced and particle reinforced composites embedding cohesive interfaces. He then showed that for fiber composites, the cohesive interface influence on the thermal expansion coefficient, transverse shear modulus, and Young's modulus is significant, whereas its influence on the axial thermal expansion coefficient and axial Young's modulus is negligible. In Refs. [358] and [359], Hashin derived the relations between the cohesive interface parameters and interphase elastic properties and thickness for particulate-composites. In Ref. [380], Hashin generalized the classical extremum principles of elasticity theory to account for cohesive interfaces in composites and obtain bounds on the overall elastic moduli of such media. He concluded that unlike the bounds for a medium with the perfect interface, which depend only on volume fractions, the bounds for a medium with a cohesive interface are substantially influenced by the interface shape. After the works of Hashin, investigation of the behavior of composites with interfacial debonding gained considerable attention, and various extensions have been proposed ever since. A nonlinear cohesive interface model for the dilatational response of fiber composites was presented by Levy [382]. Qu [383] developed a modified Eshelby tensor to incorporate cohesive interfaces and presented an integral form to predict the strain field within an ellipsoidal inclusion. The advantage of his proposed methodology was that it was generic and not restricted to certain geometries or approximations. A similar study has been conducted by Gao [384] for circular inclusions using Airy stress functions. Lee and Pyo [385] proposed a multilevel elastic damage model for particulate-composites based on a combination of a micromechanical model and a multilevel damage model. Using the micromechanical model of Ju and Chen [386], Lee and Pyo adopted Eshelby's tensor for an ellipsoidal inclusion with cohesive interfaces and predicted the effective elastic behavior of composites embedding cohesive interfaces. Further studies on Eshelby's formulation incorporating cohesive interface models include [387–393].

Qu [394] modified the Mori–Tanaka method to account for cohesive interfaces and determined the effective moduli of composites with spherical and ellipsoidal inclusions. Tan et al. [395] used the Mori–Tanaka method to examine the effect of interface debonding on the overall behavior of particulate-composites with large volume fractions. They demonstrated that particle size plays an important role in the behavior of the material with small particles stiffening the material and large ones leading to lower overall stiffness, see also Ref. [396]. A two-dimensional study using the Mori–Tanaka method was carried out by Zhao and Weng [398]. To model the debonding, they replaced the isotropic debonded inclusion with a fictitious transversely isotropic one whose tensile and shear stresses associated with vertical direction were zero. Further studies on the Mori–Tanaka method in the context of cohesive interfaces can be found in Refs. [397], and [399–404] among others.

The interfacial bonding conditions have been thoroughly investigated by Duan et al. [405]. They derived the local and average stress concentration tensors for inhomogeneities using four different interface models of which two had admissible displacement jumps across the interface. A few years later, Duan et al. [406,407] proposed a framework based on a replacement procedure and the generalized self-consistent method. Via replacing the inhomogeneity/interface system with an equivalent inclusion, they obtained the elastic properties of fiber and particulate-composites. Analysis of the stress fields throughout the constituents of a composite medium comprising a cohesive interface was carried out by Shen et al. [408] where they proposed a semi-analytic solution using the complex variable technique for the problem of an elliptic inclusion with homogeneously imperfect interface in antiplane shear. They showed that the effect of the cohesive interface parameter on the average stress inside the inclusion increases in correlation with the aspect ratio of the ellipse, see also [409]. Ru and Schiavone [410] and Sudak et al. [411] developed rigorous solutions for the problem of a circular inclusion in an infinite matrix with a circumferentially inhomogeneous interface in between. They showed that, in contrast to the results reported by Hashin [359] and Gao [384], for antiplane deformation, under a remote uniform antiplane stress field, the state of stress inside a circular inclusion remains uniform, see Ref. [413] for similar studies. Later, Ru [412] utilized the cohesive interface model to propose a framework for designing composites with neutral inclusions. In such media, the inclusions do not disturb the prescribed uniform stress field in the surrounding elastic body. Thermoelastic properties of fiber composites with interfacial debonding and slippage have been investigated by Pagano and Tandon [414,415]. They demonstrated that interfacial debonding has negligible effects on the longitudinal Young's modulus and thermal expansion coefficient. In addition, they showed that imperfect interface conditions yield a mathematical and physical mismatch between the strain field calculated using the volume average theory versus surface measurements and reported that this mismatch renders the effective stiffness tensor to be unsymmetric, see also Refs. [416] and [417].

Failure of brittle composites has been investigated by Königsberger et al. [440,441] where they extended the continuum micromechanics framework to analyze cracking in the interfacial transition zone in concrete. They proposed a multiscale model that relates the macroscopic stress to the average of the stresses in the aggregates as well as the tractions acting on the aggregates surfaces, thereby predicting the location of the potential microcracks due to macroscopic loading. Further studies on brittle failure of interfaces include [442].

Most of the aforementioned studies considered single inclusions in their analyses. The works considering multiple inclusions include Sangani and Mo [418] in which they considered the problem of multiple spherical inclusions interacting with each other in a matrix and developed a method to calculate the effective properties of such medium. Bigoni et al. [419] applied the problem of circular inclusions with imperfect bonding to crack propagation and homogenization of dilute, periodic composites. Sabina et al. [420] utilized the asymptotic homogenization method to determine the complete set of effective elastic moduli for two-phase fibrous periodic composites with imperfect contact conditions of

linear spring type, see also [421]. Sevostianov et al. [422] conducted a comprehensive comparative study on different approaches to model imperfect interfaces for fiber reinforced composites with a periodic distribution of fibers. They demonstrated that the differential approach, the three-phase model with consequent homogenization, and the spring interface model yield almost the same solutions for the effective elastic moduli when the inclusion to matrix stiffness ratio is between 0.01 and 100.

A simplification that can be applied to the cohesive interface model is to assume that the displacement jump only occurs in the interface tangential direction and not in its normal direction. Such problems are commonly referred to as sliding inclusions. Ghahremani [423] investigated the sliding phenomenon in composites for the first time and obtained the solution for a sliding spherical inhomogeneity embedded in an isotropic elastic medium subjected to uniform tension at infinity. Further studies on spherical sliding inclusions were carried out by Mura, Jasuik, and Tsuchida [424,425] where they analyzed the elastic fields in a composite under pure shear and uniaxial tension loading at infinity. They reported that, unlike the perfect bonding condition, the stress field is not uniform in a sliding inclusion and this effect is more pronounced when the inclusions is stiffer than the matrix. Mura and Furuhashi [426] extended the work by Ghahremani [423] to ellipsoidal inclusions using the Somigliana dislocation theory [678]. They concluded that under uniform shear eigenstrains, a sphere always deforms to an ellipsoid whereas an ellipsoid restores its shape and orientation by rotation after the material deformation. For further studies on modeling interfacial debonding in composites using Somigliana dislocation theory see Refs. [427] and [679]. Furuhashi et al. [428] compared the elastic fields within the spherical and ellipsoidal inclusions subject to various loadings. Huang et al. [429] extended the work [426] via introducing friction at the interface of inclusion and matrix, and presented exact analytical solutions for the stress fields in constituents via modifying Eshelby's problem to incorporate sliding inclusions. Lee et al. [430] presented an exact elasticity solution for a circular sliding inclusion embedded in a half plane matrix and determined the stress and displacement fields in the constituents. They observed that the sliding yields higher stress concentrations whose magnitude depends on the size and location of the inclusion. A similar study was carried out by Kouris and Mura [431]. A continuum theory for a fiber composite with admissible tangential debonding between the constituents was developed by Benveniste and Aboudi [432]. They applied their theory to investigate debonding effects on wave propagation in boron/epoxy composites with rectangular fibers. Prediction of the overall properties of composites containing sliding inclusions has been originally addressed by Shibata et al. [433] where they determined the overall shear modulus and the Poisson ratio of a composite embedding sliding spherical inclusions. They first analyzed the problem with a single inclusion to determine the tangential traction due to sliding and then incorporated the effects of other inclusions using a successive iteration method. Later, Devries [434,435] presented closed-form constitutive relations for the overall behavior of periodic fiber composites. Considering only tangential slipping between the fibers and the matrix, Devries obtained bounds and estimates for the effective moduli of such media. Jasiuk et al. [436,437] determined the overall elastic moduli of composites with sliding inclusions using four micromechanical techniques; the generalized self-consistent method, the self-consistent method, the Mori–Tanaka method, and the differential scheme. For further studies on sliding inclusions in heterogeneous materials see Lubarda and Markenscoff [438,439].

The cohesive interface model can also be extended to account for viscosity effects, commonly referred to as the viscous interface models. In the viscous interface model, the interface is regarded as a viscous membrane type medium where the interface traction is related to the displacement jump across the interface including interface viscosity [443,447]. The viscous interface model can be employed to understand the behavior of materials with organic-inorganic phases or materials rendering damping behavior, but such interface models can also allow for sliding inclusions as well as fluid interfaces. It has been shown [444,445,448,449] that the viscosity at the interface can play an important role in the structural integrity and creep behavior of composites. For instance, He and Liu [446] studied the mechanical damping of fiber reinforced composites with viscous interfaces. Using the composite cylinder assemblage approach, they obtained explicit expressions for specific damping capability composites embedding viscous interfaces. Shahidi et. al. [447] adopted a micromechanics continuum theory to formulate viscous interfaces into creep laws at the continuum scale for materials embedding a non-creeping solid matrix with confined fluid-filled interfaces. Further studies on viscous interfaces can be found in Refs. [450–454].

1.3.2.2 Computational studies. Computational studies on the cohesive interface model in composites can be traced back to the work of Owen and Lyness [455] where they examined debonding of a single fiber embedded in a matrix using the finite element method. Lene and Leguillon [456] employed the homogenization method in conjunction with finite element analysis to find the effects of imperfect bonding on the effective moduli of fiber composites. They found that there exists a specific spring constant for the interface beyond which the overall material stiffness decreases drastically. Employing a cohesive interface model, Needleman [457] developed a unified framework to describe the process of void nucleation in periodic particulate-composites starting from initial debonding until complete separation. In his constitutive equations, increasing the interfacial separation requires the traction across the interface to increase until it reaches a maximum. Further separation results in a decrease in traction until it vanishes which signifies complete decohesion. Steif and Hayson [458] showed that the longitudinal modulus of fiber composites embedding dilute concentration of fibers with the interfacial debonding condition can be written in terms of the perturbations that a single fiber induces in the displacement field in a homogeneous medium subject to a far field uni-axial tension. Formulating the proper boundary value problem, they calculated the perturbed displacement field and determined the medium overall longitudinal modulus in terms of the potential energy using the finite element method. Bisegna and Luciano [460] formulated the homogenization problem of periodic composites with nonlinear hyperelastic constituents embedding debonded frictionless interfaces. Using the finite element method, they obtained bounds on the homogenized free-energy density functional of the medium. Wriggers et al. [461], conducted a computational investigation on the effects of interface strength and debonding on the macroscopic response of fiber-reinforced composites with a random distribution of aligned fibers. They showed that the degree of debonding directly correlates with the loss of macroscopic stiffness of the material. Periodic fiber composites embedding cohesive interfaces were studied by Würkner et al. [462,463] using the finite element method where they determined the overall moduli of such medium and compared them with the results obtained with composite cylinder assemblage. Inspired by the works [680,681], Zheng et al. [464] proposed a dual effective-medium and finite element study to examine the interfacial partial debonding effects on the elastic stiffness of composites with aligned elliptic fibers, see also Caporale et al. [465].

Besides the finite element method, various techniques have been developed to model interfacial debonding in composites. The pioneering works on cohesive interfaces using the boundary element method were carried out by Achenbach and Zhu [466,467] where they studied transverse loading of a composite with the rectangular distribution of fibers. Substituting the interphase with a cohesive interface model, they determined the overall moduli of the medium and found that the interface parameters significantly influence the stress fields in the constituents. Zhu et al. [468] developed an efficient three-dimensional extended finite element method to model curved cohesive interfaces and

then predicted the effective elastic moduli of composites embedding such interfaces. Fritzen and Leuschner [469,470] developed a reduced-order model to predict the nonlinear response of heterogeneous materials embedding nonlinear cohesive interfaces. They examined a unidirectional fiber composite consisting of a viscoplastic matrix and a viscoelastic interface and demonstrated that the reduced-order model can be exploited to analyze rate-dependent effective moduli and interface-induced size effects. Koutsawa [471] extended the mechanics of structure genome to piezoelasticity and investigated the effective electro-elastic properties of composites embedding the spring-type interface model.

While the majority of the contributions on the topic, from a computational perspective are dealing with FEM and BEM, other approaches such as the material point method [472] have also been utilized to formulate the cohesive interface model. In the context of computational analysis on fracture and failure of composites, numerous contributions are available in the literature. Yeh [473], developed a finite element method to investigate failure mechanisms and the ultimate strength of fiber-reinforced composites with admissible interfacial debonding between the fiber and the matrix. Xu and Needleman [459] conducted a numerical analysis on size dependent dynamic crack growth in a continuum composed of a set of cohesive surfaces. Their constitutive relation for the cohesive surfaces allowed for the formation of new surfaces and their dimensional analysis was capable of capturing size effects. Camacho and Ortiz [474] developed a Lagrangian finite element method for fracture and fragmentation in brittle materials using a cohesive-law fracture model. Later, via generalizing the cohesive element of de-Andrés et al. [475], Ortiz and Pandolfi [476] extended the work in [474] to the three-dimensional setting and developed a cohesive element with a class of irreversible cohesive laws suitable to accurately track dynamic growth of cracks. Alfano and Crisfield [477], carried out a finite element analysis of the delamination in laminated composites using an interface damage model [478]. For further computational studies on applications of cohesive interfaces in fracture and failure in composites see Refs. [479,491–495], and [497–511], among others.

1.3.3 Elastic Interface Model. The third option is to assume that the displacement field is continuous across the interface while the traction field across the interface is allowed to experience a jump due to (tangential) interfacial stresses [512,516] in accordance with the generalized Young–Laplace equation [517,518,682]. This interface model is commonly referred to as the *elastic (stress-type) interface model* since it is an immediate consequence of the surface elasticity theory [519].

1.3.3.1 Analytical studies. The pioneering works of Gurtin and Murdoch [519,521] laid the mathematical foundation of incorporating surface stresses into classical continuum mechanics leading to the elastic interface model [520], see also Ref. [683]. In Gurtin–Murdoch surface elasticity theory, a surface can be regarded as a thin layer perfectly attached to the bulk with no slipping nor delamination. The material parameters of a surface/interface are assumed to be independent of the bulk material. Various theoretical studies have been carried out to generalize the Gurtin–Murdoch model [522–525,588,589]. For further studies investigating surface and interface effects in solids see Refs. [513–515,530,532–535,590], and [684–695] and the review by Javili et al. [602]. Applications of the Gurtin–Murdoch theory have emerged in a wide spectrum of studies among which, investigation of interface effects in heterogeneous materials has been a subject of increasing interest. Caillerie [526] showed that the elastic interface model is suitable to represent stiff interphases and depending on the degree of the interphase stiffness with respect to the matrix and inclusions, four different regimes of elastic interfaces could be identified, see also [527].

After almost two decades, Benveniste and Miloh [361] carried out a more generic study and demonstrated that depending on the degree of stiffness of interphases with respect to their neighboring materials, there exist seven distinct regimes of interface options which essentially boil down to perfect bonding and the two elastic and cohesive interface models with various interface parameters. Concentrating on the elastic interfaces, they derived the interface conditions and parameters based on a formal asymptotic expansion for the displacement and stress fields in the interphase, see Refs. [528,529], and [536] for similar studies. After the seminal work of Benveniste and Miloh [361], a significant body of literature has been dedicated to finding the elastic states in the constituents and overall properties of heterogeneous materials. Sharma et al. [537,538], combined the surface elasticity theory with Eshelby's formalism to analyze inhomogeneities of circular and spherical shapes bonded to their surrounding medium with an elastic interface. They derived closed-form expressions for the elastic state of inhomogeneities in a variational manner and concluded that the inclusions with a constant curvature admit a uniform elastic state. Yang [539] examined the influence of the surface energy on the effective modulus of an elastic composite material containing spherical nanovoids and reported that the effective moduli of such composites are not only size dependent but also strain dependent. Sun et al. [540], derived a new expression for the bulk modulus for a particle-reinforced composite at large deformations and questioned the results reported by Yang [539] by demonstrating that constant surface stress independent of the elastic strain should have no influence on the effective shear modulus. Later, Duan et al. [541] derived the interior and exterior field solutions for a spherical inclusion embedded in a matrix with interface stress effects subjected to a uniform eigenstrain in the inclusion and remote uniform stress.

Exploiting the composite sphere assemblage method, the Mori–Tanaka method, and the generalized self-consistent method, Duan et al. [542] established a generalized micromechanical framework to account for interface stress effects on the effective moduli of composites containing nano-inhomogeneities. Theoretical frameworks to study elasticity problems for multiphase materials embedding elastic interfaces at finite deformations were proposed by Huang and Wang [544] and Monteiro et al. [545]. Afterward, Huang and Sun [546] examined the change of the elastic fields induced by the interface energy and interface stresses in a finite deformation setting. They concluded that during the deformation, the shape, size, and curvature tensor of the interface will change, which is in contradiction to the works of Sharma and Ganti [538] and Duan et al. [541]. He [547] studied surface stresses in elastic isotropic solids with nanovoids and showed that when the voids are spherical with identical sizes, certain hydrostatic loads applied on the outer boundary result in uniform stress and strain fields within the medium. Afterward, Lim et al. [548] considered a solid with nano-inclusion under a non-hydrostatic load and demonstrated that the interface stress renders the elastic field in the inclusion to depend on both inclusion size and nonuniformity. Using a variational approach, Chen et al. [549] derived the energy potential incorporating surface effects for fiber composites. A similar study has been carried out for particulate-composites in Chen et al. [550]. Through a displacement potential formulation, Mi and Kouris [551] demonstrated that the interface effects on the stress distribution in the matrix are more pronounced when the particles are soft whereas an opposite effect holds within the particles themselves. See Refs. [551–553] for the solutions of similar problems with a single circular or spherical inhomogeneity embedded in an infinite half-space. Le-Quang and He [554,556] extended the generalized self-consistent method to account for elastic interfaces to determine thermoelastic properties of fiber- and particle-reinforced composites, see Ref. [555] for the associated bounds on effective elastic moduli. Duan et al. [406,407] employed the generalized self-consistent method and the Eshelby equivalent inclusion method to predict the effective moduli of multiphase composites embedding spherical particles or cylindrical fibers with elastic interfaces.

The solution of the nano-inhomogeneity in an infinite matrix is an important fundamental problem and its utility becomes more

apparent when its extensions are considered. These extensions include considering noncircular or nonspherical inhomogeneities or having multiple inclusions interacting with each other throughout the medium. A remarkable contribution on this topic by Mogilevskaya et al. [557] compares the original Gurtin–Murdoch interface model with a thin membrane-type interphase layer and demonstrates the validity of the approach in solving multi-inclusion problems, see also Ref. [561]. They also highlight the differences between the original theory of Gurtin and Murdoch and the simplified models in Refs. [206,537,538,541], and [696–698] and clarify the shortcomings that each simplification entail. Following their work [699], Mogilevskaya et al. [558] established a framework where periodic and random composites with inclusions interacting with each other were replaced by an equivalent inhomogeneity in an infinite plane. Their work was followed by a systematic study on nanocomposite systems in Ref. [559]. Similar studies using a vectorial spherical harmonics approach for multiple interacting inclusions have been carried out by Kushch et al. [562–564]. Tian and Rajapakse [597,598] studied the elastic field of a nanoscale elliptical inhomogeneity embedded in an infinite matrix with an elastic interface in between. Via employing the complex variable technique of Muskhelishvili [565], they showed that the elastic field of an elliptic inhomogeneity under uniform eigenstrain is no longer uniform when interfacial stress effects are taken into account, see also Ref. [566]. Benveniste and Miloh [567] investigated the possibility of modifying the contact mechanism between the inhomogeneity and the matrix in a composite medium using the elastic interface model so as to achieve inhomogeneity neutrality that would maintain the stress field within the matrix undisturbed. Moreover, the strength properties of ductile nanoporous materials with interface stress effects have been studied in Refs. [568–570] in a nonlinear homogenization framework.

One of the major shortcomings of the Gurtin–Murdoch theory was that the interface was modeled as a zero thickness layer without resistance against bending. This issue was addressed by Steigmann and Ogden [588,589] where they generalized the Gurtin–Murdoch model via incorporating the flexural resistance into the interface model. Via connecting the Steigmann–Ogden theory to atomistic simulation, Chhapadia et al. [590] investigated the effective elastic modulus of a nanostructured beam using curvature-dependent surface energy. Zemlyanova and Mogilevskaya [591,592] proposed a solution for the problem of single spherical and circular inhomogeneity embedded in a matrix with Steigmann–Ogden interface. Han et al. [593] extended their studies to account for multiple interacting inclusions. Gao et al. [525] studied the curvature-dependence of the interfacial energy and formulated interfacial energy together with an interface stress model resulting in a micromechanical framework to determine the overall elastic properties, see also Ref. [594]. Further analytical studies on the subject of the overall behavior of heterogeneous materials embedding elastic interfaces can be found in Refs. [571–587,595,596,603], and [604].

1.3.3.2 Computational studies. Besides the analytical approaches, substantial progress has been made in computational studies of interface elasticity. Tian and Rajapakse [700] presented a two-dimensional finite element formulation for analysis of multiple arbitrary shaped anisotropic inclusions in an anisotropic matrix having elastic interfaces in between. Yvonnet et al. [599] developed a computational technique combining the level set method and the extended finite element method to analyze interface effects described by the elastic interface model and to determine the size-dependent effective elastic moduli of nanocomposites. Dong and Pan [600] proposed a boundary element method to analyze the stress field in nano-inhomogeneities with elastic interface effects. Considering the inhomogeneities' interactions, they studied the effects of different inhomogeneities' shapes and interface material parameters on the overall material response. Javili et al. [602] presented a couple-field finite element method to study the thermomechanical behavior of materials embedding Kapitza interfaces. Later, Javili et al. [603] developed a computational homogenization framework for micro- to macrotransitions of porous media that accounts for size effects due to surface elasticity at the microscale. See Ref. [604] for a curvilinear-coordinate-based finite element methodology for the computational implementation of the surface elasticity theory.

Dai et al. [601] developed a new methodology to analyze composites with periodic distributions of inclusions connected to the matrix with elastic interfaces imposing periodic boundary conditions. Using FEM, they showed that when the shear modulus of the inclusions exceeds twice the shear modulus of the matrix, inclusion and matrix can be treated as being perfectly bonded. Moreover, they demonstrated that when the volume fraction of the inclusions is less than 9%, the interfacial stress can be approximated using a single inclusion with the same volume fraction embedded in an infinite plane. Koutsawa et al. [605] proposed the mechanics of the structure genome model to analyze nanocomposites embedding elastic interfaces. They exploited the full field micromechanics approach to predict the overall properties of composites containing nano-inhomogeneities. Chen et al. [606,607] incorporated interface elasticity into a finite volume-based homogenization theory to analyze materials embedding nanosized cylindrical voids with circular and ellipsoidal cross section. See Chen et al. [608] for a critical comparison between the performance of the finite element and finite volume method in determining the response of nanoporous materials embedding energetic surfaces and interfaces. Dong and Pan [600] examined the stress field in nano-inhomogeneities with different shapes. They proposed a boundary element method formulation in conjunction with the Gurtin–Murdoch interface model and investigates the elastic behavior of composites embedding inclusions with arbitrary shapes. Dong and Lo [609] employed BEM to analyze the stress state in an elastic half-plane containing nano-inhomogeneities with surface and interface effects. Their method was extended to three-dimensional (3D) in Ref. [610]. Zhao et al. [611] developed a hybrid smoothed extended finite element/level set method to model nano-inhomogeneities with interfacial energy effects. In their methodology, the finite element mesh can be completely independent of the interface geometry. They showed that considering interfacial effects, the energetically favorable shape for the inhomogeneities depends on the inhomogeneity size, misfit strain as well as elastic properties of the surrounding bulk material. Further computational studies on the surface and interface elasticity include [612–615].

1.3.4 General Interface Model. The fourth option assumes that both displacement and traction jumps across the interface are admissible as illustrated in Fig. 1. This interface model is a more inclusive model compared to the previously introduced interface models and is referred to as the *general interface model*. Note, for the general interface model, the interface always coincides with the midlayer. From the perspective of deriving the previous interface models as asymptotic limits of thin interphases, the cohesive interface model is derived as the limit case of soft interphases and the elastic interface model is obtained as the limit case of stiff interphases, see Wang et al. [362] while the general interface model covers the whole spectrum in between.

1.3.4.1 Analytical studies. The general interface model was originally proposed by Hashin [616] where he derived "imperfect" interface conditions representing the effect of thin interphases with no restriction on the magnitude of the interphase stiffness. Hashin also derived the effective elastic moduli of a unidirectional coated fiber composite embedding general imperfect interfaces and showed that the general interface model is valid for the whole range of interphase stiffness, from very small to very large. The analysis carried out by Hashin was restricted to isotropic interphases. Benveniste [617] generalized the approach adopted by Bövik [620] and developed a general interface model to capture

the effects of anisotropic interphase between two anisotropic media. Based on the works of Bövik [620] and Benveniste [617], Monchiet and Bonnet [621] extended the concept of a general imperfect interface to viscoplastic materials via a Taylor expansion approach. Later, Benveniste [618] formulated approximate models of thin interphases in plane-strain elasticity in which interphase properties were variables. Benveniste replaced the interphase with the general interface model and calculated the interfacial displacement and traction jump conditions, see Benveniste [619] for a similar study on thermal problems. Gu and He [622] introduced two orthogonal projection operators determining interfacial continuity and discontinuity of the field variables and obtained coordinate-free interfacial relations involving the surface decomposition of linear constitutive laws. Using their relations, Gu and He derived a general imperfect interface model for coupled multifield phenomena by applying a Taylor expansion to a three-dimensional curved thin interphase embedded between its two neighboring materials, see a similar study carried out by Gu et al. [623] in the context of thermal conduction. Serpilli et al. [625] derived the governing equations for general imperfect interfaces in a linear multiphysics framework for composite material. They adopted the asymptotic expansions technique via defining a general multiphysics interface law and derived zero and higher-order interface models for soft, hard, and rigid interphases. Gu et al. [624] derived estimates for the effective bulk and shear moduli of isotropic particulate-composites with general interfaces by using the generalized self-consistent scheme. They compared their results against a three-phase model comprising interphase between the constituents and observed excellent agreements, see also Ref. [626]. A similar study was conducted by Xu et al. [627] for fiber reinforced composites.

Firooz et al. [628,629] developed a unifying framework to determine the overall behavior of fiber- and particle-reinforced composites embedding general interfaces. In their study, they extended the composite cylinder assemblage, the composite sphere assemblage, and the generalized self-consistent scheme to account for general interfaces and obtained size-dependent effective elastic properties of composites. Furthermore, via incorporating the general interface model into the Mori–Tanaka method, they proposed a methodology to determine the average strain and stress fields within the constituents of a composite. They compared their analytical solutions against computational results obtained by the finite element method and observed a remarkable agreement, see also Chatzigeorgiou et al. [630].

1.3.4.2 Computational studies. Computational studies on general interfaces are fairly limited since this class of interfaces is comparatively new. Gu et al. [631] provided the preliminary steps for a numerical implementation of the work presented in [622] via establishing the weak form for the boundary value problem of composites embedding general imperfect interfaces in the context of transport phenomena, elasticity, and piezoelectricity. Javili et al. [632] established the computational framework for the general interface model at finite deformations. They presented a thermodynamically consistent formulation and governing equations of general imperfect interfaces and provided a detailed finite element implementation to study the behavior of heterogeneous materials embedding general interfaces; a similar study was conducted for thermal problems in Ref. [633]. Kaessmair et al. [634] developed a thermodynamically consistent theory for general interfaces in view of their thermomechanical behavior. They established a unified computational framework to model all classes of such interfaces using the finite element method. The variational formulation of generalized interfaces within the finite deformation continuum mechanics setting was presented by Javili [635] where he showed that elastic and cohesive interface models naturally represent two limit cases of the general interface model. A parametric study on the role of generalized interfaces in the overall material response has been carried out by Saeb et al. [636] for fiber composites and Firooz and Javili [639] for particulate-composites. Saeb et al. [637] presented a systematic study to obtain size-dependent bounds on the response of composites embedding general interfaces within a computational homogenization framework. Conducting computational analyses on periodic microstructures, they found that their response approaches asymptotically to an upper bound. Saeb et al. [638] investigated the influence of a degrading general interface on the failure of composites. They observed that in the presence of general interfaces with damage, DBC and TBC may not necessarily provide bounds for random microstructures, in contrast to classical computational homogenization.

1.4 Significance of the Interface Position. Although numerous contributions in the literature have studied the aforementioned interface models, only very few have investigated the importance of the interface position. For the elastic interface model, due to the vanishing displacement jump, the interface always coincides with the two interphase sides, and thus, the interface position becomes irrelevant. For the cohesive interface model, the topic of the interface position is commonly dismissed since the traction-separation law relates the traction to the displacement jump across the interface. Clearly, the interface position plays no role in evaluating the displacement jump and thus, it does not contribute to the governing equations associated with the interfacial behavior. When developing cohesive zone laws, special care must be taken to sufficiently satisfy the angular momentum balance at large deformations. In a continuum body, the symmetry of the Cauchy stress a priori ensures the angular momentum balance. This cannot be enforced for the cohesive zone models since the stress tensor does not exist by definition. The only equilibrium requirement is the continuity of traction which does not guarantee the moment balance at large deformations.

A commonly accepted methodology to overcome this difficulty is to postulate that the traction vector is coaxial to the displacement jump across the interface. Ortiz and Pandolfi [476] developed a three-dimensional cohesive element for finite deformation analysis together with a class of irreversible cohesive laws that were compatible with the conventional finite element discretization of the bulk material. While considering different weights for the sliding and normal opening displacements at the interface, the interface in their model was intuitively assumed to be in the middle of the two dissimilar opening materials. Gasser and Holzapfel [479] developed three different finite element formulations with embedded strong discontinuities based on the enhanced assumed strain method. They proposed an explicit expression for a transversely isotropic traction law in the form of a displacement-energy function assuming that softening phenomena in the cohesive zone is modeled by a damage law. To model the cohesive zone, they introduced a fictitious discontinuity surface in the deformed configuration which, conventionally, was located in the middle of its adjacent surfaces. Mergheim and Steinmann [480] introduced a discontinuous finite element method for computational modeling of strong and weak discontinuities in a geometrically nonlinear elasticity setting. They applied Nitsche's method [701] in their variational formulation for weak discontinuities which yielded a weighted average term for the Piola stress in their interfacial cohesive energy where they assumed the interface to be at the midplane of its adjacent constituents. Hansbo and Hansbo [481] also adopted a weighting factor for averaging the parameters across the interface and proposed a computational approach for the finite element solution of elliptic interface problems, using Nitsche's method, see also Ref. [482]. van den Bosch et al. [483] showed that most of the cohesive zone models are suited for small deformations only and proposed a large displacement formulation to overcome the issues of the classical approaches. They also introduced a 3D cohesive zone element and elaborated its numerical implementation in which the formulations were derived with respect to a midline between the two opening parts of the cohesive zone, see also van den Bosch et al. [484,485]. Vossen et al. [486] and Ottosen et al. [487] demonstrated that the commonly adopted

traction-separation laws do not necessarily satisfy the balance of angular momentum at the cohesive element level resulting in an error which becomes significant at large deformations concluding that the traction vector must be collinear with the displacement jump, see also Refs. [488] and [489].

Figure 2 schematically illustrates finite thickness interphase and its equivalent zero-thickness interface model. For uniform interphase (left), the interface is situated at the center of its associated interphase. For graded interphase (right), the interface is off-center and its position must be shifted toward the stiffer side of its corresponding interphase. The correct interface position can be obtained via comparing the interface model with direct numerical simulations of its associated interphase. While many contributions consider the interphase as an isotropic and homogeneous phase, a realistic analysis should take into account the effects of interphase anisotropy and heterogeneity. It can be shown that if the interface is assumed to coincide with the midplane, in general, it cannot capture the overall behavior of graded interphases. For the general interface model, since both interface elasticity and opening are admissible, the position of the interface plays a crucial role at large as well as small deformations. Nonetheless, the interface position has been commonly disregarded in the development of the general interface model by assuming that the interface is located at the midlayer between its bulk neighbors. This simplification sufficiently satisfies the interface rotational equilibrium and can lead to the conclusion that the only admissible position for the interface is the midplane [702]. *We argue that not only this simplification is not necessary, but also it defeats the utility of the general interface model to replace nonuniform interphases, as demonstrated in Ref. [703]. Therefore, it is imperative to introduce an extended general interface model that allows for arbitrary interface positions.*

1.5 Objectives and Key Features. In this contribution, we revisit the controversial issue of the interface position in general interfaces via introducing a weighted average operator and demonstrate that the interface does not need to be necessarily restricted to the midlayer. Therefore, we rigorously establish an extended general interface model that can assume any arbitrary position between its neighbors and still fulfill the rotational equilibrium condition. Our proposed interface model is capable of recovering all the aforementioned interface models in Sec. 1.3, see Fig. 1. In addition to the detailed review on the subject, the key features and contributions of this paper are:

- to develop an extended general interface model as depicted in Fig. 1, with arbitrary interface positions via introducing the weighted average operator;
- to show that the commonly accepted general interface model is a subclass of the *extended general interface model* and can be recovered if the weighted average operator is replaced by the classical average operator;
- to incorporate the *extended* interface model into homogenization and to develop bounds and estimates on the *size-dependent* effective properties of fiber-reinforced and particle-reinforced composites;
- to provide a comprehensive comparison between the *extended general* interface model and the already existing interface models;
- to carry out an exhaustive numerical study to compare the analytical and computational results.

Remark on accounting for softening at the interface. The proposed extended general interface model encloses the general interface model, see Fig. 1. The general interface model itself recovers both the cohesive interface model and the elastic interface model. Hence, the extended general interface model recovers anything that a cohesive interface model or an elastic interface model can capture, but it also covers more complex interfacial behavior. The extended general interface model here can, in principle, account for softening too. However, we have limited the discussion here to linear elasticity for the sake of simplicity only. More precisely, the interface orthogonal (out-of-plane) response, commonly referred to as traction-separation law, can be nonlinear and it may as well include damage and softening. Accounting for softening in the traction-separation description of a cohesive zone model translates in the current context to accounting for interface damage in the constitutive law. In the current model, since the interface has both out-of-plane response (similar to the cohesive interface model) and in-plane response (similar to the elastic interface model), accounting for interface damage requires further elaboration to distinguish between orthogonal damage and tangential damage on the interface, similar to taking damage into account for the general interface model investigated in Ref. [638]. The framework here is focused on the kinematics and kinetics of the problem at hand. More complex traction-separation laws can be introduced through a different constitutive model at the interface. Leaving out "softening" in the discussion here is not a shortcoming of the model but it is rather an assumption to have less complicated analytical expressions. Similar to softening, the interface model itself is generic enough to allow for debonding and damage too. Nonetheless, we have excluded this aspect for the sake of brevity. See, for instance, Refs. [704] and [705] for debonding and damage at the interface. Apart from softening at the interface, softening of the bulk material itself is important too, but it is also omitted from the discussion here. In particular, according to Ref. [706], it may not be possible to define an RVE in the presence of softening. For the current zero-thickness interface model, however, it is possible to retain the notion of RVE if softening and damage occur only at the interface enclosed within the domain.

1.6 Notations and Definitions. Throughout this paper, vector quantities are denoted by lowercase bold letters, tensorial quantities are denoted by uppercase bold letters, third-order tensors are denoted by lowercase blackboard letters, and fourth-order tensors are denoted by uppercase blackboard letters. For instance, α is a scalar, $\boldsymbol{a}$ is a vector, $\boldsymbol{A}$ is a second-order tensor, $\mathbb{a}$ is a third-order tensor and $\mathbb{A}$ is a fourth-order tensor. The dot product of two vectors $\boldsymbol{a}$ and $\boldsymbol{b}$ is a scalar $\alpha = \boldsymbol{a} \cdot \boldsymbol{b}$ with $\alpha = [\boldsymbol{a}]_i[\boldsymbol{b}]_i$. The cross product of two vectors $\boldsymbol{a}$ and $\boldsymbol{b}$ is a vector $\boldsymbol{c} = \boldsymbol{a} \times \boldsymbol{b}$ with $[\boldsymbol{c}]_k = [\boldsymbol{a}]_i[\boldsymbol{b}]_j[\mathbb{e}]_{ijk}$ where $[\mathbb{e}]_{ijk}$ is the third-order Levi–Civita permutation tensor with symbol $\mathbb{e}$. The dyadic product of two vectors

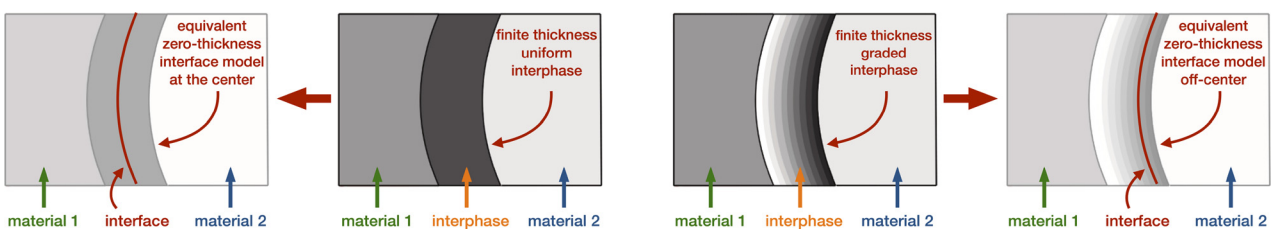

Fig. 2 Schematic illustration of finite thickness interphase and its equivalent zero-thickness interface model. For uniform interphase (left), the interface is situated at the center of its associated interphase. For graded interphase (right), the interface is off-center and its position must be shifted toward the stiffer side of its corresponding interphase.

$\boldsymbol{a}$ and $\boldsymbol{b}$ is a second-order tensor $\boldsymbol{C} = \boldsymbol{a} \otimes \boldsymbol{b}$ with $[\boldsymbol{C}]_{ij} = [\boldsymbol{a}]_i [\boldsymbol{b}]_j$. The composition of two second-order tensors $\boldsymbol{A}$ and $\boldsymbol{B}$ is a second-order tensor $\boldsymbol{C} = \boldsymbol{A} \cdot \boldsymbol{B}$ with components $[\boldsymbol{C}]_{ij} = [\boldsymbol{A}]_{ik} [\boldsymbol{B}]_{kj}$. The (double) contraction of two second-order tensors $\boldsymbol{A}$ and $\boldsymbol{B}$ is a scalar $\alpha = \boldsymbol{A} : \boldsymbol{B}$ with $\alpha = [\boldsymbol{A}]_{ij} [\boldsymbol{B}]_{ij}$. The action of a second-order tensor $\boldsymbol{A}$ on a vector $\boldsymbol{b}$ results in a vector $\boldsymbol{c} = \boldsymbol{A} \cdot \boldsymbol{b}$ with $[\boldsymbol{c}]_i = [\boldsymbol{A}]_{ij} [\boldsymbol{b}]_j$. The standard dyadic product of two second-order tensors $\boldsymbol{A}$ and $\boldsymbol{B}$ is a fourth-order tensor $\mathbb{C} = \boldsymbol{A} \otimes \boldsymbol{B}$ with $[\mathbb{C}]_{ijkl} = [\boldsymbol{A}]_{ij} [\boldsymbol{B}]_{kl}$. Two nonstandard dyadic products of two second-order tensors $\boldsymbol{A}$ and $\boldsymbol{B}$ are fourth-order tensors $\mathbb{D} = \boldsymbol{A} \overline{\otimes} \boldsymbol{B}$ and $\mathbb{E} = \boldsymbol{A} \underline{\otimes} \boldsymbol{B}$ with $[\mathbb{D}]_{ijkl} = [\boldsymbol{A}]_{ik} [\boldsymbol{B}]_{jl}$ and $[\mathbb{E}]_{ijkl} = [\boldsymbol{A}]_{il} [\boldsymbol{B}]_{jk}$, respectively.

Interface quantities are distinguished from bulk quantities by a bar placed on top of them. That is, $\{\bar{\bullet}\}$ denotes an interface quantity with its bulk counterpart $\{\bullet\}$. Moreover, the classical average and the jump operators across the interface are defined by $\{\{\{\bullet\}\}\} := \frac{1}{2}[\{\bullet\}^+ + \{\bullet\}^-]$ and $[[\{\bullet\}]] = \{\bullet\}^+ - \{\bullet\}^-$, respectively. The quantities at the macroscale are distinguished from their counterparts at the microscale by a left superscript "M." For instance, ${}^{\mathrm{M}}\{\bullet\}$ is a macroscopic quantity counterpart to $\{\bullet\}$ at the microscale. The notation and abbreviations of the paper are listed in Nomenclature.

1.7 Organization of the Manuscript. The remainder of this contribution is organized as follows. Section 2 presents the governing equations for continua embedding the proposed extended general interface model. This is then followed by establishing analytical solutions in Secs. 3 and 4 for the overall properties of fiber-reinforced and particle-reinforced composites embedding extended general interfaces between their constituents, respectively. Through a series of numerical examples, a comprehensive study to examine the effects of the interface position on the overall material response is carried out. Section 5 summarizes this work and provides further outlooks.

2 Governing Equations

This section elaborates on the governing equations of a continuum body accounting for the *extended general interface model* in the context of linear elasticity. The formulation presented here demonstrates that the interface is allowed to have any arbitrary position between its bulk neighbors. The differences and similarities between our novel formulation and the classical interface models are highlighted.

2.1 Kinematics. Figure 3 depicts a continuum body, corresponding to a heterogeneous medium, occupying the configuration ${}^{\mathrm{M}}\mathcal{B}$ at the macroscale with its underlying RVE at the microscale denoted as $\mathcal{B}$. The boundary of the domains at the macro- and microscale is denoted as $\partial {}^{\mathrm{M}}\mathcal{B}$ and $\partial \mathcal{B}$, respectively. At the microscale, it is assumed that the constitutive behavior of the constituents is known. Via solving the associated boundary value problem and proper averaging over the RVE, the overall macroscopic response of the material is obtained, see Refs. [163,164,166,167], and [707–709], among others. Within the framework of homogenization, a proper RVE must be chosen (i) large enough to include enough information about the microstructure and at the same time (ii) small enough to guarantee the separation of length scales [119–121]. To capture isotropic behavior, the RVE is assumed circular in the two-dimensional setting and spherical in the 3D setting representing fiber-reinforced and particle-reinforced composites, respectively. As shown in Fig. 3, the finite thickness interphase region is replaced by a zero-thickness interface model characterized by displacement and traction jumps. The interface $\mathcal{I}$ divides the microstructure into two disjoint subdomains $\mathcal{B}^+$ and $\mathcal{B}^-$ corresponding to bulk domains on the plus and minus sides of the interface, respectively. The intersection of the interface $\mathcal{I}$ with $\mathcal{B}^+$ is denoted as $\mathcal{I}^+$ and the intersection of the interface with $\mathcal{B}^-$ is denoted as $\mathcal{I}^-$. The unit normal to the RVE boundary $\partial \mathcal{B}$ is

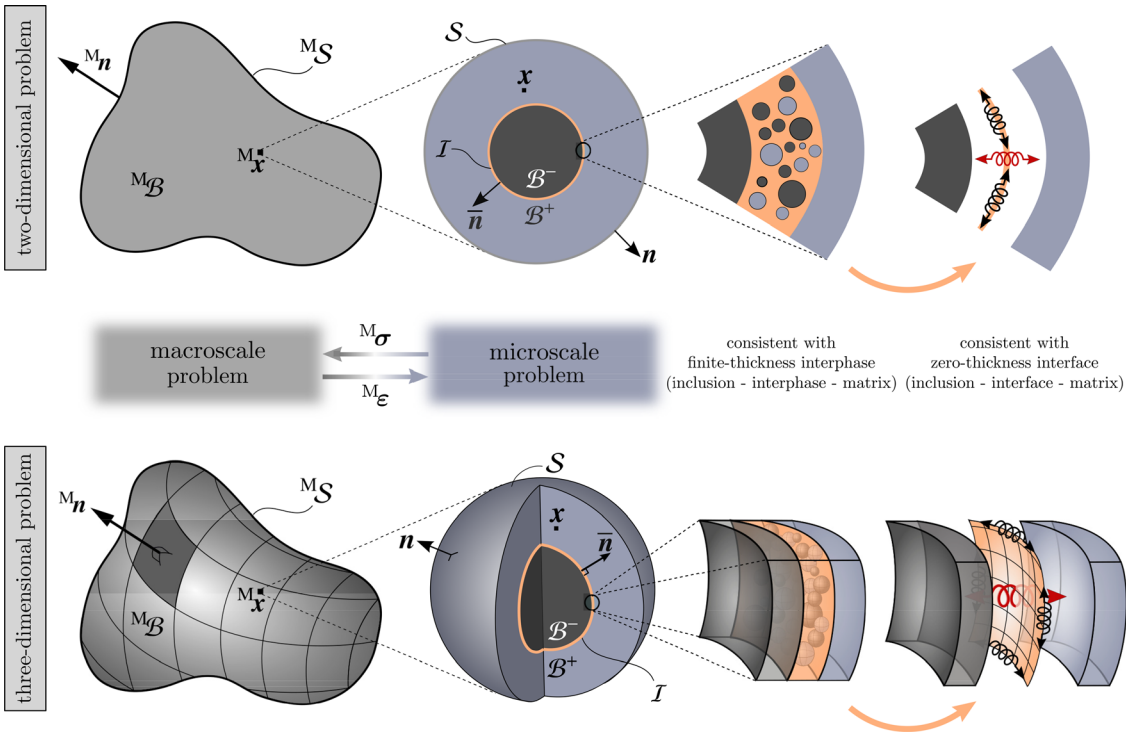

Fig. 3 Problem definition for homogenization including the extended general interface model. The macrostructure is shown with its underlying RVE. At the microscale, the constitutive laws are assumed to be known and the macroscopic behavior is obtained via solving the boundary value problem at the microscale. A finite thickness interphase is replaced with a zero-thickness interface model.

denoted as $\boldsymbol{n}$ and the unit normal to the interface I, pointing from the interface minus to the plus side, is denoted as $\overline{\boldsymbol{n}}$. The outward unit vector $\tilde{\boldsymbol{n}}$ is defined such that it is normal to the boundary of the interface but it is tangential to the interface itself. Let $\boldsymbol{u}$ and $\overline{\boldsymbol{u}}$ define the displacement fields in the bulk and on the interface, respectively. Since interface opening is admissible for the extended general interface model, the two sides $\mathcal{B}^+$ and $\mathcal{B}^-$ are allowed to depart from each other resulting in a displacement jump across the interface as

$$[[\boldsymbol{u}]] := \boldsymbol{u}^+ - \boldsymbol{u}^- \tag{1}$$

where $\boldsymbol{u}^+$ and $\boldsymbol{u}^-$ denote the displacements on the plus and minus sides of the interface, respectively. In the (classical) general interface model the interface displacement is commonly [616,617,631,632] defined as the average of the displacements between its two sides as

$$\overline{\boldsymbol{u}} := \left\{\left\{\{\{\boldsymbol{u}\}\} := \frac{1}{2}[\boldsymbol{u}^+ + \boldsymbol{u}^-]\right. \tag{2}$$

The *extended general interface model* allows the interface to occupy any arbitrary position between its two sides. In doing so, we first define the *weighted average* and the *complimentary weighted average operators*

$$\begin{aligned}\{\{\{\bullet\}\}\}^{\overline{\alpha}} &= \overline{\alpha}\,\{\bullet\}^+ + [1-\overline{\alpha}]\,\{\bullet\}^-\\ \{\{\{\bullet\}\}\}^{[1-\overline{\alpha}]} &= [1-\overline{\alpha}]\,\{\bullet\}^+ + \overline{\alpha}\,\{\bullet\}^-\end{aligned} \tag{3}$$

respectively, where $\overline{\alpha}$ is the weighting coefficient determining the interface position. These average operators are indeed the weighted forms of the classical average operator (2). As shown in Fig. 4, we have $0 \leq \overline{\alpha} \leqslant 1$. That is, $\overline{\alpha} < 0.5$ implies that the interface is closer to the minus side (inclusion) while $\overline{\alpha} > 0.5$ indicates that the interface is closer to the plus side (matrix). Clearly, $\overline{\alpha} = 0.5$ recovers the classical definition where the interface coincides with the midlayer and thus the extended general interface model coincides with the general interface model. We define the extended general interface displacement as the *weighted average* of the displacements $\boldsymbol{u}^+$ and $\boldsymbol{u}^-$. That is

$$\overline{\boldsymbol{u}} := \{\{\boldsymbol{u}\}\}^{\overline{\alpha}} = \overline{\alpha}\,\boldsymbol{u}^+ + [1-\overline{\alpha}]\,\boldsymbol{u}^- \tag{4}$$

Having the displacement fields, the strains in the bulk and on the interface can be expressed as

$$\begin{aligned}\boldsymbol{\varepsilon} &= \frac{1}{2}\left[\boldsymbol{I}\cdot\mathrm{Grad}\,\boldsymbol{u} + [\mathrm{Grad}\,\boldsymbol{u}]^T\cdot\boldsymbol{I}\right] \quad \text{in } \mathcal{B}\\ \overline{\boldsymbol{\varepsilon}} &= \frac{1}{2}\left[\overline{\boldsymbol{I}}\cdot\overline{\mathrm{Grad}}\,\overline{\boldsymbol{u}} + [\overline{\mathrm{Grad}}\,\overline{\boldsymbol{u}}]^T\cdot\overline{\boldsymbol{I}}\right] \quad \text{on } I\end{aligned} \tag{5}$$

where $\boldsymbol{I}$ is the second-order identity tensor. The operator $\overline{\mathrm{Grad}}\,\{\bullet\}$ is the interface gradient operator defined by $\overline{\mathrm{Grad}}\,\{\bullet\} := \mathrm{Grad}\,\{\bullet\}\cdot\overline{\boldsymbol{I}}$ in which $\overline{\boldsymbol{I}}$ is the interface identity tensor $\overline{\boldsymbol{I}} := \boldsymbol{I} - \overline{\boldsymbol{n}}\otimes\overline{\boldsymbol{n}}$. Thus, the interface strain $\overline{\boldsymbol{\varepsilon}}$ is not only a superficial tensor possessing the property $\overline{\boldsymbol{\varepsilon}}\cdot\overline{\boldsymbol{n}} = \boldsymbol{0}$, but it is also tangential since $\overline{\boldsymbol{n}}\cdot\overline{\boldsymbol{\varepsilon}} = \boldsymbol{0}$.

2.2 Balance Equations. Equipped with the kinematics description of the problem, we derive the balance equations and allow the interface to coincide with any arbitrary surface between its bulk neighbors. Evidently, the choice of the interface position $\overline{\alpha}$ does not alter the governing equations for the bulk. To pinpoint the novelty of our proposed methodology, we first elaborate the interface balance equations for the general interface model theory and after highlighting its shortcomings and limitations, we introduce our new formalism. Since we limit our discussion to the microscale problem, the body forces are omitted henceforth.

Let $\boldsymbol{\sigma}$ denote the stress in the bulk $\mathcal{B}$ and $\boldsymbol{t}$ the traction acting on the boundary $\partial\mathcal{B}$. According to Cauchy's postulate, on the boundary we have $\boldsymbol{t} = \boldsymbol{\sigma}\cdot\boldsymbol{n}$. In the absence of body forces, the force balance over the bulk reads

$$\int_{\partial\mathcal{B}} \boldsymbol{t}\,\mathrm{d}A = \int_{\partial\mathcal{B}} \boldsymbol{\sigma}\cdot\boldsymbol{n}\,\mathrm{d}A = \int_{\mathcal{B}} \mathrm{Div}\boldsymbol{\sigma}\,\mathrm{d}V = \boldsymbol{0} \tag{6}$$

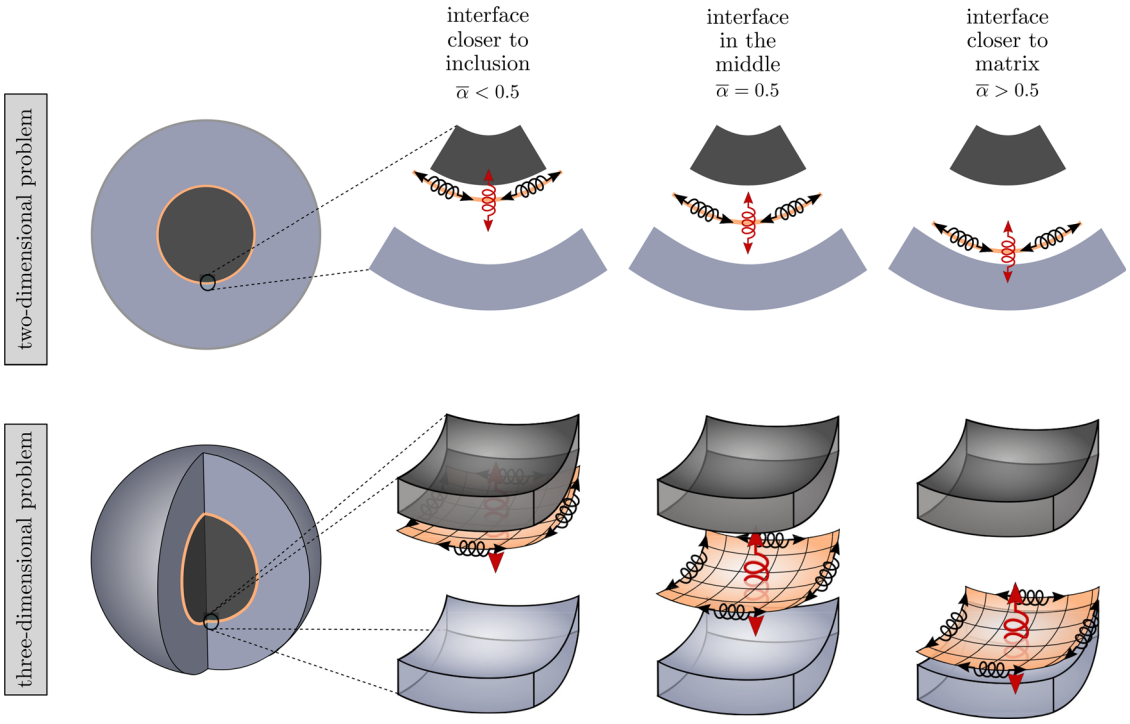

Fig. 4 Illustration of the interface position. The parameter $\overline{\alpha}$ determines the position of the interface. When $\overline{\alpha} < 0.5$ the interface is closer to the inclusion and when $\overline{\alpha} > 0.5$ the interface is closer to the matrix.

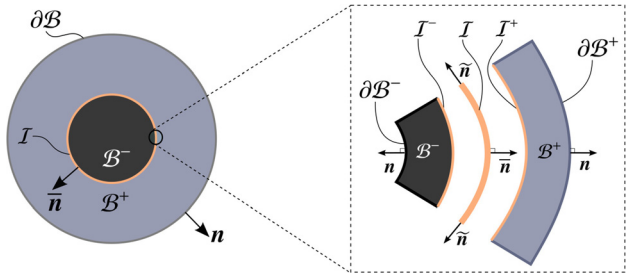

Fig. 5 Illustration of the unit normals to the body and the interface in the limit of vanishing bulk

which can be explicitly stated as

$$\mathrm{Div}\boldsymbol{\sigma} = \mathbf{0} \qquad \forall \boldsymbol{x} \in \mathcal{B} \tag{7}$$

For rotational equilibrium, we write the moments acting on the body with respect to an arbitrary point. That is

$$\begin{aligned}\int_{\partial\mathcal{B}} \boldsymbol{x}\times\boldsymbol{t}\,\mathrm{d}A &= \int_{\partial\mathcal{B}} \boldsymbol{x}\times[\boldsymbol{\sigma}\cdot\boldsymbol{n}]\,\mathrm{d}A = \int_{\mathcal{B}} \mathrm{Div}[\boldsymbol{x}\times\boldsymbol{\sigma}]\,\mathrm{d}V \\ &= \int_{\mathcal{B}} \boldsymbol{x}\times\mathrm{Div}\boldsymbol{\sigma}\,\mathrm{d}V + \int_{\mathcal{B}} \mathbb{e} : \boldsymbol{\sigma}^T\,\mathrm{d}V = \mathbf{0}\end{aligned} \tag{8}$$

where $\mathbb{e}$ is the Levi–Civita permutation tensor. The first term in (8) vanishes due to balance of forces (7), thus the moment balance can explicitly be written as

$$\mathbb{e} : \boldsymbol{\sigma}^T = 0 \;\Rightarrow\; \boldsymbol{\sigma} = \boldsymbol{\sigma}^T \qquad \forall \boldsymbol{x} \in \mathcal{B} \tag{9}$$

Next, we proceed with the interface balance equations. Let $\overline{\boldsymbol{\sigma}}$ denote the stress on the interface. The interface traction $\bar{\boldsymbol{t}}$ is defined by

$$\bar{\boldsymbol{t}} = \left\{\left\{\{\{\boldsymbol{\sigma}\}\}\cdot\overline{\boldsymbol{n}} = \frac{1}{2}\boldsymbol{\sigma}^+\cdot\overline{\boldsymbol{n}} + \frac{1}{2}\boldsymbol{\sigma}^-\cdot\overline{\boldsymbol{n}}\right.\right. \tag{10}$$

The balance of forces on a portion of the body containing the interface reads[2]

$$\int_{\partial\mathcal{B}^+\ \mathcal{I}^+} \boldsymbol{t}\,\mathrm{d}A + \int_{\partial\mathcal{B}^-\ \mathcal{I}^-} \boldsymbol{t}\,\mathrm{d}A + \int_{\partial I} \overline{\boldsymbol{\sigma}}\cdot\tilde{\boldsymbol{n}}\,\mathrm{d}L = \mathbf{0} \tag{11}$$

where $\partial\mathcal{B}^+$ and $\partial\mathcal{B}^-$ are the boundaries of cutouts of $\mathcal{B}^+$ and $\mathcal{B}^-$, respectively, as shown in Fig. 5. In the limit of vanishing bulk, the normal vector to $\partial\mathcal{B}^+\ \mathcal{I}^+$ is identical to interface unit normal $\overline{\boldsymbol{n}}$ and the unit normal to $\partial\mathcal{B}^-\ \mathcal{I}^-$ points in the opposite direction to $\overline{\boldsymbol{n}}$, see Fig. 5. The interface here denoted as $\mathcal{I}$ is essentially a two-sided surface with its two sides distinguished as $\mathcal{I}^-$ and $\mathcal{I}^+$. Prior to deformation, the two sides coincide with the interface itself and, therefore, $\mathcal{I}^-$, $\mathcal{I}^+$ and $\mathcal{I}$ collapse altogether. Therefore, Eq. (11) can be rewritten as

$$\begin{aligned}&\int_{\mathcal{I}^+} \boldsymbol{\sigma}^+\cdot\overline{\boldsymbol{n}}\,\mathrm{d}A - \int_{\mathcal{I}^-} \boldsymbol{\sigma}^-\cdot\overline{\boldsymbol{n}}\,\mathrm{d}A + \int_{\partial I} \overline{\boldsymbol{\sigma}}\cdot\tilde{\boldsymbol{n}}\,\mathrm{d}L \\ &= \int_I [[\boldsymbol{\sigma}]]\cdot\overline{\boldsymbol{n}}\,\mathrm{d}A + \int_{\partial I} \overline{\boldsymbol{\sigma}}\cdot\tilde{\boldsymbol{n}}\,\mathrm{d}L \\ &= \int_I [[\boldsymbol{\sigma}]]\cdot\overline{\boldsymbol{n}}\,\mathrm{d}A + \int_I \overline{\mathrm{Div}}\,\overline{\boldsymbol{\sigma}}\,\mathrm{d}A + \int_I \overline{C}\,\overline{\boldsymbol{\sigma}}\cdot\overline{\boldsymbol{n}}\,\mathrm{d}A = \mathbf{0}\end{aligned} \tag{12}$$

where $\overline{C} = -\overline{\mathrm{Div}}\,\overline{\boldsymbol{n}}$ is the interface curvature. The interface divergence operator is defined by $\overline{\mathrm{Div}}\{\bullet\} := \overline{\mathrm{Grad}}\{\bullet\} : \overline{\boldsymbol{I}}$. The last term integral in Eq. (12) vanishes due to the superficiality of the interface stress $\overline{\boldsymbol{\sigma}}$. The force balance on the interface therefore reads

$$\overline{\mathrm{Div}}\,\overline{\boldsymbol{\sigma}} + [[\boldsymbol{\sigma}]]\cdot\overline{\boldsymbol{n}} = \mathbf{0} \tag{13}$$

Similar to the bulk, for the interface rotational equilibrium, we write the moments acting on the interface with respect to an arbitrary origin as

$$\begin{aligned}&\int_{\mathcal{I}^+} \boldsymbol{x}\times\boldsymbol{t}\,\mathrm{d}A + \int_{\mathcal{I}^-} \boldsymbol{x}\times\boldsymbol{t}\,\mathrm{d}A + \int_{\partial I} \overline{\boldsymbol{x}}\times\overline{\boldsymbol{\sigma}}\cdot\tilde{\boldsymbol{n}}\,\mathrm{d}L \\ &= \int_{\mathcal{I}^+} \boldsymbol{x}^+\times\boldsymbol{\sigma}^+\cdot\overline{\boldsymbol{n}}\,\mathrm{d}A - \int_{\mathcal{I}^-} \boldsymbol{x}^-\times\boldsymbol{\sigma}^-\cdot\overline{\boldsymbol{n}}\,\mathrm{d}A + \int_{\partial I} \overline{\boldsymbol{x}}\times\overline{\boldsymbol{\sigma}}\cdot\tilde{\boldsymbol{n}}\,\mathrm{d}L \\ &= \int_I [[\boldsymbol{x}\times\boldsymbol{\sigma}]]\cdot\overline{\boldsymbol{n}}\,\mathrm{d}A + \int_I \overline{\mathrm{Div}}\,[\overline{\boldsymbol{x}}\times\overline{\boldsymbol{\sigma}}]\,\mathrm{d}A + \int_I \overline{C}\,\overline{\boldsymbol{x}}\times\underbrace{\overline{\boldsymbol{\sigma}}\cdot\overline{\boldsymbol{n}}}_{\mathbf{0}}\,\mathrm{d}A \\ &= \int_I [[\boldsymbol{x}\times\boldsymbol{\sigma}]]\cdot\overline{\boldsymbol{n}}\,\mathrm{d}A + \int_I \mathbb{e} : \overline{\boldsymbol{\sigma}}^T\,\mathrm{d}A + \int_I \overline{\boldsymbol{x}}\times\overline{\mathrm{Div}}\,\overline{\boldsymbol{\sigma}}\,\mathrm{d}A \\ &= \int_I [[\boldsymbol{x}\times\boldsymbol{\sigma}]]\cdot\overline{\boldsymbol{n}}\,\mathrm{d}A + \int_I \mathbb{e} : \overline{\boldsymbol{\sigma}}^T\,\mathrm{d}A - \int_I \overline{\boldsymbol{x}}\times[[\boldsymbol{\sigma}]]\cdot\overline{\boldsymbol{n}}\,\mathrm{d}A = \mathbf{0}\end{aligned} \tag{14}$$

which can be expressed as

$$[[\boldsymbol{x}\times\boldsymbol{\sigma}]]\cdot\overline{\boldsymbol{n}} + \mathbb{e} : \overline{\boldsymbol{\sigma}}^T - \overline{\boldsymbol{x}}\times[[\boldsymbol{\sigma}]]\cdot\overline{\boldsymbol{n}} = \mathbf{0} \tag{15}$$

To simplify the first term in relation (15), we utilize the following property that holds for the classical average and jump operators

$$[[\{\bullet\}\times\{\circ\}]] = \{\{\{\bullet\}\}\}\times[[\{\circ\}]] + [[\{\bullet\}]]\times\{\{\{\circ\}\}\} \tag{16}$$

which yields

$$[[\boldsymbol{x}\times\boldsymbol{\sigma}]]\cdot\overline{\boldsymbol{n}} = \{\{\boldsymbol{x}\}\}\times[[\boldsymbol{\sigma}]]\cdot\overline{\boldsymbol{n}} + [[\boldsymbol{x}]]\times\{\{\boldsymbol{\sigma}\}\}\cdot\overline{\boldsymbol{n}} \tag{17}$$

Resulting in the classical form of the interface moment balance

$$[[\boldsymbol{x}]]\times\underbrace{\{\{\boldsymbol{\sigma}\}\}\cdot\overline{\boldsymbol{n}}}_{\bar{\boldsymbol{t}}} + \mathbb{e} : \overline{\boldsymbol{\sigma}}^T + [\{\{\boldsymbol{x}\}\} - \overline{\boldsymbol{x}}]\times[[\boldsymbol{\sigma}]]\cdot\overline{\boldsymbol{n}} = \mathbf{0} \tag{18}$$

Three sufficient (yet not necessary) conditions to fulfill the rotational equilibrium (18) are

- $[[\boldsymbol{x}]] \,||\, \bar{\boldsymbol{t}} \;\Rightarrow\; [[\boldsymbol{x}]]\times\bar{\boldsymbol{t}} = \mathbf{0}$
- $\overline{\boldsymbol{\sigma}}^T = \overline{\boldsymbol{\sigma}} \;\Rightarrow\; \mathbb{e} : \overline{\boldsymbol{\sigma}} = \mathbf{0}$
- $\{\{\boldsymbol{x}\}\} = \overline{\boldsymbol{x}} \;\Rightarrow\; [\{\{\boldsymbol{x}\}\} - \overline{\boldsymbol{x}}]\times[[\boldsymbol{\sigma}]]\cdot\overline{\boldsymbol{n}} = \mathbf{0}$ (19)

The first two conditions can be achieved via a proper definition of interface constitutive laws. The last condition, however, is achieved by constraining the interface to the midlayer. Such a restriction limits the applicability of the general interface model since it is only suitable to capture uniform isotropic interphases. For example, for graded interphases, the effective position of the interface may not necessarily coincide with the midlayer.

Remark on how the canonical interface models satisfy the rotational equilibrium (19). In view of the rotational equilibrium conditions (19), it can be readily shown that the canonical interface models fulfill these conditions differently, as follows.

- *Perfect interface model:* Both the displacement jump and traction jump at the interface are zero. That is, $[[\boldsymbol{x}]] = \mathbf{0}$ and $[[\boldsymbol{\sigma}]]\cdot\overline{\boldsymbol{n}} = \mathbf{0}$ and therefore the first and third conditions are trivially fulfilled. Also, the perfect interface model does not possess elasticity along with the interface and thus, $\overline{\boldsymbol{\sigma}} = \mathbf{0}$ satisfying the second condition.

[2]Usually, cutout volumes and their boundaries are denoted by different letters, to avoid confusion. Nonetheless, we use the same letter for a domain and a cutout thereof to avoid clutter.

- *Cohesive interface model:* The interface stress and traction jump are zero but the displacement jump is not necessarily vanishing. That is, $\overline{\boldsymbol{\sigma}} = \mathbf{0}$ and $[[\boldsymbol{\sigma}]] \cdot \overline{\boldsymbol{n}} = \mathbf{0}$ and, therefore, the second and third conditions are fulfilled. Since $[[\boldsymbol{x}]] \neq \mathbf{0}$, to satisfy the first condition, the displacement jump must be co-axial to the interface traction. This requirement can be imposed via the interface traction-separation law.
- *Elastic interface model:* The displacement is continuous across the interface and therefore $[[\boldsymbol{x}]] = \mathbf{0}$ that immediately satisfies the first condition. Consequently, $\{\{\boldsymbol{x}\}\} = \overline{\boldsymbol{x}}$ and therefore, the third condition is a priori fulfilled. The rotational equilibrium reduces to the second condition which must be imposed via a consistent constitutive law for the interface elasticity.
- *General interface model:* Both the displacement jump and traction jump at the interface are admissible. To satisfy the first condition, the displacement jump must be co-axial to the interface traction that is enforced via the interface traction-separation law. The second condition is fulfilled via introducing an interface constitutive law that renders symmetric interface stresses $\overline{\boldsymbol{\sigma}}$. The third condition is fulfilled via constraining the interface to coincide with the midlayer by imposing $\{\{\boldsymbol{x}\}\} = \overline{\boldsymbol{x}}$.

Here, we propose an extended general interface model where the interface is no longer enforced to coincide with the midlayer. In doing so, we incorporate the weighted average and the complimentary weighted average operators introduced in Eq. (3) into the identity (16) resulting in

$$[[\{\bullet\} \times \{\circ\}]] = \{\{\{\bullet\}\}\}_{\overline{\alpha}} \times [[\{\circ\}]] + [[\{\bullet\}]] \times \{\{\{\circ\}\}\}_{[1-\overline{\alpha}]} \tag{20}$$

Accordingly, Eq. (17) reads

$$[[\boldsymbol{x} \times \boldsymbol{\sigma}]] \cdot \overline{\boldsymbol{n}} = \{\{\boldsymbol{x}\}\}_{\overline{\alpha}} \times [[\boldsymbol{\sigma}]] \cdot \overline{\boldsymbol{n}} + [[\boldsymbol{x}]] \times \{\{\boldsymbol{\sigma}\}\}_{[1-\overline{\alpha}]} \cdot \overline{\boldsymbol{n}} \tag{21}$$

which yields

$$[[\boldsymbol{x}]] \times \{\{\boldsymbol{\sigma}\}\}_{[1-\overline{\alpha}]} \cdot \overline{\boldsymbol{n}} + \mathbb{e} : \overline{\boldsymbol{\sigma}} + \{\{\boldsymbol{x}\}\}_{\overline{\alpha}} \times [[\boldsymbol{\sigma}]] \cdot \overline{\boldsymbol{n}} - \overline{\boldsymbol{x}} \times [[\boldsymbol{\sigma}]] \cdot \overline{\boldsymbol{n}} = \mathbf{0} \tag{22}$$

Motivated by the structure of Eq. (22), we define the interface position $\overline{\boldsymbol{x}} := \{\{\boldsymbol{x}\}\}_{\overline{\alpha}}$ and the interface traction $\overline{\boldsymbol{t}} = \{\{\boldsymbol{\sigma}\}\}_{[1-\overline{\alpha}]} \cdot \overline{\boldsymbol{n}}$ as

$$\begin{aligned} \overline{\boldsymbol{x}} &:= \{\{\boldsymbol{x}\}\}_{\overline{\alpha}} = \overline{\alpha}\boldsymbol{x}^{+} + [1-\overline{\alpha}]\boldsymbol{x}^{-} \\ \overline{\boldsymbol{t}} &= \{\{\boldsymbol{\sigma}\}\}_{[1-\overline{\alpha}]} \cdot \overline{\boldsymbol{n}} = [1-\overline{\alpha}]\boldsymbol{\sigma}^{+} \cdot \overline{\boldsymbol{n}} + \overline{\alpha}\,\boldsymbol{\sigma}^{-} \cdot \overline{\boldsymbol{n}} \end{aligned} \tag{23}$$

Note that while the interface kinematics is enforced by the weighted average operator, it is the complementary weighted average operator that defines the interface kinetics. For example, when the interface coincides with its minus side, $\overline{\alpha} = 0$, the interface displacement solely depends on the displacement of the minus side whereas the interface traction consists of only the contribution from the plus side. On the other hand, when the interface coincides with its plus side, $\overline{\alpha} = 1$, the interface displacement solely depends on the displacement of the plus side whereas the interface traction consists of only the contribution from the minus side. Based on the definition $(23)_1$, the third and fourth terms in Eq. (22) cancel each other and the interface momentum balance reads

$$[[\boldsymbol{x}]] \times \overline{\boldsymbol{t}} + \mathbb{e} : \overline{\boldsymbol{\sigma}} = \mathbf{0} \tag{24}$$

which is sufficiently fulfilled if

$$\begin{aligned} &\bullet \quad [[\boldsymbol{x}]] \;||\; \overline{\boldsymbol{t}} \;\Rightarrow\; [[\boldsymbol{x}]] \times \overline{\boldsymbol{t}} = \mathbf{0} \\ &\bullet \quad \overline{\boldsymbol{\sigma}}^{T} = \overline{\boldsymbol{\sigma}} \;\Rightarrow\; \mathbb{e} : \overline{\boldsymbol{\sigma}} = \mathbf{0} \end{aligned} \tag{25}$$

The new form of interface rotational equilibrium (24) is fulfilled via a suitable choice of the interface material behavior without constraining the interface position. Table 4 gathers the fundamental equations governing the bulk and the extended general interface model.

Remark on interface curvature and Young–Laplace equation. The governing Eq. (13) is local and does not explicitly take advantage of the geometry of the problem. That is, the interface may or may not be curved, or a self-closed geometry for that matter. Equation (13) guarantees the tangential equilibrium at the interface. For example, if the interface is flat and if $\overline{\boldsymbol{\sigma}}$ is constant, then the equilibrium on the interface reduces to $[[\boldsymbol{\sigma}]] \cdot \overline{\boldsymbol{n}} = \mathbf{0}$, indicating that the traction jump across the interface is zero, as expected. On the other hand, in the case of a uniform surface-tension-like interface stress $\overline{\boldsymbol{\sigma}} = \overline{\gamma}\overline{\boldsymbol{I}}$, with $\overline{\gamma}$ being the surface tension, any traction jump across the interface involves the curvature of the interface according to

$$\begin{aligned} &\overline{\mathrm{Div}}\,\overline{\boldsymbol{\sigma}} + [[\boldsymbol{\sigma}]] \cdot \overline{\boldsymbol{n}} = \mathbf{0} \quad \text{with} \quad \overline{\boldsymbol{\sigma}} = \overline{\gamma}\overline{\boldsymbol{I}} \\ &\Rightarrow \overline{\mathrm{Div}}(\overline{\gamma}\overline{\boldsymbol{I}}) + [[\boldsymbol{\sigma}]] \cdot \overline{\boldsymbol{n}} = \mathbf{0} \quad \Rightarrow \quad \overline{C}\,\overline{\boldsymbol{n}} = -[[\boldsymbol{\sigma}]] \cdot \overline{\boldsymbol{n}} \end{aligned} \tag{26}$$

that is indeed the generalized Young–Laplace equation. In the case of inviscid fluids, the bulk stress reads $\boldsymbol{\sigma} = p\boldsymbol{I}$ and Eq. (26) reduces to its classical format $\overline{C} = [[p]]$ with $\overline{C}$ being twice the mean curvature, or simply the curvature, and $[[p]]$ being the pressure jump across the interface. Note that the interface curvature $\overline{C}$ is captured via the interface divergence operator and $\overline{\mathrm{Div}}(\overline{\boldsymbol{I}}) = \overline{C}\,\overline{\boldsymbol{n}}$. It shall be emphasized that the interface model here, similar to all other canonical interface models to date, is a zero-thickness model and therefore, the interface does not possess a "flexural resistance" against bending. More precisely, the in-plane elastic response of the interface follows the Gurtin–Murdoch interface elasticity theory [519] and mimics a membrane behavior rather than a shell theory. In principle, it is possible to introduce flexural stiffness to the interface model similar to the Steigmann–Ogden extension [589] of the Gurtin–Murdoch theory.

2.3 Strain Energy Density-Based Elastic Modeling. In the context of elasticity, the constitutive material behavior of a body embedding an extended general interface can be obtained in a variationally consistent manner based on the existence of a free energy density. The free energy density of the medium is composed of the bulk free energy density ψ and the interface free energy density $\overline{\psi}$. The bulk free energy density is only a function of the strain field in the bulk as $\psi = \psi(\boldsymbol{\varepsilon})$. The interface free energy density, however, is a function of both interface strain and interface displacement jump as $\overline{\psi} = \overline{\psi}(\overline{\boldsymbol{\varepsilon}}, [[\boldsymbol{u}]])$. More complicated choices for energy densities can be obtained via introducing implicit constitutive theories [710], however, they are not considered here to avoid digression. That bulk and interface free energy densities read

$$\begin{aligned} \psi &= \frac{1}{2}\,\boldsymbol{\varepsilon} : \mathbb{C} : \boldsymbol{\varepsilon} && \text{in } \mathcal{B} \\ \overline{\psi} &= \frac{1}{2}\left[\overline{\boldsymbol{\varepsilon}} : \overline{\mathbb{C}}_{\parallel} : \overline{\boldsymbol{\varepsilon}} + [[\boldsymbol{u}]] \cdot \overline{\boldsymbol{C}}_{\perp} \cdot [[\boldsymbol{u}]]\right] && \text{on } I \end{aligned} \tag{27}$$

with $\mathbb{C}$ being the fourth-order constitutive tensor in the bulk. The fourth-order constitutive tensor of the interface is $\overline{\mathbb{C}}_{\parallel}$, and $\overline{\boldsymbol{C}}_{\perp}$ is a

Table 4 Summary of fundamental governing equations for the bulk and the extended general interface model

Linear momentum balance	$\mathrm{Div}\boldsymbol{\sigma} = \mathbf{0}$	in $\mathcal{B}$	$\overline{\mathrm{Div}}\,\overline{\boldsymbol{\sigma}} + [[\boldsymbol{\sigma}]] \cdot \overline{\boldsymbol{n}} = \mathbf{0}$	on I
Angular momentum balance	$\mathbb{e} : \boldsymbol{\sigma} = \mathbf{0}$	in $\mathcal{B}$	$[[\boldsymbol{x}]] \times \overline{\boldsymbol{t}} + \mathbb{e} : \overline{\boldsymbol{\sigma}} = \mathbf{0}$	on I
Traction	$\boldsymbol{t} = \boldsymbol{\sigma} \cdot \boldsymbol{n}$	on $\partial\mathcal{B}$	$\overline{\boldsymbol{t}} = \{\{\boldsymbol{\sigma}\}\}_{[1-\overline{\alpha}]} \cdot \overline{\boldsymbol{n}}$	on I

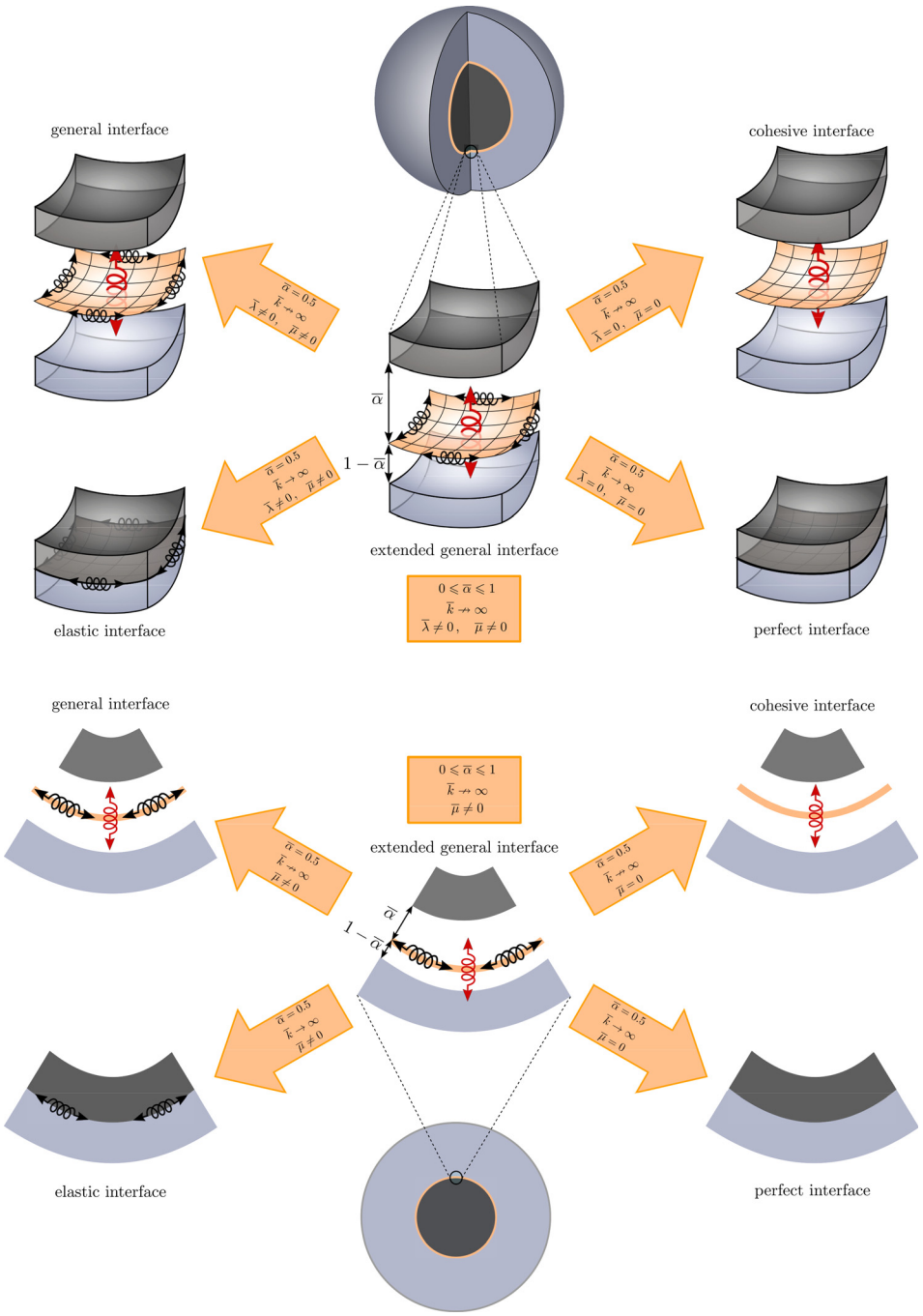

Fig. 6 Illustration of recovering all the previously introduced interface models by the current proposed interface model. The classical general interface model can be recovered by setting $\overline{\alpha} = 0.5$. The cohesive interface model is recovered when $\overline{\lambda} = \overline{\mu} = 0$ and $\overline{\alpha} = 0.5$. The conditions $\overline{\lambda} \neq 0$, $\overline{\mu} \neq 0$ and $\overline{k} \to \infty$ and $\overline{\alpha} = 0.5$ recover the elastic interface model. Finally, the perfect interface model is recovered when $\overline{\lambda} = \overline{\mu} = 0$ and $\overline{k} \to \infty$ and $\overline{\alpha} = 0.5$.

second-order tensor characterizing the interface cohesive behavior.[3] The resulting linear stresses and traction relate to the energy densities (27) via the constitutive laws

$$\boldsymbol{\sigma} = \frac{\partial \psi}{\partial \boldsymbol{\varepsilon}} = \mathbb{C} : \boldsymbol{\varepsilon} \qquad \text{in } \mathcal{B}$$

$$\overline{\boldsymbol{\sigma}} = \frac{\partial \overline{\psi}}{\partial \overline{\boldsymbol{\varepsilon}}} = \overline{\mathbb{C}}_{\parallel} : \overline{\boldsymbol{\varepsilon}} \qquad \text{along } I \tag{28}$$

$$\overline{\boldsymbol{t}} = \frac{\partial \overline{\psi}}{\partial [[\boldsymbol{u}]]} = \overline{\boldsymbol{C}}_{\perp} \cdot [[\boldsymbol{u}]] \quad \text{across } I$$

[3]The tangential interface stress $\overline{\boldsymbol{\sigma}}$ accounts only for the elastic interface response assuming a stress-free interface in the absence of strains. In other words, for the sake of brevity, we preclude surface tension from the discussion here. Accounting for a stress-tension-like behavior is fairly straightforward and can be achieved by adding a term $\overline{\gamma}\overline{\boldsymbol{I}}$ to $\overline{\boldsymbol{\sigma}}$, where $\overline{\gamma}$ is the isotropic surface tension.

The bulk material response is assumed to be standard and (linear) isotropic elastic taking the form

$$\mathbb{C} = \mu\left[\boldsymbol{I}\overline{\otimes}\boldsymbol{I} + \boldsymbol{I}\underline{\otimes}\boldsymbol{I}\right] + \lambda\boldsymbol{I}\otimes\boldsymbol{I} \quad \Rightarrow \quad \boldsymbol{\sigma} = 2\mu\boldsymbol{\varepsilon} + \lambda\left[\boldsymbol{\varepsilon} : \boldsymbol{I}\right]\boldsymbol{I},$$
$$[\mu] = [\lambda] = [\boldsymbol{\sigma}] = \frac{\mathrm{N}}{\mathrm{m}^2} \tag{29}$$

with λ and μ being the bulk Lamé parameters. For the interface, the material response reads

$$\overline{\mathbb{C}}_{\parallel} = \overline{\mu}\left[\overline{\boldsymbol{I}}\,\overline{\otimes}\,\overline{\boldsymbol{I}} + \overline{\boldsymbol{I}}\,\underline{\otimes}\,\overline{\boldsymbol{I}}\right] + \overline{\lambda}\,\overline{\boldsymbol{I}}\otimes\overline{\boldsymbol{I}} \quad \Rightarrow \quad \overline{\boldsymbol{\sigma}} = 2\overline{\mu}\,\overline{\boldsymbol{\varepsilon}} + \overline{\lambda}\left[\overline{\boldsymbol{\varepsilon}} : \overline{\boldsymbol{I}}\right]\overline{\boldsymbol{I}},$$
$$[\overline{\mu}] = [\overline{\lambda}] = [\overline{\boldsymbol{\sigma}}] = \frac{\mathrm{N}}{\mathrm{m}}$$
$$\overline{\boldsymbol{C}}_{\perp} = \overline{k}\,\boldsymbol{I} \quad \Rightarrow \quad \overline{\boldsymbol{t}} = \overline{k}\,[[\boldsymbol{u}]], \quad [\overline{k}] = \frac{[\overline{\boldsymbol{t}}]}{\mathrm{m}} = \frac{\mathrm{N}}{\mathrm{m}^3} \tag{30}$$

Corresponding to its tangential and normal directions, respectively. The parameters $\overline{\lambda}$ and $\overline{\mu}$ are the interface Lamé-like parameters representing the interface tangential elasticity relating to the resistance against the stretches along with the interface. The interface normal resistance is denoted $\overline{k}$ representing the stiffness against its opening. It shall be emphasized that depending on the choice of the interface parameters, the extended general interface model can recover any of the classical interface models, schematically illustrated in Fig. 6. The general interface model can be recovered by setting $\overline{\alpha} = 0.5$. The cohesive interface model is recovered when $\overline{\lambda} = \overline{\mu} = 0$ and $\overline{\alpha} = 0.5$. The conditions $\overline{\lambda} \neq 0$, $\overline{\mu} \neq 0$ and $\overline{k} \to \infty$ and $\overline{\alpha} = 0.5$ recover the elastic interface model. Finally, the perfect interface model is recovered when $\overline{\lambda} = \overline{\mu} = 0$ and $\overline{k} \to \infty$ and $\overline{\alpha} = 0.5$. It can be shown that in a two-dimensional setting, associated with fiber-reinforced composites, the resistance along the interface can be sufficiently captured with only one interface Lamé parameter hence the assumption $\overline{\lambda} = 0$ in two-dimensional. Similar to the bulk material, the form of the energy of the interface as well as its parameters can be obtained from fundamental reasoning or atomistic modeling as it has been established for the surface elasticity theory [365,532–534,695]. For instance, Yvonnet et al. [711] extracted the surface elastic parameters from ab initio calculations. Moreover, interface energy can be constructed using the surface/interface Cauchy–Born hypothesis [712,713]. In general, mechanical constants can be obtained using inverse parameter identification.

2.4 Micro- to Macrotransition. The final step to complete our homogenization framework is to elaborate on the micro- to macrotransition. Following classical homogenization, macroscopic quantities are related to their microscopic counterparts through volume averaging over the RVE. Accordingly, it is possible to define the macroscopic strain and stress fields ${}^{\mathrm{M}}\boldsymbol{\varepsilon}$ and ${}^{\mathrm{M}}\boldsymbol{\sigma}$, respectively, as surface integrals of microscopic quantities over the RVE's boundary as

$${}^{\mathrm{M}}\boldsymbol{\varepsilon} = \frac{1}{\mathscr{V}}\int_S \frac{1}{2}\left[\boldsymbol{u}\otimes\boldsymbol{n} + \boldsymbol{n}\otimes\boldsymbol{u}\right]\mathrm{d}A\,,$$
$${}^{\mathrm{M}}\boldsymbol{\sigma} = \frac{1}{\mathscr{V}}\int_S \boldsymbol{t}\otimes\boldsymbol{x}\,\mathrm{d}A \tag{31}$$

Using the extended divergence theorem [632], both relations can be written as a summation of integrals in the bulk and on the interface. That is

$${}^{\mathrm{M}}\boldsymbol{\varepsilon} = \frac{1}{\mathscr{V}}\int_{\mathcal{B}} \boldsymbol{\varepsilon}\,\mathrm{d}V + \frac{1}{\mathscr{V}}\int_I \frac{1}{2}\left[[[\boldsymbol{u}]]\otimes\overline{\boldsymbol{n}} + \overline{\boldsymbol{n}}\otimes[[\boldsymbol{u}]]\right]\mathrm{d}A$$
$${}^{\mathrm{M}}\boldsymbol{\sigma} = \frac{1}{\mathscr{V}}\int_{\mathcal{B}} \boldsymbol{\sigma}\,\mathrm{d}V + \frac{1}{\mathscr{V}}\int_I \overline{\boldsymbol{\sigma}}\,\mathrm{d}A \tag{32}$$

The incremental energy at the macroscale reads

$$\delta^{\mathrm{M}}\psi = {}^{\mathrm{M}}\boldsymbol{\sigma} : \delta^{\mathrm{M}}\boldsymbol{\varepsilon} \tag{33}$$

At the microscale, the incremental energy densities read

$$\begin{aligned} \delta\psi &= \boldsymbol{\sigma} : \delta\boldsymbol{\varepsilon} && \text{in } \mathcal{B} \\ \delta\overline{\psi} &= \overline{\boldsymbol{\sigma}} : \delta\overline{\boldsymbol{\varepsilon}} + \overline{\boldsymbol{t}}\cdot\delta[[\boldsymbol{u}]] && \text{on } I \end{aligned} \tag{34}$$

Central to homogenization is the Hill–Mandel condition which imposes an incremental energy equivalence between the scales. The Hill–Mandel condition extended to account for interfaces reads

$$\delta^{\mathrm{M}}\psi \overset{!}{=} \frac{1}{V\int_{\mathcal{B}}\delta\psi\,\mathrm{d}V + \frac{1}{\mathscr{V}}\int_I \delta\overline{\psi}\,\mathrm{d}A} \tag{35}$$

with $\overset{!}{=}$ indicating that equality is a condition. Inserting the incremental energies (34) and (33) at both scales into the Hill–Mandel condition (35) yields

$$\frac{1}{\mathscr{V}}\int_{\mathcal{B}} \boldsymbol{\sigma} : \delta\boldsymbol{\varepsilon}\,\mathrm{d}V + \frac{1}{\mathscr{V}}\int_I \left[\overline{\boldsymbol{\sigma}} : \delta\overline{\boldsymbol{\varepsilon}} + \overline{\boldsymbol{t}}\cdot\delta[[\boldsymbol{u}]]\right]\mathrm{d}A - {}^{\mathrm{M}}\boldsymbol{\sigma} : \delta^{\mathrm{M}}\boldsymbol{\varepsilon} \overset{!}{=} 0 \tag{36}$$

Finally, importing the macrostrain and macrostress relations from Eq. (32) into Eq. (36) furnishes the extended Hill–Mandel condition in terms of the boundary integral

$$\int_S \left[\delta\boldsymbol{u} - \delta^{\mathrm{M}}\boldsymbol{\varepsilon}\cdot\boldsymbol{x}\right]\cdot\left[\boldsymbol{t} - {}^{\mathrm{M}}\boldsymbol{\sigma}\cdot\boldsymbol{n}\right]\mathrm{d}A \overset{!}{=} 0 \tag{37}$$

Among all boundary conditions satisfying the condition (37), the linear DBC and constant TBC are of particular interest here. This choice of boundary conditions is suitable to make meaningful comparisons between the computational and analytical solutions. See Firooz et al. [95] for a comprehensive study on the boundary conditions and the RVE types within the framework of homogenization.

3 Fiber-Reinforced Composites

The objective of this section is to derive the bounds and estimates of the overall bulk and shear moduli of fiber-reinforced composites embedding extended general interfaces between the fibers and the matrix. In doing so, the CCA approach and the GSCM are extended to account for extended general interfaces where the interface position is not restricted to the midlayer. Firstly, the preliminaries of the RVE problem for fiber-reinforced composites are introduced. Afterward, CCA and GSCM are enhanced with interfaces. Our methodology is commonly accepted for transversely isotropic problems, see Ref. [57] among others. Throughout this section, the fiber and matrix quantities are distinguished by superscripts (1) and (2), respectively.

3.1 Preliminaries. Figure 7 depicts a fiber-reinforced composite with its underlying simplified RVE together with a cylindrical coordinate system appropriate to analyze such a medium. The RVE consists of a fiber located at the center of the matrix. The volume fraction of the fiber is $f = r_1^2/r_2^2$. Figure 8 illustrates a schematic definition of the size and how it is related to the volume fraction and the radii of the constituents. The term size here refers to the physical "size" of the RVE. Given a length scale ℓ and the volume fraction f, the radii of the fiber and the matrix can be calculated. Note, ℓ refers to the side length of a unit square. The unit circle is chosen such that it satisfies the area equivalence $\ell^2 = \pi r_2^2$ hence $\ell \propto r_2$. The constitutive material behavior for an isotropic material, in Voigt notation, reads

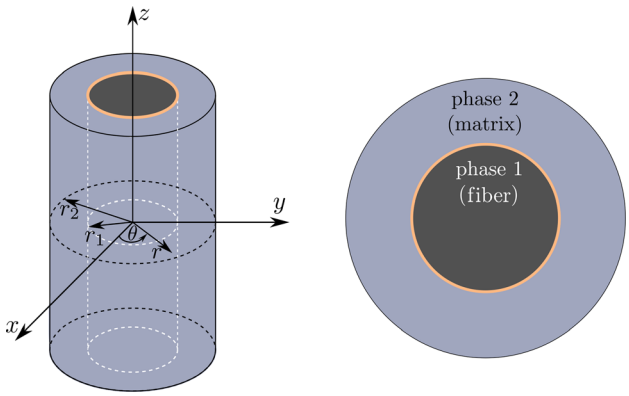

Fig. 7 Simplified RVE (right) and a cylindrical coordinate system (left) to examine such a medium

$$\begin{bmatrix}\sigma_{rr}\\ \sigma_{\theta\theta}\\ \sigma_{zz}\\ \sigma_{r\theta}\\ \sigma_{rz}\\ \sigma_{\theta z}\end{bmatrix} = \begin{bmatrix}\lambda+2\mu & \lambda & \lambda & 0 & 0 & 0\\ \lambda & \lambda+2\mu & \lambda & 0 & 0 & 0\\ \lambda & \lambda & \lambda+2\mu & 0 & 0 & 0\\ 0 & 0 & 0 & \mu & 0 & 0\\ 0 & 0 & 0 & 0 & \mu & 0\\ 0 & 0 & 0 & 0 & 0 & \mu\end{bmatrix}\begin{bmatrix}\varepsilon_{rr}\\ \varepsilon_{\theta\theta}\\ \varepsilon_{zz}\\ 2\varepsilon_{r\theta}\\ 2\varepsilon_{rz}\\ 2\varepsilon_{\theta z}\end{bmatrix} \tag{38}$$

Under the assumption that the transverse shear modulus is equal to the axial shear modulus. Note that in plane-strain linear elasticity, the bulk modulus κ relates to the Lamé parameters via $\kappa = \lambda + \mu$. In a cylindrical coordinate system, the strains in the bulk read

$$\begin{aligned}\varepsilon_{rr} &= \frac{\partial u_r}{\partial r}, \quad \varepsilon_{\theta\theta} = \frac{1}{r}\frac{\partial u_\theta}{\partial \theta} + \frac{u_r}{r}, \quad \varepsilon_{zz} = \frac{\partial u_z}{\partial z}\\ 2\varepsilon_{r\theta} &= \frac{\partial u_\theta}{\partial r} + \frac{1}{r}\frac{\partial u_r}{\partial \theta} - \frac{u_\theta}{r}\\ 2\varepsilon_{\theta z} &= \frac{1}{r}\frac{\partial u_z}{\partial \theta} + \frac{\partial u_\theta}{\partial z}\\ 2\varepsilon_{rz} &= \frac{\partial u_z}{\partial r} + \frac{\partial u_r}{\partial z}\end{aligned} \tag{39}$$

and the balance equations associated with the bulk (7) expand as

$$\begin{aligned}&\frac{\partial \sigma_{rr}}{\partial r} + \frac{1}{r}\frac{\partial \sigma_{r\theta}}{\partial \theta} + \frac{\partial \sigma_{rz}}{\partial z} + \frac{\sigma_{rr} - \sigma_{\theta\theta}}{r} = 0\\ &\frac{\partial \sigma_{r\theta}}{\partial r} + \frac{1}{r}\frac{\partial \sigma_{\theta\theta}}{\partial \theta} + \frac{\partial \sigma_{\theta z}}{\partial z} + \frac{2}{r}\sigma_{r\theta} = 0\\ &\frac{\partial \sigma_{rz}}{\partial r} + \frac{1}{r}\frac{\partial \sigma_{\theta z}}{\partial \theta} + \frac{\partial \sigma_{zz}}{\partial z} + \frac{1}{r}\sigma_{rz} = 0\end{aligned} \tag{40}$$

For the interface, the constitutive tangential behavior reads

$$\begin{bmatrix}\overline{\sigma}_{\theta\theta}\\ \overline{\sigma}_{zz}\\ \overline{\sigma}_{\theta z}\end{bmatrix} = \begin{bmatrix}\overline{\lambda}+2\overline{\mu} & \overline{\lambda} & 0\\ \overline{\lambda} & \overline{\lambda}+2\overline{\mu} & 0\\ 0 & 0 & \overline{\mu}\end{bmatrix}\begin{bmatrix}\overline{\varepsilon}_{\theta\theta}\\ \overline{\varepsilon}_{zz}\\ 2\overline{\varepsilon}_{\theta z}\end{bmatrix} \tag{41}$$

Under the assumption that the interface transverse shear modulus is equal to the interface axial shear modulus. For fiber-reinforced composites, the resistance along the interface can be sufficiently captured with only one interface Lamé parameter, thus we assume $\overline{\lambda} = 0$. According to Eq. (30), the interface cohesive response reads

$$\begin{bmatrix}\overline{t}_r\\ \overline{t}_\theta\\ \overline{t}_z\end{bmatrix} = \begin{bmatrix}\overline{k}\,[[u_r]]\\ \overline{k}\,[[u_\theta]]\\ \overline{k}\,[[u_z]]\end{bmatrix} \tag{42}$$

assuming isotropic cohesive behavior. The strains on the interface read

$$\begin{aligned}\overline{\varepsilon}_{\theta\theta} &= \frac{1}{r_1}\frac{\partial \overline{u}_\theta}{\partial \theta} + \frac{\overline{u}_r}{r_1}\\ \overline{\varepsilon}_{zz} &= \frac{\partial \overline{u}_z}{\partial z}\\ 2\overline{\varepsilon}_{\theta z} &= \frac{1}{r_1}\frac{\partial \overline{u}_z}{\partial \theta} + \frac{\partial \overline{u}_\theta}{\partial z}\end{aligned} \tag{43}$$

and the interface balance equations (13) can be written as

$$\begin{aligned}&\frac{\overline{\sigma}_{\theta\theta}}{r_1} - [[\sigma_{rr}]] = 0\\ &\frac{1}{r_1}\frac{\partial \overline{\sigma}_{\theta\theta}}{\partial \theta} + \frac{\partial \overline{\sigma}_{\theta z}}{\partial z} + [[\sigma_{r\theta}]] = 0\\ &\frac{1}{r_1}\frac{\partial \overline{\sigma}_{\theta z}}{\partial \theta} + \frac{\partial \overline{\sigma}_{zz}}{\partial z} + [[\sigma_{rz}]] = 0\end{aligned} \tag{44}$$

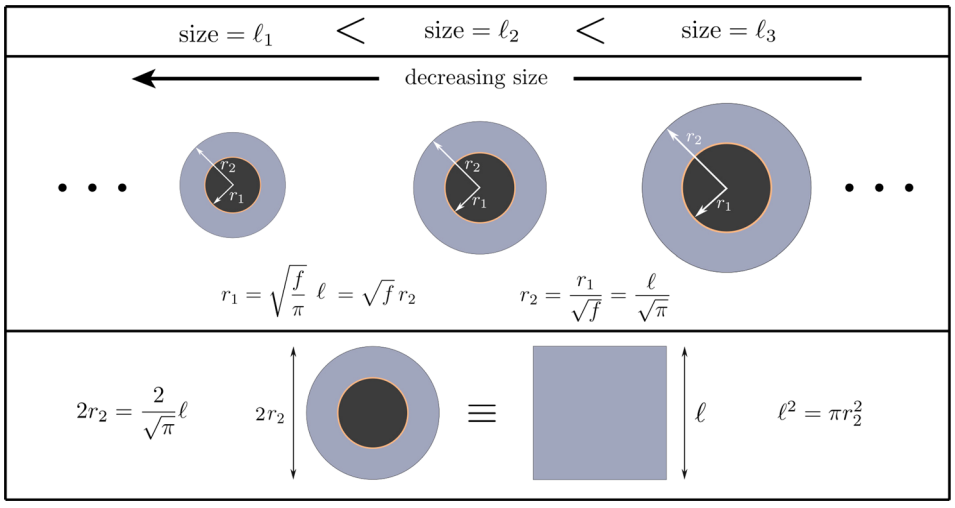

Fig. 8 Definition of the size for fiber-reinforced composites. Given the size ℓ and the volume fraction *f*, the radii of the fiber and the matrix can be calculated.

The three normal basis vectors in cylindrical coordinates are

$$\boldsymbol{n}_r = \begin{bmatrix} \cos\theta \\ \sin\theta \\ 0 \end{bmatrix}, \quad \boldsymbol{n}_\theta = \begin{bmatrix} -\sin\theta \\ \cos\theta \\ 0 \end{bmatrix}, \quad \boldsymbol{n}_z = \begin{bmatrix} 0 \\ 0 \\ 1 \end{bmatrix} \tag{45}$$

and the displacements and stresses can accordingly be expressed as

$$\begin{aligned} \boldsymbol{u} &= u_r\,\boldsymbol{n}_r + u_\theta\,\boldsymbol{n}_\theta + u_z\,\boldsymbol{n}_z \\ \boldsymbol{\sigma} &= \sigma_{rr}\,\boldsymbol{n}_r \otimes \boldsymbol{n}_r + \sigma_{\theta\theta}\,\boldsymbol{n}_\theta \otimes \boldsymbol{n}_\theta + \sigma_{zz}\,\boldsymbol{n}_z \otimes \boldsymbol{n}_z \\ &\quad + \sigma_{r\theta}[\boldsymbol{n}_r \otimes \boldsymbol{n}_\theta + \boldsymbol{n}_\theta \otimes \boldsymbol{n}_r] + \sigma_{rz}[\boldsymbol{n}_r \otimes \boldsymbol{n}_z + \boldsymbol{n}_z \otimes \boldsymbol{n}_r] \\ &\quad + \sigma_{\theta z}[\boldsymbol{n}_\theta \otimes \boldsymbol{n}_z + \boldsymbol{n}_z \otimes \boldsymbol{n}_\theta] \\ \overline{\boldsymbol{\sigma}} &= \overline{\sigma}_{\theta\theta}\,\boldsymbol{n}_\theta \otimes \boldsymbol{n}_\theta + \overline{\sigma}_{zz}\,\boldsymbol{n}_z \otimes \boldsymbol{n}_z + \overline{\sigma}_{\theta z}[\boldsymbol{n}_\theta \otimes \boldsymbol{n}_z + \boldsymbol{n}_z \otimes \boldsymbol{n}_\theta] \end{aligned} \tag{46}$$

The mechanical energy stored in the RVE reads

$$\begin{aligned} U^{(\mathrm{RVE})} &= \frac{1}{2}\int_{\mathcal{B}} \boldsymbol{\sigma} : \boldsymbol{\varepsilon}\,\mathrm{d}V + \frac{1}{2}\int_I \overline{\boldsymbol{\sigma}} : \overline{\boldsymbol{\varepsilon}}\,\mathrm{d}A + \frac{1}{2}\int_I \overline{\boldsymbol{t}} \cdot [[\boldsymbol{u}]]\,\mathrm{d}A \\ &= \frac{1}{2}\int_{\partial\mathcal{B}} [\boldsymbol{\sigma}\cdot\boldsymbol{n}] \cdot \boldsymbol{u}\,\mathrm{d}A = \frac{1}{2}\int_{\partial\mathcal{B}} \boldsymbol{t}\cdot\boldsymbol{u}\,\mathrm{d}A \end{aligned} \tag{47}$$

Under prescribed boundary conditions associated with expansion and in-plane shear, the average mechanical energy density stored in the RVE reads

$$U^{(\mathrm{RVE})} = \frac{1}{4\pi r_2^2 L}\int_{-L}^{L}\int_0^{2\pi} \left[\sigma_{rr}^{(2)}\,u_r^{(2)} + \sigma_{r\theta}^{(2)}\,u_\theta^{(2)}\right]_{r=r_2} r_2\,\mathrm{d}\theta\,\mathrm{d}z \tag{48}$$

where L is half of the height of the RVE in the z-direction shown in the middle of Fig. 7. Accordingly, the mechanical energy stored in an equivalent homogeneous medium reads

$$\begin{aligned} U^{(\mathrm{eq})} &= \frac{1}{2}\int_{\mathcal{B}} \boldsymbol{\sigma}^{(\mathrm{eq})} : \boldsymbol{\varepsilon}^{(\mathrm{eq})}\,\mathrm{d}V = \frac{1}{2}\int_{\partial\mathcal{B}} [\boldsymbol{\sigma}^{(\mathrm{eq})}\cdot\boldsymbol{n}] \cdot \boldsymbol{u}^{(\mathrm{eq})}\,\mathrm{d}A \\ &= \frac{1}{2}\int_{\partial\mathcal{B}} \boldsymbol{t}^{(\mathrm{eq})} \cdot \boldsymbol{u}^{(\mathrm{eq})}\,\mathrm{d}A \end{aligned} \tag{49}$$

Under prescribed boundary conditions associated with expansion and in-plane shear, the average mechanical energy density stored in the equivalent homogeneous medium reads

$$U^{(\mathrm{eq})} = \frac{1}{4\pi r_2^2 L}\int_{-L}^{L}\int_0^{2\pi} \left[\sigma_{rr}^{(\mathrm{eq})}\,u_r^{(\mathrm{eq})} + \sigma_{r\theta}^{(\mathrm{eq})}\,u_\theta^{(\mathrm{eq})}\right]_{r=r_2} r_2\,\mathrm{d}\theta\,\mathrm{d}z \tag{50}$$

Equating the energies (48) and (50) renders the overall macroscopic properties. Note that the generic form of the average mechanical energy density in principle includes other components of stress and displacement but they vanish for expansion and in-plane shear boundary conditions that are imposed here.

In CCA [26], the RVE resembles the right microstructure in Fig. 7. Applying expansion and simple shear under both displacement and traction boundary conditions renders bounds on the overall bulk and shear moduli. While the bounds on the shear modulus are distinct, they coincide with the bulk modulus and therefore, they are collectively referred to as the effective bulk modulus. To obtain an estimate for the effective shear modulus, Christensen and Lo [52] developed GSCM via introducing an infinite effective medium surrounding the matrix whose properties are the unknowns of the problem. Here, we extend CCA and GSCM to account for extended general interfaces with arbitrary interface positions and obtain bounds and estimates for the effective bulk and shear moduli of fiber composites.

3.2 Effective Bulk Modulus. To calculate the effective bulk modulus ${}^{\mathrm{M}}\kappa$, the RVE is subject to a uniform radial expansion characterized by

$$\boldsymbol{u}^0_{(r,\theta,z)} = \begin{bmatrix} \beta r \\ 0 \\ 0 \end{bmatrix} \tag{51}$$

where the superscript 0 denotes the prescribed deformation mode. As demonstrated by Hashin and Rosen [26], the developed displacement fields within each constituent read

$$\begin{aligned} u_r^{(1)} &= \beta r\left[X_1 + X_2\frac{1}{[r/r_1]^2}\right] \\ u_\theta^{(1)} &= u_z^{(1)} = 0 \\ u_r^{(2)} &= \beta r\left[X_3 + X_4\frac{1}{[r/r_1]^2}\right] \\ u_\theta^{(2)} &= u_z^{(2)} = 0 \end{aligned} \tag{52}$$

Resulting in the four unknowns X_1 to X_4 that can be determined via imposing the boundary and interface conditions

- finite displacement at $r = 0$

$$u_r^{(1)}(r=0) \to \infty \;\Rightarrow\; X_2 = 0 \tag{53}$$

- radial equilibrium at $r = r_1$

$$\begin{aligned} \overline{t}_r = \overline{k}\,[[u_r]] \;&\Rightarrow\; [1-\overline{\alpha}]\sigma_{rr}^{(2)}(r_1) + \overline{\alpha}\sigma_{rr}^{(1)}(r_1) \\ &= \overline{k}[u_r^{(2)}(r_1) - u_r^{(1)}(r_1)] \end{aligned} \tag{54}$$

- tangential equilibrium at $r = r_1$

$$[\overline{\mathrm{div}}\,\overline{\sigma}]_r + [[t_r]] = 0 \;\Rightarrow\; -\frac{\overline{\sigma}_{\theta\theta}}{r_1} + \sigma_{rr}^{(2)}(r_1) - \sigma_{rr}^{(1)}(r_1) = 0 \tag{55}$$

- prescribed displacement at $r = r_2$

$$u_r^{(2)}(r_2) = \beta r_2 \tag{56}$$

The conditions (53)–(56) lead to the system of equations

$$\begin{bmatrix} \dfrac{2\overline{\alpha}\kappa^{(1)} + \overline{k}r_1}{\overline{k}} & \dfrac{2[1-\overline{\alpha}]\kappa^{(2)} - \overline{k}r_1}{\overline{k}} & \dfrac{-2[1-\overline{\alpha}]\mu^{(2)} - \overline{k}r_1}{\overline{k}} \\ \dfrac{-2\kappa^{(1)}r_1 - 2[1-\overline{\alpha}]\overline{\mu}}{r_1} & \dfrac{2\kappa^{(2)}r_1 - 2\overline{\alpha}\overline{\mu}}{r_1} & \dfrac{-2\mu^{(2)}r_1 - 2\overline{\alpha}\overline{\mu}}{r_1} \\ 0 & 1 & f \end{bmatrix} \begin{bmatrix} X_1 \\ X_3 \\ X_4 \end{bmatrix} = \begin{bmatrix} 0 \\ 0 \\ 1 \end{bmatrix} \tag{57}$$

Applying the same displacement (51) to the equivalent homogeneous medium leads to the displacement field $u_r^{(\mathrm{eq})} = \beta r$ and $u_\theta^{(\mathrm{eq})} = u_z^{(\mathrm{eq})} = 0$. Using Eqs. (48) and (50), the overall energy densities in the RVE and the equivalent homogeneous medium read

$$\begin{aligned} U^{(\mathrm{RVE})} &= 2\beta^2[X_3\kappa^{(2)} - X_4 f\mu^{(2)}] \\ U^{(\mathrm{eq})} &= 2\beta^2\,{}^{\mathrm{M}}\kappa. \end{aligned} \tag{58}$$

Imposing $U^{(\mathrm{RVE})} = U^{(\mathrm{eq})}$ results in a closed-form explicit expression for the overall bulk modulus ${}^{\mathrm{M}}\kappa$ as

$$
{}^{M}\kappa = \frac{\left[\kappa^{(2)} + f\mu^{(2)}\right]\left[\overline{k}\,\overline{\mu} r_1 + 2\overline{\alpha}^2\kappa^{(1)}\overline{\mu} + \overline{k}\kappa^{(1)} r_1^2\right] + 2\kappa^{(2)}\mu^{(2)}[1-f]\left[\overline{\mu}(1-\overline{\alpha})^2 + \kappa^{(1)} r_1 + \overline{k} r_1^2/2\right]}{\left[\mu^{(2)} + f\kappa^{(2)}\right]\left[2\overline{\mu}(1-\overline{\alpha})^2 + 2\kappa^{(1)} r_1 + \overline{k} r_1^2\right] + [1-f]\left[\overline{k}\,\overline{\mu} r_1 + 2\overline{\alpha}^2\kappa^{(1)}\overline{\mu} + \overline{k}\kappa^{(1)} r_1^2\right]} \tag{59}
$$

with $\overline{\alpha}$ determining the interface position. Figure 9 shows the overall bulk modulus ${}^{M}\kappa$ versus $\overline{\alpha}$ for the extended general interface model against the classical interface models. Three different inclusion to matrix stiffness ratios is considered. The ratio incl./matr. $= 0.1$ represents an inclusion being 10 softer than the matrix whereas incl./matr. $= 10$ implies a 10 times stiffer inclusion than the matrix. Obviously, incl./matr. $= 1$ corresponds to identical inclusion and matrix properties. The position of the interface does not influence the effective material response for perfect, elastic, cohesive, and general interface models. For the extended general interface model, it is observed that for small $\overline{\alpha}$ the material renders a closer behavior to the cohesive interface model. Increasing $\overline{\alpha}$ yields a stiffer response where the solution due to the extended general interface model approaches that of the elastic interface model.

Remark on the choice of interface parameters. The material parameters are chosen to clearly illustrate the significance of interfaces on the effective material parameters and to demonstrate the analytical expressions. To avoid clutter, the units are omitted throughout but obviously, they must be consistent. For example, assuming that size is expressed in mm, the bulk material properties λ and μ will be in N/mm^2 while the interface parameters $\overline{\lambda}$ and $\overline{\mu}$ will be in N/mm. The interface orthogonal resistance $\overline{k}$ is then measured in N/mm^3. In other words, we treat the material parameters as numerical values to perform parametric studies without limiting our attention to any particular material.

3.3 Upper Bound on Shear Modulus. To obtain the upper bound on the overall in-plane shear modulus, the simple shear boundary condition

$$
\boldsymbol{u}^0_{(r,\theta,z)} = \begin{bmatrix} \beta r \sin(2\theta) \\ \beta r \cos(2\theta) \\ 0 \end{bmatrix} \tag{60}
$$

is applied to the RVE boundary at $r = r_2$. For this boundary condition, following Christensen and Lo [52], the displacement fields developed in the constituents read

$$
\begin{aligned}
u_r^{(1)} &= \beta r \sin(2\theta)\left[\frac{\kappa^{(1)} - \mu^{(1)}}{\left[2\kappa^{(1)} + \mu^{(1)}\right]}[r/r_1]^2 X_1 + X_2 - \frac{X_3}{[r/r_1]^4} + \frac{\kappa^{(1)} + \mu^{(1)}}{\mu^{(1)}}\frac{X_4}{[r/r_1]^2}\right] \\
u_\theta^{(1)} &= \beta r \cos(2\theta)\left[[r/r_1]^2 X_1 + X_2 + \frac{X_3}{[r/r_1]^4} + \frac{X_4}{[r/r_1]^2}\right] \\
u_z^{(1)} &= 0 \\
u_r^{(2)} &= \beta r \sin(2\theta)\left[\frac{\kappa^{(2)} - \mu^{(2)}}{\left[2\kappa^{(2)} + \mu^{(2)}\right]}[r/r_1]^2 X_5 + X_6 - \frac{X_7}{[r/r_1]^4} + \frac{\kappa^{(2)} + \mu^{(2)}}{\mu^{(2)}}\frac{X_8}{[r/r_1]^2}\right] \\
u_\theta^{(2)} &= \beta r \cos(2\theta)\left[[r/r_1]^2 X_5 + X_6 + \frac{X_7}{[r/r_1]^4} + \frac{X_8}{[r/r_1]^2}\right] \\
u_z^{(2)} &= 0
\end{aligned} \tag{61}
$$

with the eight unknowns X_1–X_8 which can be determined via applying the boundary and interface conditions

- finite displacement at $r = 0$

$$
u_r^{(1)}(r=0) \to \infty \quad \text{and} \quad u_\theta^{(1)}(r=0) \to \infty \Rightarrow X_3 = 0 \quad \text{and} \quad X_4 = 0 \tag{62}
$$

- radial equilibrium at $r = r_1$

$$
\bar{t}_r = \overline{k}\,[[u_r]] \Rightarrow [1-\overline{\alpha}]\sigma_{rr}^{(2)}(r_1) + \overline{\alpha}\sigma_{rr}^{(1)}(r_1) = \overline{k}[u_r^{(2)}(r_1) - u_r^{(1)}(r_1)] \tag{63}
$$

- circumferential equilibrium at $r = r_1$

$$
\bar{t}_\theta = \overline{k}\,[[u_\theta]] \Rightarrow [1-\overline{\alpha}]\sigma_{r\theta}^{(2)}(r_1) + \overline{\alpha}\sigma_{r\theta}^{(1)}(r_1) = \overline{k}[u_\theta^{(2)}(r_1) - u_\theta^{(1)}(r_1)] \tag{64}
$$

- tangential equilibrium in r direction at $r = r_1$

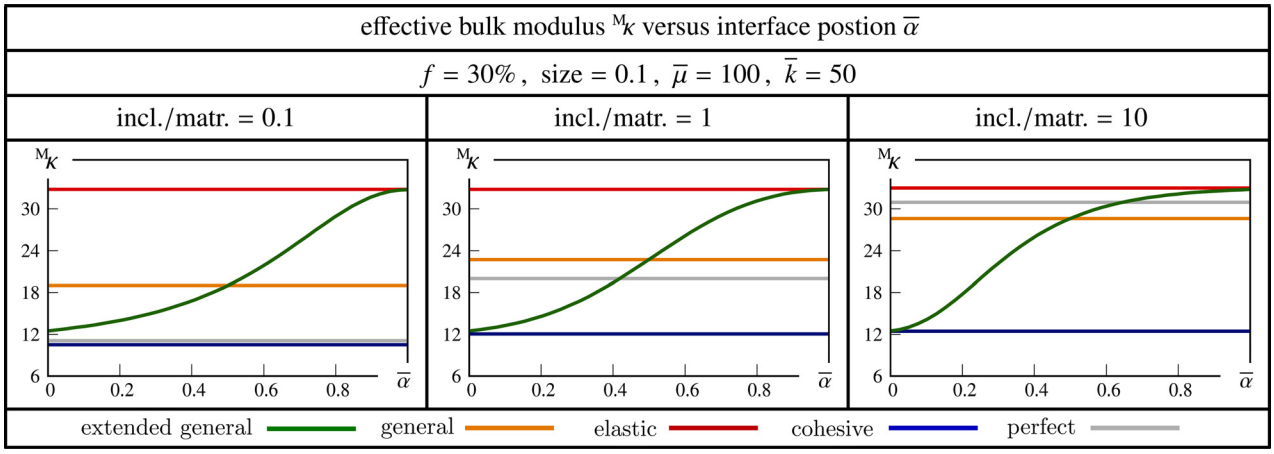

Fig. 9 Effective bulk modulus ${}^{M}\kappa$ versus interface position $\overline{\alpha}$ for fiber-reinforced composites. Different interface models are compared against each other.

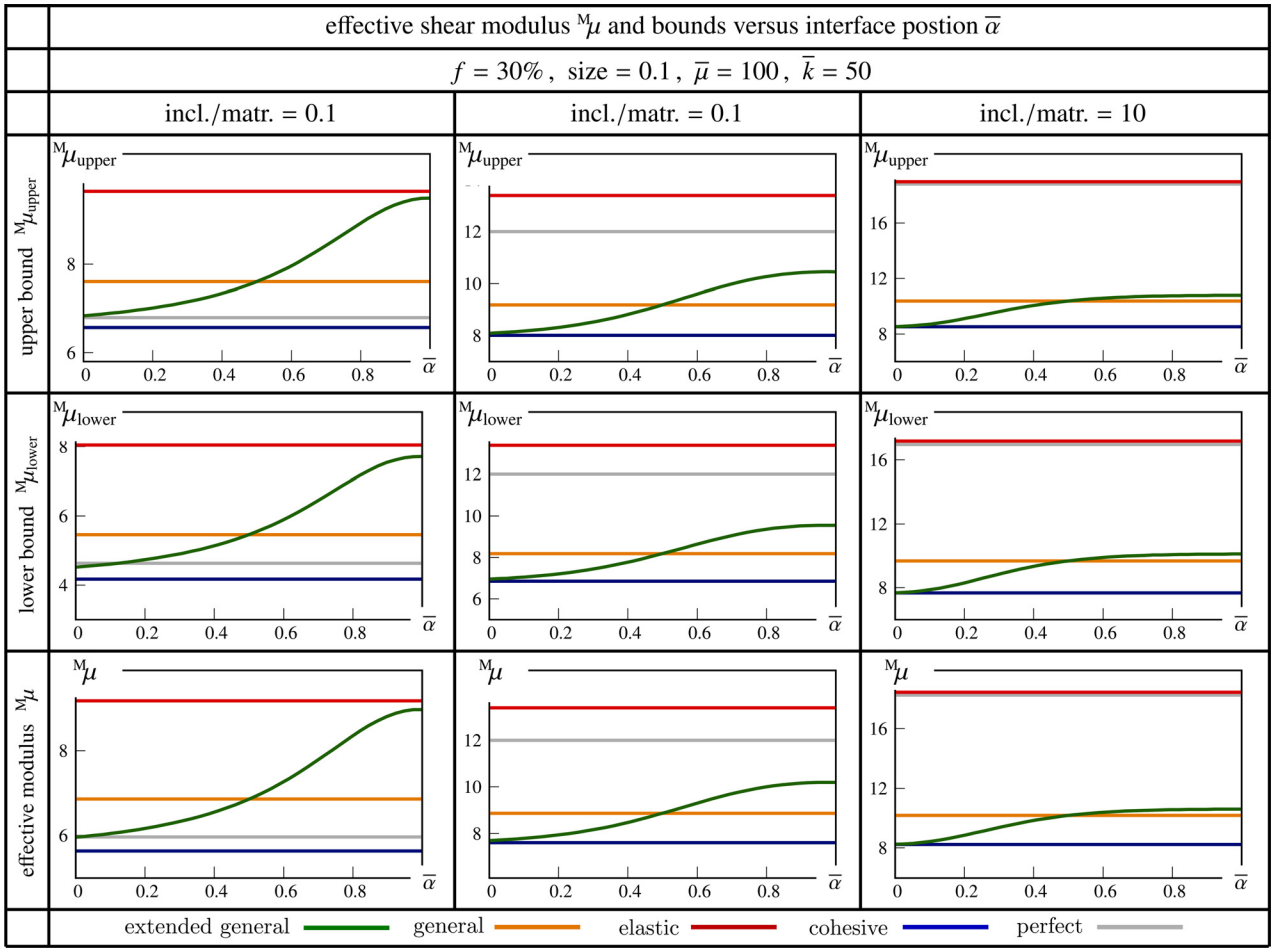

Fig. 10 Effective shear modulus $^{M}\mu$ and its bounds versus interface position $\bar{\alpha}$ for fiber-reinforced composites. Different interface models are compared against each other.

$$[\overline{\operatorname{div}}\,\overline{\sigma}]_r + [[t_r]] = 0 \Rightarrow -\frac{\overline{\sigma}_{\theta\theta}}{r_1} + \sigma_{rr}^{(2)}(r_1) - \sigma_{rr}^{(1)}(r_1) = 0 \tag{65}$$

- tangential equilibrium in θ direction at $r = r_1$

$$[\overline{\operatorname{div}}\,\overline{\sigma}]_\theta + [[t_\theta]] = 0 \Rightarrow \frac{1}{r_1}\frac{\partial \overline{\sigma}_{\theta\theta}}{\partial \theta} + \sigma_{r\theta}^{(2)}(r_1) - \sigma_{r\theta}^{(1)}(r_1) = 0 \tag{66}$$

- prescribed displacements at $r = r_2$

$$u_r^{(2)}(r_2) = \beta r_2 \sin(2\theta) \quad \text{and} \quad u_\theta^{(2)}(r_2) = \beta r_2 \cos(2\theta) \tag{67}$$

The conditions (62)–(67) lead to the system of equations

$$\begin{bmatrix} D_{11} & D_{12} & D_{13} & D_{14} & D_{15} & D_{16} \\ D_{21} & D_{22} & D_{23} & D_{24} & D_{25} & D_{26} \\ D_{31} & D_{32} & D_{33} & D_{34} & D_{35} & D_{36} \\ D_{41} & D_{42} & D_{43} & D_{44} & D_{45} & D_{46} \\ D_{51} & D_{52} & D_{53} & D_{54} & D_{55} & D_{56} \\ D_{61} & D_{62} & D_{63} & D_{64} & D_{65} & D_{66} \end{bmatrix} \begin{bmatrix} X_1 \\ X_2 \\ X_5 \\ X_6 \\ X_7 \\ X_8 \end{bmatrix} = \begin{bmatrix} 0 \\ 0 \\ 0 \\ 0 \\ 1 \\ 1 \end{bmatrix} \tag{68}$$

with the components of $\boldsymbol{D}$ detailed in Eq. (A1). For an equivalent homogeneous medium subject to the same boundary conditions, the displacement field reads

$$u_r^{(\mathrm{eq})} = \beta r \sin(2\theta), \quad u_\theta^{(\mathrm{eq})} = \beta r \cos(2\theta), \quad u_z^{(\mathrm{eq})} = 0 \tag{69}$$

Subsequently, using Eqs. (48) and (50), the average mechanical energy densities in the RVE and the equivalent homogeneous medium read

$$U^{(\mathrm{RVE})} = \frac{\beta^2}{2}\left[\frac{6\mu^{(2)}\kappa^{(2)}r_2^2}{2\kappa^{(2)}+\mu^{(2)}}X_5 + 4\mu^{(2)}X_6 - \frac{2\kappa^{(2)}}{r_2^2}X_8\right] \tag{70}$$

$$U^{(\mathrm{eq})} = 2\beta^2\, {}^{M}\mu$$

Imposing $U^{(\mathrm{RVE})} = U^{(\mathrm{eq})}$ renders the upper bound on the effective in-plane shear modulus

$$^{M}\mu_{\mathrm{upper}} = \frac{1}{4}\left[\frac{6\mu^{(2)}\kappa^{(2)}r_2^2}{2\kappa^{(2)}+\mu^{(2)}}X_5 + 4\mu^{(2)}X_6 - \frac{2\kappa^{(2)}}{r_2^2}X_8\right] \tag{71}$$

where X_5, X_6, and X_8 can be calculated via solving the system of Eqs. (68). Figure 10 illustrates the effective shear modulus and its bounds with respect to the interface position $\bar{\alpha}$ for various interface models. The top row corresponds to the upper bound on the shear modulus $^{M}\mu_{\mathrm{upper}}$. The middle row corresponds to the lower bound on the shear modulus $^{M}\mu_{\mathrm{lower}}$ which will be discussed in the next section. The last row corresponds to the effective shear modulus $^{M}\mu$ which will be discussed in Sec. 3.5. Similar to the bulk modulus, it is observed that for small $\bar{\alpha}$ the material associated with the extended general interface model renders a closer behavior to the cohesive interface model. However, increasing $\bar{\alpha}$ results in a stiffer response but not as stiff as the elastic interface.

3.4 Lower Bound on Shear Modulus. To obtain the lower bound on the overall in-plane shear modulus, a traction field is applied to the RVE boundary as

$$\boldsymbol{t}^0_{(r,\theta,z)} = \begin{bmatrix} \beta \sin 2\theta \\ \beta \cos 2\theta \\ 0 \end{bmatrix} \tag{72}$$

The displacement fields developed in the constituents due to the prescribed traction (72) mimic Eq. (61) with eight unknowns. The boundary and interface conditions are similar to Eqs. (62)–(66) and instead of condition (67), we have

- prescribed stresses at $r = r_2$

$$\sigma_{rr}^{(2)}(r_2) = \beta \sin(2\theta) \quad \text{and} \quad \sigma_{r\theta}^{(2)}(r_2) = \beta \cos(2\theta) \tag{73}$$

leading to the system of equations

$$\begin{bmatrix} E_{11} & E_{12} & E_{13} & E_{14} & E_{15} & E_{16} \\ E_{21} & E_{22} & E_{23} & E_{24} & E_{25} & E_{26} \\ E_{31} & E_{32} & E_{33} & E_{34} & E_{35} & E_{36} \\ E_{41} & E_{42} & E_{43} & E_{44} & E_{45} & E_{46} \\ E_{51} & E_{52} & E_{53} & E_{54} & E_{55} & E_{56} \\ E_{61} & E_{62} & E_{63} & E_{64} & E_{65} & E_{66} \end{bmatrix} \begin{bmatrix} X_1 \\ X_2 \\ X_5 \\ X_6 \\ X_7 \\ X_8 \end{bmatrix} = \begin{bmatrix} 0 \\ 0 \\ 0 \\ 0 \\ 1 \\ 1 \end{bmatrix} \tag{74}$$

The components of $\boldsymbol{E}$ are given in Eq. (A2). For an equivalent homogeneous medium subject to the same boundary condition, the displacement field reads

$$u_r^{(\mathrm{eq})} = \frac{\beta}{2^{\mathrm{M}}\mu} r \sin(2\theta), \quad u_\theta^{(\mathrm{eq})} = \frac{\beta}{2^{\mathrm{M}}\mu} r \cos(2\theta), \quad u_z^{(\mathrm{eq})} = 0 \tag{75}$$

Using Eqs. (48) and (50), the average mechanical energies stored in the RVE and the equivalent homogeneous medium are

$$\begin{aligned} U^{(\mathrm{RVE})} &= \frac{\beta^2}{2}\left[\frac{3\kappa^{(2)} r_2^2}{2\kappa^{(2)} + \mu^{(2)}} X_5 + 2X_6 + \frac{\kappa^{(2)} + 2\mu^{(2)}}{\mu^{(2)} r_2^2} X_8\right] \\ U^{(\mathrm{eq})} &= \frac{\beta^2}{2^{\mathrm{M}}\mu} \end{aligned} \tag{76}$$

Imposing $U^{(\mathrm{RVE})} = U^{(\mathrm{eq})}$ renders the lower bound on the macroscopic in-plane shear modulus

$$^{\mathrm{M}}\mu_{\mathrm{lower}} = \frac{1}{\dfrac{3\kappa^{(2)} r_2^2}{2\kappa^{(2)} + \mu^{(2)}} X_5 + 2X_6 + \dfrac{\kappa^{(2)} + 2\mu^{(2)}}{\mu^{(2)} r_2^2} X_8} \tag{77}$$

where X_5, X_6, and X_8 are the solution of the system (74). See Fig. 10 for the illustration of the lower bound on the shear modulus $^{\mathrm{M}}\mu_{\mathrm{lower}}$ versus the interface position $\bar{\alpha}$. Similar to the upper bound, it is observed that small $\bar{\alpha}$ associated with the extended general interface model renders a closer behavior to the cohesive interface. However, increasing $\bar{\alpha}$ results in a stiffer response but not as stiff as the elastic interface.

3.5 Effective Shear Modulus. To obtain the effective shear modulus $^{\mathrm{M}}\mu$, we employ GSCM developed by Christensen and Lo [52] where an infinite effective medium is bonded to the matrix and the properties of the effective medium are the unknowns of the problem. To obtain an estimate for the effective shear modulus, let the medium be subject to the displacement

$$\boldsymbol{u}^0_{(r,\theta,z)} = \begin{bmatrix} \beta r \sin(2\theta) \\ \beta r \cos(2\theta) \\ 0 \end{bmatrix} \tag{78}$$

The displacement (78) is applied on the boundary of the effective medium. The displacement fields generated in the fiber and the matrix due to the boundary condition (78) are similar to Eq. (61), hence the eight unknowns X_1 to X_8. In addition, the displacement field in the effective medium reads

$$\begin{aligned} u_r^{(\mathrm{eff})} &= \beta r \sin(2\theta)\left[1 - \frac{X_9}{r^4} + \frac{^{\mathrm{M}}\kappa + {}^{\mathrm{M}}\mu}{^{\mathrm{M}}\mu}\frac{X_{10}}{r^2}\right] \\ u_\theta^{(\mathrm{eff})} &= \beta r \cos(2\theta)\left[1 + \frac{X_9}{r^4} + \frac{X_{10}}{r^2}\right] \\ u_z^{(\mathrm{eff})} &= 0 \end{aligned} \tag{79}$$

with X_9 and X_{10} being the ninth and the tenth unknowns. Note, the displacement field in the effective medium indeed mimics the ones in Eq. (61), and the first and second unknowns are determined considering the conditions at $r \to \infty$. Before considering the boundary and the interface conditions, the additional energetic criterion

$$\int_0^{2\pi} [\sigma_{rr}^{(\mathrm{eff})} u_r^{(\mathrm{eq})} + \sigma_{r\theta}^{(\mathrm{eff})} u_\theta^{(\mathrm{eq})} - \sigma_{rr}^{(\mathrm{eq})} u_r^{(\mathrm{eff})} - \sigma_{r\theta}^{(\mathrm{eq})} u_\theta^{(\mathrm{eff})}]_{r=r_2} \mathrm{d}\theta = 0 \tag{80}$$

Deduced from the Eshelby's energy principle [52] must be imposed and yields $X_{10} = 0$. The remaining nine unknowns can be determined via imposing the boundary and interface conditions which are similar to Eqs. (62)–(66) and instead of condition (67), we have

- displacement continuity at $r = r_2$

$$u_r^{(2)}(r_2) = u_r^{(\mathrm{eff})}(r_2) \quad \text{and} \quad u_\theta^{(2)}(r_2) = u_\theta^{(\mathrm{eff})}(r_2) \tag{81}$$

leading to the system of equations

$$\begin{bmatrix} F_{11} & F_{12} & F_{13} & F_{14} & F_{15} & F_{16} \\ F_{21} & F_{22} & F_{23} & F_{24} & F_{25} & F_{26} \\ F_{31} & F_{32} & F_{33} & F_{34} & F_{35} & F_{36} \\ F_{41} & F_{42} & F_{43} & F_{44} & F_{45} & F_{46} \\ F_{51} & F_{52} & F_{53} & F_{54} & F_{55} & F_{56} \\ F_{61} & F_{62} & F_{63} & F_{64} & F_{65} & F_{66} \end{bmatrix} \begin{bmatrix} X_1 \\ X_2 \\ X_5 \\ X_6 \\ X_7 \\ X_8 \end{bmatrix} = \begin{bmatrix} 0 \\ 0 \\ 0 \\ 0 \\ 1 \\ 1 \end{bmatrix} + \begin{bmatrix} 0 \\ 0 \\ 0 \\ 0 \\ -f^2 \\ f^2 \end{bmatrix} X_9 \tag{82}$$

with $\boldsymbol{F} = \boldsymbol{D}$ thus, see Eq. (A1). The remaining six unknowns can be written as a function of X_9 as

$$\underbrace{\begin{bmatrix} X_1 \\ X_2 \\ X_5 \\ X_6 \\ X_7 \\ X_8 \end{bmatrix}}_{\boldsymbol{X}} = \underbrace{\boldsymbol{F}^{-1}\begin{bmatrix} 0 \\ 0 \\ 0 \\ 0 \\ 1 \\ 1 \end{bmatrix}}_{\boldsymbol{a}} + \underbrace{\boldsymbol{F}^{-1}\begin{bmatrix} 0 \\ 0 \\ 0 \\ 0 \\ -f^2 \\ f^2 \end{bmatrix}}_{\boldsymbol{b}} X_9 = \begin{bmatrix} a_1 \\ a_2 \\ a_5 \\ a_6 \\ a_7 \\ a_8 \end{bmatrix} + \begin{bmatrix} b_1 \\ b_2 \\ b_5 \\ b_6 \\ b_7 \\ b_8 \end{bmatrix} X_9 \tag{83}$$

Note, the components of the arrays $\boldsymbol{a}$ and $\boldsymbol{b}$ are numbered according to the indices in $\boldsymbol{X}$ to facilitate the understanding of the procedure. Imposing the stress continuity between the matrix and the effective medium yields

$$\begin{aligned} \sigma_{rr}^{(2)}(r_2) = \sigma_{rr}^{(\mathrm{eff})}(r_2) &\Rightarrow g_1 + h_1 X_9 = {}^{\mathrm{M}}\mu + 3f^2 X_9 {}^{\mathrm{M}}\mu \\ \sigma_{r\theta}^{(2)}(r_2) = \sigma_{r\theta}^{(\mathrm{eff})}(r_2) &\Rightarrow g_2 + h_2 X_9 = {}^{\mathrm{M}}\mu - 3f^2 X_9 {}^{\mathrm{M}}\mu \end{aligned} \tag{84}$$

Table 5 Explicit formulations for the bounds and estimates on the overall bulk and shear moduli of fiber-composites embedding general interfaces

General interface model	
$^{M}\kappa = \dfrac{[\kappa^{(2)}+f\mu^{(2)}][\overline{k}\overline{\mu}r_1+\frac{1}{2}\kappa^{(1)}\overline{\mu}+\overline{k}\kappa^{(1)}r_1^2]+2\kappa^{(2)}\mu^{(2)}[1-f][\frac{1}{4}\overline{\mu}+\kappa^{(1)}r_1+\overline{k}r_1^2/2]}{[\mu^{(2)}+f\kappa^{(2)}][\frac{1}{2}\overline{\mu}+2\kappa^{(1)}r_1+\overline{k}r_1^2]+[1-f][\overline{k}\overline{\mu}r_1+\frac{1}{2}\kappa^{(1)}\overline{\mu}+\overline{k}\kappa^{(1)}r_1^2]}$	
$^{M}\mu_{\text{upper}} = \dfrac{1}{4}\left[\dfrac{6\mu^{(2)}\kappa^{(2)}r_2^2}{2\kappa^{(2)}+\mu^{(2)}}X_5+4\mu^{(2)}X_6-\dfrac{2\kappa^{(2)}}{r_2^2}X_8\right]$	See Appendix (B1)
$^{M}\mu_{\text{lower}} = \dfrac{1}{\dfrac{3\kappa^{(2)}r_2^2}{2\kappa^{(2)}+\mu^{(2)}}X_5+2X_6+\dfrac{\kappa^{(2)}+2\mu^{(2)}}{\mu^{(2)}r_2^2}X_8}$	see Appendix (B2)
$6f^{2M}\mu^2+[h_2-h_1-3f^2[g_1+g_2]]^{M}\mu+[h_1g_2-h_2g_1]=0$	see Appendix (B1)

Table 6 Explicit formulations for the bounds and estimates on the overall bulk and shear moduli of fiber-composites embedding elastic interfaces

Elastic interface model	
$^{M}\kappa = \dfrac{[\kappa^{(2)}+f\mu^{(2)}][\overline{\mu}r_1+\kappa^{(1)}r_1^2]+\kappa^{(2)}\mu^{(2)}[1-f]r_1^2}{[\mu^{(2)}+f\kappa^{(2)}]r_1^2+[1-f][\overline{\mu}r_1+\kappa^{(1)}r_1^2]}$	
$^{M}\mu_{\text{upper}} = \dfrac{1}{4}\left[\dfrac{6\mu^{(2)}\kappa^{(2)}r_2^2}{2\kappa^{(2)}+\mu^{(2)}}X_5+4\mu^{(2)}X_6-\dfrac{2\kappa^{(2)}}{r_2^2}X_8\right]$	see Appendix (C1)
$^{M}\mu_{\text{lower}} = \dfrac{1}{\dfrac{3\kappa^{(2)}r_2^2}{2\kappa^{(2)}+\mu^{(2)}}X_5+2X_6+\dfrac{\kappa^{(2)}+2\mu^{(2)}}{\mu^{(2)}r_2^2}X_8}$	see Appendix (C2)
$6f^{2M}\mu^2+[h_2-h_1-3f^2[g_1+g_2]]^{M}\mu+[h_1g_2-h_2g_1]=0$	see Appendix (C1)

Table 7 Explicit formulations for the bounds and estimates on the overall bulk and shear moduli of fiber-composites embedding cohesive interfaces

Cohesive interface model	
$^{M}\kappa = \dfrac{[\kappa^{(2)}+f\mu^{(2)}][\overline{k}\kappa^{(1)}r_1^2]+2\kappa^{(2)}\mu^{(2)}[1-f][\kappa^{(1)}r_1+\overline{k}r_1^2/2]}{[\mu^{(2)}+f\kappa^{(2)}][2\kappa^{(1)}r_1+\overline{k}r_1^2]+[1-f][\overline{k}\kappa^{(1)}r_1^2]}$	
$^{M}\mu_{\text{upper}} = \dfrac{1}{4}\left[\dfrac{6\mu^{(2)}\kappa^{(2)}r_2^2}{2\kappa^{(2)}+\mu^{(2)}}X_5+4\mu^{(2)}X_6-\dfrac{2\kappa^{(2)}}{r_2^2}X_8\right]$	see Appendix (D1)
$^{M}\mu_{\text{lower}} = \dfrac{1}{\dfrac{3\kappa^{(2)}r_2^2}{2\kappa^{(2)}+\mu^{(2)}}X_5+2X_6+\dfrac{\kappa^{(2)}+2\mu^{(2)}}{\mu^{(2)}r_2^2}X_8}$	see Appendix (D2)
$6f^{2M}\mu^2+[h_2-h_1-3f^2[g_1+g_2]]^{M}\mu+[h_1g_2-h_2g_1]=0$	see Appendix (D1)

with

$$
\begin{aligned}
g_1 &= a_6\mu^{(2)}+3f^2\mu^{(2)}a_7-2f\kappa^{(2)}a_8\\
h_1 &= b_6\mu^{(2)}+3f^2\mu^{(2)}b_7-2f\kappa^{(2)}b_8\\
g_2 &= \frac{3\kappa^{(2)}\mu^{(2)}}{f\left[2\kappa^{(2)}+\mu^{(2)}\right]}a_5+\mu^{(2)}a_6-3f^2\mu^{(2)}a_7+f\kappa^{(2)}a_8\\
h_2 &= \frac{3\kappa^{(2)}\mu^{(2)}}{f\left[2\kappa^{(2)}+\mu^{(2)}\right]}b_5+\mu^{(2)}b_6-3f^2\mu^{(2)}b_7+f\kappa^{(2)}b_8
\end{aligned}
\tag{85}
$$

Adding up Eqs. $(84)_1$ and $(84)_2$ renders

$$
X_9 = \frac{2^{M}\mu-[g_1+g_2]}{h_1+h_2} \tag{86}
$$

and via replacing X_9 from Eq. (86) into Eq. $(84)_1$ we obtain

$$
6f^{2M}\mu^2+[h_2-h_1-3f^2[g_1+g_2]]^{M}\mu+[h_1g_2-h_2g_1]=0 \tag{87}
$$

From the two possible solutions of the quadratic Eq. (87), the positive value is the effective shear modulus $^{M}\mu$. See Fig. 10 for the illustration of the effective shear modulus $^{M}\mu$ versus the interface position $\overline{\alpha}$. Similar to the bounds, it is observed that small $\overline{\alpha}$ associated with the extended general interface model renders a closer behavior to the cohesive interface. However, increasing $\overline{\alpha}$ results in a stiffer response but not as stiff as the elastic interface.

3.6 Recovering General, Elastic, Cohesive, and Interface Models. This section briefly provides the previously obtained solutions for the bounds and estimates on the elastic moduli for the general, cohesive, elastic, and perfect interface models. As mentioned before, the general interface model can be recovered by setting $\overline{\alpha}=0.5$. The cohesive interface model is recovered when $\overline{\lambda}=\overline{\mu}=0$ and $\overline{\alpha}=0.5$. The elastic interface model is recovered when $\overline{\lambda}\neq 0$, $\overline{\mu}\neq 0$ and $\overline{k}\to\infty$ and $\overline{\alpha}=0.5$. Finally, the perfect interface model is recovered when $\overline{\lambda}=\overline{\mu}=0$ and $\overline{k}\to\infty$ and $\overline{\alpha}=0.5$. Tables 5–8 show the formulations for the effective bulk and shear moduli and the bounds on the shear modulus for fiber-

Table 8 Explicit formulations for the bounds and estimates on the overall bulk and shear moduli of fiber-composites embedding perfect interfaces

Perfect interface model	
${}^{\mathrm{M}}\kappa = \dfrac{[\kappa^{(2)}+f\mu^{(2)}]\kappa^{(1)}+\kappa^{(2)}\mu^{(2)}[1-f]}{[\mu^{(2)}+f\kappa^{(2)}]+[1-f]\kappa^{(1)}}$	
${}^{\mathrm{M}}\mu_{\mathrm{upper}} = \dfrac{1}{4}\left[\dfrac{6\mu^{(2)}\kappa^{(2)}r_2^2}{2\kappa^{(2)}+\mu^{(2)}}X_5+4\mu^{(2)}X_6-\dfrac{2\kappa^{(2)}}{r_2^2}X_8\right]$	see Appendix (E1)
${}^{\mathrm{M}}\mu_{\mathrm{lower}} = \dfrac{1}{\dfrac{3\kappa^{(2)}r_2^2}{2\kappa^{(2)}+\mu^{(2)}}X_5+2X_6+\dfrac{\kappa^{(2)}+2\mu^{(2)}}{\mu^{(2)}r_2^2}X_8}$	see Appendix (E2)
$6f^2{}^{\mathrm{M}}\mu^2+[h_2-h_1-3f^2[g_1+g_2]]{}^{\mathrm{M}}\mu+[h_1g_2-h_2g_1]=0$	see Appendix (E1)

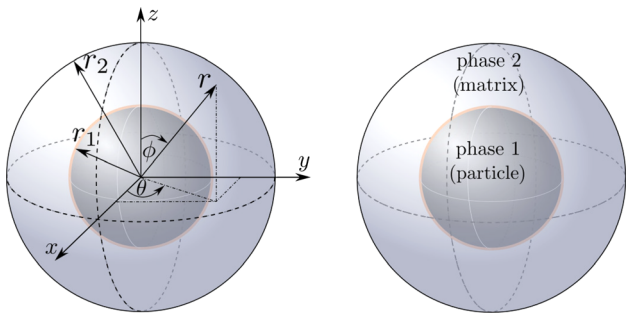

Fig. 11 Simplified RVE (right) and a spherical coordinate system (left) to examine such a medium

reinforced composites embedding the general, elastic, cohesive and perfect interfaces, respectively.

4 Particle-Reinforced Composites

This section aims to examine particle-reinforced composites accounting for extended general interfaces between the constituents where the interface is allowed to occupy any arbitrary position between the particle and the matrix. Bounds and estimates for the overall bulk and shear moduli of such composites are obtained via extending the CSA approach and the GSCM to account for the extended general interface model. First, the preliminaries of the RVE problem for these composites are introduced. Second, the interface enhanced CSA and GSCM approaches are elaborated resulting in bounds and estimates on the overall moduli of composites. Throughout this section, the particle-related properties are denoted by a superscript (1) whereas the matrix-related properties are denoted by a superscript (2). We intentionally develop this section in a manner that reflects the similarities between the particle-reinforced composites here and the fiber-reinforced composites elaborated in Sec. 3.

4.1 Preliminaries. Figure 11 shows a particle-reinforced composite with its underlying simplified RVE together with a spherical coordinate system suitable to analyze such a medium. The RVE consists of a particle located at the center of the matrix. The particle volume fraction is $f = r_1^3/r_2^3$. Figure 12 illustrates a schematic definition of the size and how it is related to the volume fraction and the radii of the constituents. Clearly, having the size ℓ and the volume fraction f, one can determine the radii of the particle and the matrix. Note, ℓ refers to the side length of an equivalent unit cube and is introduced for simplicity. The unit sphere is chosen such that it satisfies the volume equivalence $\ell^3 = 4/3\pi r_2^3$ hence $\ell \propto r_2$. The constitutive material behavior for the bulk, in Voigt notation, reads

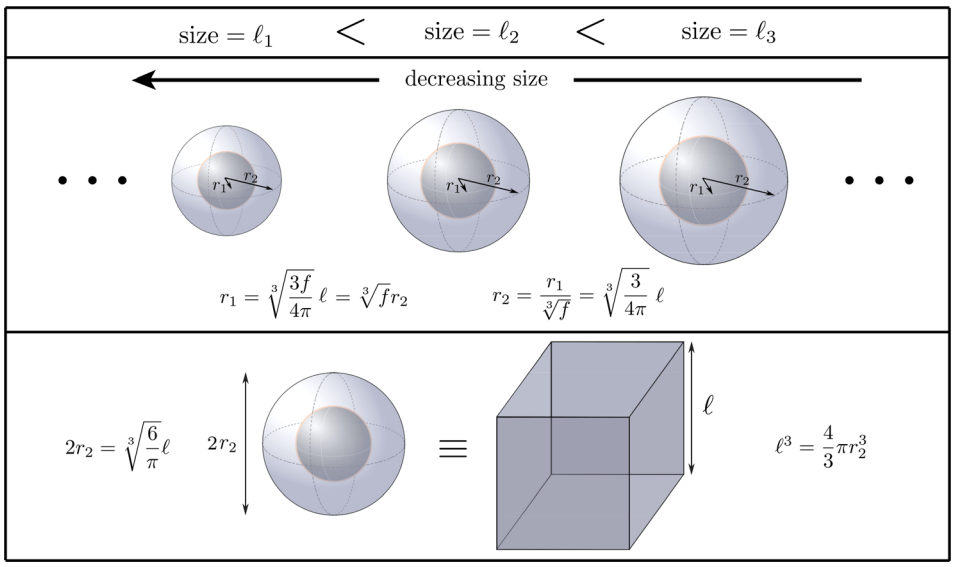

Fig. 12 Definition of the size for particle-reinforced composites. Given the size ℓ and the volume fraction *f*, the radii of the fiber and the matrix can be calculated.

$$\begin{bmatrix}\sigma_{rr}\\ \sigma_{\theta\theta}\\ \sigma_{\phi\phi}\\ \sigma_{r\theta}\\ \sigma_{r\phi}\\ \sigma_{\theta\phi}\end{bmatrix}=\begin{bmatrix}\lambda+2\mu & \lambda & \lambda & 0 & 0 & 0\\ \lambda & \lambda+2\mu & \lambda & 0 & 0 & 0\\ \lambda & \lambda & \lambda+2\mu & 0 & 0 & 0\\ 0 & 0 & 0 & \mu & 0 & 0\\ 0 & 0 & 0 & 0 & \mu & 0\\ 0 & 0 & 0 & 0 & 0 & \mu\end{bmatrix}\begin{bmatrix}\varepsilon_{rr}\\ \varepsilon_{\theta\theta}\\ \varepsilon_{\phi\phi}\\ 2\varepsilon_{r\theta}\\ 2\varepsilon_{r\phi}\\ 2\varepsilon_{\theta\phi}\end{bmatrix} \tag{88}$$

For this case, the bulk modulus κ relates to the Lamé parameters via $\kappa=\lambda+2\mu/3$. In a spherical coordinate system, the strain field in the bulk reads

$$\begin{aligned}\varepsilon_{rr}&=\frac{\partial u_r}{\partial r},\quad \varepsilon_{\theta\theta}=\frac{1}{r}\frac{\partial u_\theta}{\partial\theta}+\frac{u_r}{r}\\ \varepsilon_{\phi\phi}&=\frac{1}{r\sin\theta}\frac{\partial u_\phi}{\partial\phi}+\frac{u_r}{r}+\frac{u_\theta\cos\theta}{r\sin\theta}\\ 2\varepsilon_{r\phi}&=\frac{\partial u_\phi}{\partial r}+\frac{1}{r\sin\theta}\frac{\partial u_r}{\partial\phi}-\frac{u_\phi}{r}\\ 2\varepsilon_{\theta\phi}&=\frac{1}{r}\frac{\partial u_\phi}{\partial\theta}+\frac{1}{r\sin\theta}\frac{\partial u_\theta}{\partial\phi}-\frac{u_\phi\cos\theta}{r\sin\theta}\\ 2\varepsilon_{r\theta}&=\frac{\partial u_\theta}{\partial r}+\frac{1}{r}\frac{\partial u_r}{\partial\theta}-\frac{u_\theta}{r}\end{aligned} \tag{89}$$

and the balance equations for the bulk expand to

$$\begin{aligned}&\frac{\partial\sigma_{rr}}{\partial r}+\frac{1}{r}\frac{\partial\sigma_{r\theta}}{\partial\theta}+\frac{\sigma_{r\theta}\cos\theta}{r\sin\theta}+\frac{2\sigma_{rr}-\sigma_{\theta\theta}-\sigma_{\phi\phi}}{r}+\frac{1}{r\sin\theta}\frac{\partial\sigma_{r\phi}}{\partial\phi}=0\\ &\frac{\partial\sigma_{r\theta}}{\partial r}+\frac{1}{r}\frac{\partial\sigma_{\theta\theta}}{\partial\theta}+\frac{3\sigma_{r\theta}}{r}+\frac{[\sigma_{\theta\theta}-\sigma_{\phi\phi}]\cos\theta}{r\sin\theta}+\frac{1}{r\sin\theta}\frac{\partial\sigma_{\theta\phi}}{\partial\phi}=0\\ &\frac{\partial\sigma_{r\phi}}{\partial r}+\frac{1}{r}\frac{\partial\sigma_{\theta\phi}}{\partial\theta}+\frac{3\sigma_{r\phi}}{r}+\frac{2\sigma_{\theta\phi}\cos\theta}{r\sin\theta}+\frac{1}{r\sin\theta}\frac{\partial\sigma_{\phi\phi}}{\partial\phi}=0\end{aligned} \tag{90}$$

The interface tangential behavior follows from the constitutive relation:

$$\begin{bmatrix}\overline{\sigma}_{\theta\theta}\\ \overline{\sigma}_{\phi\phi}\\ \overline{\sigma}_{\theta\phi}\end{bmatrix}=\begin{bmatrix}\overline{\lambda}+2\overline{\mu} & \overline{\lambda} & 0\\ \overline{\lambda} & \overline{\lambda}+2\overline{\mu} & 0\\ 0 & 0 & \overline{\mu}\end{bmatrix}\begin{bmatrix}\overline{\varepsilon}_{\theta\theta}\\ \overline{\varepsilon}_{\phi\phi}\\ 2\overline{\varepsilon}_{\theta\phi}\end{bmatrix} \tag{91}$$

The interface cohesive behavior is characterized by

$$\begin{bmatrix}\overline{t}_r\\ \overline{t}_\theta\\ \overline{t}_\phi\end{bmatrix}=\begin{bmatrix}\overline{k}\,[[u_r]]\\ \overline{k}\,[[u_\theta]]\\ \overline{k}\,[[u_\phi]]\end{bmatrix} \tag{92}$$

Under the assumption of identical cohesive stiffness in all three directions. The (tangential) strain field on the interface reads

$$\begin{aligned}\overline{\varepsilon}_{\theta\theta}&=\frac{1}{r_1}\frac{\partial\overline{u}_\theta}{\partial\theta}+\frac{\overline{u}_r}{r_1}\\ \overline{\varepsilon}_{\phi\phi}&=\frac{1}{r_1\sin\theta}\frac{\partial\overline{u}_\phi}{\partial\phi}+\frac{\overline{u}_r}{r_1}+\frac{\overline{u}_\theta\cos\theta}{r_1\sin\theta}\\ 2\overline{\varepsilon}_{\theta\phi}&=\frac{1}{r_1}\frac{\partial\overline{u}_\phi}{\partial\theta}+\frac{1}{r_1\sin\theta}\frac{\partial\overline{u}_\theta}{\partial\phi}-\frac{\overline{u}_\phi\cos\theta}{r_1\sin\theta}\end{aligned} \tag{93}$$

and the interface balance equations can be expanded to

$$\begin{aligned}&\frac{\overline{\sigma}_{\theta\theta}+\overline{\sigma}_{\phi\phi}}{r_1}-[[\sigma_{rr}]]=0\\ &\frac{1}{r_1}\frac{\partial\overline{\sigma}_{\theta\theta}}{\partial\theta}+\frac{1}{r_1\sin\theta}\frac{\partial\overline{\sigma}_{\theta\phi}}{\partial\phi}+\frac{[\overline{\sigma}_{\theta\theta}-\overline{\sigma}_{\phi\phi}]\cos\theta}{r_1\sin\theta}+[[\sigma_{r\theta}]]=0\\ &\frac{1}{r_1}\frac{\partial\overline{\sigma}_{\theta\phi}}{\partial\theta}+\frac{1}{r_1\sin\theta}\frac{\partial\overline{\sigma}_{\phi\phi}}{\partial\phi}+\frac{2\overline{\sigma}_{\theta\phi}\cos\theta}{r_1\sin\theta}+[[\sigma_{r\phi}]]=0\end{aligned} \tag{94}$$

The normal basis vectors in spherical coordinates are

$$\boldsymbol{n}_r=\begin{bmatrix}\sin\theta\cos\phi\\ \sin\theta\sin\phi\\ \cos\theta\end{bmatrix},\quad \boldsymbol{n}_\theta=\begin{bmatrix}\cos\theta\cos\phi\\ \cos\theta\sin\phi\\ -\sin\theta\end{bmatrix},\quad \boldsymbol{n}_\phi=\begin{bmatrix}-\sin\phi\\ \cos\phi\\ 0\end{bmatrix} \tag{95}$$

and the displacements and stresses can be accordingly expressed as

$$\begin{aligned}\boldsymbol{u}&=u_r\boldsymbol{n}_r+u_\theta\boldsymbol{n}_\theta+u_\phi\boldsymbol{n}_\phi\\ \boldsymbol{\sigma}&=\sigma_{rr}\boldsymbol{n}_r\otimes\boldsymbol{n}_r+\sigma_{\theta\theta}\boldsymbol{n}_\theta\otimes\boldsymbol{n}_\theta+\sigma_{\phi\phi}\boldsymbol{n}_\phi\otimes\boldsymbol{n}_\phi\\ &\quad+\sigma_{r\theta}[\boldsymbol{n}_r\otimes\boldsymbol{n}_\theta+\boldsymbol{n}_\theta\otimes\boldsymbol{n}_r]+\sigma_{r\phi}[\boldsymbol{n}_r\otimes\boldsymbol{n}_\phi+\boldsymbol{n}_\phi\otimes\boldsymbol{n}_r]\\ \overline{\boldsymbol{\sigma}}&=\overline{\sigma}_{\theta\theta}\boldsymbol{n}_\theta\otimes\boldsymbol{n}_\theta+\overline{\sigma}_{\phi\phi}\boldsymbol{n}_\phi\otimes\boldsymbol{n}_\phi+\overline{\sigma}_{\theta\phi}[\boldsymbol{n}_\theta\otimes\boldsymbol{n}_z+\boldsymbol{n}_z\otimes\boldsymbol{n}_\theta]\end{aligned} \tag{96}$$

The mechanical energy stored in the RVE reads

$$\begin{aligned}U^{(\mathrm{RVE})}&=\frac{1}{2}\int_{\mathcal{B}}\boldsymbol{\sigma}:\boldsymbol{\varepsilon}\,\mathrm{d}V+\frac{1}{2}\int_I\overline{\boldsymbol{\sigma}}:\overline{\boldsymbol{\varepsilon}}\,\mathrm{d}A+\frac{1}{2}\int_I\overline{\boldsymbol{t}}\cdot[[\boldsymbol{u}]]\,\mathrm{d}A\\ &=\frac{1}{2}\int_{\partial\mathcal{B}}[\boldsymbol{\sigma}\cdot\boldsymbol{n}]\cdot\boldsymbol{u}\,\mathrm{d}A=\frac{1}{2}\int_{\partial\mathcal{B}}\boldsymbol{t}\cdot\boldsymbol{u}\,\mathrm{d}A\end{aligned} \tag{97}$$

Under prescribed boundary conditions associated with expansion and in-plane shear, the average mechanical energy density stored in the RVE reads

$$U^{(\mathrm{RVE})}=\frac{3}{8\pi r_2^3}\int_0^{2\pi}\int_0^{\pi}\left[\sigma_{rr}^{(2)}u_r^{(2)}+\sigma_{r\theta}^{(2)}u_\theta^{(2)}+\sigma_{r\phi}^{(2)}u_\phi^{(2)}{}_{]r=r_2}\right]\sin\theta\,\mathrm{d}\theta\,\mathrm{d}\phi \tag{98}$$

Accordingly, the mechanical energy stored in an equivalent homogeneous medium reads

$$\begin{aligned}U^{(\mathrm{eq})}&=\frac{1}{2}\int_{\mathcal{B}}\boldsymbol{\sigma}^{(\mathrm{eq})}:\boldsymbol{\varepsilon}^{(\mathrm{eq})}\,\mathrm{d}V=\frac{1}{2}\int_{\partial\mathcal{B}}[\boldsymbol{\sigma}^{(\mathrm{eq})}\cdot\boldsymbol{n}]\cdot\boldsymbol{u}^{(\mathrm{eq})}\,\mathrm{d}A\\ &=\frac{1}{2}\int_{\partial\mathcal{B}}\boldsymbol{t}^{(\mathrm{eq})}\cdot\boldsymbol{u}^{(\mathrm{eq})}\,\mathrm{d}A\end{aligned} \tag{99}$$

Under prescribed boundary conditions associated with expansion and in-plane shear, the average mechanical energy density stored in the equivalent homogeneous medium reads

$$U(eq)=\frac{3}{8\pi r_2^3}\int_0^{2\pi}\int_0^{\pi}\left[\sigma_{rr}^{(\mathrm{eq})}u_r^{(\mathrm{eq})}+\sigma_{r\theta}^{(\mathrm{eq})}u_\theta^{(\mathrm{eq})}+\sigma_{r\phi}^{(\mathrm{eq})}u_\phi^{(\mathrm{eq})}\right]_{r=r_2}\sin\theta\mathrm{d}\theta\mathrm{d}\phi \tag{100}$$

Equating the energies (98) and (100) renders the overall macroscopic properties. Note that the generic form of the average mechanical energy density in principle includes other components of stress and displacement but they vanish for expansion and in-plane shear boundary conditions that are imposed here.

In CSA [14], the RVE resembles the right microstructure in Fig. 11. Applying expansion and simple shear under both displacement and traction boundary conditions renders bounds on the overall bulk and shear moduli. While the bounds for the shear modulus are distinct, for the bulk modulus the bounds coincide

and therefore, they are collectively referred to as the effective bulk modulus. To obtain an estimate for the effective shear modulus, Christensen and Lo [52] developed GSCM via introducing an infinite effective medium surrounding the matrix whose properties are the unknowns of the problem. Here, we extend CSA and GSCM to account for extended general interfaces with arbitrary interface positions and obtain bounds and estimates for the effective bulk and shear moduli of particulate-composites.

4.2 Effective Bulk Modulus. To obtain the effective bulk modulus ${}^{\mathrm{M}}\kappa$, consider the RVE subject to a uniform radial expansion via

$$\boldsymbol{u}^{0}_{(r,\theta,\phi)} = \begin{bmatrix} \beta r \\ 0 \\ 0 \end{bmatrix} \tag{101}$$

where the superscript 0 denotes the prescribed deformation mode. As demonstrated by Hashin [14], the generated displacement fields in the constituents due to the boundary condition (101) are

$$\begin{aligned} u_r^{(1)} &= \beta r\left[X_1 + \frac{1}{[r/r_1]^3}X_2\right] \\ u_\theta^{(1)} &= u_\phi^{(1)} = 0 \\ u_r^{(2)} &= \beta r\left[X_3 + \frac{1}{[r/r_1]^3}X_4\right] \\ u_\theta^{(2)} &= u_\phi^{(2)} = 0 \end{aligned} \tag{102}$$

with the four unknowns X_1–X_4 that can be determined via imposing the boundary and interface conditions

- finite displacement at $r=0$

$$u_r^{(1)}(r=0) \to \infty \;\Rightarrow\; X_2 = 0 \tag{103}$$

- radial equilibrium at $r=r_1$

$$\bar{t}_r = \overline{k}\,[[u_r]] \Rightarrow [1-\overline{\alpha}]\sigma_{rr}^{(2)}(r_1) + \overline{\alpha}\sigma_{rr}^{(1)}(r_1) = \overline{k}[u_r^{(2)}(r_1) - u_r^{(1)}(r_1)] \tag{104}$$

- tangential equilibrium at $r=r_1$

$$[\overline{\operatorname{div}}\,\overline{\sigma}]_r + [[t_r]] = 0 \;\Rightarrow\; -\frac{\overline{\sigma}_{\theta\theta} + \overline{\sigma}_{\phi\phi}}{r_1} + \sigma_{rr}^{(2)}(r_1) - \sigma_{rr}^{(1)}(r_1) = 0 \tag{105}$$

- prescribed displacement at $r=r_2$

$$u_r^{(2)}(r_2) = \beta r \tag{106}$$

The conditions (103)–(106) lead to the system of equations

$$\begin{bmatrix} \dfrac{3\overline{\alpha}\kappa^{(1)} + \overline{k}r_1}{\overline{k}} & \dfrac{3[1-\overline{\alpha}]\kappa^{(2)} - \overline{k}r_1}{\overline{k}} & \dfrac{-4[1-\overline{\alpha}]\mu^{(2)} - \overline{k}r_1}{\overline{k}} \\ \dfrac{-4[1-\overline{\alpha}]\left[\overline{\lambda}+\overline{\mu}\right] - 3\kappa^{(1)}r_1}{r_1} & \dfrac{-4\overline{\alpha}\left[\overline{\lambda}+\overline{\mu}\right] + 3\kappa^{(2)}r_1}{r_1} & \dfrac{-4\overline{\alpha}\left[\overline{\lambda}+\overline{\mu}\right] - 4\mu^{(2)}r_1}{r_1} \\ 0 & 1 & f \end{bmatrix} \begin{bmatrix} X_1 \\ X_3 \\ X_4 \end{bmatrix} = \begin{bmatrix} 0 \\ 0 \\ 1 \end{bmatrix} \tag{107}$$

Applying the same boundary condition (101) to the equivalent homogeneous medium leads to the displacement field $u_r^{(\mathrm{eq})} = \beta r$ and $u_\theta^{(\mathrm{eq})} = u_\phi^{(\mathrm{eq})} = 0$. Employing Eqs. (98) and (100), the average mechanical energy densities in the RVE and the equivalent homogeneous medium read

$$\begin{aligned} U(RVE) &= \frac{3\beta^2\left[3\kappa^{(2)}X_3 - 4f\mu^{(2)}X_4\right]}{2r_2^2} \\ U^{(\mathrm{eq})} &= \frac{9\beta^2\,{}^{\mathrm{M}}\kappa}{2r_2^2} \end{aligned} \tag{108}$$

where X_3 and X_4 are the solutions of the system (107). Imposing $U(\mathrm{RVE}) = U^{(\mathrm{eq})}$ renders the overall bulk modulus

$${}^{\mathrm{M}}\kappa = \frac{3\kappa^{(2)}S_1 + 4f\mu^{(2)}S_2}{3S_3}$$

with

$$\begin{aligned} S_1 &= 4\overline{k}\left[\overline{\lambda}+\overline{\mu}\right]r_1 + \overline{k}r_1^2\left[3\kappa^{(1)} + 4\mu^{(2)}\right] + 4\left[\overline{\lambda}+\overline{\mu}\right]\left[3\overline{\alpha}^2\kappa^{(1)} + 4[1-\overline{\alpha}]^2\mu^{(2)}\right] + 12\kappa^{(1)}\mu^{(2)}r_1 \\ S_2 &= 4\overline{k}\left[\overline{\lambda}+\overline{\mu}\right]r_1 + 3\overline{k}r_1^2\left[\kappa^{(1)} - \kappa^{(2)}\right] + 12\left[\overline{\lambda}+\overline{\mu}\right]\left[\overline{\alpha}^2\kappa^{(1)} - [1-\overline{\alpha}]^2\kappa^{(2)}\right] - 9\kappa^{(1)}\kappa^{(2)}r_1 \\ S_3 &= 4\overline{k}\left[\overline{\lambda}+\overline{\mu}\right]r_1[1-f] + \overline{k}r_1^2\left[3\kappa^{(1)}[1-f] + 3f\kappa^{(2)} + 4\mu^{(2)}\right] + 4\left[\overline{\lambda}+\overline{\mu}\right]\left[\left[4\mu^{(2)} + 3f\kappa^{(2)}\right][1-\overline{\alpha}]^2 + 3\overline{\alpha}^2\kappa^{(1)}[1-f]\right] \\ &\quad + 3\kappa^{(1)}r_1\left[4\mu^{(2)} + 3f\kappa^{(2)}\right] \end{aligned} \tag{109}$$

where $\overline{\alpha}$ determines the interface position. Figure 13 shows the overall bulk modulus ${}^{M}\kappa$ versus $\overline{\alpha}$ for various interface models. Clearly, the position of the interface does not influence the material response for the classical interface models. Similar to the two-dimensional case, for the extended general interface model, it is observed that for small $\overline{\alpha}$ the material renders a closer behavior to the cohesive interface. Increasing $\overline{\alpha}$ yields a stiffer response where the solution due to the extended general interface model approaches that of the elastic interface model. The extended general interface model coincides with the general interface model if $\overline{\alpha} = 0.5$.

4.3 Upper Bound on Shear Modulus. To obtain the upper bound on the overall shear modulus, the simple shear deformation

$$\boldsymbol{u}^0_{(r,\theta,\phi)} = \begin{bmatrix} \beta r \sin^2\theta \cos 2\phi \\ \beta r \sin\theta \cos\theta \cos 2\phi \\ -\beta r \sin\theta \sin 2\phi \end{bmatrix} \tag{110}$$

is applied to the RVE boundary at $r = r_2$. For this boundary condition, following Christensen and Lo [52], the displacement fields developed in the constituents read

$$\begin{aligned}
u_r^{(1)} &= \beta r \sin^2(\theta)\cos(2\phi)\left[X_1 + \left[2 - 3\frac{\kappa^{(1)}}{\mu^{(1)}}\right][r/r_1]^2 X_2 + \frac{3X_3}{[r/r_1]^5} + \left[3 + 3\frac{\kappa^{(1)}}{\mu^{(1)}}\right]\frac{X_4}{[r/r_1]^3}\right] \\
u_\theta^{(1)} &= \beta r \sin(\theta)\cos(\theta)\cos(2\phi)\left[X_1 - \left[\frac{11}{3} + 5\frac{\kappa^{(1)}}{\mu^{(1)}}\right][r/r_1]^2 X_2 - \frac{2X_3}{[r/r_1]^5} + \frac{2X_4}{[r/r_1]^3}\right] \\
u_\phi^{(1)} &= -\beta r \sin(\theta)\sin(2\phi)\left[X_1 - \left[\frac{11}{3} + 5\frac{\kappa^{(1)}}{\mu^{(1)}}\right][r/r_1]^2 X_2 - \frac{2X_3}{[r/r_1]^5} + \frac{2X_4}{[r/r_1]^3}\right] \\
u_r^{(2)} &= \beta r \sin^2(\theta)\cos(2\phi)\left[X_5 + \left[2 - 3\frac{\kappa^{(2)}}{\mu^{(2)}}\right][r/r_1]^2 X_6 + \frac{3X_7}{[r/r_1]^5} + \left[3 + 3\frac{\kappa^{(2)}}{\mu^{(2)}}\right]\frac{X_8}{[r/r_1]^3}\right] \\
u_\theta^{(2)} &= \beta r \sin(\theta)\cos(\theta)\cos(2\phi)\left[X_5 - \left[\frac{11}{3} + 5\frac{\kappa^{(2)}}{\mu^{(2)}}\right][r/r_1]^2 X_6 - \frac{2X_7}{[r/r_1]^5} + \frac{2X_8}{[r/r_1]^3}\right] \\
u_\phi^{(2)} &= -\beta r \sin(\theta)\sin(2\phi)\left[X_5 - \left[\frac{11}{3} + 5\frac{\kappa^{(2)}}{\mu^{(2)}}\right][r/r_1]^2 X_6 - \frac{2X_7}{[r/r_1]^5} + \frac{2X_8}{[r/r_1]^3}\right]
\end{aligned} \tag{111}$$

with the eight unknowns X_1–X_8 which can be determined via imposing the boundary and interface conditions

- finite displacement at $r = 0$

$$u_r^{(1)}(r=0) \to \infty \quad \text{and} \quad u_\theta^{(1)}(r=0) \to \infty \;\Rightarrow\; X_3 = 0 \quad \text{and} \quad X_4 = 0 \tag{112}$$

- radial equilibrium in r direction at $r = r_1$

$$\bar{t}_r = \overline{k}\,[[u_r]] \;\Rightarrow\; [1-\overline{\alpha}]\sigma_{rr}^{(2)}(r_1) + \overline{\alpha}\sigma_{rr}^{(1)}(r_1) = \overline{k}[u_r^{(2)}(r_1) - u_r^{(1)}(r_1)] \tag{113}$$

- circumferential equilibrium in θ direction at $r = r_1$

$$\bar{t}_\theta = \overline{k}\,[[u_\theta]] \;\Rightarrow\; [1-\overline{\alpha}]\sigma_{r\theta}^{(2)}(r_1) + \overline{\alpha}\sigma_{r\theta}^{(1)}(r_1) = \overline{k}[u_\theta^{(2)}(r_1) - u_\theta^{(1)}(r_1)] \tag{114}$$

- tangential equilibrium in r direction at $r = r_1$

$$[\overline{\operatorname{div}}\,\overline{\sigma}]_r + [[t_r]] = 0 \;\Rightarrow\; -\frac{\overline{\sigma}_{\theta\theta} + \overline{\sigma}_{\phi\phi}}{r_1} + \sigma_{rr}^{(2)}(r_1) - \sigma_{rr}^{(1)}(r_1) = 0 \tag{115}$$

- tangential equilibrium in θ direction at $r = r_1$

$$[\overline{\operatorname{div}}\,\overline{\sigma}]_\theta + [[t_\theta]] = 0 \;\Rightarrow\; \frac{1}{r_1}\frac{\partial\overline{\sigma}_{\theta\theta}}{\partial\theta} + \frac{1}{r_1\sin\theta}\frac{\partial\overline{\sigma}_{\theta\phi}}{\partial\phi} + \frac{[\overline{\sigma}_{\theta\theta} - \overline{\sigma}_{\phi\phi}]\cos\theta}{r_1\sin\theta} + \sigma_{r\theta}^{(2)}(r_1) - \sigma_{r\theta}^{(1)}(r_1) = 0 \tag{116}$$

- prescribed displacements at $r = r_2$

$$u_r^{(2)}(r_2) = \beta r_2 \sin^2\theta\cos 2\phi \quad \text{and} \quad u_\theta^{(2)}(r_2) = \beta r_2 \sin\theta\cos\theta\cos 2\phi \tag{117}$$

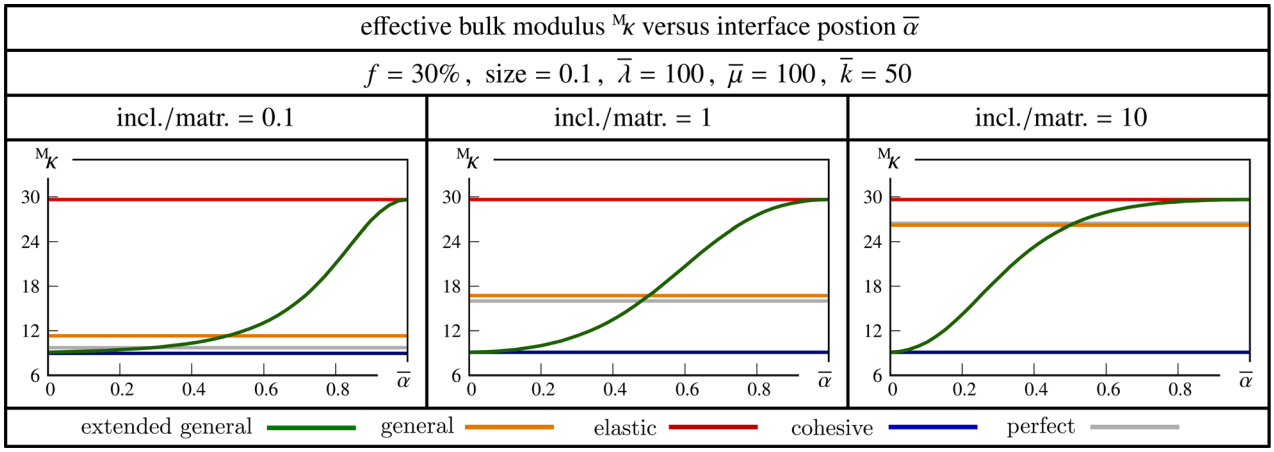

Fig. 13 Effective bulk modulus $^{M}\kappa$ versus interface position $\bar{\alpha}$ for particle-reinforced composites. Different interface models are compared against each other.

The conditions (112)–(117) lead to the system of equations

$$\begin{bmatrix} P_{11} & P_{12} & P_{13} & P_{14} & P_{15} & P_{16} \\ P_{21} & P_{22} & P_{23} & P_{24} & P_{25} & P_{26} \\ P_{31} & P_{32} & P_{33} & P_{34} & P_{35} & P_{36} \\ P_{41} & P_{42} & P_{43} & P_{44} & P_{45} & P_{46} \\ P_{51} & P_{52} & P_{53} & P_{54} & P_{55} & P_{56} \\ P_{61} & P_{62} & P_{63} & P_{64} & P_{65} & P_{66} \end{bmatrix} \begin{bmatrix} X_1 \\ X_2 \\ X_5 \\ X_6 \\ X_7 \\ X_8 \end{bmatrix} = \begin{bmatrix} 0 \\ 0 \\ 0 \\ 0 \\ 1 \\ 1 \end{bmatrix} \tag{118}$$

where the components of $\boldsymbol{P}$ are detailed in Eq. (A3). Applying the same boundary condition to the equivalent homogeneous medium results in the displacement field

$$\begin{aligned} u_r^{(\mathrm{eq})} &= \beta r \sin^2\theta \cos 2\phi \\ u_\theta^{(\mathrm{eq})} &= \beta r \sin\theta \cos\theta \cos 2\phi \\ u_\phi^{(\mathrm{eq})} &= -\beta r \sin\theta \sin 2\phi \end{aligned} \tag{119}$$

Equipped with the displacement and stress fields in both constituents, the overall mechanical energy densities in both RVE and the equivalent homogeneous medium according to Eqs. (98) and (100) read

$$\begin{aligned} U^{(\mathrm{RVE})} &= \frac{\beta^2}{5r_2^2}\Big[10\mu^{(2)}X_5 - 14\Big[3\kappa^{(2)} + \mu^{(2)}\Big]f^{-2/3}X_6 \\ &\quad - 2\Big[9\kappa^{(2)} + 8\mu^{(2)}\Big]fX_8\Big] \\ U^{(\mathrm{eq})} &= \frac{2\beta^2\,{}^{M}\mu}{r_2^2} \end{aligned} \tag{120}$$

From $U^{(\mathrm{RVE})} = U^{(\mathrm{eq})}$ the upper bound on the macroscopic shear modulus is obtained as

$$\begin{aligned} {}^{M}\mu_{\mathrm{upper}} = \frac{1}{10}\Big[&10\mu^{(2)}X_5 - 14\Big[3\kappa^{(2)} + \mu^{(2)}\Big]f^{-2/3}X_6 \\ &-2\Big[9\kappa^{(2)} + 8\mu^{(2)}\Big]fX_8\Big] \end{aligned} \tag{121}$$

where X_5, X_6, and X_8 can be calculated via solving the system of Eq. (118). Figure 14 illustrates the effective shear modulus and its bounds with respect to the interface position $\bar{\alpha}$ for various interface models. The top row corresponds to the upper bound on the shear modulus $^{M}\mu_{\mathrm{upper}}$. The middle row corresponds to the lower bound on the shear modulus $^{M}\mu_{\mathrm{lower}}$ which will be discussed in the next section. The last row corresponds to the effective shear modulus $^{M}\mu$ that we derive in Sec. 4.5. Similar to the bulk modulus, it is observed that for small $\bar{\alpha}$ the composite embedding the extended general interface model renders a closer behavior to the cohesive interface model. Unlike the fiber-reinforced composites, here, increasing $\bar{\alpha}$ yields a stiffer response where the solution due to the extended general interface model approaches that of the elastic interface model.

4.4 Lower Bound on Shear Modulus. To obtain the lower bound on the overall shear modulus, a traction field is applied to the boundary of the RVE as

$$\boldsymbol{t}^0_{(r,\theta,\phi)} = \begin{bmatrix} \beta \sin^2\theta \cos 2\phi \\ \beta \sin\theta \cos\theta \cos 2\phi \\ -\beta \sin\theta \sin 2\phi \end{bmatrix} \tag{122}$$

The displacement fields developed in the constituents due to the applied traction are analogous to Eq. (111) with the eight unknowns X_1–X_8. The boundary and interface conditions are similar to Eqs. (112)–(116) and instead of condition (117), we have

- prescribed stresses at $r = r_2$

$$\sigma_{rr}^{(2)}(r_2) = \beta \sin^2\theta \cos 2\phi \quad \text{and} \quad \sigma_{r\theta}^{(2)}(r_2) = \beta \sin\theta \cos\theta \cos 2\phi \tag{123}$$

which leads to the system of equations

$$\begin{bmatrix} Q_{11} & Q_{12} & Q_{13} & Q_{14} & Q_{15} & Q_{16} \\ Q_{21} & Q_{22} & Q_{23} & Q_{24} & Q_{25} & Q_{26} \\ Q_{31} & Q_{32} & Q_{33} & Q_{34} & Q_{35} & Q_{36} \\ Q_{41} & Q_{42} & Q_{43} & Q_{44} & Q_{45} & Q_{46} \\ Q_{51} & Q_{52} & Q_{53} & Q_{54} & Q_{55} & Q_{56} \\ Q_{61} & Q_{62} & Q_{63} & Q_{64} & Q_{65} & Q_{66} \end{bmatrix} \begin{bmatrix} X_1 \\ X_2 \\ X_5 \\ X_6 \\ X_7 \\ X_8 \end{bmatrix} = \begin{bmatrix} 0 \\ 0 \\ 0 \\ 0 \\ 1 \\ 1 \end{bmatrix} \tag{124}$$

Further details regarding the components of $\boldsymbol{Q}$ are available in Eq. (A4). Applying the same boundary conditions to the equivalent homogeneous medium leads to the displacement field

$$\begin{aligned} u_r^{\mathrm{eq}} &= \frac{\beta}{2\,{}^{M}\mu} r \sin^2\theta \cos 2\phi \\ u_\theta^{\mathrm{eq}} &= \frac{\beta}{2\,{}^{M}\mu} r \sin\theta \cos\theta \cos 2\phi \\ u_\phi^{\mathrm{eq}} &= -\frac{\beta}{2\,{}^{M}\mu} r \sin\theta \sin 2\phi \end{aligned} \tag{125}$$

Equipped with the displacement and stress fields in both constituents, the overall mechanical energy in both RVE and the equivalent homogeneous medium according to Eqs. (98) and (100) read

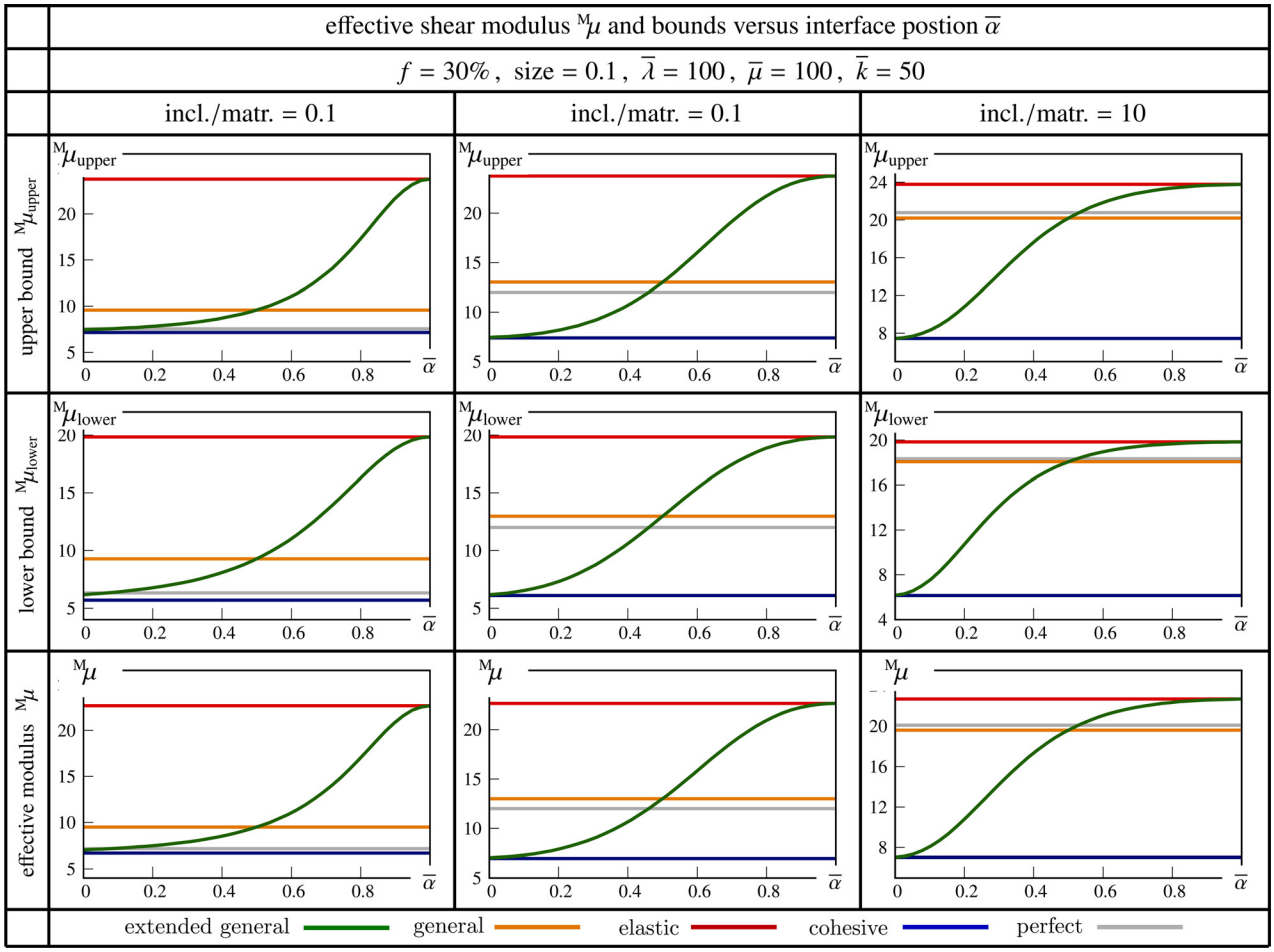

Fig. 14 Effective shear modulus $^{M}\mu$ and its bounds versus interface position $\bar{\alpha}$ for particle-reinforced composites. Different interface models are compared against each other.

$$U^{(\mathrm{RVE})} = \frac{\beta^2}{5r_2^2}\left[5X_5^{(2)} - 7\left[1 + 3\frac{\kappa^{(2)}}{\mu^{(2)}}\right]f^{-2/3}X_6 + 6\left[2 + \frac{\kappa^{(2)}}{\mu^{(2)}}\right]fX_8\right]$$
$$U^{(\mathrm{eq})} = \frac{\beta^2}{2^{\mathrm{M}}\mu r_2^2} \tag{126}$$

Imposing $U^{(\mathrm{RVE})} = U^{(\mathrm{eq})}$ furnishes the lower bound on the macroscopic shear modulus

$$^{\mathrm{M}}\mu_{\mathrm{lower}} = \frac{5}{2\left[5X_5 - 7\left[1 + 3\frac{\kappa^{(2)}}{\mu^{(2)}}\right]f^{-2/3}X_6 + 6\left[2 + \frac{\kappa^{(2)}}{\mu^{(2)}}\right]fX_8\right]} \tag{127}$$

where in X_5, X_6, and X_8 can be calculated via solving the system (124). See Fig. 14 for the illustration of the lower bound on the shear modulus $^{\mathrm{M}}\mu_{\mathrm{lower}}$ versus the interface position $\bar{\alpha}$. Similar to the upper bound, it is observed that smaller $\bar{\alpha}$ renders a closer behavior to the cohesive interface. Increasing $\bar{\alpha}$ yields a stiffer response but unlike the fiber-reinforced composites, the solution due to the general interface model approaches that of the elastic interface model.

4.5 Effective Shear Modulus. To obtain the effective shear modulus $^{\mathrm{M}}\mu$, GSCM [52] is employed. No traction or displacement jump between the matrix and the effective medium is allowed. To obtain the effective shear modulus, let the medium be subject to the displacement boundary condition

$$\boldsymbol{u}^0_{(r,\theta,\phi)} = \begin{bmatrix} \beta r \sin^2\theta \cos 2\phi \\ \beta r \sin\theta \cos\theta \cos 2\phi \\ -\beta r \sin\theta \sin 2\phi \end{bmatrix} \tag{128}$$

The resultant displacement fields in the fiber and the matrix due to the boundary condition (128) are similar to Eq. (111), hence the eight unknowns X_1–X_8. Furthermore, the displacement field in the effective medium reads

$$u_r^{(\mathrm{eff})} = \beta r \sin^2\theta \cos 2\phi\left[1 + \frac{3X_9}{[r/r_1]^5} + \left[3 + 3\frac{^{\mathrm{M}}\kappa}{^{\mathrm{M}}\mu}\right]\frac{X_{10}}{[r/r_1]^3}\right]$$
$$u_\theta^{(\mathrm{eff})} = \beta r \sin\theta \cos\theta \cos 2\phi\left[1 - \frac{2X_9}{[r/r_1]^5} + \frac{2X_{10}}{[r/r_1]^3}\right]$$
$$u_\phi^{(\mathrm{eff})} = -\beta r \sin\theta \sin 2\phi\left[1 - \frac{2X_9}{[r/r_1]^5} + \frac{2X_{10}}{[r/r_1]^3}\right] \tag{129}$$

with X_9 and X_{10} being the ninth and the tenth unknowns. Before considering the boundary and interface conditions, the energetic criterion (130) deduced from the Eshelby's energy principle [52] is imposed

$$\int_0^{2\pi}\int_0^{\pi}[\sigma_{rr}^{(\mathrm{eff})}u_r^{(\mathrm{eq})} + \sigma_{r\theta}^{(\mathrm{eff})}u_\theta^{(\mathrm{eq})} + \sigma_{r\phi}^{(\mathrm{eff})}u_\phi^{(\mathrm{eq})} - \sigma_{rr}^{(\mathrm{eq})}u_r^{(\mathrm{eff})} - \sigma_{r\theta}^{(\mathrm{eq})}u_\theta^{(\mathrm{eff})} - \sigma_{r\phi}^{(\mathrm{eq})}u_\phi^{(\mathrm{eff})}]_{r=r_2}\sin\theta\,\mathrm{d}\theta\,\mathrm{d}\phi = 0 \tag{130}$$

Table 9 Explicit formulations for the bounds and estimates on the overall bulk and shear moduli of fiber-composites embedding general interfaces

General interface model	
${}^{\mathrm{M}}\kappa = \dfrac{3\kappa^{(2)}S_1 + 4f\mu^{(2)}S_2}{3S_3}$	
$S_1 = 4\overline{k}[\overline{\lambda}+\overline{\mu}]r_1 + \overline{k}r_1^2[3\kappa^{(1)}+4\mu^{(2)}] + [\overline{\lambda}+\overline{\mu}][3\kappa^{(1)}+4\mu^{(2)}] + 12\kappa^{(1)}\mu^{(2)}r_1$	
$S_2 = 4\overline{k}[\overline{\lambda}+\overline{\mu}]r_1 + 3\overline{k}r_1^2[\kappa^{(1)}-\kappa^{(2)}] + 3[\overline{\lambda}+\overline{\mu}][\kappa^{(1)}-\kappa^{(2)}] - 9\kappa^{(1)}\kappa^{(2)}r_1$	
$S_3 = 4\overline{k}[\overline{\lambda}+\overline{\mu}]r_1[1-f] + \overline{k}r_1^2[3\kappa^{(1)}[1-f]+3f\kappa^{(2)}+4\mu^{(2)}] + [\overline{\lambda}+\overline{\mu}][[4\mu^{(2)}+3f\kappa^{(2)}]+3\kappa^{(1)}[1-f]] + 3\kappa^{(1)}r_1[4\mu^{(2)}+3f\kappa^{(2)}]$	
${}^{\mathrm{M}}\mu_{\mathrm{upper}} = \dfrac{1}{10}[10\mu^{(2)}X_5 - 14[3\kappa^{(2)}+\mu^{(2)}]f^{-2/3}X_6 - 2[9\kappa^{(2)}+8\mu^{(2)}]fX_8]$	see Appendix (B3)
${}^{\mathrm{M}}\mu_{\mathrm{lower}} = \dfrac{5}{2[5X_5 - 7\left[1+3\dfrac{\kappa^{(2)}}{\mu^{(2)}}\right]f^{-2/3}X_6 + 6\left[2+\dfrac{\kappa^{(2)}}{\mu^{(2)}}\right]fX_8]}$	see Appendix (B4)
$120f^{5/3\,\mathrm{M}}\mu^2 + [3h_1 - 2h_2 - 24[g_1+g_2]f^{5/3}]^{\mathrm{M}}\mu + [g_1h_2 - g_2h_1] = 0$	see Appendix (B3)

that yields $X_{10} = 0$. The remaining unknowns can be determined via imposing the boundary and interface conditions which are similar to Eqs. (112)–(116) and instead of condition (117), we have

- displacement continuity at $r = r_2$

$$u_r^{(2)}(r_2) = u_r^{(\mathrm{eff})}(r_2) \quad \text{and} \quad u_\theta^{(2)}(r_2) = u_\theta^{(\mathrm{eff})}(r_2) \tag{131}$$

that lead to the system of equations

$$\begin{bmatrix} R_{11} & R_{12} & R_{13} & R_{14} & R_{15} & R_{16} \\ R_{21} & R_{22} & R_{23} & R_{24} & R_{25} & R_{26} \\ R_{31} & R_{32} & R_{33} & R_{34} & R_{35} & R_{36} \\ R_{41} & R_{42} & R_{43} & R_{44} & R_{45} & R_{46} \\ R_{51} & R_{52} & R_{53} & R_{54} & R_{55} & R_{56} \\ R_{61} & R_{62} & R_{63} & R_{64} & R_{65} & R_{66} \end{bmatrix} \begin{bmatrix} X_1 \\ X_2 \\ X_5 \\ X_6 \\ X_7 \\ X_8 \end{bmatrix} = \begin{bmatrix} 0 \\ 0 \\ 0 \\ 0 \\ 1 \\ 1 \end{bmatrix} + \begin{bmatrix} 0 \\ 0 \\ 0 \\ 0 \\ 3f^{5/3} \\ -2f^{5/3} \end{bmatrix} X_9 \tag{132}$$

with $\boldsymbol{R} = \boldsymbol{P}$ thus, see Eq. (A3). The remaining six unknowns can be obtained as a function of X_9. That is

$$\underbrace{\begin{bmatrix} X_1 \\ X_2 \\ X_5 \\ X_6 \\ X_7 \\ X_8 \end{bmatrix}}_{\boldsymbol{X}} = \boldsymbol{R}^{-1}\underbrace{\begin{bmatrix} 0 \\ 0 \\ 0 \\ 0 \\ 1 \\ 1 \end{bmatrix}}_{\boldsymbol{a}} + \boldsymbol{R}^{-1}\underbrace{\begin{bmatrix} 0 \\ 0 \\ 0 \\ 0 \\ 3f^{5/3} \\ -2f^{5/3} \end{bmatrix}}_{\boldsymbol{b}} X_9 = \begin{bmatrix} a_1 \\ a_2 \\ a_5 \\ a_6 \\ a_7 \\ a_8 \end{bmatrix} + \begin{bmatrix} b_1 \\ b_2 \\ b_5 \\ b_6 \\ b_7 \\ b_8 \end{bmatrix} X_9 \tag{133}$$

Note, the components of the arrays $\boldsymbol{a}$ and $\boldsymbol{b}$ are numbered according to the indices in $\boldsymbol{X}$. Imposing the stress continuity between the matrix and the effective medium yields

$$\begin{aligned} \sigma_{rr}^{(2)}(r_2) = \sigma_{rr}^{(\mathrm{eff})}(r_2) &\Rightarrow g_1 + h_1X_9 = 2^{\mathrm{M}}\mu - \frac{24X_9{}^{\mathrm{M}}\mu r_1^5}{r_2^5} \\ \sigma_{r\theta}^{(2)}(r_2) = \sigma_{r\theta}^{(\mathrm{eff})}(r_2) &\Rightarrow g_2 + h_2X_9 = 3^{\mathrm{M}}\mu + \frac{24X_9{}^{\mathrm{M}}\mu r_1^5}{r_2^5} \end{aligned} \tag{134}$$

with

$$\begin{aligned} g_1 &= 2\mu^{(2)}a_5 + [3\kappa^{(2)} - 2\mu^{(2)}]f^{-2/3}a_6 - 24\mu^{(2)}f^{5/3}a_7 \\ &\quad - [18\kappa^{(2)} + 8\mu^{(2)}]fa_8 \\ h_1 &= 2\mu^{(2)}b_5 + [3\kappa^{(2)} - 2\mu^{(2)}]f^{-2/3}b_6 - 24\mu^{(2)}f^{5/3}b_7 \\ &\quad - [18\kappa^{(2)} + 8\mu^{(2)}]fb_8 \\ g_2 &= 3\mu^{(2)}a_5 - [24\kappa^{(2)} + 5\mu^{(2)}]f^{-2/3}a_6 + 24\mu^{(2)}f^{5/3}a_7 + 9\kappa^{(2)}fa_8 \\ h_2 &= 3\mu^{(2)}b_5 - [24\kappa^{(2)} + 5\mu^{(2)}]f^{-2/3}b_6 + 24\mu^{(2)}f^{5/3}b_7 + 9\kappa^{(2)}fb_8 \end{aligned} \tag{135}$$

Equation (134) furnishes

$$X_9 = \frac{5^{\mathrm{M}}\mu - g_1 - g_2}{h_1 + h_2}, \tag{136}$$

and via replacing X_9 from Eq. (136) into Eq. (134) we obtain

$$120f^{5/3\,\mathrm{M}}\mu^2 + [3h_1 - 2h_2 - 24[g_1+g_2]f^{5/3}]^{\mathrm{M}}\mu + [g_1h_2 - g_2h_1] = 0 \tag{137}$$

From the two possible solutions of the quadratic Eq. (137), the positive one is the effective shear modulus. See Fig. 14 for the illustration of the effective shear modulus ${}^{\mathrm{M}}\mu$ versus the interface position $\overline{\alpha}$. Again, smaller $\overline{\alpha}$ renders a closer behavior to the cohesive interface model and increasing $\overline{\alpha}$ yields a stiffer response closer to that of the elastic interface model.

4.6 Recovering General, Elastic, Cohesive, and Interface Models. This section briefly provides the previously obtained solutions for the bounds and estimates on the elastic moduli for the general, cohesive, elastic, and perfect interface models. As mentioned before, the general interface model can be recovered by setting $\overline{\alpha} = 0.5$. The cohesive interface model is recovered when $\overline{\lambda} = \overline{\mu} = 0$ and $\overline{\alpha} = 0.5$. The cohesive interface model is recovered when $\overline{\lambda} \neq 0$, $\overline{\mu} \neq 0$ and $\overline{k} \to \infty$ and $\overline{\alpha} = 0.5$. Finally, the perfect interface model is recovered when $\overline{\lambda} = \overline{\mu} = 0$ and $\overline{k} \to \infty$ and $\overline{\alpha} = 0.5$. Tables 9–12 show the formulations for the effective bulk and shear moduli and the bounds on the shear modulus for particle-reinforced composites embedding the general, elastic, cohesive, and perfect interfaces, respectively.

Remark on computational implementation using FEM. Limiting the analysis here to monodisperse particles/fibers is an underlying assumption to derive meaningful analytical estimates. While analytical homogenization proves useful in understanding the

Table 10 Explicit formulations for the bounds and estimates on the overall bulk and shear moduli of fiber-composites embedding elastic interfaces

Elastic interface model	
$^{\mathrm{M}}\kappa = \dfrac{3\kappa^{(2)}[4[\overline{\lambda}+\overline{\mu}]r_1 + r_1^2[3\kappa^{(1)}+4\mu^{(2)}]] + 4f\mu^{(2)}[4[\overline{\lambda}+\overline{\mu}]r_1 + 3r_1^2[\kappa^{(1)}-\kappa^{(2)}]]}{3[4[\overline{\lambda}+\overline{\mu}]r_1[1-f] + r_1^2[3\kappa^{(1)}[1-f]+3f\kappa^{(2)}+4\mu^{(2)}]]}$	
$^{\mathrm{M}}\mu_{\mathrm{upper}} = \dfrac{1}{10}[10\mu^{(2)}X_5 - 14[3\kappa^{(2)}+\mu^{(2)}]f^{-2/3}X_6 - 2[9\kappa^{(2)}+8\mu^{(2)}]fX_8]$	see Appendix (C3)
$^{\mathrm{M}}\mu_{\mathrm{lower}} = \dfrac{5}{2[5X_5 - 7\left[1+3\dfrac{\kappa^{(2)}}{\mu^{(2)}}\right]f^{-2/3}X_6 + 6\left[2+\dfrac{\kappa^{(2)}}{\mu^{(2)}}\right]fX_8]}$	see Appendix (C4)
$120f^{5/3\,\mathrm{M}}\mu^2 + [3h_1 - 2h_2 - 24[g_1+g_2]f^{5/3}]^{\mathrm{M}}\mu + [g_1h_2 - g_2h_1] = 0$	see Appendix (C3)

Table 11 Explicit formulations for the bounds and estimates on the overall bulk and shear moduli of fiber-composites embedding cohesive interfaces

Cohesive interface model	
$^{\mathrm{M}}\kappa = \dfrac{3\kappa^{(2)}[\overline{k}r_1^2[3\kappa^{(1)}+4\mu^{(2)}] + 12\kappa^{(1)}\mu^{(2)}r_1] + 4f\mu^{(2)}[3\overline{k}r_1^2[\kappa^{(1)}-\kappa^{(2)}] - 9\kappa^{(1)}\kappa^{(2)}r_1]}{3[\overline{k}r_1^2[3\kappa^{(1)}[1-f]+3f\kappa^{(2)}+4\mu^{(2)}] + 3\kappa^{(1)}r_1[4\mu^{(2)}+3f\kappa^{(2)}]]}$	
$^{\mathrm{M}}\mu_{\mathrm{upper}} = \dfrac{1}{10}[10\mu^{(2)}X_5 - 14[3\kappa^{(2)}+\mu^{(2)}]f^{-2/3}X_6 - 2[9\kappa^{(2)}+8\mu^{(2)}]fX_8]$	see Appendix (D3)
$^{\mathrm{M}}\mu_{\mathrm{lower}} = \dfrac{5}{2[5X_5 - 7\left[1+3\dfrac{\kappa^{(2)}}{\mu^{(2)}}\right]f^{-2/3}X_6 + 6\left[2+\dfrac{\kappa^{(2)}}{\mu^{(2)}}\right]fX_8]}$	see Appendix (D4)
$120f^{5/3\,\mathrm{M}}\mu^2 + [3h_1 - 2h_2 - 24[g_1+g_2]f^{5/3}]^{\mathrm{M}}\mu + [g_1h_2 - g_2h_1] = 0$	see Appendix (D3)

Table 12 Explicit formulations for the bounds and estimates on the overall bulk and shear moduli of fiber-composites embedding perfect interfaces

Perfect interface model	
$^{\mathrm{M}}\kappa = \dfrac{\kappa^{(2)}[3\kappa^{(1)}+4\mu^{(2)}] + 4f\mu^{(2)}[\kappa^{(1)}-\kappa^{(2)}]}{3\kappa^{(1)}[1-f]+3f\kappa^{(2)}+4\mu^{(2)}}$	
$^{\mathrm{M}}\mu_{\mathrm{upper}} = \dfrac{1}{10}[10\mu^{(2)}X_5 - 14[3\kappa^{(2)}+\mu^{(2)}]f^{-2/3}X_6 - 2[9\kappa^{(2)}+8\mu^{(2)}]fX_8]$	see Appendix (E3)
$^{\mathrm{M}}\mu_{\mathrm{lower}} = \dfrac{5}{2[5X_5 - 7\left[1+3\dfrac{\kappa^{(2)}}{\mu^{(2)}}\right]f^{-2/3}X_6 + 6\left[2+\dfrac{\kappa^{(2)}}{\mu^{(2)}}\right]fX_8]}$	see Appendix (E4)
$120f^{5/3\,\mathrm{M}}\mu^2 + [3h_1 - 2h_2 - 24[g_1+g_2]f^{5/3}]^{\mathrm{M}}\mu + [g_1h_2 - g_2h_1] = 0$	see Appendix (E3)

behavior of composites accounting for extended general interfaces, it is virtually impossible to explain the effective response of more complex microstructures with polydisperse particles/fibers, shown in Fig. 15, without recourse to computational methods such as FEM. The first step toward the finite element implementation of our theory is to derive the weak form of the governing equations. To do so, the strong form of the linear momentum balance for the bulk and interface is contracted from left by a vector-valued test function $\delta\boldsymbol{\varphi} \in \mathcal{H}^1(\mathcal{B})$ and $\delta\overline{\boldsymbol{\varphi}} \in \mathcal{H}^1(I)$, respectively, where $\mathcal{H}^1$ denotes the Sobolev space of order one. Then the resulting equation is integrated over the corresponding domain. The test functions are specified to be zero on the Dirichlet part of the boundary. Integrating Eqs. (7) and (13) over their respective domains, the integral form of the linear momentum balance reads

$$\int_{\mathcal{B}} \mathrm{Div}\boldsymbol{\sigma}\,\mathrm{d}V + \int_I \overline{\mathrm{Div}}\overline{\boldsymbol{\sigma}}\,\mathrm{d}A + \int_I [[\boldsymbol{\sigma}]]\cdot\overline{\boldsymbol{n}}\,\mathrm{d}A = \boldsymbol{0} \tag{138}$$

Upon contracting with the test functions and using the divergence theorem, after some mathematical steps, the weak form of the linear momentum balance reads

$$\int_{\mathcal{B}} \boldsymbol{\sigma} : \mathrm{Grad}\,\delta\boldsymbol{\varphi}\,\mathrm{d}V + \int_I \overline{\boldsymbol{\sigma}} : \overline{\mathrm{Grad}}\,\delta\overline{\boldsymbol{\varphi}}\,\mathrm{d}A + \int_I \overline{\boldsymbol{t}}\cdot[[\delta\boldsymbol{\varphi}]]\,\mathrm{d}A - \int_{\partial\mathcal{B}} \delta\boldsymbol{\varphi}\cdot\boldsymbol{t}_0\,\mathrm{d}A = 0 \tag{139}$$

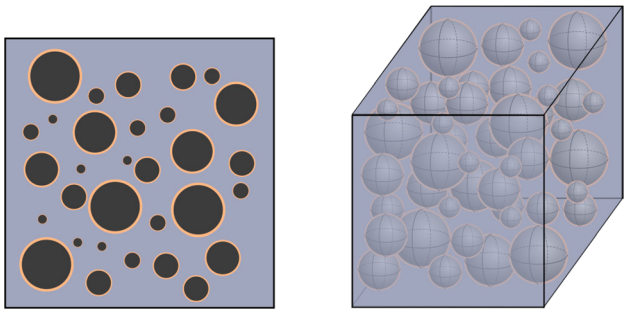

Fig. 15 Schematic illustration of complex polydisperse microstructures for fiber-composites (left) and particulate-composites (right)

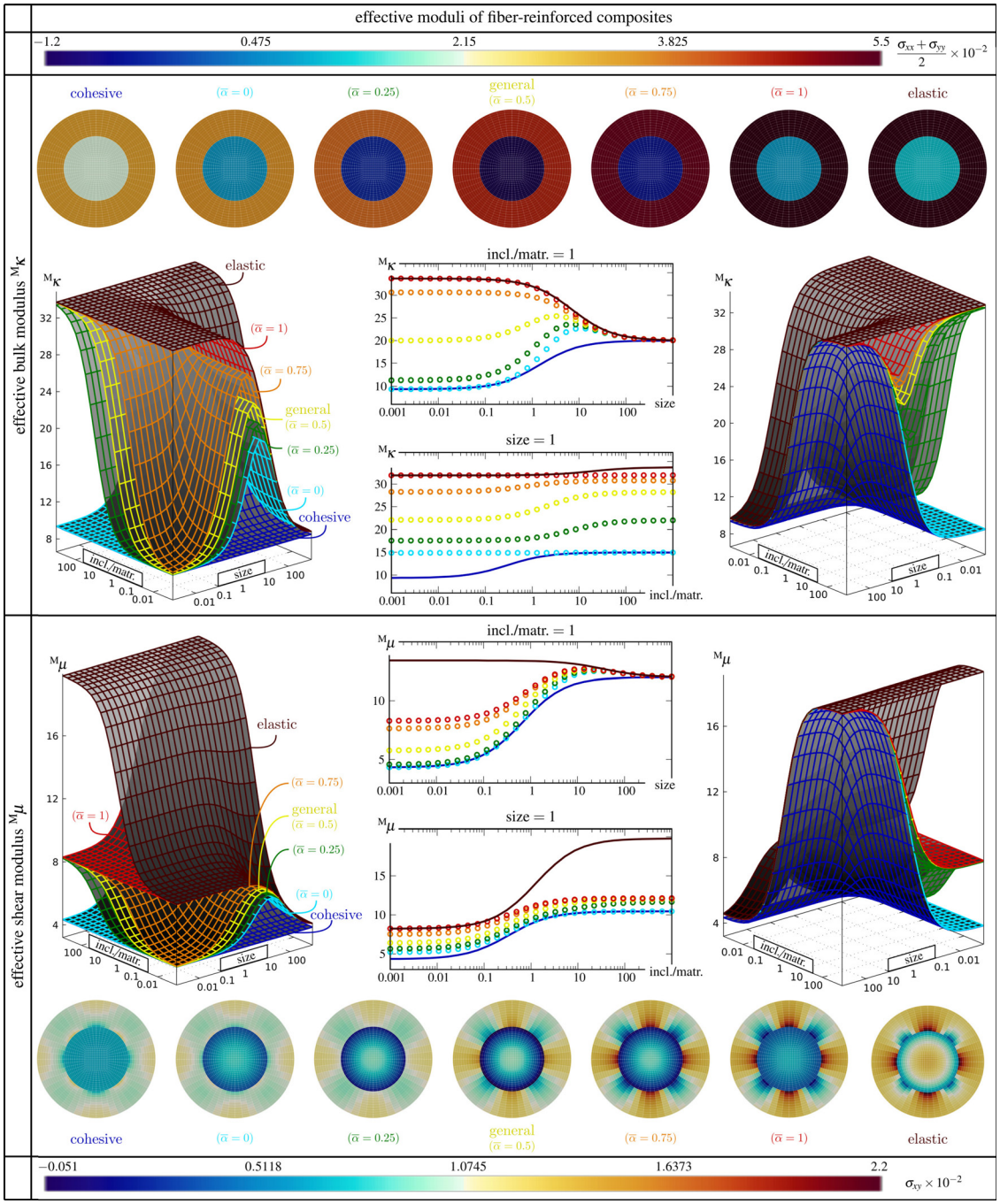

Fig. 16 Comparison of the overall material response obtained from the extended general interface model, general interface model, cohesive interface model, and elastic interface model. The top segment corresponds to the effective bulk modulus and the bottom segment corresponds to the effective shear modulus. The left and right plots in each segment exhibit two different views of the same graph representing the variation of the overall modulus with respect to stiffness ratio as well as RVE size. To better illustrate the variation of the moduli, the two plots at the center depict two cutouts of the side plots; one cut at incl./matr. = 1 with varying size and one cut at size = 1 with varying stiffness ratio.

where $\boldsymbol{t}_0$ is the prescribed traction on the boundary of the body. In view of the weak form Eq. (139), the interface position enters through $\overline{\alpha}$ reflected in $\overline{\boldsymbol{t}} = \{\{\boldsymbol{\sigma}\}\}_{[1-\overline{\alpha}]} \cdot \overline{\boldsymbol{n}}$. As mentioned earlier, the body forces are neglected since we limit our discussion to the microscale problem. The last integral in Eq. (139) acts on the boundary of the domain and is therefore not influenced by the interface at the microscale. This term is standard in all computational homogenization schemes dependent on the boundary condition imposed on the RVE. For further details on implementing boundary conditions in computational homogenization, see, e.g., Saeb et al. [166]. Note that in this context, it proves convenient to use a curvilinear-coordinate-based finite element method [633] since it mimics the underlying geometrical and mathematical concepts for two-dimensional manifolds embedded into a three-dimensional space. Further details of the computational implementation of the scheme are omitted, for the sake of brevity. The analytical solutions here are compared with our computational simulations and an excellent agreement is observed consistently.

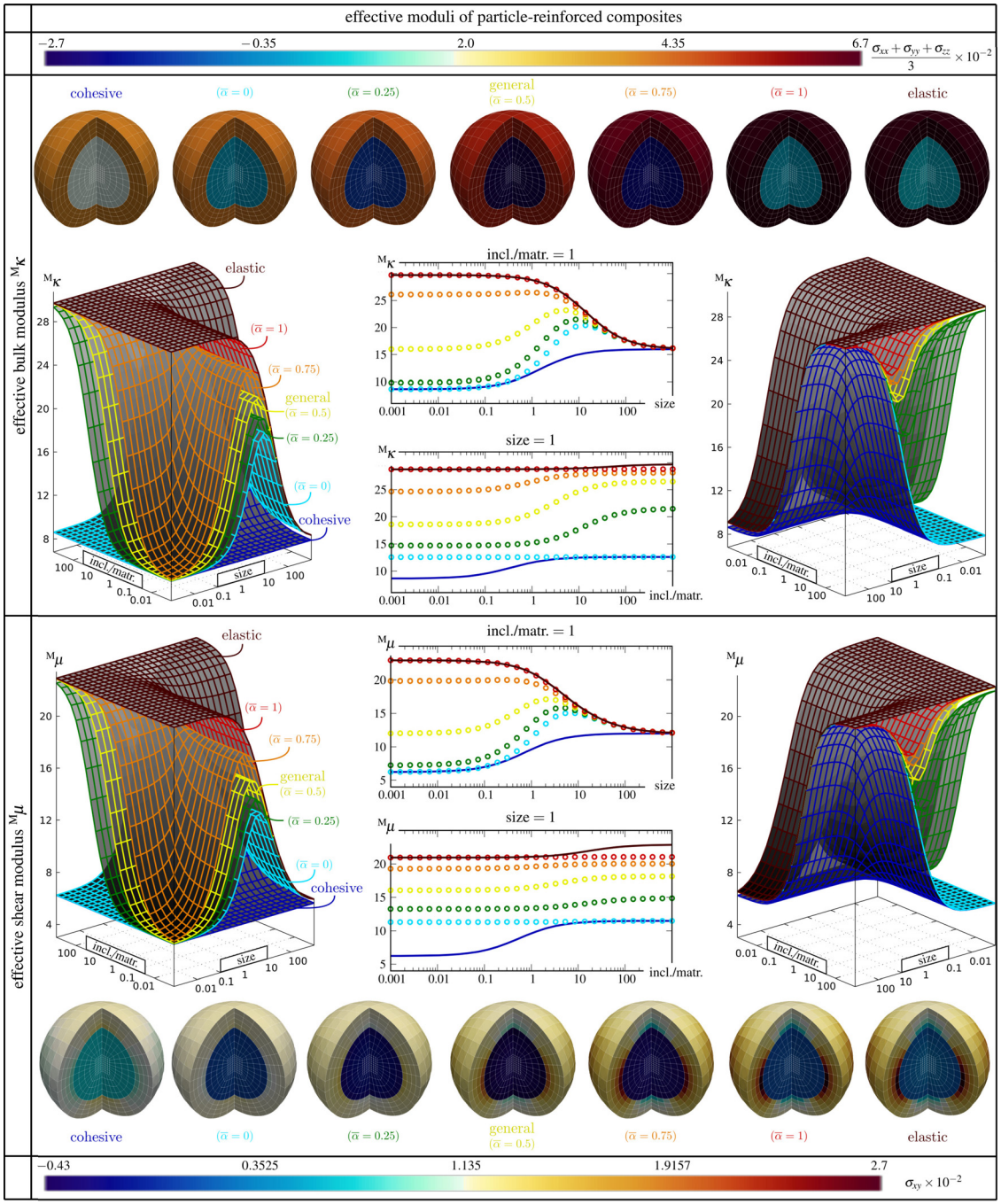

Fig. 17 Comparison of the overall material response obtained from the extended general interface model, general interface model, cohesive interface model, and elastic interface model. The top segment corresponds to the effective bulk modulus and the bottom segment corresponds to the effective shear modulus. The left and right plots in each segment exhibit two different views of the same graph representing the variation of the overall modulus with respect to stiffness ratio as well as RVE size. To better illustrate the variation of the moduli, the two plots at the center depict two cutouts of the side plots; one cut at incl./matr. = 1 with varying size and one cut at size = 1 with varying stiffness ratio.

Figures 16 and 17 provide a thorough comparison between the extended general interface model and the classical interface models for both fiber-reinforced and particle-reinforced composites. The general interface model is recovered via setting $\overline{\alpha} = 0.5$. The elastic interface model can be recovered from our model via setting $\overline{k} \to \infty$ and $\overline{\alpha} = 0.5$, the cohesive interface model can be recovered via setting $\overline{\lambda} = 0$, $\overline{\mu} = 0$ and $\overline{\alpha} = 0.5$. The top segment in each figure corresponds to the effective bulk modulus and the bottom segment corresponds to the effective shear modulus. For the top segments, volumetric expansion is prescribed on the RVE to compute the effective bulk modulus $^{M}\kappa$ and the stress distribution throughout the RVEs is depicted. Pressure-like quantities $[\sigma_{xx} + \sigma_{yy}]/2$ for the two-dimensional case and $[\sigma_{xx} + \sigma_{yy} + \sigma_{zz}]/3$ for the three-dimensional case are illustrated as relevant stress measures. On the other hand, for the bottom segments, simple shear is prescribed on the RVE to compute the effective shear modulus $^{M}\mu$ in which case the shear stress σ_{xy} is provided as a more appropriate quantity. The left and right plots in each segment exhibit two different views of the same graph representing the variation of the overall modulus with respect to stiffness ratio

as well as RVE size. In these graphs, the extended general interface model with various interface positions $\overline{\alpha}$ is compared against the general, cohesive, and elastic interface models. To better understand the surface plots, the two plots at the center depict two sections of the plots on the sides; one at incl./matr. $= 1$ with varying size and one at size $= 1$ with varying stiffness ratio. In these plots, the solutions associated with the extended general interface model are illustrated by points and the solutions obtained by the cohesive and elastic interface models are depicted by lines. Again, note that the extended general interface model at $\overline{\alpha} = 0.5$ coincides with the general interface model. The stress distributions are elaborated for incl./matr. $= 1$ and at size $= 1$. It is observed that the material response due to extended general interfaces is always bounded between the response due to the cohesive interface from below and the elastic interface from above. When $\overline{\alpha} = 0$ the material response is closer to the cohesive interface. Increasing $\overline{\alpha}$ results in a stiffer response where the material behavior tends to approach the elastic interface model. Another interesting observation is that the effective properties obtained by the elastic interface model are identical to the extended general interface model with $\overline{\alpha} = 1$ for compliant inclusions or in other words small stiffness ratios (left surface plots). However, for large stiffness ratios, the elastic interface response overestimates the response due to the extended general interface model with $\overline{\alpha} = 1$ (right surface plots). An opposite trend can be seen between the cohesive interface model and the extended general interface model with $\overline{\alpha} = 0$. For very stiff inclusions, the material renders identical behavior for these two interface models whereas, for compliant inclusions, their responses deviate from each other with the cohesive interface model rendering a more compliant response. This trend can be observed more clearly in the bottom plots at the center in each figure where the effective moduli versus the stiffness ratio are shown at size $= 1$. Looking at the top plots at the center associated with incl./matr. $= 1$, we observe that all the interface models tend to converge at large sizes that is intuitive due to diminishing interface effects. On the other hand, at small sizes, the solutions are distinct from each other. Moving the interface from the inclusion toward the matrix (increasing $\overline{\alpha}$) leads the overall material response to shift from smaller-weaker to smaller-stronger.

5 Conclusion

This paper provides a comprehensive review of homogenization of composites embedding interfaces. First, the historical development of analytical and computational methods available in the literature to model heterogeneous materials have been reviewed; their specific features were extensively discussed and compared in several cases. Next, interphases between the constituents of a heterogeneous medium were introduced. Various interphase types as well different analytical and computational schemes developed to analyze them were extensively studied. This was then followed by an extensive review of canonical interface models developed to capture interphases. Balance equations governing the interface models were revisited and a major conjecture restricting the position of the interface to the midlayer in the general interface model was pointed out. We demonstrated that the assumption of enforcing the interface to coincide with the midlayer is unnecessary and consequently, we developed an extended general interface model where the interface is allowed to occupy any arbitrary position between its bulk neighbors. We extended the homogenization technique to account for this novel interface model and, for the first time, proposed explicit expressions for the effective bulk modulus, effective shear modulus as well as the upper and lower bound on the effective shear modulus of fiber-reinforced and particle-reinforced composites embedding the extended general interface model. We showed that the choice of the interface position can lead to smaller-stronger or smaller-weaker responses, which were usually attributed to the elastic and cohesive interface models, respectively. Our proposed interface model can recover any of the general interface model, elastic interface model, cohesive interface model, and perfect interface model. A finite element framework suitable for the extended general interface model was established. Finally, we presented an exhaustive parametric study through numerical examples and examined the overall behavior of composites. Excellent agreements between the computational and our proposed analytical solutions were observed. The presented examples show the potential of the extended general interface model to understand and design architected materials with extraordinary properties. We believe that this paper deepens our understanding of the interface effects and size-dependent behavior of composites which, in turn, paves the way toward the computational design of metamaterials.

Funding Data

- Scientific and Technological Research Council of Turkey (TÜBITAK) Career Development Program (Grant No. 218M700; Funder ID: 10.13039/501100004410).

Nomenclature

$\mathcal{B}$ = bulk domain
$\mathcal{B}^h$ = discretized bulk domain
$\mathcal{B}^-$ = bulk domain on the minus side of the interface
$\mathcal{B}^+$ = bulk domain on the plus side of the interface
$\mathbb{C}$ = bulk constitutive fourth-order tensor
$\overline{\mathbb{C}}_{\parallel}$ = interface tangential constitutive tensor
$\overline{\boldsymbol{C}}_{\perp}$ = interface orthogonal constitutive tensor
$\underline{\mathrm{Div}}$ = divergence operator
$\overline{\mathrm{Div}}$ = interface divergence operator
$\mathbb{e}$ = Levi-Civita permutation tensor
f = inclusion volume fraction
$\underline{\mathrm{Grad}}$ = gradient operator
$\overline{\mathrm{Grad}}$ = interface gradient operator
$\overline{k}$ = interface orthogonal resistance
I = second-order identity tensor
$\mathcal{I}$ = interface domain
$\mathcal{I}^h$ = discretized interface domain
$\mathcal{I}^+$ = plus side of the interface domain
$\mathcal{I}^-$ = minus side of the interface domain
$\overline{\boldsymbol{I}}$ = second-order interface identity tensor
n = unit normal to the boundary of the bulk
$\tilde{\boldsymbol{n}}$ = unit normal along with the interface
$\overline{\boldsymbol{n}}$ = unit normal across the interface
r_1 = radius of the inclusion
r_2 = radius of the matrix
size = size of the RVE
t = traction field in the bulk
$\overline{\boldsymbol{t}}$ = traction field on the interface
u = displacement field in the bulk
$\boldsymbol{u}^+$ = displacement on the plus side of the interface
$\overline{\boldsymbol{u}}$ = displacement field on the interface
$\boldsymbol{u}^-$ = displacement on the minus side of the interface
$\overline{\boldsymbol{\varepsilon}}$ = strain field on the interface
κ_2 = matrix bulk modulus
λ_2 = matrix first Lamé parameter
μ_2 = matrix shear modulus
$\overline{\mu}$ = shear modulus of the interface
${}^{\mathrm{M}}\mu_{\mathrm{lower}}$ = lower bound on macro shear modulus
${}^{\mathrm{M}}\mu$ = macroscopic shear modulus
M_{κ} = macroscopic bulk modulus
$\overline{\boldsymbol{\sigma}}$ = stress field on the interface
$\boldsymbol{\sigma}^-$ = stress on the minus side of the interface
$\boldsymbol{\sigma}$ = stress field in the bulk
$\boldsymbol{\sigma}^+$ = stress on plus side of the interface
$\overline{\psi}$ = interface free energy density
x = position vector for a point in the domain
$\overline{\alpha}$ = weighted average parameter
δ = Kronecker delta

$\overline{\lambda}$ = first Lamé parameter of the interface
λ = first Lamé parameter of the bulk
λ_1 = inclusion first Lamé parameter
μ = shear modulus of the bulk
μ_1 = inclusion shear modulus
$\boldsymbol{\varepsilon}$ = strain field in the bulk
κ_1 = inclusion bulk modulus
${}^{M}\mu_{\text{upper}}$ = upper bound on macro shear modulus
ψ = bulk free energy density
$\partial\mathcal{B}$ = boundary of $\mathcal{B}$
$\partial\mathcal{B}^{+}$ = boundary of $\mathcal{B}^{+}$
$\partial\mathcal{B}^{-}$ = boundary of $\mathcal{B}^{-}$
∂I = boundary of I
$\{\bullet\}$ = an arbitrary bulk quantity
$\{\bullet\}\overline{\alpha}$ = weighted average of $\{\bullet\}$
$[[\{\bullet\}]]$ = jump of $\{\bullet\}$
${}^{M}\{\bullet\}$ = macroscopic counterpart of $\{\bullet\}$
$\{\bullet\}_{[1-\overline{\alpha}]}$ = a complimentary weighted average of $\{\bullet\}$
$\{\}$ = an arbitrary interface quantity
$\{\{\{\bullet\}\}\}$ = classical average of $\{\bullet\}$

Abbreviations

CCA = composite cylinder assemblage
CSA = composite sphere assemblage
DBC = displacement boundary condition
FEM = finite element method
GSCM = generalized self-consistent method
PBC = periodic boundary condition
PD = problem dimension
RVE = representative volume element
SCM = self-consistent method
TBC = traction boundary condition

Appendix A: Coefficients for Bounds and Estimates on the Shear Modulus of Composites Embedding Extended General Interfaces

This section elaborates on the components of the matrices constructed from the system of equations that were obtained via imposing the boundary and the interface conditions.

A.1 Upper Bound on the Shear Modulus and Effective Shear Modulus for Fiber Composites Embedding Extended General Interfaces

$$
\begin{aligned}
D_{11} &= \frac{\lambda^{(1)} r_1}{\left[2\kappa^{(1)} + \mu^{(1)}\right]}, & D_{21} &= \frac{6\overline{\alpha}\mu^{(1)}\kappa^{(1)} + \overline{k}\left[2\kappa^{(1)} + \mu^{(1)}\right] r_1}{\overline{k}\left[2\kappa^{(1)} + \mu^{(1)}\right]}, & D_{31} &= \frac{6[1-\overline{\alpha}]\overline{\mu}\left[\kappa^{(1)} + \mu^{(1)}\right]}{r_1\left[2\kappa^{(1)} + \mu^{(1)}\right]} \\
D_{12} &= \frac{2\overline{\alpha}\mu^{(1)} + \overline{k} r_1}{\overline{k}}, & D_{22} &= \frac{2\overline{\alpha}\mu^{(1)} + \overline{k} r_1}{\overline{k}}, & D_{32} &= \frac{2[1-\overline{\alpha}]\overline{\mu} - 2\mu^{(1)} r_1}{r_1} \\
D_{13} &= \frac{-\lambda_2 r_1}{\left[2\kappa^{(2)} + \mu^{(2)}\right]}, & D_{23} &= \frac{6[1-\overline{\alpha}]\kappa^{(2)}\mu^{(2)} - \overline{k}\left[2\kappa^{(2)} + \mu^{(2)}\right] r_1}{\overline{k}\left[2\kappa^{(2)} + \mu^{(2)}\right]}, & D_{33} &= \frac{6\overline{\alpha}\overline{\mu}\left[\kappa^{(2)} + \mu^{(2)}\right]}{r_1\left[2\kappa^{(2)} + \mu^{(2)}\right]} \\
D_{14} &= \frac{2[1-\overline{\alpha}]\mu^{(2)} - \overline{k} r_1}{\overline{k}}, & D_{24} &= \frac{2[1-\overline{\alpha}]\mu^{(2)} - \overline{k} r_1}{\overline{k}}, & D_{34} &= \frac{2\overline{\alpha}\overline{\mu} + 2\mu^{(2)} r_1}{r_1} \\
D_{15} &= \frac{6[1-\overline{\alpha}]\mu^{(2)} + \overline{k} r_1}{\overline{k}}, & D_{25} &= \frac{-6[1-\overline{\alpha}]\mu^{(2)} - \overline{k} r_1}{\overline{k}}, & D_{35} &= \frac{6\overline{\alpha}\overline{\mu} + 6\mu^{(2)} r_1}{r_1} \\
D_{16} &= \frac{-4[1-\overline{\alpha}]\kappa^{(2)}\mu^{(2)} - \overline{k} r_1\left[\kappa^{(2)} + \mu^{(2)}\right]}{\mu^{(2)}\overline{k}}, & D_{26} &= \frac{2[1-\overline{\alpha}]\kappa^{(2)} - \overline{k} r_1}{\overline{k}}, & D_{36} &= \frac{-2\overline{\alpha}\overline{\mu}\lambda_2 - 4\kappa^{(2)}\mu^{(2)} r_1}{\mu^{(2)} r_1} \\
D_{41} &= -\frac{-12[1-\overline{\alpha}]\overline{\mu}\left[\kappa^{(1)} + \mu^{(1)}\right] - 6\mu^{(1)}\kappa^{(1)} r_1}{r_1\left[2\kappa^{(1)} + \mu^{(1)}\right]}, & D_{51} &= 0, & D_{61} &= 0 \\
D_{42} &= \frac{-4[1-\overline{\alpha}]\overline{\mu} - 2\mu^{(1)} r_1}{r_1}, & D_{52} &= 0, & D_{62} &= 0 \\
D_{43} &= \frac{-12\overline{\alpha}\overline{\mu}\left[\kappa^{(2)} + \mu^{(2)}\right] + 6\mu^{(2)}\kappa^{(2)} r_1}{r_1\left[2\kappa^{(2)} + \mu^{(2)}\right]}, & D_{53} &= \frac{\lambda_2}{f\left[2\kappa^{(2)} + \mu^{(2)}\right]}, & D_{63} &= \frac{1}{f} \\
D_{44} &= \frac{-4\overline{\alpha}\overline{\mu} + 2\mu^{(2)} r_1}{r_1}, & D_{54} &= 1 & D_{64} &= 1 \\
D_{45} &= \frac{-12\overline{\alpha}\overline{\mu} - 6\mu^{(2)} r_1}{r_1}, & D_{55} &= -f^2, & D_{65} &= f^2 \\
D_{46} &= \frac{4\overline{\alpha}\overline{\mu}\lambda_2 + 2\kappa^{(2)}\mu^{(2)} r_1}{\mu^{(2)} r_1}, & D_{56} &= \frac{f\left[\kappa^{(2)} + \mu^{(2)}\right]}{\mu^{(2)}}, & D_{66} &= f
\end{aligned}
\tag{A1}
$$

A.2 Lower Bound on the Shear Modulus for Fiber Composites Embedding Extended General Interfaces

$$
\begin{aligned}
E_{11} &= \frac{\lambda^{(1)} r_1}{\left[2\kappa^{(1)} + \mu^{(1)}\right]}, & E_{21} &= \frac{6\overline{\alpha}\mu^{(1)}\kappa^{(1)} + \overline{k}\left[2\kappa^{(1)} + \mu^{(1)}\right] r_1}{\overline{k}\left[2\kappa^{(1)} + \mu^{(1)}\right]}, & E_{31} &= \frac{6[1-\overline{\alpha}]\overline{\mu}\left[\kappa^{(1)} + \mu^{(1)}\right]}{r_1\left[2\kappa^{(1)} + \mu^{(1)}\right]} \\
E_{12} &= \frac{2\overline{\alpha}\mu^{(1)} + \overline{k} r_1}{\overline{k}}, & E_{22} &= \frac{2\overline{\alpha}\mu^{(1)} + \overline{k} r_1}{\overline{k}}, & E_{32} &= \frac{2[1-\overline{\alpha}]\overline{\mu} - 2\mu^{(1)} r_1}{r_1} \\
E_{13} &= \frac{-\lambda_2 r_1}{\left[2\kappa^{(2)} + \mu^{(2)}\right]}, & E_{23} &= \frac{6[1-\overline{\alpha}]\kappa^{(2)}\mu^{(2)} - \overline{k}\left[2\kappa^{(2)} + \mu^{(2)}\right] r_1}{\overline{k}\left[2\kappa^{(2)} + \mu^{(2)}\right]} & E_{33} &= \frac{6\overline{\alpha}\overline{\mu}\left[\kappa^{(2)} + \mu^{(2)}\right]}{r_1\left[2\kappa^{(2)} + \mu^{(2)}\right]}, \\
E_{14} &= \frac{2[1-\overline{\alpha}]\mu^{(2)} - \overline{k} r_1}{\overline{k}}, & E_{24} &= \frac{2[1-\overline{\alpha}]\mu^{(2)} - \overline{k} r_1}{\overline{k}}, & E_{34} &= \frac{2\overline{\alpha}\overline{\mu} + 2\mu^{(2)} r_1}{r_1} \\
E_{15} &= \frac{6[1-\overline{\alpha}]\mu^{(2)} + \overline{k} r_1}{\overline{k}}, & E_{25} &= \frac{-6[1-\overline{\alpha}]\mu^{(2)} - \overline{k} r_1}{\overline{k}}, & E_{35} &= \frac{6\overline{\alpha}\overline{\mu} + 6\mu^{(2)} r_1}{r_1} \\
E_{16} &= \frac{-4[1-\overline{\alpha}]\kappa^{(2)}\mu^{(2)} - \overline{k} r_1\left[\kappa^{(2)} + \mu^{(2)}\right]}{\mu^{(2)}\overline{k}}, & E_{26} &= \frac{2[1-\overline{\alpha}]\kappa^{(2)} - \overline{k} r_1}{\overline{k}}, & E_{36} &= \frac{-2\overline{\alpha}\overline{\mu}\lambda_2 - 4\kappa^{(2)}\mu^{(2)} r_1}{\mu^{(2)} r_1} \\
E_{41} &= -\frac{-12[1-\overline{\alpha}]\overline{\mu}\left[\kappa^{(1)} + \mu^{(1)}\right] - 6\mu^{(1)}\kappa^{(1)} r_1}{r_1\left[2\kappa^{(1)} + \mu^{(1)}\right]}, & E_{51} &= 0, & E_{61} &= 0 \\
E_{42} &= \frac{-4[1-\overline{\alpha}]\overline{\mu} - 2\mu^{(1)} r_1}{r_1}, & E_{52} &= 0, & E_{62} &= 0 \\
E_{43} &= \frac{-12\overline{\alpha}\overline{\mu}\left[\kappa^{(2)} + \mu^{(2)}\right] + 6\mu^{(2)}\kappa^{(2)} r_1}{r_1\left[2\kappa^{(2)} + \mu^{(2)}\right]}, & E_{53} &= 0, & E_{63} &= \frac{6\kappa^{(2)}\mu^{(2)}}{f\left[2\kappa^{(2)} + \mu^{(2)}\right]} \\
E_{44} &= \frac{-4\overline{\alpha}\overline{\mu} + 2\mu^{(2)} r_1}{r_1}, & E_{54} &= 2\mu^{(2)}, & E_{64} &= 2\mu^{(2)} \\
E_{45} &= \frac{-12\overline{\alpha}\overline{\mu} - 6\mu^{(2)} r_1}{r_1}, & E_{55} &= 6\mu^{(2)} f^2, & E_{65} &= -6\mu^{(2)} f^2 \\
E_{46} &= \frac{4\overline{\alpha}\overline{\mu}\lambda_2 + 2\kappa^{(2)}\mu^{(2)} r_1}{\mu^{(2)} r_1}, & E_{56} &= -4\kappa^{(2)} f, & E_{66} &= 2\kappa^{(2)} f
\end{aligned}
\tag{A2}
$$

A.3 Upper Bound on the Shear Modulus and Effective Shear Modulus for Particulate Composites Embedding Extended General Interfaces

$$
\begin{aligned}
P_{11} &= \frac{2\overline{\alpha}\mu^{(1)} + \overline{k}r_1}{\overline{k}}, & P_{12} &= \frac{\left[\overline{\alpha}\mu^{(1)} - \overline{k}r_1\right]\left[3\kappa^{(1)} - 2\mu^{(1)}\right]}{\overline{k}\mu^{(1)}} \\
P_{13} &= \frac{2[1-\overline{\alpha}]\mu^{(2)} - \overline{k}r_1}{\overline{k}}, & P_{14} &= \frac{\left[3\kappa^{(2)} - 2\mu^{(2)}\right]\left[[1-\overline{\alpha}]\mu^{(2)} + \overline{k}r_1\right]}{\overline{k}\mu^{(2)}} \\
P_{15} &= \frac{-24[1-\overline{\alpha}]\mu^{(2)} - 3\overline{k}r_1}{\overline{k}}, & P_{16} &= \frac{-2[1-\overline{\alpha}]\mu^{(2)}\left[9\kappa^{(2)} + 4\mu^{(2)}\right] - 3\overline{k}r_1\left[\kappa^{(2)} + \mu^{(2)}\right]}{\overline{k}\mu^{(2)}} \\
P_{21} &= \frac{2\overline{\alpha}\mu^{(1)} + \overline{k}r_1}{\overline{k}}, & P_{22} &= \frac{-2\overline{\alpha}\mu^{(1)}\left[24\kappa^{(1)} + 5\mu^{(1)}\right] - \overline{k}r_1\left[15\kappa^{(1)} + 11\mu^{(1)}\right]}{3\overline{k}\mu^{(1)}} \\
P_{23} &= \frac{2[1-\overline{\alpha}]\mu^{(2)} - \overline{k}r_1}{\overline{k}}, & P_{24} &= \frac{-2[1-\overline{\alpha}]\mu^{(2)}\left[24\kappa^{(2)} + 5\mu^{(2)}\right] + \overline{k}r_1\left[15\kappa^{(2)} + 11\mu^{(2)}\right]}{3\overline{k}\mu^{(2)}} \\
P_{25} &= \frac{16[1-\overline{\alpha}]\mu^{(2)} + 2\overline{k}r_1}{\overline{k}}, & P_{26} &= \frac{6[1-\overline{\alpha}]\kappa^{(2)} - 2\overline{k}r_1}{\overline{k}} \\
P_{31} &= \frac{2[1-\overline{\alpha}]\left[\overline{\lambda} + \overline{\mu}\right] - 2\mu^{(1)}r_1}{r_1}, & P_{32} &= \frac{-2[1-\overline{\alpha}]\left[\overline{\lambda} + \overline{\mu}\right]\left[9\kappa^{(1)} + 15\mu^{(1)}\right] - \mu^{(1)}r_1\left[3\kappa^{(1)} - 2\mu^{(1)}\right]}{\mu^{(1)}r_1} \\
P_{33} &= \frac{2\overline{\alpha}\left[\overline{\lambda} + \overline{\mu}\right] + 2\mu^{(2)}r_1}{r_1}, & P_{34} &= \frac{-2\overline{\alpha}\left[\overline{\lambda} + \overline{\mu}\right]\left[9\kappa^{(2)} + 15\mu^{(2)}\right] + \mu^{(2)}r_1\left[3\kappa^{(2)} - 2\mu^{(2)}\right]}{\mu^{(2)}r_1} \\
P_{35} &= -\frac{24\left[\overline{\alpha}\left[\overline{\lambda} + \overline{\mu}\right] + \mu^{(2)}r_1\right]}{r_1}, & P_{36} &= -\frac{2\left[6\overline{\alpha}\kappa^{(2)}\left[\overline{\lambda} + \overline{\mu}\right] + \mu^{(2)}r_1\left[9\kappa^{(2)} + 4\mu^{(2)}\right]\right]}{\mu^{(2)}r_1} \\
P_{41} &= \frac{-2[1-\overline{\alpha}]\left[\overline{\lambda} + 3\overline{\mu}\right] - 2\mu^{(1)}r_1}{r_1}, & P_{42} &= \frac{2[1-\overline{\alpha}]\kappa^{(1)}\left[27\overline{\lambda} + 57\overline{\mu}\right] + 2[1-\overline{\alpha}]\mu^{(1)}\left[45\overline{\lambda} + 67\overline{\mu}\right] + 2\mu^{(1)}r_1\left[24\kappa^{(1)} + 5\mu^{(1)}\right]}{3\mu^{(1)}r_1} \\
P_{43} &= \frac{-2\overline{\alpha}\left[\overline{\lambda} + 3\overline{\mu}\right] + 2\mu^{(2)}r_1}{r_1}, & P_{44} &= \frac{2\overline{\alpha}\kappa^{(2)}\left[27\overline{\lambda} + 57\overline{\mu}\right] + 2\overline{\alpha}\mu^{(2)}\left[45\overline{\lambda} + 67\overline{\mu}\right] - 2\mu^{(2)}r_1\left[24\kappa^{(2)} + 5\mu^{(2)}\right]}{3\mu^{(2)}r_1} \\
P_{45} &= \frac{8\left[\overline{\alpha}\left[3\overline{\lambda} + 4\overline{\mu}\right] + 2\mu^{(2)}r_1\right]}{r_1}, & P_{46} &= \frac{2\left[6\overline{\alpha}\kappa^{(2)}\left[\overline{\lambda} + \overline{\mu}\right] - 4\overline{\alpha}\mu^{(2)}\overline{\mu} + 3\kappa^{(2)}\mu^{(2)}r_1\right]}{\mu^{(2)}r_1} \\
P_{51} &= 0, & P_{52} &= 0 \\
P_{53} &= 1, & P_{54} &= \left[2 - 3\frac{\kappa^{(2)}}{\mu^{(2)}}\right]f^{-2/3} \\
P_{55} &= 3f^{5/3}, & P_{56} &= \left[3 + \frac{3\kappa^{(2)}}{\mu^{(2)}}\right]f \\
P_{61} &= 0, & P_{62} &= 0 \\
P_{63} &= 1, & P_{64} &= -\left[\frac{11}{3} + 5\frac{\kappa^{(2)}}{\mu^{(2)}}\right]f^{-2/3} \\
P_{65} &= -2f^{5/3}, & P_{66} &= 2f
\end{aligned}
\tag{A3}
$$

A.4 Lower Bound on the Shear Modulus for Particulate Composites Embedding Extended General Interfaces

$$
\begin{aligned}
Q_{11} &= \frac{2\overline{\alpha}\mu^{(1)} + \overline{k}r_1}{\overline{k}}, & Q_{12} &= \frac{\left[\overline{\alpha}\mu^{(1)} - \overline{k}r_1\right]\left[3\kappa^{(1)} - 2\mu^{(1)}\right]}{\overline{k}\mu^{(1)}} \\
Q_{13} &= \frac{2[1-\overline{\alpha}]\mu^{(2)} - \overline{k}r_1}{\overline{k}}, & Q_{14} &= \frac{\left[3\kappa^{(2)} - 2\mu^{(2)}\right]\left[[1-\overline{\alpha}]\mu^{(2)} + \overline{k}r_1\right]}{\overline{k}\mu^{(2)}} \\
Q_{15} &= \frac{-24[1-\overline{\alpha}]\mu^{(2)} - 3\overline{k}r_1}{\overline{k}}, & Q_{16} &= \frac{-2[1-\overline{\alpha}]\mu^{(2)}\left[9\kappa^{(2)} + 4\mu^{(2)}\right] - 3\overline{k}r_1\left[\kappa^{(2)} + \mu^{(2)}\right]}{\overline{k}\mu^{(2)}} \\
Q_{21} &= \frac{2\overline{\alpha}\mu^{(1)} + \overline{k}r_1}{\overline{k}}, & Q_{22} &= \frac{-2\overline{\alpha}\mu^{(1)}\left[24\kappa^{(1)} + 5\mu^{(1)}\right] - \overline{k}r_1\left[15\kappa^{(1)} + 11\mu^{(1)}\right]}{3\overline{k}\mu^{(1)}} \\
Q_{23} &= \frac{2[1-\overline{\alpha}]\mu^{(2)} - \overline{k}r_1}{\overline{k}}, & Q_{24} &= \frac{-2[1-\overline{\alpha}]\mu^{(2)}\left[24\kappa^{(2)} + 5\mu^{(2)}\right] + \overline{k}r_1\left[15\kappa^{(2)} + 11\mu^{(2)}\right]}{3\overline{k}\mu^{(2)}} \\
Q_{25} &= \frac{16[1-\overline{\alpha}]\mu^{(2)} + 2\overline{k}r_1}{\overline{k}}, & Q_{26} &= \frac{6[1-\overline{\alpha}]\kappa^{(2)} - 2\overline{k}r_1}{\overline{k}} \\
Q_{31} &= \frac{2[1-\overline{\alpha}]\left[\overline{\lambda} + \overline{\mu}\right] - 2\mu^{(1)}r_1}{r_1}, & Q_{32} &= \frac{-2[1-\overline{\alpha}]\left[\overline{\lambda} + \overline{\mu}\right]\left[9\kappa^{(1)} + 15\mu^{(1)}\right] - \mu^{(1)}r_1\left[3\kappa^{(1)} - 2\mu^{(1)}\right]}{\mu^{(1)}r_1} \\
Q_{33} &= \frac{2\overline{\alpha}\left[\overline{\lambda} + \overline{\mu}\right] + 2\mu^{(2)}r_1}{r_1}, & Q_{34} &= \frac{-2\overline{\alpha}\left[\overline{\lambda} + \overline{\mu}\right]\left[9\kappa^{(2)} + 15\mu^{(2)}\right] + \mu^{(2)}r_1\left[3\kappa^{(2)} - 2\mu^{(2)}\right]}{\mu^{(2)}r_1} \\
Q_{35} &= -\frac{24\left[\overline{\alpha}\left[\overline{\lambda} + \overline{\mu}\right] + \mu^{(2)}r_1\right]}{r_1}, & Q_{36} &= -\frac{2\left[6\overline{\alpha}\kappa^{(2)}\left[\overline{\lambda} + \overline{\mu}\right] + \mu^{(2)}r_1\left[9\kappa^{(2)} + 4\mu^{(2)}\right]\right]}{\mu^{(2)}r_1} \\
Q_{41} &= \frac{-2[1-\overline{\alpha}]\left[\overline{\lambda} + 3\overline{\mu}\right] - 2\mu^{(1)}r_1}{r_1}, & Q_{42} &= \frac{2[1-\overline{\alpha}]\kappa^{(1)}\left[27\overline{\lambda} + 57\overline{\mu}\right] + 2[1-\overline{\alpha}]\mu^{(1)}\left[45\overline{\lambda} + 67\overline{\mu}\right] + 2\mu^{(1)}r_1\left[24\kappa^{(1)} + 5\mu^{(1)}\right]}{3\mu^{(1)}r_1} \\
Q_{43} &= \frac{-2\overline{\alpha}\left[\overline{\lambda} + 3\overline{\mu}\right] + 2\mu^{(2)}r_1}{r_1}, & Q_{44} &= \frac{2\overline{\alpha}\kappa^{(2)}\left[27\overline{\lambda} + 57\overline{\mu}\right] + 2\overline{\alpha}\mu^{(2)}\left[45\overline{\lambda} + 67\overline{\mu}\right] - 2\mu^{(2)}r_1\left[24\kappa^{(2)} + 5\mu^{(2)}\right]}{3\mu^{(2)}r_1} \\
Q_{45} &= \frac{8\left[\overline{\alpha}\left[3\overline{\lambda} + 4\overline{\mu}\right] + 2\mu^{(2)}r_1\right]}{r_1}, & Q_{46} &= \frac{2\left[6\overline{\alpha}\kappa^{(2)}\left[\overline{\lambda} + \overline{\mu}\right] - 4\overline{\alpha}\mu^{(2)}\overline{\mu} + 3\kappa^{(2)}\mu^{(2)}r_1\right]}{\mu^{(2)}r_1} \\
Q_{51} &= 0, & Q_{52} &= 0 \\
Q_{53} &= 2\mu^{(2)}, & Q_{54} &= \left[3\kappa^{(2)} - 2\mu^{(2)}\right]f^{-2/3} \\
Q_{55} &= -24\mu^{(2)}f^{5/3}, & Q_{56} &= -2\left[9\kappa^{(2)} + 4\mu^{(2)}\right]f \\
Q_{61} &= 0, & Q_{62} &= 0 \\
Q_{63} &= 2\mu^{(2)}, & Q_{64} &= -\frac{2}{3}\left[24\kappa^{(2)} + 5\mu^{(2)}\right]f^{-2/3} \\
Q_{65} &= 16\mu^{(2)}f^{5/3}, & Q_{66} &= 6\kappa^{(2)}f
\end{aligned}
\tag{A4}
$$

Appendix B: Coefficients for Bounds and Estimates on the Shear Modulus of Composites Embedding General Interfaces

In this section, the coefficient matrices corresponding to the bounds and estimates on the shear modulus of composites embedding general interfaces are presented.

B.1 Upper Bound on the Shear Modulus and Effective Shear Modulus for Fiber Composites Embedding General Interfaces

$$
\begin{aligned}
D_{11} &= \frac{\lambda^{(1)} r_1}{\left[2\kappa^{(1)} + \mu^{(1)}\right]}, & D_{21} &= \frac{3\mu^{(1)}\kappa^{(1)} + \overline{k}\left[2\kappa^{(1)} + \mu^{(1)}\right] r_1}{\overline{k}\left[2\kappa^{(1)} + \mu^{(1)}\right]}, & D_{31} &= \frac{3\overline{\mu}\left[\kappa^{(1)} + \mu^{(1)}\right]}{r_1\left[2\kappa^{(1)} + \mu^{(1)}\right]} \\
D_{12} &= \frac{\mu^{(1)} + \overline{k} r_1}{\overline{k}}, & D_{22} &= \frac{\mu^{(1)} + \overline{k} r_1}{\overline{k}}, & D_{32} &= \frac{\overline{\mu} - 2\mu^{(1)} r_1}{r_1} \\
D_{13} &= \frac{-\lambda_2 r_1}{\left[2\kappa^{(2)} + \mu^{(2)}\right]}, & D_{23} &= \frac{3\kappa^{(2)}\mu^{(2)} - \overline{k}\left[2\kappa^{(2)} + \mu^{(2)}\right] r_1}{\overline{k}\left[2\kappa^{(2)} + \mu^{(2)}\right]}, & D_{33} &= \frac{3\overline{\mu}\left[\kappa^{(2)} + \mu^{(2)}\right]}{r_1\left[2\kappa^{(2)} + \mu^{(2)}\right]} \\
D_{14} &= \frac{\mu^{(2)} - \overline{k} r_1}{\overline{k}}, & D_{24} &= \frac{\mu^{(2)} - \overline{k} r_1}{\overline{k}}, & D_{34} &= \frac{\overline{\mu} + 2\mu^{(2)} r_1}{r_1} \\
D_{15} &= \frac{3\mu^{(2)} + \overline{k} r_1}{\overline{k}}, & D_{25} &= \frac{-3\mu^{(2)} - \overline{k} r_1}{\overline{k}}, & D_{35} &= \frac{3\overline{\mu} + 6\mu^{(2)} r_1}{r_1} \\
D_{16} &= \frac{-2\kappa^{(2)}\mu^{(2)} - \overline{k} r_1\left[\kappa^{(2)} + \mu^{(2)}\right]}{\mu^{(2)}\overline{k}}, & D_{26} &= \frac{\kappa^{(2)} - \overline{k} r_1}{\overline{k}}, & D_{36} &= \frac{-\overline{\mu}\lambda_2 - 4\kappa^{(2)}\mu^{(2)} r_1}{\mu^{(2)} r_1} \\
D_{41} &= -\frac{-6\overline{\mu}\left[\kappa^{(1)} + \mu^{(1)}\right] - 6\mu^{(1)}\kappa^{(1)} r_1}{r_1\left[2\kappa^{(1)} + \mu^{(1)}\right]}, & D_{51} &= 0, & D_{61} &= 0 \\
D_{42} &= \frac{-2\overline{\mu} - 2\mu^{(1)} r_1}{r_1}, & D_{52} &= 0, & D_{62} &= 0 \\
D_{43} &= \frac{-6\overline{\mu}\left[\kappa^{(2)} + \mu^{(2)}\right] + 6\mu^{(2)}\kappa^{(2)} r_1}{r_1\left[2\kappa^{(2)} + \mu^{(2)}\right]}, & D_{53} &= \frac{\lambda_2}{f\left[2\kappa^{(2)} + \mu^{(2)}\right]}, & D_{63} &= \frac{1}{f} \\
D_{44} &= \frac{-2\overline{\mu} + 2\mu^{(2)} r_1}{r_1}, & D_{54} &= 1, & D_{64} &= 1 \\
D_{45} &= \frac{-6\overline{\mu} - 6\mu^{(2)} r_1}{r_1}, & D_{55} &= -f^2, & D_{65} &= f^2 \\
D_{46} &= \frac{2\overline{\mu}\lambda_2 + 2\kappa^{(2)}\mu^{(2)} r_1}{\mu^{(2)} r_1}, & D_{56} &= \frac{f\left[\kappa^{(2)} + \mu^{(2)}\right]}{\mu^{(2)}}, & D_{66} &= f
\end{aligned}
\tag{B1}
$$

B.2 Lower Bound on the Shear Modulus for Fiber Composites Embedding General Interfaces

$$
\begin{aligned}
E_{11} &= \frac{\lambda^{(1)} r_1}{\left[2\kappa^{(1)} + \mu^{(1)}\right]}, & E_{21} &= \frac{3\mu^{(1)}\kappa^{(1)} + \overline{k}\left[2\kappa^{(1)} + \mu^{(1)}\right] r_1}{\overline{k}\left[2\kappa^{(1)} + \mu^{(1)}\right]}, & E_{31} &= \frac{3\overline{\mu}\left[\kappa^{(1)} + \mu^{(1)}\right]}{r_1\left[2\kappa^{(1)} + \mu^{(1)}\right]} \\
E_{12} &= \frac{\mu^{(1)} + \overline{k} r_1}{\overline{k}}, & E_{22} &= \frac{\mu^{(1)} + \overline{k} r_1}{\overline{k}}, & E_{32} &= \frac{\overline{\mu} - 2\mu^{(1)} r_1}{r_1} \\
E_{13} &= \frac{-\lambda_2 r_1}{\left[2\kappa^{(2)} + \mu^{(2)}\right]}, & E_{23} &= \frac{3\kappa^{(2)}\mu^{(2)} - \overline{k}\left[2\kappa^{(2)} + \mu^{(2)}\right] r_1}{\overline{k}\left[2\kappa^{(2)} + \mu^{(2)}\right]}, & E_{33} &= \frac{3\overline{\mu}\left[\kappa^{(2)} + \mu^{(2)}\right]}{r_1\left[2\kappa^{(2)} + \mu^{(2)}\right]} \\
E_{14} &= \frac{\mu^{(2)} - \overline{k} r_1}{\overline{k}}, & E_{24} &= \frac{\mu^{(2)} - \overline{k} r_1}{\overline{k}}, & E_{34} &= \frac{\overline{\mu} + 2\mu^{(2)} r_1}{r_1} \\
E_{15} &= \frac{3\mu^{(2)} + \overline{k} r_1}{\overline{k}}, & E_{25} &= \frac{-3\mu^{(2)} - \overline{k} r_1}{\overline{k}}, & E_{35} &= \frac{3\overline{\mu} + 6\mu^{(2)} r_1}{r_1} \\
E_{16} &= \frac{-2\kappa^{(2)}\mu^{(2)} - \overline{k} r_1\left[\kappa^{(2)} + \mu^{(2)}\right]}{\mu^{(2)}\overline{k}}, & E_{26} &= \frac{\kappa^{(2)} - \overline{k} r_1}{\overline{k}}, & E_{36} &= \frac{-\overline{\mu}\lambda_2 - 4\kappa^{(2)}\mu^{(2)} r_1}{\mu^{(2)} r_1} \\
E_{41} &= -\frac{-6\overline{\mu}\left[\kappa^{(1)} + \mu^{(1)}\right] - 6\mu^{(1)}\kappa^{(1)} r_1}{r_1\left[2\kappa^{(1)} + \mu^{(1)}\right]}, & E_{51} &= 0, & E_{61} &= 0 \\
E_{42} &= \frac{-2\overline{\mu} - 2\mu^{(1)} r_1}{r_1}, & E_{52} &= 0, & E_{62} &= 0 \\
E_{43} &= \frac{-6\overline{\mu}\left[\kappa^{(2)} + \mu^{(2)}\right] + 6\mu^{(2)}\kappa^{(2)} r_1}{r_1\left[2\kappa^{(2)} + \mu^{(2)}\right]}, & E_{53} &= 0, & E_{63} &= \frac{6\kappa^{(2)}\mu^{(2)}}{f\left[2\kappa^{(2)} + \mu^{(2)}\right]} \\
E_{44} &= \frac{-2\overline{\mu} + 2\mu^{(2)} r_1}{r_1}, & E_{54} &= 2\mu^{(2)}, & E_{64} &= 2\mu^{(2)} \\
E_{45} &= \frac{-6\overline{\mu} - 6\mu^{(2)} r_1}{r_1}, & E_{55} &= 6\mu^{(2)} f^2, & E_{65} &= -6\mu^{(2)} f^2 \\
E_{46} &= \frac{2\overline{\mu}\lambda_2 + 2\kappa^{(2)}\mu^{(2)} r_1}{\mu^{(2)} r_1}, & E_{56} &= -4\kappa^{(2)} f, & E_{66} &= 2\kappa^{(2)} f
\end{aligned}
\tag{B2}
$$

B.3 Upper Bound on the Shear Modulus and Effective Shear Modulus for Particulate Composites Embedding General Interfaces

$$
\begin{aligned}
P_{11} &= \frac{\mu^{(1)} + \overline{k} r_1}{\overline{k}}, & P_{12} &= \frac{\left[\frac{1}{2}\mu^{(1)} - \overline{k} r_1\right]\left[3\kappa^{(1)} - 2\mu^{(1)}\right]}{\overline{k}\mu^{(1)}} \\
P_{13} &= \frac{\mu^{(2)} - \overline{k} r_1}{\overline{k}}, & P_{14} &= \frac{\left[3\kappa^{(2)} - 2\mu^{(2)}\right]\left[\frac{1}{2}\mu^{(2)} + \overline{k} r_1\right]}{\overline{k}\mu^{(2)}} \\
P_{15} &= \frac{-12\mu^{(2)} - 3\overline{k} r_1}{\overline{k}}, & P_{16} &= \frac{-\mu^{(2)}\left[9\kappa^{(2)} + 4\mu^{(2)}\right] - 3\overline{k} r_1\left[\kappa^{(2)} + \mu^{(2)}\right]}{\overline{k}\mu^{(2)}} \\
P_{21} &= \frac{\mu^{(1)} + \overline{k} r_1}{\overline{k}}, & P_{22} &= \frac{-\mu^{(1)}\left[24\kappa^{(1)} + 5\mu^{(1)}\right] - \overline{k} r_1\left[15\kappa^{(1)} + 11\mu^{(1)}\right]}{3\overline{k}\mu^{(1)}} \\
P_{23} &= \frac{\mu^{(2)} - \overline{k} r_1}{\overline{k}}, & P_{24} &= \frac{-\mu^{(2)}\left[24\kappa^{(2)} + 5\mu^{(2)}\right] + \overline{k} r_1\left[15\kappa^{(2)} + 11\mu^{(2)}\right]}{3\overline{k}\mu^{(2)}} \\
P_{25} &= \frac{8\mu^{(2)} + 2\overline{k} r_1}{\overline{k}}, & P_{26} &= \frac{3\kappa^{(2)} - 2\overline{k} r_1}{\overline{k}} \\
P_{31} &= \frac{\left[\overline{\lambda} + \overline{\mu}\right] - 2\mu^{(1)} r_1}{r_1}, & P_{32} &= \frac{-\left[\overline{\lambda} + \overline{\mu}\right]\left[9\kappa^{(1)} + 15\mu^{(1)}\right] - \mu^{(1)} r_1\left[3\kappa^{(1)} - 2\mu^{(1)}\right]}{\mu^{(1)} r_1} \\
P_{33} &= \frac{\left[\overline{\lambda} + \overline{\mu}\right] + 2\mu^{(2)} r_1}{r_1}, & P_{34} &= \frac{-\left[\overline{\lambda} + \overline{\mu}\right]\left[9\kappa^{(2)} + 15\mu^{(2)}\right] + \mu^{(2)} r_1\left[3\kappa^{(2)} - 2\mu^{(2)}\right]}{\mu^{(2)} r_1} \\
P_{35} &= \frac{-12\left[\overline{\lambda} + \overline{\mu}\right] - 24\mu^{(2)} r_1}{r_1}, & P_{36} &= -\frac{6\kappa^{(2)}\left[\overline{\lambda} + \overline{\mu}\right] + 2\mu^{(2)} r_1\left[9\kappa^{(2)} + 4\mu^{(2)}\right]}{\mu^{(2)} r_1} \\
P_{41} &= \frac{-\left[\overline{\lambda} + 3\overline{\mu}\right] - 2\mu^{(1)} r_1}{r_1}, & P_{42} &= \frac{\kappa^{(1)}\left[27\overline{\lambda} + 57\overline{\mu}\right] + \mu^{(1)}\left[45\overline{\lambda} + 67\overline{\mu}\right] + 2\mu^{(1)} r_1\left[24\kappa^{(1)} + 5\mu^{(1)}\right]}{3\mu^{(1)} r_1} \\
P_{43} &= \frac{-\left[\overline{\lambda} + 3\overline{\mu}\right] + 2\mu^{(2)} r_1}{r_1}, & P_{44} &= \frac{\kappa^{(2)}\left[27\overline{\lambda} + 57\overline{\mu}\right] + \mu^{(2)}\left[45\overline{\lambda} + 67\overline{\mu}\right] - 2\mu^{(2)} r_1\left[24\kappa^{(2)} + 5\mu^{(2)}\right]}{3\mu^{(2)} r_1} \\
P_{45} &= \frac{12\overline{\lambda} + 16\overline{\mu} + 16\mu^{(2)} r_1}{r_1}, & P_{46} &= \frac{6\kappa^{(2)}\left[\overline{\lambda} + \overline{\mu}\right] - 4\mu^{(2)}\overline{\mu} + 6\kappa^{(2)}\mu^{(2)} r_1}{\mu^{(2)} r_1} \\
P_{51} &= 0, & P_{52} &= 0 \\
P_{53} &= 1, & P_{54} &= \left[2 - 3\frac{\kappa^{(2)}}{\mu^{(2)}}\right] f^{-2/3} \\
P_{55} &= 3f^{5/3}, & P_{56} &= \left[3 + \frac{3\kappa^{(2)}}{\mu^{(2)}}\right] f \\
P_{61} &= 0, & P_{62} &= 0 \\
P_{63} &= 1, & P_{64} &= -\left[\frac{11}{3} + 5\frac{\kappa^{(2)}}{\mu^{(2)}}\right] f^{-2/3} \\
P_{65} &= -2f^{5/3}, & P_{66} &= 2f
\end{aligned}
\tag{B3}
$$

B.4 Lower Bound on the Shear Modulus for Particulate Composites Embedding General Interfaces

$$
\begin{aligned}
Q_{11} &= \frac{\mu^{(1)} + \overline{k} r_1}{\overline{k}}, & Q_{12} &= \frac{\left[\frac{1}{2}\mu^{(1)} - \overline{k} r_1\right]\left[3\kappa^{(1)} - 2\mu^{(1)}\right]}{\overline{k}\mu^{(1)}} \\
Q_{13} &= \frac{\mu^{(2)} - \overline{k} r_1}{\overline{k}}, & Q_{14} &= \frac{\left[3\kappa^{(2)} - 2\mu^{(2)}\right]\left[\frac{1}{2}\mu^{(2)} + \overline{k} r_1\right]}{\overline{k}\mu^{(2)}} \\
Q_{15} &= \frac{-12\mu^{(2)} - 3\overline{k} r_1}{\overline{k}}, & Q_{16} &= \frac{-\mu^{(2)}\left[9\kappa^{(2)} + 4\mu^{(2)}\right] - 3\overline{k} r_1\left[\kappa^{(2)} + \mu^{(2)}\right]}{\overline{k}\mu^{(2)}} \\
Q_{21} &= \frac{\mu^{(1)} + \overline{k} r_1}{\overline{k}}, & Q_{22} &= \frac{-\mu^{(1)}\left[24\kappa^{(1)} + 5\mu^{(1)}\right] - \overline{k} r_1\left[15\kappa^{(1)} + 11\mu^{(1)}\right]}{3\overline{k}\mu^{(1)}} \\
Q_{23} &= \frac{\mu^{(2)} - \overline{k} r_1}{\overline{k}}, & Q_{24} &= \frac{-\mu^{(2)}\left[24\kappa^{(2)} + 5\mu^{(2)}\right] + \overline{k} r_1\left[15\kappa^{(2)} + 11\mu^{(2)}\right]}{3\overline{k}\mu^{(2)}} \\
Q_{25} &= \frac{8\mu^{(2)} + 2\overline{k} r_1}{\overline{k}}, & Q_{26} &= \frac{3\kappa^{(2)} - 2\overline{k} r_1}{\overline{k}} \\
Q_{31} &= \frac{\left[\overline{\lambda} + \overline{\mu}\right] - 2\mu^{(1)} r_1}{r_1}, & Q_{32} &= \frac{-\left[\overline{\lambda} + \overline{\mu}\right]\left[9\kappa^{(1)} + 15\mu^{(1)}\right] - \mu^{(1)} r_1\left[3\kappa^{(1)} - 2\mu^{(1)}\right]}{\mu^{(1)} r_1} \\
Q_{33} &= \frac{\left[\overline{\lambda} + \overline{\mu}\right] + 2\mu^{(2)} r_1}{r_1}, & Q_{34} &= \frac{-\left[\overline{\lambda} + \overline{\mu}\right]\left[9\kappa^{(2)} + 15\mu^{(2)}\right] + \mu^{(2)} r_1\left[3\kappa^{(2)} - 2\mu^{(2)}\right]}{\mu^{(2)} r_1} \\
Q_{35} &= \frac{-12\left[\overline{\lambda} + \overline{\mu}\right] - 24\mu^{(2)} r_1}{r_1}, & Q_{36} &= \frac{-6\kappa^{(2)}\left[\overline{\lambda} + \overline{\mu}\right] - 2\mu^{(2)} r_1\left[9\kappa^{(2)} + 4\mu^{(2)}\right]}{\mu^{(2)} r_1} \\
Q_{41} &= \frac{-\left[\overline{\lambda} + 3\overline{\mu}\right] - 2\mu^{(1)} r_1}{r_1}, & Q_{42} &= \frac{\kappa^{(1)}\left[27\overline{\lambda} + 57\overline{\mu}\right] + \mu^{(1)}\left[45\overline{\lambda} + 67\overline{\mu}\right] + 2\mu^{(1)} r_1\left[24\kappa^{(1)} + 5\mu^{(1)}\right]}{3\mu^{(1)} r_1} \\
Q_{43} &= \frac{-\left[\overline{\lambda} + 3\overline{\mu}\right] + 2\mu^{(2)} r_1}{r_1}, & Q_{44} &= \frac{\kappa^{(2)}\left[27\overline{\lambda} + 57\overline{\mu}\right] + \mu^{(2)}\left[45\overline{\lambda} + 67\overline{\mu}\right] - 2\mu^{(2)} r_1\left[24\kappa^{(2)} + 5\mu^{(2)}\right]}{3\mu^{(2)} r_1} \\
Q_{45} &= \frac{12\overline{\lambda} + 16\overline{\mu} + 16\mu^{(2)} r_1}{r_1}, & Q_{46} &= \frac{6\kappa^{(2)}\left[\overline{\lambda} + \overline{\mu}\right] - 4\mu^{(2)}\overline{\mu} + 6\kappa^{(2)}\mu^{(2)} r_1}{\mu^{(2)} r_1} \\
Q_{51} &= 0, & Q_{52} &= 0 \\
Q_{53} &= 2\mu^{(2)}, & Q_{54} &= \left[3\kappa^{(2)} - 2\mu^{(2)}\right] f^{-2/3} \\
Q_{55} &= -24\mu^{(2)} f^{5/3}, & Q_{56} &= -2\left[9\kappa^{(2)} + 4\mu^{(2)}\right] f \\
Q_{61} &= 0, & Q_{62} &= 0 \\
Q_{63} &= 2\mu^{(2)}, & Q_{64} &= -\frac{2}{3}\left[24\kappa^{(2)} + 5\mu^{(2)}\right] f^{-2/3} \\
Q_{65} &= 16\mu^{(2)} f^{5/3}, & Q_{66} &= 6\kappa^{(2)} f
\end{aligned}
\tag{B4}
$$

Appendix C: Coefficients for Bounds and Estimates on the Shear Modulus of Composites Embedding Elastic Interfaces

In this section, the coefficient matrices corresponding to the bounds and estimates on the shear modulus of composites embedding elastic interfaces are presented.

C.1 Upper Bound on the Shear Modulus and Effective Shear Modulus for Fiber Composites Embedding Elastic Interfaces

$$
\begin{aligned}
&D_{11} = \frac{\lambda^{(1)} r_1}{\left[2\kappa^{(1)} + \mu^{(1)}\right]}, && D_{21} = r_1, && D_{31} = \frac{3\overline{\mu}\left[\kappa^{(1)} + \mu^{(1)}\right]}{r_1\left[2\kappa^{(1)} + \mu^{(1)}\right]}\\
&D_{12} = r_1, && D_{22} = r_1, && D_{32} = \frac{\overline{\mu} - 2\mu^{(1)} r_1}{r_1}\\
&D_{13} = \frac{-\lambda_2 r_1}{\left[2\kappa^{(2)} + \mu^{(2)}\right]}, && D_{23} = -r_1, && D_{33} = \frac{3\overline{\mu}\left[\kappa^{(2)} + \mu^{(2)}\right]}{r_1\left[2\kappa^{(2)} + \mu^{(2)}\right]}\\
&D_{14} = -r_1, && D_{24} = -r_1, && D_{34} = \frac{\overline{\mu} + 2\mu^{(2)} r_1}{r_1}\\
&D_{15} = r_1, && D_{25} = -r_1, && D_{35} = \frac{3\overline{\mu} + 6\mu^{(2)} r_1}{r_1}\\
&D_{16} = \frac{-r_1\left[\kappa^{(2)} + \mu^{(2)}\right]}{\mu^{(2)}}, && D_{26} = -r_1, && D_{36} = \frac{-\overline{\mu}\lambda_2 - 4\kappa^{(2)}\mu^{(2)} r_1}{\mu^{(2)} r_1}\\
&D_{41} = -\frac{-6\overline{\mu}\left[\kappa^{(1)} + \mu^{(1)}\right] - 6\mu^{(1)}\kappa^{(1)} r_1}{r_1\left[2\kappa^{(1)} + \mu^{(1)}\right]}, && D_{51} = 0, && D_{61} = 0\\
&D_{42} = \frac{-2\overline{\mu} - 2\mu^{(1)} r_1}{r_1}, && D_{52} = 0, && D_{62} = 0\\
&D_{43} = \frac{-6\overline{\mu}\left[\kappa^{(2)} + \mu^{(2)}\right] + 6\mu^{(2)}\kappa^{(2)} r_1}{r_1\left[2\kappa^{(2)} + \mu^{(2)}\right]}, && D_{53} = \frac{\lambda_2}{f\left[2\kappa^{(2)} + \mu^{(2)}\right]}, && D_{63} = \frac{1}{f}\\
&D_{44} = \frac{-2\overline{\mu} + 2\mu^{(2)} r_1}{r_1}, && D_{54} = 1, && D_{64} = 1\\
&D_{45} = \frac{-6\overline{\mu} - 6\mu^{(2)} r_1}{r_1}, && D_{55} = -f^2, && D_{65} = f^2\\
&D_{46} = \frac{2\overline{\mu}\lambda_2 + 2\kappa^{(2)}\mu^{(2)} r_1}{\mu^{(2)} r_1}, && D_{56} = \frac{f\left[\kappa^{(2)} + \mu^{(2)}\right]}{\mu^{(2)}}, && D_{66} = f
\end{aligned}
\tag{C1}
$$

C.2 Lower Bound on the Shear Modulus for Fiber Composites Embedding Elastic Interfaces

$$
\begin{aligned}
&E_{11} = \frac{\lambda^{(1)} r_1}{\left[2\kappa^{(1)} + \mu^{(1)}\right]}, && E_{21} = r_1, && E_{31} = \frac{3\overline{\mu}\left[\kappa^{(1)} + \mu^{(1)}\right]}{r_1\left[2\kappa^{(1)} + \mu^{(1)}\right]}\\
&E_{12} = r_1, && E_{22} = r_1, && E_{32} = \frac{\overline{\mu} - 2\mu^{(1)} r_1}{r_1}\\
&E_{13} = \frac{-\lambda_2 r_1}{\left[2\kappa^{(2)} + \mu^{(2)}\right]}, && E_{23} = -r_1, && E_{33} = \frac{3\overline{\mu}\left[\kappa^{(2)} + \mu^{(2)}\right]}{r_1\left[2\kappa^{(2)} + \mu^{(2)}\right]}\\
&E_{14} = -r_1, && E_{24} = -r_1, && E_{34} = \frac{\overline{\mu} + 2\mu^{(2)} r_1}{r_1}\\
&E_{15} = r_1, && E_{25} = -r_1, && E_{35} = \frac{3\overline{\mu} + 6\mu^{(2)} r_1}{r_1}\\
&E_{16} = \frac{-r_1\left[\kappa^{(2)} + \mu^{(2)}\right]}{\mu^{(2)}}, && E_{26} = -r_1, && E_{36} = \frac{-\overline{\mu}\lambda_2 - 4\kappa^{(2)}\mu^{(2)} r_1}{\mu^{(2)} r_1}\\
&E_{41} = -\frac{-6\overline{\mu}\left[\kappa^{(1)} + \mu^{(1)}\right] - 6\mu^{(1)}\kappa^{(1)} r_1}{r_1\left[2\kappa^{(1)} + \mu^{(1)}\right]}, && E_{51} = 0, && E_{61} = 0\\
&E_{42} = \frac{-2\overline{\mu} - 2\mu^{(1)} r_1}{r_1}, && E_{52} = 0, && E_{62} = 0\\
&E_{43} = \frac{-6\overline{\mu}\left[\kappa^{(2)} + \mu^{(2)}\right] + 6\mu^{(2)}\kappa^{(2)} r_1}{r_1\left[2\kappa^{(2)} + \mu^{(2)}\right]}, && E_{53} = 0, && E_{63} = \frac{6\kappa^{(2)}\mu^{(2)}}{f\left[2\kappa^{(2)} + \mu^{(2)}\right]}\\
&E_{44} = \frac{-2\overline{\mu} + 2\mu^{(2)} r_1}{r_1}, && E_{54} = 2\mu^{(2)}, && E_{64} = 2\mu^{(2)}\\
&E_{45} = \frac{-6\overline{\mu} - 6\mu^{(2)} r_1}{r_1}, && E_{55} = 6\mu^{(2)} f^2, && E_{65} = -6\mu^{(2)} f^2\\
&E_{46} = \frac{2\overline{\mu}\lambda_2 + 2\kappa^{(2)}\mu^{(2)} r_1}{\mu^{(2)} r_1}, && E_{56} = -4\kappa^{(2)} f, && E_{66} = 2\kappa^{(2)} f
\end{aligned}
\tag{C2}
$$

C.3 Upper Bound on the Shear Modulus and Effective Shear Modulus for Particulate Composites Embedding Elastic Interfaces

$$
\begin{aligned}
&P_{11} = r_1, && P_{12} = \frac{-r_1\left[3\kappa^{(1)} - 2\mu^{(1)}\right]}{\mu^{(1)}}\\
&P_{13} = -r_1, && P_{14} = \frac{r_1\left[3\kappa^{(2)} - 2\mu^{(2)}\right]}{\mu^{(2)}}\\
&P_{15} = -3r_1, && P_{16} = \frac{-3r_1\left[\kappa^{(2)} + \mu^{(2)}\right]}{\mu^{(2)}}\\
&P_{21} = r_1, && P_{22} = \frac{-r_1\left[15\kappa^{(1)} + 11\mu^{(1)}\right]}{3\mu^{(1)}}\\
&P_{23} = -r_1, && P_{24} = \frac{r_1\left[15\kappa^{(2)} + 11\mu^{(2)}\right]}{3\mu^{(2)}}\\
&P_{25} = 2r_1, && P_{26} = -2r_1\\
&P_{31} = \frac{\left[\overline{\lambda} + \overline{\mu}\right] - 2\mu^{(1)}r_1}{r_1}, && P_{32} = \frac{-\left[\overline{\lambda} + \overline{\mu}\right]\left[9\kappa^{(1)} + 15\mu^{(1)}\right] - \mu^{(1)}r_1\left[3\kappa^{(1)} - 2\mu^{(1)}\right]}{\mu^{(1)}r_1}\\
&P_{33} = \frac{\left[\overline{\lambda} + \overline{\mu}\right] + 2\mu^{(2)}r_1}{r_1}, && P_{34} = \frac{-\left[\overline{\lambda} + \overline{\mu}\right]\left[9\kappa^{(2)} + 15\mu^{(2)}\right] + \mu^{(2)}r_1\left[3\kappa^{(2)} - 2\mu^{(2)}\right]}{\mu^{(2)}r_1}\\
&P_{35} = \frac{-12\left[\overline{\lambda} + \overline{\mu}\right] - 24\mu^{(2)}r_1}{r_1}, && P_{36} = -\frac{6\kappa^{(2)}\left[\overline{\lambda} + \overline{\mu}\right] + 2\mu^{(2)}r_1\left[9\kappa^{(2)} + 4\mu^{(2)}\right]}{\mu^{(2)}r_1}\\
&P_{41} = \frac{-\left[\overline{\lambda} + 3\overline{\mu}\right] - 2\mu^{(1)}r_1}{r_1}, && P_{42} = \frac{\kappa^{(1)}\left[27\overline{\lambda} + 57\overline{\mu}\right] + \mu^{(1)}\left[45\overline{\lambda} + 67\overline{\mu}\right] + 2\mu^{(1)}r_1\left[24\kappa^{(1)} + 5\mu^{(1)}\right]}{3\mu^{(1)}r_1}\\
&P_{43} = \frac{-\left[\overline{\lambda} + 3\overline{\mu}\right] + 2\mu^{(2)}r_1}{r_1}, && P_{44} = \frac{\kappa^{(2)}\left[27\overline{\lambda} + 57\overline{\mu}\right] + \mu^{(2)}\left[45\overline{\lambda} + 67\overline{\mu}\right] - 2\mu^{(2)}r_1\left[24\kappa^{(2)} + 5\mu^{(2)}\right]}{3\mu^{(2)}r_1}\\
&P_{45} = \frac{12\overline{\lambda} + 16\overline{\mu} + 16\mu^{(2)}r_1}{r_1}, && P_{46} = \frac{6\kappa^{(2)}\left[\overline{\lambda} + \overline{\mu}\right] - 4\mu^{(2)}\overline{\mu} + 6\kappa^{(2)}\mu^{(2)}r_1}{\mu^{(2)}r_1}\\
&P_{51} = 0, && P_{52} = 0\\
&P_{53} = 1, && P_{54} = \left[2 - 3\frac{\kappa^{(2)}}{\mu^{(2)}}\right]f^{-2/3}\\
&P_{55} = 3f^{5/3}, && P_{56} = \left[3 + \frac{3\kappa^{(2)}}{\mu^{(2)}}\right]f\\
&P_{61} = 0, && P_{62} = 0\\
&P_{63} = 1, && P_{64} = -\left[\frac{11}{3} + 5\frac{\kappa^{(2)}}{\mu^{(2)}}\right]f^{-2/3}\\
&P_{65} = -2f^{5/3}, && P_{66} = 2f
\end{aligned}
\tag{C3}
$$

C.4 Lower Bound on the Shear Modulus for Particulate Composites Embedding Elastic Interfaces

$$
\begin{aligned}
Q_{11} &= r_1, & Q_{12} &= \frac{-r_1\left[3\kappa^{(1)} - 2\mu^{(1)}\right]}{\overline{k}\mu^{(1)}} \\
Q_{13} &= -r_1, & Q_{14} &= \frac{r_1\left[3\kappa^{(2)} - 2\mu^{(2)}\right]}{\overline{k}\mu^{(2)}} \\
Q_{15} &= -3r_1, & Q_{16} &= \frac{-3r_1\left[\kappa^{(2)} + \mu^{(2)}\right]}{\mu^{(2)}} \\
Q_{21} &= r_1, & Q_{22} &= \frac{-r_1\left[15\kappa^{(1)} + 11\mu^{(1)}\right]}{3\mu^{(1)}} \\
Q_{23} &= -r_1, & Q_{24} &= \frac{r_1\left[15\kappa^{(2)} + 11\mu^{(2)}\right]}{3\mu^{(2)}} \\
Q_{25} &= 2r_1, & Q_{26} &= -2r_1 \\
Q_{31} &= \frac{\left[\overline{\lambda} + \overline{\mu}\right] - 2\mu^{(1)}r_1}{r_1}, & Q_{32} &= \frac{-\left[\overline{\lambda} + \overline{\mu}\right]\left[9\kappa^{(1)} + 15\mu^{(1)}\right] - \mu^{(1)}r_1\left[3\kappa^{(1)} - 2\mu^{(1)}\right]}{\mu^{(1)}r_1} \\
Q_{33} &= \frac{\left[\overline{\lambda} + \overline{\mu}\right] + 2\mu^{(2)}r_1}{r_1}, & Q_{34} &= \frac{-\left[\overline{\lambda} + \overline{\mu}\right]\left[9\kappa^{(2)} + 15\mu^{(2)}\right] + \mu^{(2)}r_1\left[3\kappa^{(2)} - 2\mu^{(2)}\right]}{\mu^{(2)}r_1} \\
Q_{35} &= \frac{-12\left[\overline{\lambda} + \overline{\mu}\right] - 24\mu^{(2)}r_1}{r_1}, & Q_{36} &= \frac{-6\kappa^{(2)}\left[\overline{\lambda} + \overline{\mu}\right] - 2\mu^{(2)}r_1\left[9\kappa^{(2)} + 4\mu^{(2)}\right]]}{\mu^{(2)}r_1} \\
Q_{41} &= \frac{-\left[\overline{\lambda} + 3\overline{\mu}\right] - 2\mu^{(1)}r_1}{r_1}, & Q_{42} &= \frac{\kappa^{(1)}\left[27\overline{\lambda} + 57\overline{\mu}\right] + \mu^{(1)}\left[45\overline{\lambda} + 67\overline{\mu}\right] + 2\mu^{(1)}r_1\left[24\kappa^{(1)} + 5\mu^{(1)}\right]}{3\mu^{(1)}r_1} \\
Q_{43} &= \frac{-\left[\overline{\lambda} + 3\overline{\mu}\right] + 2\mu^{(2)}r_1}{r_1}, & Q_{44} &= \frac{\kappa^{(2)}\left[27\overline{\lambda} + 57\overline{\mu}\right] + \mu^{(2)}\left[45\overline{\lambda} + 67\overline{\mu}\right] - 2\mu^{(2)}r_1\left[24\kappa^{(2)} + 5\mu^{(2)}\right]}{3\mu^{(2)}r_1} \\
Q_{45} &= \frac{12\overline{\lambda} + 16\overline{\mu} + 16\mu^{(2)}r_1}{r_1}, & Q_{46} &= \frac{6\kappa^{(2)}\left[\overline{\lambda} + \overline{\mu}\right] - 4\mu^{(2)}\overline{\mu} + 6\kappa^{(2)}\mu^{(2)}r_1}{\mu^{(2)}r_1} \\
Q_{51} &= 0, & Q_{52} &= 0 \\
Q_{53} &= 2\mu^{(2)}, & Q_{54} &= \left[3\kappa^{(2)} - 2\mu^{(2)}\right]f^{-2/3} \\
Q_{55} &= -24\mu^{(2)}f^{5/3}, & Q_{56} &= -2\left[9\kappa^{(2)} + 4\mu^{(2)}\right]f \\
Q_{61} &= 0, & Q_{62} &= 0 \\
Q_{63} &= 2\mu^{(2)}, & Q_{64} &= -\frac{2}{3}\left[24\kappa^{(2)} + 5\mu^{(2)}\right]f^{-2/3} \\
Q_{65} &= 16\mu^{(2)}f^{5/3}, & Q_{66} &= 6\kappa^{(2)}f
\end{aligned}
\tag{C4}
$$

Appendix D: Coefficients for Bounds and Estimates on the Shear Modulus of Composites Embedding Cohesive Interfaces

In this section, the coefficient matrices corresponding to the bounds and estimates on the shear modulus of composites embedding cohesive interfaces are presented.

D.1 Upper Bound on the Shear Modulus and Effective Shear Modulus for Fiber Composites Embedding Cohesive Interfaces

$$
\begin{aligned}
&D_{11}=\frac{\lambda^{(1)}r_1}{\left[2\kappa^{(1)}+\mu^{(1)}\right]}, && D_{21}=\frac{3\mu^{(1)}\kappa^{(1)}+\overline{k}\left[2\kappa^{(1)}+\mu^{(1)}\right]r_1}{\overline{k}\left[2\kappa^{(1)}+\mu^{(1)}\right]}, && D_{31}=0\\
&D_{12}=\frac{\mu^{(1)}+\overline{k}r_1}{\overline{k}}, && D_{22}=\frac{\mu^{(1)}+\overline{k}r_1}{\overline{k}}, && D_{32}=-2\mu^{(1)}\\
&D_{13}=\frac{-\lambda_2 r_1}{\left[2\kappa^{(2)}+\mu^{(2)}\right]}, && D_{23}=\frac{3\kappa^{(2)}\mu^{(2)}-\overline{k}\left[2\kappa^{(2)}+\mu^{(2)}\right]r_1}{\overline{k}\left[2\kappa^{(2)}+\mu^{(2)}\right]}, && D_{33}=0\\
&D_{14}=\frac{\mu^{(2)}-\overline{k}r_1}{\overline{k}}, && D_{24}=\frac{\mu^{(2)}-\overline{k}r_1}{\overline{k}}, && D_{34}=2\mu^{(2)}\\
&D_{15}=\frac{3\mu^{(2)}+\overline{k}r_1}{\overline{k}}, && D_{25}=\frac{-3\mu^{(2)}-\overline{k}r_1}{\overline{k}}, && D_{35}=6\mu^{(2)}\\
&D_{16}=\frac{-2\kappa^{(2)}\mu^{(2)}-\overline{k}r_1\left[\kappa^{(2)}+\mu^{(2)}\right]}{\mu^{(2)}\overline{k}}, && D_{26}=\frac{\kappa^{(2)}-\overline{k}r_1}{\overline{k}}, && D_{36}=-4\kappa^{(2)}\\
&D_{41}=-\frac{6\mu^{(1)}\kappa^{(1)}r_1}{r_1\left[2\kappa^{(1)}+\mu^{(1)}\right]}, && D_{51}=0, && D_{61}=0\\
&D_{42}=-2\mu^{(1)}, && D_{52}=0, && D_{62}=0\\
&D_{43}=\frac{6\mu^{(2)}\kappa^{(2)}r_1}{r_1\left[2\kappa^{(2)}+\mu^{(2)}\right]}, && D_{53}=\frac{\lambda_2}{f\left[2\kappa^{(2)}+\mu^{(2)}\right]}, && D_{63}=\frac{1}{f}\\
&D_{44}=2\mu^{(2)}, && D_{54}=1, && D_{64}=1\\
&D_{45}=-6\mu^{(2)}, && D_{55}=-f^2, && D_{65}=f^2\\
&D_{46}=2\kappa^{(2)}, && D_{56}=\frac{f\left[\kappa^{(2)}+\mu^{(2)}\right]}{\mu^{(2)}}, && D_{66}=f
\end{aligned}
\tag{D1}
$$

D.2 Lower Bound on the Shear Modulus for Fiber Composites Embedding Cohesive Interfaces

$$
\begin{aligned}
&E_{11}=\frac{\lambda^{(1)}r_1}{\left[2\kappa^{(1)}+\mu^{(1)}\right]}, && E_{21}=\frac{3\mu^{(1)}\kappa^{(1)}+\overline{k}\left[2\kappa^{(1)}+\mu^{(1)}\right]r_1}{\overline{k}\left[2\kappa^{(1)}+\mu^{(1)}\right]}, && E_{31}=0\\
&E_{12}=\frac{\mu^{(1)}+\overline{k}r_1}{\overline{k}}, && E_{22}=\frac{\mu^{(1)}+\overline{k}r_1}{\overline{k}}, && E_{32}=-2\mu^{(1)}\\
&E_{13}=\frac{-\lambda_2 r_1}{\left[2\kappa^{(2)}+\mu^{(2)}\right]}, && E_{23}=\frac{3\kappa^{(2)}\mu^{(2)}-\overline{k}\left[2\kappa^{(2)}+\mu^{(2)}\right]r_1}{\overline{k}\left[2\kappa^{(2)}+\mu^{(2)}\right]}, && E_{33}=0\\
&E_{14}=\frac{\mu^{(2)}-\overline{k}r_1}{\overline{k}}, && E_{24}=\frac{\mu^{(2)}-\overline{k}r_1}{\overline{k}}, && E_{34}=2\mu^{(2)}\\
&E_{15}=\frac{3\mu^{(2)}+\overline{k}r_1}{\overline{k}}, && E_{25}=\frac{-3\mu^{(2)}-\overline{k}r_1}{\overline{k}}, && E_{35}=6\mu^{(2)}\\
&E_{16}=\frac{-2\kappa^{(2)}\mu^{(2)}-\overline{k}r_1\left[\kappa^{(2)}+\mu^{(2)}\right]}{\mu^{(2)}\overline{k}}, && E_{26}=\frac{\kappa^{(2)}-\overline{k}r_1}{\overline{k}}, && E_{36}=-4\kappa^{(2)}\\
&E_{41}=-\frac{6\mu^{(1)}\kappa^{(1)}r_1}{r_1\left[2\kappa^{(1)}+\mu^{(1)}\right]}, && E_{51}=0, && E_{61}=0\\
&E_{42}=-2\mu^{(1)}, && E_{52}=0, && E_{62}=0\\
&E_{43}=\frac{6\mu^{(2)}\kappa^{(2)}r_1}{r_1\left[2\kappa^{(2)}+\mu^{(2)}\right]}, && E_{53}=0, && E_{63}=\frac{6\kappa^{(2)}\mu^{(2)}}{f\left[2\kappa^{(2)}+\mu^{(2)}\right]}\\
&E_{44}=2\mu^{(2)}, && E_{54}=2\mu^{(2)}, && E_{64}=2\mu^{(2)}\\
&E_{45}=-6\mu^{(2)}, && E_{55}=6\mu^{(2)}f^2, && E_{65}=-6\mu^{(2)}f^2\\
&E_{46}=2\kappa^{(2)}, && E_{56}=-4\kappa^{(2)}f, && E_{66}=2\kappa^{(2)}f
\end{aligned}
\tag{D2}
$$

D.3 Upper Bound on the Shear Modulus and Effective Shear Modulus for Particulate Composites Embedding Cohesive Interfaces

$$
\begin{aligned}
P_{11} &= \frac{\mu^{(1)} + \overline{k} r_1}{\overline{k}}, & P_{12} &= \frac{\left[\frac{1}{2}\mu^{(1)} - \overline{k} r_1\right]\left[3\kappa^{(1)} - 2\mu^{(1)}\right]}{\overline{k}\mu^{(1)}} \\
P_{13} &= \frac{\mu^{(2)} - \overline{k} r_1}{\overline{k}}, & P_{14} &= \frac{\left[3\kappa^{(2)} - 2\mu^{(2)}\right]\left[\frac{1}{2}\mu^{(2)} + \overline{k} r_1\right]}{\overline{k}\mu^{(2)}} \\
P_{15} &= \frac{-12\mu^{(2)} - 3\overline{k} r_1}{\overline{k}}, & P_{16} &= \frac{-\mu^{(2)}\left[9\kappa^{(2)} + 4\mu^{(2)}\right] - 3\overline{k} r_1\left[\kappa^{(2)} + \mu^{(2)}\right]}{\overline{k}\mu^{(2)}} \\
P_{21} &= \frac{\mu^{(1)} + \overline{k} r_1}{\overline{k}}, & P_{22} &= \frac{-\mu^{(1)}\left[24\kappa^{(1)} + 5\mu^{(1)}\right] - \overline{k} r_1\left[15\kappa^{(1)} + 11\mu^{(1)}\right]}{3\overline{k}\mu^{(1)}} \\
P_{23} &= \frac{\mu^{(2)} - \overline{k} r_1}{\overline{k}}, & P_{24} &= \frac{-\mu^{(2)}\left[24\kappa^{(2)} + 5\mu^{(2)}\right] + \overline{k} r_1\left[15\kappa^{(2)} + 11\mu^{(2)}\right]}{3\overline{k}\mu^{(2)}} \\
P_{25} &= \frac{8\mu^{(2)} + 2\overline{k} r_1}{\overline{k}}, & P_{26} &= \frac{3\kappa^{(2)} - 2\overline{k} r_1}{\overline{k}} \\
P_{31} &= -2\mu^{(1)}, & P_{32} &= -3\kappa^{(1)} + 2\mu^{(1)} \\
P_{33} &= 2\mu^{(2)}, & P_{34} &= 3\kappa^{(2)} - 2\mu^{(2)} \\
P_{35} &= -24\mu^{(2)}, & P_{36} &= -18\kappa^{(2)} - 8\mu^{(2)} \\
P_{41} &= -2\mu^{(1)}, & P_{42} &= \frac{48\kappa^{(1)} + 10\mu^{(1)}}{3} \\
P_{43} &= 2\mu^{(2)}, & P_{44} &= \frac{-48\kappa^{(2)} - 10\mu^{(2)}}{3} \\
P_{45} &= 16\mu^{(2)}, & P_{46} &= 6\kappa^{(2)} \\
P_{51} &= 0, & P_{52} &= 0 \\
P_{53} &= 1, & P_{54} &= \left[2 - 3\frac{\kappa^{(2)}}{\mu^{(2)}}\right] f^{-2/3} \\
P_{55} &= 3f^{5/3}, & P_{56} &= \left[3 + \frac{3\kappa^{(2)}}{\mu^{(2)}}\right] f \\
P_{61} &= 0, & P_{62} &= 0 \\
P_{63} &= 1, & P_{64} &= -\left[\frac{11}{3} + 5\frac{\kappa^{(2)}}{\mu^{(2)}}\right] f^{-2/3} \\
P_{65} &= -2f^{5/3}, & P_{66} &= 2f
\end{aligned}
\tag{D3}
$$

D.4 Lower Bound on the Shear Modulus for Particulate Composites Embedding Cohesive Interfaces

$$
\begin{aligned}
Q_{11} &= \frac{\mu^{(1)} + \overline{k} r_1}{\overline{k}}, & Q_{12} &= \frac{\left[\frac{1}{2}\mu^{(1)} - \overline{k} r_1\right]\left[3\kappa^{(1)} - 2\mu^{(1)}\right]}{\overline{k}\mu^{(1)}} \\
Q_{13} &= \frac{\mu^{(2)} - \overline{k} r_1}{\overline{k}}, & Q_{14} &= \frac{\left[3\kappa^{(2)} - 2\mu^{(2)}\right]\left[[1-\overline{\alpha}]\mu^{(2)} + \overline{k} r_1\right]}{\overline{k}\mu^{(2)}} \\
Q_{15} &= \frac{-12\mu^{(2)} - 3\overline{k} r_1}{\overline{k}}, & Q_{16} &= \frac{-\mu^{(2)}\left[9\kappa^{(2)} + 4\mu^{(2)}\right] - 3\overline{k} r_1\left[\kappa^{(2)} + \mu^{(2)}\right]}{\overline{k}\mu^{(2)}} \\
Q_{21} &= \frac{\mu^{(1)} + \overline{k} r_1}{\overline{k}}, & Q_{22} &= \frac{-\mu^{(1)}\left[24\kappa^{(1)} + 5\mu^{(1)}\right] - \overline{k} r_1\left[15\kappa^{(1)} + 11\mu^{(1)}\right]}{3\overline{k}\mu^{(1)}} \\
Q_{23} &= \frac{\mu^{(2)} - \overline{k} r_1}{\overline{k}}, & Q_{24} &= \frac{-\mu^{(2)}\left[24\kappa^{(2)} + 5\mu^{(2)}\right] + \overline{k} r_1\left[15\kappa^{(2)} + 11\mu^{(2)}\right]}{3\overline{k}\mu^{(2)}} \\
Q_{25} &= \frac{8\mu^{(2)} + 2\overline{k} r_1}{\overline{k}}, & Q_{26} &= \frac{3\kappa^{(2)} - 2\overline{k} r_1}{\overline{k}} \\
Q_{31} &= -2\mu^{(1)}, & Q_{32} &= -3\kappa^{(1)} + 2\mu^{(1)} \\
Q_{33} &= 2\mu^{(2)}, & Q_{34} &= 3\kappa^{(2)} - 2\mu^{(2)} \\
Q_{35} &= -24\mu^{(2)}, & Q_{36} &= -18\kappa^{(2)} - 8\mu^{(2)} \\
Q_{41} &= -2\mu^{(1)}, & Q_{42} &= \frac{48\kappa^{(1)} + 10\mu^{(1)}}{3} \\
Q_{43} &= 2\mu^{(2)}, & Q_{44} &= \frac{-48\kappa^{(2)} - 10\mu^{(2)}}{3} \\
Q_{45} &= 16\mu^{(2)}, & Q_{46} &= 6\kappa^{(2)} \\
Q_{51} &= 0, & Q_{52} &= 0 \\
Q_{53} &= 2\mu^{(2)}, & Q_{54} &= \left[3\kappa^{(2)} - 2\mu^{(2)}\right] f^{-2/3} \\
Q_{55} &= -24\mu^{(2)} f^{5/3}, & Q_{56} &= -2\left[9\kappa^{(2)} + 4\mu^{(2)}\right] f \\
Q_{61} &= 0, & Q_{62} &= 0 \\
Q_{63} &= 2\mu^{(2)}, & Q_{64} &= -\frac{2}{3}\left[24\kappa^{(2)} + 5\mu^{(2)}\right] f^{-2/3} \\
Q_{65} &= 16\mu^{(2)} f^{5/3}, & Q_{66} &= 6\kappa^{(2)} f
\end{aligned}
\tag{D4}
$$

Appendix E: Coefficients for Bounds and Estimates on the Shear Modulus of Composites Embedding Perfect Interfaces

In this section, the coefficient matrices corresponding to the bounds and estimates on the shear modulus of composites embedding perfect interfaces are presented.

E.1 Upper Bound on the Shear Modulus and Effective Shear Modulus for Fiber Composites Embedding Perfect Interfaces

$$
\begin{aligned}
D_{11} &= \frac{\lambda^{(1)} r_1}{\left[2\kappa^{(1)} + \mu^{(1)}\right]}, & D_{21} &= r_1, & D_{31} &= 0 \\
D_{12} &= r_1, & D_{22} &= r_1, & D_{32} &= -2\mu^{(1)} \\
D_{13} &= \frac{-\lambda_2 r_1}{\left[2\kappa^{(2)} + \mu^{(2)}\right]}, & D_{23} &= -r_1, & D_{33} &= 0 \\
D_{14} &= -r_1, & D_{24} &= -r_1, & D_{34} &= 2\mu^{(2)} \\
D_{15} &= r_1, & D_{25} &= -r_1, & D_{35} &= 6\mu^{(2)} \\
D_{16} &= \frac{-r_1\left[\kappa^{(2)} + \mu^{(2)}\right]}{\mu^{(2)}}, & D_{26} &= -r_1, & D_{36} &= -4\kappa^{(2)} \\
D_{41} &= -\frac{6\mu^{(1)}\kappa^{(1)} r_1}{r_1\left[2\kappa^{(1)} + \mu^{(1)}\right]}, & D_{51} &= 0, & D_{61} &= 0 \\
D_{42} &= -2\mu^{(1)}, & D_{52} &= 0, & D_{62} &= 0 \\
D_{43} &= \frac{6\mu^{(2)}\kappa^{(2)} r_1}{r_1\left[2\kappa^{(2)} + \mu^{(2)}\right]}, & D_{53} &= \frac{\lambda_2}{f\left[2\kappa^{(2)} + \mu^{(2)}\right]}, & D_{63} &= \frac{1}{f} \\
D_{44} &= 2\mu^{(2)}, & D_{54} &= 1, & D_{64} &= 1 \\
D_{45} &= -6\mu^{(2)}, & D_{55} &= -f^2, & D_{65} &= f^2 \\
D_{46} &= 2\kappa^{(2)}, & D_{56} &= \frac{f\left[\kappa^{(2)} + \mu^{(2)}\right]}{\mu^{(2)}}, & D_{66} &= f
\end{aligned}
\tag{E1}
$$

E.2 Lower Bound on the Shear Modulus for Fiber Composites Embedding Perfect Interfaces

$$
\begin{aligned}
&E_{11} = \frac{\lambda^{(1)} r_1}{\left[2\kappa^{(1)} + \mu^{(1)}\right]}, && E_{21} = r_1, && E_{31} = 0\\
&E_{12} = r_1, && E_{22} = r_1, && E_{32} = -2\mu^{(1)}\\
&E_{13} = \frac{-\lambda_2 r_1}{\left[2\kappa^{(2)} + \mu^{(2)}\right]}, && E_{23} = -r_1, && E_{33} = 0\\
&E_{14} = -r_1, && E_{24} = -r_1, && E_{34} = 2\mu^{(2)}\\
&E_{15} = r_1, && E_{25} = -r_1, && E_{35} = 6\mu^{(2)}\\
&E_{16} = \frac{-r_1\left[\kappa^{(2)} + \mu^{(2)}\right]}{\mu^{(2)}}, && E_{26} = -r_1, && E_{36} = -4\kappa^{(2)}\\
&E_{41} = -\frac{6\mu^{(1)}\kappa^{(1)} r_1}{r_1\left[2\kappa^{(1)} + \mu^{(1)}\right]}, && E_{51} = 0, && E_{61} = 0\\
&E_{42} = -2\mu^{(1)}, && E_{52} = 0, && E_{62} = 0\\
&E_{43} = \frac{6\mu^{(2)}\kappa^{(2)} r_1}{r_1\left[2\kappa^{(2)} + \mu^{(2)}\right]}, && E_{53} = 0, && E_{63} = \frac{6\kappa^{(2)}\mu^{(2)}}{f\left[2\kappa^{(2)} + \mu^{(2)}\right]}\\
&E_{44} = 2\mu^{(2)}, && E_{54} = 2\mu^{(2)}, && E_{64} = 2\mu^{(2)}\\
&E_{45} = -6\mu^{(2)}, && E_{55} = 6\mu^{(2)} f^2, && E_{65} = -6\mu^{(2)} f^2\\
&E_{46} = 2\kappa^{(2)}, && E_{56} = -4\kappa^{(2)} f, && E_{66} = 2\kappa^{(2)} f
\end{aligned}
\tag{E2}
$$

E.3 Upper Bound on the Shear Modulus and Effective Shear Modulus for Particulate Composites Embedding Perfect Interfaces

$$
\begin{aligned}
&P_{11} = r_1, && P_{12} = \frac{-r_1\left[3\kappa^{(1)} - 2\mu^{(1)}\right]}{\mu^{(1)}}\\
&P_{13} = -r_1, && P_{14} = \frac{r_1\left[3\kappa^{(2)} - 2\mu^{(2)}\right]}{\mu^{(2)}}\\
&P_{15} = -3r_1, && P_{16} = \frac{-3r_1\left[\kappa^{(2)} + \mu^{(2)}\right]}{\mu^{(2)}}\\
&P_{21} = r_1, && P_{22} = \frac{-r_1\left[15\kappa^{(1)} + 11\mu^{(1)}\right]}{3\mu^{(1)}}\\
&P_{23} = \frac{\mu^{(2)} - \overline{k} r_1}{\overline{k}}, && P_{24} = \frac{r_1\left[15\kappa^{(2)} + 11\mu^{(2)}\right]}{3\mu^{(2)}}\\
&P_{25} = 2r_1, && P_{26} = -2r_1\\
&P_{31} = -2\mu^{(1)}, && P_{32} = -3\kappa^{(1)} + 2\mu^{(1)}\\
&P_{33} = 2\mu^{(2)}, && P_{34} = 3\kappa^{(2)} - 2\mu^{(2)}\\
&P_{35} = -24\mu^{(2)}, && P_{36} = -18\kappa^{(2)} - 8\mu^{(2)}\\
&P_{41} = -2\mu^{(1)}, && P_{42} = \frac{48\kappa^{(1)} + 10\mu^{(1)}}{3}\\
&P_{43} = 2\mu^{(2)}, && P_{44} = \frac{-48\kappa^{(2)} - 10\mu^{(2)}}{3}\\
&P_{45} = 16\mu^{(2)}, && P_{46} = 6\kappa^{(2)}\\
&P_{51} = 0, && P_{52} = 0\\
&P_{53} = 1, && P_{54} = \left[2 - 3\frac{\kappa^{(2)}}{\mu^{(2)}}\right] f^{-2/3}\\
&P_{55} = 3f^{5/3}, && P_{56} = \left[3 + \frac{3\kappa^{(2)}}{\mu^{(2)}}\right] f\\
&P_{61} = 0, && P_{62} = 0\\
&P_{63} = 1, && P_{64} = -\left[\frac{11}{3} + 5\frac{\kappa^{(2)}}{\mu^{(2)}}\right] f^{-2/3}\\
&P_{65} = -2f^{5/3}, && P_{66} = 2f
\end{aligned}
\tag{E3}
$$

E.4 Lower Bound on the Shear Modulus for Particulate Composites Embedding Perfect Interfaces

$$
\begin{aligned}
&Q_{11} = r_1, && Q_{12} = \frac{-r_1\left[3\kappa^{(1)} - 2\mu^{(1)}\right]}{\mu^{(1)}}\\
&Q_{13} = -r_1, && Q_{14} = \frac{r_1\left[3\kappa^{(2)} - 2\mu^{(2)}\right]}{\mu^{(2)}}\\
&Q_{15} = -3r_1, && Q_{16} = \frac{-3r_1\left[\kappa^{(2)} + \mu^{(2)}\right]}{\mu^{(2)}}\\
&Q_{21} = r_1, && Q_{22} = \frac{-r_1\left[15\kappa^{(1)} + 11\mu^{(1)}\right]}{3\mu^{(1)}}\\
&Q_{23} = -r_1, && Q_{24} = \frac{r_1\left[15\kappa^{(2)} + 11\mu^{(2)}\right]}{3\mu^{(2)}}\\
&Q_{25} = 2r_1, && Q_{26} = -2r_1\\
&Q_{31} = -2\mu^{(1)}, && Q_{32} = -3\kappa^{(1)} + 2\mu^{(1)}\\
&Q_{33} = 2\mu^{(2)}, && Q_{34} = 3\kappa^{(2)} - 2\mu^{(2)}\\
&Q_{35} = -24\mu^{(2)}, && Q_{36} = -18\kappa^{(2)} - 8\mu^{(2)}\\
&Q_{41} = -2\mu^{(1)}, && Q_{42} = \frac{48\kappa^{(1)} + 10\mu^{(1)}}{3}\\
&Q_{43} = 2\mu^{(2)}, && Q_{44} = \frac{-48\kappa^{(2)} - 10\mu^{(2)}}{3}\\
&Q_{45} = 16\mu^{(2)}, && Q_{46} = 6\kappa^{(2)}\\
&Q_{51} = 0, && Q_{52} = 0\\
&Q_{53} = 2\mu^{(2)}, && Q_{54} = \left[3\kappa^{(2)} - 2\mu^{(2)}\right] f^{-2/3}\\
&Q_{55} = -24\mu^{(2)} f^{5/3}, && Q_{56} = -2\left[9\kappa^{(2)} + 4\mu^{(2)}\right] f\\
&Q_{61} = 0, && Q_{62} = 0\\
&Q_{63} = 2\mu^{(2)}, && Q_{64} = -\frac{2}{3}\left[24\kappa^{(2)} + 5\mu^{(2)}\right] f^{-2/3}\\
&Q_{65} = 16\mu^{(2)} f^{5/3}, && Q_{66} = 6\kappa^{(2)} f
\end{aligned}
\tag{E4}
$$

References

[1] Voigt, W., 1889, "Ueber Die Beziehung Zwischen Den Beiden Elasticitätsconstanten Isotroper Körper," Ann. Phys., **274**(12), pp. 573–578.
[2] Reuss, V. A., 1929, "Berechnung Der Fliehgrenze Von Mischkristallen Auf Grund Der Plastizittitsbedingung Fiir Einkristalle," Z. Angew. Math. Mech, **9**(1), pp. 49–58.
[3] Hill, R., 1952, "The Elastic Behaviour of a Crystalline Aggregate," Proc. Phys. Soc. A, **65**(5), pp. 349–354.
[4] Hill, R., 1963, "Elastic Properties of Reinforced Solids: Some Theoretical Principles," J. Mech. Phys. Solids, **11**(5), pp. 357–372.
[5] Hill, R., 1964, "Theory of Mechanical Properties of Fiber-Strengthened Materials: I. Elastic Behavior," J. Mech. Phys. Solids, **12**(4), pp. 199–202.
[6] Hill, R., 1964, "Theory of Mechanical Properties of Fiber-Strengthened Materials: II. Inelastic Behaviour," J. Mech. Phys. Solids, **12**(4), pp. 213–218.
[7] Hill, R., 1965, "A Self-Consistent Mechanics of Composite Materials," J. Mech. Phys. Solids, **13**(4), pp. 213–222.
[8] Hill, R., 1965, "Theory of Mechanical Properties of Fiber-Strengthened Materials—III. Self-Consistent Model," J. Mech. Phys. Solids, **13**(4), pp. 189–198.
[9] Hill, R., "On Constitutive Macro-Variables for Heterogeneous Solids at Finite Strain," Proc. R. Soc. London A, **326**(1972), pp. 131–147.
[10] Taylor, G. I., 1938, "Plastic Strain in Metals," J. Inst. Met., **62**, pp. 307–324.
[11] Sachs, G., 1929, "Zur Ableitung Einer Fließbedingung," *Mitteilungen Der Deutschen Materialprüfungsanstalten*, Vol. 72, Springer, Berlin, pp. 94–96.
[12] Bishop, J. F. W., and Hill, R., 1951, "A Theory of the Plastic Distortion of a Polycrystalline Aggregate Under Combined Stresses," Philosophical Magazine, **42**(327), pp. 414–427.
[13] Hashin, Z., and Shtrikman, S., 1962, "On Some Variational Principles in Anisotropic and Nonhomogeneous Elasticity," J. Mech. Phys. Solids, **10**(4), pp. 335–342.
[14] Hashin, Z., and Shtrikman, S., 1962, "A Variational Approach to the Theory of the Elastic Behaviour of Polycrystals," J. Mech. Phys. Solids, **10**(4), pp. 343–352.
[15] Hashin, Z., and Shtrikman, S., 1963, "Variational Approach to the Theory of the Elastic Behavior of Multiphase Materials," J. Mech. Phys. Solids, **11**(2), pp. 127–140.
[16] Hashin, Z., and Shtrikman, S., 1962, "A Variational Approach to the Theory of the Effective Magnetic Permeability of Multiphase Materials," J. Appl. Phys., **33**(10), pp. 3125–3131.
[17] Hashin, Z., 1965, "On Elastic Behaviour of Fibre Reinforced Materials of Arbitrary Transverse Phase Geometry," J. Mech. Phys. Solids, **13**(3), pp. 119–134.
[18] Hashin, Z., 1962, "The Elastic Moduli of Heterogeneous Materials," ASME J. Appl. Mech., **29**(1), pp. 143–150.

[19] Hashin, Z., 1983, "Analysis of Composite Materials—A Survey," ASME J. Appl. Mech., **50**(3), pp. 481–505.
[20] Beran, M., and Molyneux, J., 1966, "Use of Classical Variational Principles to Determine Bounds for the Effective Bulk Modulus in Heterogeneous Media," Q. Appl. Math., **24**(2), pp. 107–118.
[21] Walpole, L. J., 1966, "On Bounds for the Overall Elastic Moduli of Inhomogeneous Systems-I," J. Mech. Phys. Solids, **14**(3), pp. 151–162.
[22] Walpole, L. J., 1966, "On Bounds for the Overall Elastic Moduli of Inhomogeneous Systems-II," J. Mech. Phys. Solids, **14**(5), pp. 289–301.
[23] Walpole, L. J., 1969, "On the Overall Elastic Moduli of Composite Materials," J. Mech. Phys. Solids, **17**(4), pp. 235–251.
[24] Fan, Z., Tsakiropoulos, P., and Miodownik, A. P., 1992, "Prediction of Young's Modulus of Particulate Two Phase Composites," Mater. Sci. Technol., **8**(10), pp. 922–929.
[25] Zimmerman, R. W., 1992, "Hashin-Shtrikman Bounds on the Poisson Ratio of a Composite Material," Mech. Res. Commun., **19**(6), pp. 563–569.
[26] Hashin, Z., and Rosen, B. W., 1964, "The Elastic Moduli of Fiber-Reinforced Materials," ASME J. Appl. Mech., **31**(2), pp. 223–232.
[27] Rosen, B. W., and Hashin, Z., 1970, "Effective Thermal Expansion Coefficients and Specific Heats of Composite Materials," Int. J. Eng. Sci., **8**(2), pp. 157–173.
[28] Milton, G. W., 1982, "New Bounds on Effective Elastic Moduli of Two-Component Materials," Proc. R. Soc. A, **380**, pp. 305–331.
[29] Bornert, M., Stolz, C., and Zaoui, A., 1996, "Morphologically Representative Pattern-Based Bounding in Elasticity," J. Mech. Phys. Solids, **44**(3), pp. 307–331.
[30] Nemat-Nasser, S., Yu, N., and Hori, M., 1993, "Bounds and Estimates of Overall Moduli of Composites With Periodic Microstructure," Mech. Mater., **15**(3), pp. 163–181.
[31] Aboudi, J., 1983, "The Effective Moduli of Short-Fiber Composites," Int. J. Solids Struct., **19**(8), pp. 693–707.
[32] Torquato, S., 1991, "Random Heterogeneous Media: Hicrosttucture and Improwed Bounds on Effective Properties," ASME Appl. Mech. Rev., **44**(2), pp. 37–76.
[33] Milton, G. W., and Kohn, R. V., 1988, "Variational Bounds of the Effective Moduli of Piezoelectric Composites," J. Mech. Phys. Solids, **36**(6), pp. 597–629.
[34] Bisegna, P., and Luciano, R., 1996, "Variational Bounds for the Overall Properties of Piezoelectric Composites," J. Mech. Phys. Solids, **44**(4), pp. 583–602.
[35] Bisegna, P., and Luciano, R., 1997, "On Methods for Bounding the Overall Properties of Periodic Piezoelectric Fibrous Composites," J. Mech. Phys. Solids, **45**(8), pp. 1329–1356.
[36] Hori, M., and Nemat-Nasser, S., 1998, "Universal Bounds for Effective Piezoelectric Moduli," Mech. Mater., **30**(1), pp. 1–19.
[37] Hori, M., and Nemat-Nasser, S., 1993, "Double-Inclusion Model and Overall Moduli of Multi-Phase Composites," Mech. Mater., **14**(3), pp. 189–206.
[38] Nemat-Nasser, S., and Hori, M., 1993, *Micromechanics: Overall Properties of Heterogeneous Materials*, Elsevier, Amsterdam, The Netherlands.
[39] Li, J. Y., and Dunn, M. L., 2001, "Variational Bounds for the Effective Moduli of Heterogeneous Piezoelectric Solids," Philos. Mag. A, **81**(4), pp. 903–926.
[40] Gibiansky, L. V., and Torquato, S., 1997, "Thermal Expansion of Isotropic Multiphase Composites and Polycrystals," J. Mech. Phys. Solids, **45**(7), pp. 1223–1252.
[41] Eshelby, J. D., 1957, "The Determination of the Elastic Field of an Ellipsoidal Inclusion, and Related Problems," Proc. R. Soc. London. Ser. A, **241**, pp. 376–396.
[42] Rodin, J. G., 1996, "Eshelby's Inclusion Problem for Polygons and Polyhedra," J. Mech. Phys. Solids, **44**(12), pp. 1977–1995.
[43] Markenscoff, X., 1997, "On the Shape of the Eshelby Inclusions," J. Elasticity, **49**(2), pp. 163–166.
[44] Mura, T., 1997, "The Determination of the Elastic Field of a Polygonal Star Shaped Inclusion," Mech. Res. Commun., **24**(5), pp. 473–482.
[45] Lubarda, V. A., and Markenscoff, X., 1998, "On the Absence of Eshelby Property for Non-Ellipsoidal Inclusions," Int. J. Solids Struct., **35**(25), pp. 3405–3411.
[46] Zohdi, T. I., and Wriggers, P., 2001, "Computational Micro-Macro Material Testing," Arch. Comput. Methods Eng., **8**(2), pp. 131–228.
[47] Hershey, A., 1954, "The Elasticity of an Isotropic Aggregate of Anisotropic Cubic Crystals," ASME J. Appl. Mech., **21**(3), pp. 236–240.
[48] Kröner, E., 1958, "Berechnung Der Elastischen Konstanten Des Vielkristalls Aus Den Konstanten Des Einkristalls," Z. Für Phys., **151**, pp. 504–518.
[49] Budiansky, B., 1965, "On the Elastic Moduli of Some Heterogeneous Materials," J. Mech. Phys. Solids, **13**(4), pp. 223–227.
[50] Laws, N., 1973, "On the Thermostatics of Composite Materials," J. Mech. Phys. Solids, **21**(1), pp. 9–17.
[51] Kerner, E. H., 1956, "The Elastic and Thermo-Elastic Properties of Composite Media," Proc. Phys. Soc. B, **69**(8), pp. 808–813.
[52] Christensen, R. M., and Lo, K. N., 1979, "Solutions for Effective Shear Properties in Three Phase Sphere and Cylinder Models," J. Mech. Phys. Solids, **27**(4), pp. 315–330.
[53] Huang, Y., Hu, K. X., Wei, X., and Chandra, A., 1994, "A Generalized Self-Consistent Mechanics Method for Composite Materials With Multiphase Inclusions," J. Mech. Phys. Solids, **42**(3), pp. 491–504.
[54] Huang, Y., and Hu, K. X., 1995, "A Generalized Self-Consistent Mechanics Method for Solids Containing Elliptical Inclusions," ASME J. Appl. Mech., **62**(3), pp. 566–572.
[55] Benveniste, Y., and Berdichevsky, O., 2010, "On Two Models of Arbitrarily Curved Three-Dimensional Thin Interphases in Elasticity," Int. J. Solids Struct., **47**(14–15), pp. 1899–1915.
[56] Benveniste, Y., and Milton, G. W., 2010, "The Effective Medium and the Average Field Approximations Vis-Vis the HashinShtrikman Bounds—I: The Self-Consistent Scheme in Matrix-Based Composites," J. Mech. Phys. Solids, **58**(7), pp. 1026–1038.
[57] Chatzigeorgiou, G., Seidel, G. D., and Lagoudas, D. C., 2012, "Effective Mechanical Properties of "Fuzzy Fiber" Composites," Compos. Part B, **43**(6), pp. 2577–2593.
[58] Boucher, S., 1976, "Modulus Effectifs de Materiaux Quasi Homogenes et Quasi Isotropes, Constitues D'une Matrice Elastique et D'inclusions Elastiques," Rev. Metall., **22**, pp. 31–36.
[59] McLaughlin, R., 1977, "A Study of the Differential Scheme for Composite Materials," Int. J. Eng. Sci., **15**(4), pp. 237–244.
[60] Norris, A. N., 1985, "A Differential Scheme for the Effective Moduli of Composites," Mech. Mater., **4**(1), pp. 1–16.
[61] Mori, T., and Tanaka, K., 1973, "Average Stress in Matrix and Average Elastic Energy of Materials With Misfitting Inclusions," Acta Metall., **21**(5), pp. 571–574.
[62] Pierard, O., Friebel, C., and Doghri, I., 2004, "Mean-Field Homogenization of Multi-Phase Thermo-Elastic Composites : A General Framework and Its Validation," Compos. Sci. Technol., **64**(10–11), pp. 1587–1603.
[63] Benveniste, Y., 1987, "A New Approach to the Application of Mori-Tanaka's Theory in Composite Materials," Mech. Mater., **6**(2), pp. 147–157.
[64] Luo, H. A., and Weng, G. J., 1987, "On Eshelby's Inclusion Problem in a Three-Phase Spherically Concentric Solid, and a Modification of Mori-Tanaka's Method," Mech. Mater., **6**(4), pp. 347–361.
[65] Luo, H. A., and Weng, G. J., 1989, "On Eshelby's S-Tensor in a Three-Phase Cylindrically Concentric Solid, and the Elastic Moduli of Fiber-Reinforced Composites," Mech. Mater., **8**(2–3), pp. 77–88.
[66] Weng, G. J., 1990, "The Theoretical Connection Between Mori-Tanaka's Theory and the Hashin-Shtrikman-Walpole Bounds," Int. J. Eng. Sci., **28**(11), pp. 1111–1120.
[67] Qiu, Y. P., and Weng, G. J., 1990, "On the Application of Mori-Tanaka's Theory Involving Transversely Isotropic Spheroidal Inclusions," Int. J. Eng. Sci., **28**(11), pp. 1121–1137.
[68] Tandon, G. P., and Weng, G. J., 1984, "The Effect of Aspect Ratio of Inclusions on the Elastic Properties of Unidirectionally Aligned Composites," Polym. Compos., **5**(4), pp. 327–333.
[69] Hu, G. K., and Weng, G. J., 2000, "The Connections Between the Double-Inclusion Model and the Ponte Castaneda-Willis, Mori-Tanaka, and Kuster-Toksoz Models," Mech. Mater., **32**(8), pp. 495–503.
[70] Aboutajeddine, A., and Neale, K. W., 2005, "The Double-Inclusion Model: A New Formulation and New Estimates," Mech. Mater., **37**(2–3), pp. 331–341.
[71] Riccardi, A., and Montheillet, F., 1999, "A Generalized Self-Consistent Method for Solids Containing Randomly Oriented Spheroidal Inclusions," Acta Mech., **133**(1–4), pp. 39–56.
[72] Ogden, R. W., 1974, "On the Overall Moduli of Non-Linear Elastic Composite Materials," J. Mech. Phys. Solids, **22**(6), pp. 541–553.
[73] Talbot, D. R. S., and Willis, J. R., 1985, "Variational Principles for Inhomogeneous Non-Linear Media," IMA J. Appl. Math., **35**(1), pp. 39–54.
[74] Talbot, D. R. S., and Willis, J. R., 1987, "Bounds and Self-Consistent Estimates for the Overall Properties of Nonlinear Composites," IMA J. Appl. Math., **39**(3), pp. 215–240.
[75] Talbot, D. R. S., and Willis, J. R., 1992, "Some Simple Explicit Bounds for the Overall Behaviour of Nonlinear Composites," Int. J. Solids Struct., **29**(14–15), pp. 1981–1987.
[76] Willis, J. R., 1977, "Bounds and Self-Consistent Estimates for the Overall Properties of Anisotropic Composites," J. Mech. Phys. Solids, **25**(3), pp. 185–202.
[77] Willis, J. R., 1983, "The Overall Elastic Response of Composite Materials," ASME J. Appl. Mech., **50**(4b), pp. 1202–1209.
[78] Willis, J. R., 1991, "On Methods for Bounding the Overall Properties of Nonlinear Composites," J. Mech. Phys. Solids, **39**(1), pp. 73–86.
[79] Ponte Castañeda, P., DeBotton, G., and Li, G., 1992, "Effective Properties of Nonlinear Inhomogeneous Dielectrics," Phys. Rev. B, **46**(8), pp. 4387–4394.
[80] Castañeda, P. P., and Willis, J. R., "On the Overall Properties of Nonlinearly Viscous Composites," Proc. R. Soc. London A, **416**(1988), pp. 217–244.
[81] Suquet, P. M., 1993, "Overall Potentials and Extremal Surfaces of Power Law or Ideally Plastic Composites," J. Mech. Phys. Solids, **41**(6), pp. 981–1002.
[82] DeBotton, G., and Ponte Castañeda, P., 1993, "Elastoplastic Constitutive Relations for Fiber-Reinforced Solids," Int. J. Solids Struct., **30**(14), pp. 1865–1890.
[83] Olson, T., 1994, "Improvements on Taylor's Upper Bound for Rigid-Plastic Composites," Mater. Sci. Eng. A, **175**(1–2), pp. 15–20.
[84] Ponte Castañeda, P., "The Overall Constitutive Behaviour of Nonlinearly Elastic Composites," Proc. R. Soc. A, **422**(1989), pp. 147–171.
[85] Ponte Castañeda, P., 1996, "Exact Second-Order Estimates for the Effective Mechanical Properties of Nonlinear Composite Materials," J. Mech. Phys. Solids, **44**(6), pp. 827–862.
[86] Ponte Castañeda, P., 2002, "Second-Order Homogenization Estimates for Nonlinear Composites Incorporating Field Fluctuations: I—Theory," J. Mech. Phys. Solids, **50**(4), pp. 737–757.
[87] Ponte Castañeda, P., 2002, "Second-Order Homogenization Estimates for Nonlinear Composites Incorporating Field Fluctuations: II—Applications," J. Mech. Phys. Solids, **50**(4), pp. 759–782.

[88] Ponte Castañeda, P., 1992, "New Variational Principles in Plasticity and Their Application to Composite Materials," J. Mech. Phys. Solids, **40**(8), pp. 1757–1788.
[89] Ponte Castañeda, P., 1991, "The Effective Mechanical Properties of Nonlinear Isotropic Composites," J. Mech. Phys. Solids, **39**(1), pp. 45–71.
[90] Castañeda, P. P., and Suquet, P., 1997, Nonlinear Composites, Vol. 34, Elsevier, Amsterdam, The Netherlands.
[91] Leroy, Y., and Ponte Castañeda, P., 2001, "Bounds on the Self-Consistent Approximation for Nonlinear Media and Implications for the Second-Order Method," C. R. L'Académie Des Sci., **329**(8), pp. 571–577.
[92] Lopez-Pamies, O., and Ponte Castañeda, P., 2003, "Second-Order Estimates for the Large-Deformation Response of Particle-Reinforced Rubbers," C. R. Mec., **331**(1), pp. 1–8.
[93] Mura, T., 1988, "Inclusion Problems," ASME Appl. Mech. Rev., **41**(1), pp. 15–20.
[94] Charalambakis, N., 2010, "Homogenization Techniques and Micromechanics. A Survey and Perspectives," ASME Appl. Mech. Rev., **63**(3), p. 030803.
[95] Firooz, S., Saeb, S., Chatzigeorgiou, G., Meraghni, F., Steinmann, P., and Javili, A., 2019, "Systematic Study of Homogenization and the Utility of Circular Simplified Representative Volume Element," Math. Mech. Solids, **24**(9), pp. 2961–2985.
[96] Mandel, J., 1966, *Contribution Theorique a L'etude de L'ecrouissage et Des Lois de L'ecoulement Plastique*, Springer, Berlin.
[97] Tvergaard, V., 1990, "Analysis of Tensile Properties for a Whisker-Reinforced Metal-Matrix Composite," Acta Metall. Et Mater., **38**(2), pp. 185–194.
[98] Smit, R. J. M., Brekelmans, W. A. M., and Meijer, H. E. H., 1998, "Prediction of the Mechanical Behavior of Nonlinear Heterogeneous Systems by Multi-Level Finite Element Modeling," Comput. Methods Appl. Mech. Eng., **155**(1–2), pp. 181–192.
[99] Bao, Y., Hutchinson, W., and McMeeking, R. M., 1991, "Plastic Reinforcement of Ductile Materials Against Plastic Flow and Creep," Acta Metall. Mater., **39**(8), pp. 1871–1882.
[100] Sluis, OV. D., Vosbeek, P. H. J., Schreurs, P. J. G., and Jer, H. E. H. M., 1999, "Homogenization of Heterogeneous Polymers," Int. J. Solids Struct., **36**(21), pp. 3193–3214.
[101] van der Sluis, O., Schreurs, P. J. G. Brekelmans, W. A. M., and Meijer, H. E. H., 2000, "Overall Behaviour of Heterogeneous Elastoviscoplastic Materials: Effect of Microstructural Modelling," Mech. Mater., **32**(8), pp. 449–462.
[102] Nemat-Nasser, S., and Hori, M., 1995, "Universal Bounds for Overall Properties of Linear and Nonlinear Heterogeneous Solids," ASME J. Eng. Mater. Technol., **117**(4), pp. 412–432.
[103] Miehe, C., 2002, "Strain-Driven Homogenization of Inelastic Microstructures and Composites Based on an Incremental Variational Formulation," Int. J. Numer. Methods Eng., **55**(11), pp. 1285–1322.
[104] Kaczmarczyk, Ł. C., Pearce, J., and Bićanić, N., 2008, "Scale Transition and Enforcement of RVE Boundary Conditions in Second-Order Computational Homogenization," Int. J. Numer. Methods Eng., **74**(3), pp. 506–522.
[105] Terada, K., Hori, M., Kyoya, T., and Kikuchi, N., 2000, "Simulation of the Multi-Scale Convergence in Computational Homogenization Approaches," Int. J. Solids Struct., **37**(16), pp. 2285–2311.
[106] Drago, A., and Pindera, M. J., 2007, "Micro-Macromechanical Analysis of Heterogeneous Materials: Macroscopically Homogeneous Vs Periodic Microstructures," Compos. Sci. Technol., **67**(6), pp. 1243–1263.
[107] Irving, J. H., and Kirkwood, J. G., 1950, "The Statistical Mechanical Theory of Transport Processes: IV—The Equations of Hydrodynamics," J. Chem. Phys., **18**(6), pp. 817–829.
[108] Mercer, B. S., Mandadapu, K. K., and Papadopoulos, P., 2015, "Novel Formulations of Microscopic Boundary-Value Problems in Continuous Multiscale Finite Element Methods," Comput. Methods Appl. Mech. Eng., **286**, pp. 268–292.
[109] Fritzen, F., and Böhlke, T., 2010, "Influence of the Type of Boundary Conditions on the Numerical Properties of Unit Cell Problems," Tech. Mech., **30**(4), pp. 354–363.
[110] Yuan, X., and Tomita, Y., 2001, "Effective Properties of Cosserat Composites With Periodic Microstructure," Mech. Res. Commun., **28**(3), pp. 265–270.
[111] Jiang, C. P., and Cheung, Y. K., 2001, "An Exact Solution for the Three-Phase Piezoelectric Cylinder Model Under Antiplane Shear and Its Applications to Piezoelectric Composites," Int. J. Solids Struct., **38**(28–29), pp. 4777–4796.
[112] Inglis, H. M., Geubelle, P. H., and Matouš, K., 2008, "Boundary Condition Effects on Multiscale Analysis of Damage Localization," Philos. Mag., **88**(16), pp. 2373–2397.
[113] Larsson, F., Runesson, K., Saroukhani, S., and Vafadari, R., 2011, "Computational Homogenization Based on a Weak Format of Micro-Periodicity for RVE-Problems," Comput. Methods Appl. Mech. Eng., **200**(1–4), pp. 11–26.
[114] Glüge, R., 2013, "Generalized Boundary Conditions on Representative Volume Elements and Their Use in Determining the Effective Material Properties," Comput. Mater. Sci., **79**, pp. 408–416.
[115] Saroukhani, S., Vafadari, R., Andersson, R., Larsson, F., and Runesson, K., 2015, "On Statistical Strain and Stress Energy Bounds From Homogenization and Virtual Testing," Eur. J. Mech., A/Solids, **51**, pp. 77–95.
[116] Nguyen, V. D., Wu, L., and Noels, L., 2017, "Unified Treatment of Microscopic Boundary Conditions and Efficient Algorithms for Estimating Tangent Operators of the Homogenized Behavior in the Computational Homogenization Method," Comput. Mech., **59**(3), pp. 483–505.
[117] Drugan, W. J., and Willis, J. R., 1996, "A Micromechanics-Based Nonlocal Constitutive Equation and Estimates of Representative Volume Element Size for Elastic Composites," J. Mech. Phys. Solids, **44**(4), pp. 497–524.
[118] Kanit, T., Forest, S., Galliet, I., Mounoury, V., and Jeulin, D., 2003, "Determination of the Size of the Representative Volume Element for Random Composites: Statistical and Numerical Approach," Int. J. Solids Struct., **40**(13–14), pp. 3647–3679.
[119] Gitman, I. M., Askes, H., and Aifantis, E. C., 2005, "The Representative Volume Size in Static and Dynamic Micro-Macro Transitions," Int. J. Fract., **135**(1–4), pp. L3–9.
[120] Khisaeva, Z. F., and Ostoja-Starzewski, M., 2006, "On the Size of RVE in Finite Elasticity of Random Composites," J. Elasticity, **85**(2), pp. 153–173.
[121] Temizer, I., and Zohdi, T. I., 2007, "A Numerical Method for Homogenization in Non-Linear Elasticity," Comput. Mech., **40**(2), pp. 281–298.
[122] Thomas, M., Boyard, N., Perez, L., Jarny, Y., and Delaunay, D., 2008, "Representative Volume Element of Anisotropic Unidirectional Carbon-Epoxy Composite With High-Fibre Volume Fraction," Compos. Sci. Technol., **68**(15–16), pp. 3184–3192.
[123] Temizer, I., Wu, T., and Wriggers, P., 2013, "On the Optimality of the Window Method in Computational Homogenization," Int. J. Eng. Sci., **64**, pp. 66–73.
[124] Dirrenberger, J., Forest, S., and Jeulin, D., 2014, "Towards Gigantic RVE Sizes for 3D Stochastic Fibrous Networks," Int. J. Solids Struct., **51**(2), pp. 359–376.
[125] Dai, M., Schiavone, P., and Gao, C. F., 2017, "A New Method for the Evaluation of the Effective Properties of Composites Containing Unidirectional Periodic Nanofibers," Arch. Appl. Mech., **87**(4), pp. 647–665.
[126] Ostoja-Starzewski, M., 2006, "Material Spatial Randomness: From Statistical to Representative Volume Element," Prob. Eng. Mech., **21**(2), pp. 112–132.
[127] Ghosh, S., Lee, K., and Moorthy, S., 1995, "Multiple Scale Analysis of Heterogeneous Elastic Structures Using Homogenization Theory and Voronoi Cell Finite Element Method," Int. J. Solids Struct., **32**(1), pp. 27–62.
[128] Ghosh, S., and Moorthy, S., 1995, "Elastic-Plastic Analysis of Arbitrary Heterogeneous Materials With the Voronoi Cell Finite Element Method," Comput. Methods Appl. Mech. Eng., **121**(1–4), pp. 373–409.
[129] Moorthy, S., and Ghosh, S., 1996, "A Model for Analysis of Arbitrary Composite and Porous Microstructures With Voronoi Cell Finite Elements," Int. J. Numer. Methods Eng., **39**(14), pp. 2363–2398.
[130] Moulinec, H., and Suquet, P., 1998, "A Numerical Method for Computing the Overall Response of Nonlinear Composites With Complex Microstructure," Comput. Methods Appl. Mech. Eng., **157**(1–2), pp. 69–94.
[131] Michel, J. C., Moulinec, H., and Suquet, P., 1999, "Effective Properties of Composite Materials With Periodic Microstructure: A Computational Approach," Comput. Methods Appl. Mech. Eng., **172**(1–4), pp. 109–143.
[132] Vinogradov, V., and Milton, G. W., 2008, "An Accelerated FFT Algorithm for Thermoelastic and Non-Linear Composites," Int. J. Numer. Methods Eng., **76**(11), pp. 1678–1695.
[133] Lee, S. B., Lebensohn, R. A., and Rollett, A. D., 2011, "Modeling the Viscoplastic Micromechanical Response of Two-Phase Materials Using Fast Fourier Transforms," Int. J. Plasticity, **27**(5), pp. 707–727.
[134] Monchiet, V., and Bonnet, G., 2012, "A Polarization-Based FFT Iterative Scheme for Computing the Effective Properties of Elastic Composites With Arbitrary Contrast," Int. J. Numer. Methods Eng., **89**(11), pp. 1419–1436.
[135] Moulinec, H., and Silva, F., 2014, "Comparison of Three Accelerated FFT-Based Schemes for Computing the Mechanical Response of Composite Materials," Int. J. Numer. Methods Eng., **97**(13), pp. 960–985.
[136] Kabel, M., Merkert, D., and Schneider, M., 2015, "Use of Composite Voxels in FFT-Based Homogenization," Comput. Methods Appl. Mech. Eng., **294**, pp. 168–188.
[137] Kamiński, M., 1999, "Boundary Element Method Homogenization of the Periodic Linear Elastic Fiber Composites," Eng. Anal. Bound. Elem., **23**(10), pp. 815–823.
[138] Okada, H., Fukui, Y., and Kumazawa, N., 2001, "Homogenization Method for Heterogeneous Material Based on Boundary Element Method," Comput. Struct., **79**(20–21), pp. 1987–2007.
[139] Procházka, P., 2001, "Homogenization of Linear and of Debonding Composites Using the BEM," Eng. Anal. Bound. Elem., **25**(9), pp. 753–769.
[140] Renard, J., and Marmonier, M. F., 1987, "Etude de L'initiation de L'endommagement Dans la Matrice D'un Matériau Composite Par Une Méthode D'homogénéisation," La Recherche Aérospatiale, **6**, pp. 43–51.
[141] Takano, N., Ohnishi, Y., Zako, M., and Nishiyabu, K., 2000, "The Formulation of Homogenization Method Applied to Large Deformation Problem for Composite Materials," Int. J. Solids Struct., **37**(44), pp. 6517–6535.
[142] Feyel, F., and Chaboche, J. L., 2000, "FE2 Multiscale Approach for Modelling the Elastoviscoplastic Behaviour of Long Fibre SiC/Ti Composite Materials," Comput. Methods Appl. Mech. Eng., **183**(3–4), pp. 309–330.
[143] Terada, K., and Kikuchi, N., 2001, "A Class of General Algorithms for Multi-Scale Analyses of Heterogeneous Media," Comput. Methods Appl. Mech. Eng., **190**(40–41), pp. 5427–5464.
[144] Miehe, C., and Koch, A., 2002, "Computational Micro-to-Macro Transitions of Discretized Microstructures Undergoing Small Strains," Arch. Appl. Mech., **72**(4–5), pp. 300–317.
[145] Segurado, J., and Llorca, J., 2002, "A Numerical Approximation to the Elastic Properties of Sphere-Reinforced Composites," J. Mech. Phys. Solids, **50**(10), pp. 2107–2121.
[146] Segurado, J., and LLorca, J., 2006, "Computational Micromechanics of Composites: The Effect of Particle Spatial Distribution," Mech. Mater., **38**(8–10), pp. 873–883.

[147] Miehe, C., Schröder, J., and Bayreuther, C., 2002, "On the Homogenization Analysis of Composite Materials Based on Discretized Fluctuations on the Micro-Structure," Acta Mech., **155**(1–2), pp. 1–16.
[148] Feyel, F., 2003, "A Multilevel Finite Element Method (FE2) to Describe the Response of Highly Non-Linear Structures Using Generalized Continua," Comput. Methods Appl. Mech. Eng., **192**(28–30), pp. 3233–3244.
[149] Terada, K., Saiki, I., Matsui, K., and Yamakawa, Y., 2003, "Two-Scale Kinematics and Linearization for Simultaneous Two-Scale Analysis of Periodic Heterogeneous Solids at Finite Strain," Comput. Methods Appl. Mech. Eng., **192**(31–32), pp. 3531–3563.
[150] Klinge, S., and Hackl, K., 2012, "Application of the Multiscale Fem to the Modeling of Nonlinear Composites With a Random Microstructure," Int. J. Multiscale Comput. Eng., **10**(3), pp. 213–227.
[151] Moës, N., and Belytschko, T., 2002, "Extended Finite Element Method for Cohesive Crack Growth," Eng. Fract. Mech., **69**(7), pp. 813–833.
[152] Spieler, C., Kästner, M., Goldmann, J., Brummund, J., and Ulbricht, V., 2013, "XFEM Modeling and Homogenization of Magnetoactive Composites," Acta Mech., **224**(11), pp. 2453–2469.
[153] Savvas, D., Stefanou, G., Papadrakakis, M., and Deodatis, G., 2014, "Homogenization of Random Heterogeneous Media With Inclusions of Arbitrary Shape Modeled by XFEM," Comput. Mech., **54**(5), pp. 1221–1235.
[154] Patil, R. U., Mishra, B. K., and Singh, I. V., 2017, "A New Multiscale XFEM for the Elastic Properties Evaluation of Heterogeneous Materials," Int. J. Mech. Sci., **122**, pp. 277–287.
[155] Lee, B. J., and Mear, M. E., 1991, "Effect of Inclusion Shape on Stiffness of Isotropic and Transversely Isotropic Two-Phase Composites," J. Mech. Phys. Solids, **39**(5), pp. 627–649.
[156] Wang, Y. M., and Weng, G. J., 1992, "The Influence of Inclusion Shape on the Overall Viscoelastic Behavior of Composites," ASME J. Appl. Mech., **59**(3), pp. 510–518.
[157] Monette, L., Anderson, M. P., and Grest, G. S., 1994, "Effect of Volume Fraction and Morphology of Reinforcing Phases in Composites," J. Appl. Phys., **75**(2), pp. 1155–1170.
[158] BöHm, H. J., Rammerstorfer, F. G., Fischer, F. D., and Siegmund, T., 1994, "Microscale Arrangement Effects on the Thermomechanical Behavior of Advanced Two-Phase Materials," ASME J. Eng. Mater. Technol., **116**(3), pp. 268–273.
[159] Ghosh, S., Nowak, Z., and Lee, K., 1997, "Quantitative Characterization and Modeling of Composite Microstructures by Voronoi Cells," Acta Mater., **45**(6), pp. 2215–2234.
[160] Brockenbrough, J. R., Suresh, S., and Wienecke, H. A., 1991, "Deformation of Metal-Matrix Composites With Continuous Fibers: Geometrical Effects of Fiber Distribution and Shape," Acta Metall. Mater., **39**(5), pp. 735–752.
[161] Kouznetsova, V., Brekelmans, W. A. M., and Baaijens, F. P. T., 2001, "An Approach to Micro-Macro Modeling of Heterogeneous Materials," Comput. Mech., **27**(1), pp. 37–48.
[162] Chawla, N., Sidhu, R. S., and Ganesh, V. V., 2006, "Three-Dimensional Visualization and Microstructure-Based Modeling of Deformation in Particle-Reinforced Composites," Acta Mater., **54**(6), pp. 1541–1548.
[163] Kanouté, P., Boso, D. P., Chaboche, J. L., and Schrefler, B. A., 2009, "Multiscale Methods for Composites: A Review," Arch. Comput. Methods Eng., **16**(1), pp. 31–75.
[164] Geers, M. G. D., Kouznetsova, V. G., and Brekelmans, W. A. M., 2010, "Multi-Scale Computational Homogenization: Trends and Challenges," J. Comput. Appl. Math., **234**(7), pp. 2175–2182.
[165] Nguyen, V. P., Stroeven, M., and Sluys, L. J., 2011, "Multiscale Continuous and Discontinuous Modeling of Heterogeneous Materials: A Review on Recent Developments," J. Multiscale Modell., **03**(04), pp. 229–270.
[166] Saeb, S., Steinmann, P., and Javili, A., 2016, "Aspects of Computational Homogenization at Finite Deformations: A Unifying Review From Reuss' to Voigt's," ASME Bound, Appl. Mech. Rev., **68**(5), p. 050801.
[167] Matouš, K., Geers, M. G. D., Kouznetsova, V. G., and Gillman, A., 2017, "A Review of Predictive Nonlinear Theories for Multiscale Modeling of Heterogeneous Materials," J. Comput. Phys., **330**, pp. 192–220.
[168] Hancox, N. L., and Wells, H., 1977, "The Effects of Fibre Surface Coatings on the Mechanical Properties of CFRP," Fibre Sci. Technol., **10**(1), pp. 9–22.
[169] Williams, J. H., and Kousiounelos, P. N., 1978, "Thermoplastic Fibre Coatings Enhance Composite Strength and Toughness," Fibre Sci. Technol., **11**(2), pp. 83–88.
[170] Drzal, L. T., Rich, M. J., Koenig, M. F., and Lloyd, P. F., 1983, "Adhesion of Graphite Fibers to Epoxy Matrices: I—The Role of Fivber Surface Treatment," J. Adhes., **16**(1), pp. 1–30.
[171] Drzal, L. T., Rich, M. J., Koenig, M. F., and Lloyd, P. F., 1983, "Adhesion of Graphite Fibers to Epoxy Matrices: II—The Effect of Fiber Finish," J. Adhes., **16**(2), pp. 133–152.
[172] Subramanian, R. V., and Crasto, A. S., 1986, "Electrodeposition of a Polymer Interphase in Carbon-Fiber Composites," Polym. Compos., **7**(4), pp. 201–218.
[173] Adams, D. F., 1987, "A Micromechanics Analysis of the Influence of the Interface on the Performance of Polymer-Matrix Composites," J. Reinf. Plast. Compos., **6**(1), pp. 66–88.
[174] Sinien, L., Lin, Y., Xiaoguang, Z., and Zongneng, Q., 1992, "Microdamage and Interfacial Adhesion in Glass Bead-Filled High-Density Polyethylene," J. Mater. Sci., **27**(17), pp. 4633–4638.
[175] Mascia, L., Dhillon, J., and Harper, J. F., 1993, "Adhesion Enhancement of Rubbery and Ductile Polyolefin Coatings on Glass Fibers for Epoxy Composites and Effects on Failure Mechanism," J. Appl. Polym. Sci., **47**(3), pp. 487–498.
[176] Kouris, D., 1993, "Stress Concentration Due to the Interaction Between Two Imperfectly Bonded Fibers in a Continuous Fiber Composite," ASME J. Appl. Mech., **60**(1), pp. 203–206.
[177] Torquato, S., and Rintoul, M. D., 1995, "Effect of the Interface on the Properties of Composite Media," Phys. Rev. Lett., **75**(22), pp. 4067–4070.
[178] Chamis, C. C., 1972, *Mechanics of Load Transfer at the Fiber/Matrix Interface*, National Aeronautics and Space Administration, Washington, DC.
[179] Jang, B. Z., Hwang, L. R., and Lieu, Y. K., 1986, "The Assessment of Interfacial Adhesion in Fibrous Composites," Interfaces in Metal-Matrix Composites, Proceedings of a Symposium Held at the Annual Meeting of the Metallurgical Society, New Orleans, LA, pp. 95–109.
[180] Narkis, M., Chen, E. J. H., and Pipes, R. B., 1988, "Review of Methods for Characterization of Interfacial Fiber-Matrix Interactions," Polym. Compos., **9**(4), pp. 245–251.
[181] Wang, Q., and Chiang, F. P., 1996, "Experimental Characterization of Interphase Mechanical Properties of Composites," Compos. Part B, **27**(2), pp. 123–128.
[182] Drzal, L. T., 1983, "Composite Interphase Characterization," Sampe J., **19**, pp. 7–14.
[183] Drzal, L. T., 1986, "The Interphase in Epoxy Composites," K. Dušek, ed., *Epoxy Resins and Composites II. Advances in Polymer Science*, Vol. 75. Springer, Berlin, Heidelberg, pp. 1–32.
[184] Wang, W., and Jasiuk, I., 1998, "Effective Elastic Constants of Participate Composites With Inhomogeneous Interphases," J. Compos. Mater., **32**(15), pp. 1391–1424.
[185] Crasto, A. S., Own, S. H., and Subramanian, R. V., 1988, "The Influence of the Interphase on Composite Properties: Poly(Ethylene-co-Acrylic Acid) and Poly(Methyl Vinyl Ether-co-Maleic Anhydride) Electrodeposited on Graphite Fibers," Polym. Compos., **9**(1), pp. 78–92.
[186] Kerans, R. J., Hay, R. S., Pagano, N. J., and Parthasarathy, T. A., 1989, "The Role of the Fiber-Matrix Interface in Ceramic Composites," Am. Ceram. Soc. Bull., **68**, pp. 429–442.
[187] Swain, R. E., Reifsnider, K. L., Jayaraman, K., and El-Zein, M., 1990, "Interface/Interphase Concepts in Composite Material Systems," J. Thermoplastic Compos. Mater., **3**(1), pp. 13–23.
[188] Evans, A. G., Zok, F. W., and Davis, J., 1991, "The Role of Interfaces in Fiber-Reinforced Brittle Matrix Composites," Compos. Sci. Technol., **42**(1–3), pp. 3–24.
[189] Hughes, J. D. H., 1991, "The Carbon Fibre/Epoxy Interface-A Review," Compos. Sci. Technol., **41**(1), pp. 13–45.
[190] Podgaiz, R. H., and Williams, R. J. J., 1997, "Effects of Fiber Coatings on Mechanical Properties of Unidirectional Glass-Reinforced Composites," Compos. Sci. Technol., **57**(8), pp. 1071–1076.
[191] Wacker, G., Bledzki, A. K., and Chate, A., 1998, "Effect of Interphase on the Transverse Young's Modulus of Glass/Epoxy Composites," Compos. Part A, **29**(5–6), pp. 619–626.
[192] Gao, S. L., and Mäder, E., 2002, "Characterisation of Interphase Nanoscale Property Variations in Glass Fibre Reinforced Polypropylene and Epoxy Resin Composites," Compos. Part A, **33**(4), pp. 559–576.
[193] Mäder, E., Gao, S. L., and Plonka, R., 2004, "Enhancing the Properties of Composites by Controlling Their Interphase Parameters," Adv. Eng. Mater., **6**(3), pp. 147–150.
[194] Walpole, L. J., 1978, "A Coated Inclusion in an Elastic Medium," Math. Proc. Cambridge Philos. Soc., **83**(3), pp. 495–506.
[195] Theocaris, P. S., and Papanicolaou, G. C., 1979, "The Effect of the Boundary Interphase on the Thermomechanical Behaviour of Composites Reinforced With Short Fibres," Fibre Sci. Technol., **12**(6), pp. 421–433.
[196] Rosen, B. W., 1965, "Mechanics of Composite Strengthening," Fibre Composite Materials, American Society for Metals, pp. 37–75.
[197] Benveniste, Y., Dvorak, G. J., and Chen, T., 1989, "Stress Fields in Composites With Coated Inclusions," Mech. Mater., **7**(4), pp. 305–317.
[198] Benveniste, Y., Dvorak, G. J., and Chen, T., 1991, "On Effective Properties of Composites With Coated Cylindrically Orthotropic Fibers," Mech. Mater., **12**(3–4), pp. 289–297.
[199] Chen, T., Dvorak, G. J., and Benveniste, Y., 1990, "Stress Fields in Composites Reinforced by Coated Cylindrically Orthotropic Fibers," Mech. Mater., **9**(1), pp. 17–32.
[200] Carman, G. P., Averill, R. C., Reifsnider, K. L., and Reddy, J. N., 1993, "Optimization of Fiber Coatings to Minimize Stress Concentrations in Composite Materials," J. Compos. Mater., **27**(6), pp. 589–612.
[201] Mikata, Y., and Taya, M., 1985, "Stress Field in a Coated Continuous Fiber Composite Subjected to Thermo-Mechanical Loadings," J. Compos. Mater., **19**(6), pp. 554–578.
[202] Mikata, Y., and Taya, M., 1985, "Stress Field in and Around a Coated Short Fiber in an Infinite Matrix Subjected to Uniaxial and Biaxial Loadings," ASME J. Appl. Mech., **52**(1), pp. 19–24.
[203] Hatta, H., and Taya, M., 1987, "Thermal Stress in a Coated Short Fiber Composite," ASME J. Eng. Mater. Technol., **109**(1), pp. 59–63.
[204] Pagano, N. J., and Tandon, G. P., 1988, "Elastic Response of Multi-Directional Coated-Fiber Composites," Compos. Sci. Technol., **31**(4), pp. 273–293.
[205] Pagano, N. J., and Tandon, G. P., 1990, "Thermo-Elastic Model for Multidirectional Coated-Fiber Composites: Traction Formulation," Compos. Sci. Technol., **38**(3), pp. 247–269.

[206] Duan, H. L., Wang, J., Huang, Z. P., and Zhong, Y., 2005, "Stress Fields of a Spheroidal Inhomogeneity With an Interphase in an Infinite Medium Under Remote Loadings," Proc. R. Soc. A, **461**(2056), pp. 1055–1080.
[207] Sullvian, B. J., and Hashin, Z., 1990, "Determination of Mechanical Properties of Interfacial Region Between Fiber and Matrix in Organic Matrix Composites," Controlled Interphases in Composite Materials, Springer, Dordrecht, The Netherlands, pp. 521–537.
[208] Maurer, F. H. J., 1990, "An Interlayer Model to Describe the Physical Properties of Particulate Composites," Controlled Interphases in Composite Materials, Springer, Dordrecht, The Netherlands, pp. 491–504.
[209] Qiu, Y. P., and Weng, G. J., 1991, "Elastic Moduli of Thickly Coated Particle and Fiber-Reinforced Composites," ASME J. Appl. Mech., **58**(2), pp. 388–398.
[210] Cherkaoui, M., Sabar, H., and Berveiller, M., 1994, "Micramechanical Approach of the Coated Inclusion Problem and Applications to Composite Materials," ASME J. Eng. Mater. Technol., **116**(3), pp. 274–278.
[211] Cherkaoui, M., Sabar, H., and Berveiller, M., 1995, "Elastic Composites With Coated Reinforcements: A Micromechanical Approach for Nonhomothetic Topology," Int. J. Eng. Sci., **33**(6), pp. 829–843.
[212] Barhdadi, E. H., Lipinski, P., and Cherkaoui, M., 2007, "Four Phase Model: A New Formulation to Predict the Effective Elastic Moduli of Composites," ASME J. Eng. Mater. Technol., **129**(2), pp. 313–320.
[213] El Mouden, M., Cherkaoui, M., Molinari, A., and Berveiller, M., 1998, "The Overall Elastic Response of Materials Containing Coated Inclusions in a Periodic Array," Int. J. Eng. Sci., **36**(7–8), pp. 813–829.
[214] Sarvestani, A. S., 2003, "On the Overall Elastic Moduli of Composites With Spherical Coated Fillers," Int. J. Solids Struct., **40**(26), pp. 7553–7566.
[215] Nazarenko, L., Bargmann, S., and Stolarski, H., 2016, "Lurie Solution for Spherical Particle and Spring Layer Model of Interphases: Its Application in Analysis of Effective Properties of Composites," Mech. Mater., **96**, pp. 39–52.
[216] Nazarenko, L., Stolarski, H., and Altenbach, H., 2017, "Thermo-Elastic Properties of Random Particulate Nano-Materials for Various Models of Interphase," Int. J. Mech. Sci., **126**, pp. 130–141.
[217] Nazarenko, L., Stolarski, H., and Altenbach, H., 2018, "Thermo-Elastic Properties of Random Composites With Unidirectional Anisotropic Short-Fibers and Interphases," Eur. J. Mech., A/Solids, **70**, pp. 249–266.
[218] Seidel, G. D., and Lagoudas, D. C., 2006, "Micromechanical Analysis of the Effective Elastic Properties of Carbon Nanotube Reinforced Composites," Mech. Mater., **38**(8–10), pp. 884–907.
[219] Xu, W., Ma, H., Ji, S., and Chen, H., 2016, "Analytical Effective Elastic Properties of Particulate Composites With Soft Interfaces Around Anisotropic Particles," Compos. Sci. Technol., **129**, pp. 10–18.
[220] Xu, W., Wu, F., Jiao, Y., and Liu, M., 2017, "A General Micromechanical Framework of Effective Moduli for the Design of Nonspherical Nano- and Micro-Particle Reinforced Composites With Interface Properties," Mater. Des., **127**, pp. 162–172.
[221] Xu, W., Jia, M., Zhu, Z., Liu, M., Lei, D., and Gou, X., 2018, "n-Phase Micromechanical Framework for the Conductivity and Elastic Modulus of Particulate Composites: Design to Microencapsulated Phase Change Materials (MPCMs)-Cementitious Composites," Mater. Des., **145**, pp. 108–115.
[222] Xu, W., Zhang, D., Lan, P., and Jiao, Y., 2019, "Multiple-Inclusion Model for the Transport Properties of Porous Composites Considering Coupled Effects of Pores and Interphase Around Spheroidal Particles," Int. J. Mech. Sci., **150**, pp. 610–616.
[223] Wu, Y., Ling, Z., and Dong, Z., 2000, "Stress-Strain Fields and the Effectiveness Shear Properties for Three-Phase Composites With Imperfect Interface," Int. J. Solids Struct., **37**(9), pp. 1275–1292.
[224] Nie, S., and Basaran, C., 2005, "A Micromechanical Model for Effective Elastic Properties of Particulate Composites With Imperfect Interfacial Bonds," Int. J. Solids Struct., **42**(14), pp. 4179–4191.
[225] Lu, P., Leong, Y. W., Pallathadka, P. K., and He, C. B., 2013, "Effective Moduli of Nanoparticle Reinforced Composites Considering Interphase Effect by Extended Double-Inclusion model - Theory and Explicit Expressions," Int. J. Eng. Sci., **73**, pp. 33–55.
[226] Shi, C., Tu, Q., Fan, H., Rios, C. A. O., and Li, S., 2016, "Interphase Models for Nanoparticle-Polymer Composites," J. Nanomech. Micromech., **6**(2), p. 04016003.
[227] Marcadon, V., Herve, E., and Zaoui, A., 2007, "Micromechanical Modeling of Packing and Size Effects in Particulate Composites," Int. J. Solids Struct., **44**(25–26), pp. 8213–8228.
[228] Liu, H. T., and Sun, L. Z., 2008, "A Micromechanics-Based Elastoplastic Model for Amorphous Composites With Nanoparticle Interactions," ASME J. Appl. Mech., **75**(3), p. 0310091.
[229] Deng, F., and Van Vliet, K. J., 2011, "Prediction of Elastic Properties for Polymer-Particle Nanocomposites Exhibiting an Interphase," Nanotechnology, **22**(16), p. 165703.
[230] Gardner, S. D., Pittman, C. U., and Hackett, R. M., 1993, "Polymeric Composite Materials Incorporating an Elastomeric Interphase: A Mathematical Assessment," Compos. Sci. Technol., **46**(4), pp. 307–318.
[231] Gardner, S. D., Pittman, C. U., and Hackett, R. M., 1993, "Residual Thermal Stresses in Filamentary Polymer-Matrix Composites Containing an Elastomeric Interphase," J. Compos. Mater., **27**(8), pp. 830–860.
[232] Gardner, S. D., Pittman, C. U., Chang, T. C., Low, B. Y., and Hackett, R. M., 1995, "Microstress Distribution in Graphite Fibre/Epoxy Composites Containing an Elastomeric Interphase: Response to Uniaxial and Biaxial Loading Conditions," Composite, **26**(4), pp. 269–280.
[233] Ordóñez-Miranda, J., Alvarado-Gil, J. J., and Medina-Ezquivel, R., 2010, "Generalized Bruggeman Formula for the Effective Thermal Conductivity of Particulate Composites With an Interface Layer," Int. J. Thermophys., **31**(4–5), pp. 975–986.
[234] Pham, D. C., and Torquato, S., 2003, "Strong-Contrast Expansions and Approximations for the Effective Conductivity of Isotropic Multiphase Composites," J. Appl. Phys., **94**(10), pp. 6591–6602.
[235] Tong, Y., and Jasiuk, I., 1990, "Transverse Elastic Moduli of Composites Reinforced With Cylindrical Coated Fibers: Successive Iteration Method," Proceedings of Fifth Technical Conference of the American Society for Composites, Lancaster, PA, May 1, pp. 117–126.
[236] Chouchaoui, C. S., and Benzeggagh, M. L., 1997, "The Effect of Interphase on the Elastic Behavior of a Glass/Epoxy Bundle," Compos. Sci. Technol., **57**(6), pp. 617–622.
[237] Guinovart-Díaz, R., Rodríguez-Ramos, R., Bravo-Castillero, J., and Sabina, F. J., 2003, "Modeling of Three-Phase Fibrous Composite Using the Asymptotic Homogenization Method," Mech. Adv. Mater. Struct., **10**(4), pp. 319–333.
[238] Lurie, S., Belov, P., Volkov-Bogorodsky, D., and Tuchkova, N., 2006, "Interphase Layer Theory and Application in the Mechanics of Composite Materials," J. Mater. Sci., **41**(20), pp. 6693–6707.
[239] Lebon, F., and Rizzoni, R., 2010, "Asymptotic Analysis of a Thin Interface: The Case Involving Similar Rigidity," Int. J. Eng. Sci., **48**(5), pp. 473–486.
[240] Lebon, F., and Rizzoni, R., 2011, "Asymptotic Behavior of a Hard Thin Linear Elastic Interphase: An Energy Approach," Int. J. Solids Struct., **48**(3–4), pp. 441–449.
[241] Papanicolaou, G. C., Theocaris, P. S., and Spathis, G. D., 1980, "Adhesion Efficiency Between phases in fibre-Reinforced Polymers by Means of the Concept of Boundary Interphase," Colloid Polym. Sci., **258**(11), pp. 1231–1237.
[242] Ostoja-Starzewski, M., Jasiuk, I., Wang, W., and Alzebdeh, K., 1996, "Composites With Functionally Graded Interphases: Mesocontinuum Concept and Effective Transverse Conductivity," Acta Mater., **44**(5), pp. 2057–2066.
[243] Sottos, N. R., McCullough, R. L., and Guceri, S. I., 1989, "Thermal Stresses Due to Property Gradients at the Fiber/Matrix Interface, in: American Society of Mechanical Engineers," Appl. Mech. Div., **100**, pp. 11–20.
[244] Jayaraman, K., Gao, Z., and Reifsnider, K. L., 1991, "Stress Fields in Continuous Fiber Composites With Interphasial Property Gradients," Proceedings of the American Society for Composites. Sixth Technical Conference. Composite Materials, Mechanics and Processing, Albany, New York, Oct. 7–9, pp. 759–768.
[245] Jayaraman, K., Reifsnider, K. L., and Giacco, A., 1992, "Local Stress Fields in a Unidirectional Fiber-Reinforced Composite With a Non-Homogeneous Interphase Region: Formulation," Adv. Compos. Lett., **1**(2), pp. 54–57.
[246] Jayaraman, K., and Reifsnider, K. L., 1993, "The Interphase in Unidirectional Fiber-Reinforced Epoxies: Effect on Residual Thermal Stress," Compos. Sci. Technol., **47**(2), pp. 119–129.
[247] Mikata, Y., 1994, "Stress Fields in a Continuous Fiber Composite With a Variable Interphase Under Thermo-Mechanical Loadings," ASME J. Eng. Mater. Technol., **116**(3), pp. 367–377.
[248] Ru, C. Q., 1999, "A New Method for an Inhomogeneity With Stepwise Graded Interphase Under Thermomechanical Loadings," J. Elasticity, **56**(2), pp. 107–127.
[249] Theocaris, P. S., Spathis, G., and Sideridis, E., 1982, "Elastic and Viscoelastic Properties of Fibre-Reinforced Composite Materials," Fibre Sci. Technol., **17**(3), pp. 169–181.
[250] Theocaris, P. S., Sideridis, E. P., and Papanicolaou, G. C., 1985, "The Elastic Longitudinal Modulus and Poisson's Ratio of Fiber Composites," J. Reinf. Plast. Compos., **4**(4), pp. 396–418.
[251] Sideridis, E., 1988, "The In-Plane Shear Modulus of Fibre Reinforced Composites as Defined by the Concept of Interphase," Compos. Sci. Technol., **31**(1), pp. 35–53.
[252] Theocaris, P. S., 1987, *The Mesophase Concept in Composites*, Springer-Verlag, Berlin.
[253] Theocaris, P. S., 1985, "The Unfolding Model for the Representation of the Mesophase Layer in Composites," J. Appl. Polym. Sci., **30**(2), pp. 621–645.
[254] Dasgupta, A., and Bhandarkar, S. M., 1992, "A Generalized Self-Consistent Mori-Tanaka Scheme for Fiber-Composites With Multiple Interphases," Mech. Mater., **14**(1), pp. 67–82.
[255] Shabana, Y. M., 2013, "A Micromechanical Model for Composites Containing Multi-Layered Interphases," Compos. Struct., **101**, pp. 265–273.
[256] Herve, E., and Zaoui, A., 1993, "n-Layered Inclusion-Based Micromechanical Modelling," Int. J. Eng. Sci., **31**(1), pp. 1–10.
[257] Herve, E., and Zaoui, A., 1995, "Elastic Behaviour of Multiply Coated Fibre-Reinforced Composites," Int. J. Eng. Sci., **33**(10), pp. 1419–1433.
[258] Berbenni, S., and Cherkaoui, M., 2010, "Homogenization of Multicoated Inclusion-Reinforced Linear Elastic Composites With Eigenstrains: Application to Thermoelastic Behavior," Philos. Mag., **90**(22), pp. 3003–3026.
[259] Bonfoh, N., Coulibaly, M., and Sabar, H., 2014, "Effective Properties of Elastic Composite Materials With Multi-Coated Reinforcements: A New Micromechanical Modelling and Applications," Compos. Struct., **115**, pp. 111–119.
[260] Jasiuk, I., and Kouider, M. W., 1993, "The Effect of an Inhomogeneous Interphase on the Elastic Constants of Transversely Isotropic Composites," Mech. Mater., **15**(1), pp. 53–63.
[261] Wu, Y. M., Huang, Z. P., Zhong, Y., and Wang, J., 2004, "Effective Moduli of Particle-Filled Composite With Inhomogeneous Interphase: Part I—Bounds," Compos. Sci. Technol., **64**(9), pp. 1345–1351.

[262] Zhong, Y., Wang, J., Wu, Y. M., and Huang, Z. P., 2004, "Effective Moduli of Particle-Filled Composite With Inhomogeneous Interphase: Part II - Mapping Method and Evaluation," Compos. Sci. Technol., **64**(9), pp. 1353–1362.
[263] Xu, W., Wu, Y., and Gou, X., 2019, "Effective Elastic Moduli of Nonspherical Particle-Reinforced Composites With Inhomogeneous Interphase Considering Graded Evolutions of Elastic Modulus and Porosity," Comput. Methods Appl. Mech. Eng., **350**, pp. 535–553.
[264] Lutz, M. P., and Zimmerman, R. W., 1996, "Effect of an Inhomogeneous Interphase Zone on the Bulk Modulus of a Particulate Composite," Compos. Part B, **63**(4), pp. 855–561.
[265] Lutz, M. P., Monteiro, P. J. M., and Zimmerman, R. W., 1997, "Inhomogeneous Interfacial Transition Zone Model for the Bulk Modulus of Mortar," Cem. Concrete Res., **27**(7), pp. 1113–1122.
[266] Lutz, M. P., and Zimmerman, R. W., 2005, "Effect of an Inhomogeneous Interphase Zone on the Bulk Modulus and Conductivity of a Particulate Composite," Int. J. Solids Struct., **42**(2), pp. 429–437.
[267] Lutz, M. P., and Zimmerman, R. W., 2016, "Effect of the Interphase Zone on the Conductivity or Diffusivity of a Particulate Composite Using Maxwell's Homogenization Method," Int. J. Eng. Sci., **98**, pp. 51–59.
[268] Low, B. Y., Gardner, S. D., Pittman, C. U., and Hackett, R. M., 1994, "A Micromechanical Characterization of Graphite-Fiber/Epoxy Composites Containing a Heterogeneous Interphase Region," Compos. Sci. Technol., **52**(4), pp. 589–606.
[269] Low, B. Y., Gardner, S. D., Pittman, C. U., and Hackett, R. M., 1995, "A Micromechanical Characterization of Residual Thermal Stresses in Carbon Fiber/Epoxy Composites Containing a Non-Uniform Interphase Region," Compos. Eng., **5**(4), pp. 375–396.
[270] Li, J. Y., 2000, "Thermoelastic Behavior of Composites With Functionally Graded Interphase: A Multi-Inclusion Model," Int. J. Solids Struct., **37**(39), pp. 5579–5597.
[271] Shen, L., and Yi, S., 2001, "An Effective Inclusion Model for Effective Moduli of Heterogeneous Materials With Ellipsoidal Inhomogeneities," Int. J. Solids Struct., **38**(32–33), pp. 5789–5805.
[272] Shen, L., and Li, J., 2003, "Effective Elastic Moduli of Composites Reinforced by Particle or Fiber With an Inhomogeneous Interphase," Int. J. Solids Struct., **40**(6), pp. 1393–1409.
[273] Shen, L., and Li, J., 2005, "Homogenization of a Fibre/Sphere With an Inhomogeneous Interphase for the Effective Elastic Moduli of Composites," Proc. R. Soc. A, **461**(2057), pp. 1475–1504.
[274] Sevostianov, I., and Kachanov, M., 2007, "Effect of Interphase Layers on the Overall Elastic and Conductive Properties of Matrix Composites. Applications to Nanosize Inclusion," Int. J. Solids Struct., **44**(3–4), pp. 1304–1315.
[275] Jiang, Y., Tohgo, K., and Shimamura, Y., 2009, "A Micro-Mechanics Model for Composites Reinforced by Regularly Distributed Particles With an Inhomogeneous Interphase," Comput. Mater. Sci., **46**(2), pp. 507–515.
[276] Li, Y., Waas, A. M., and Arruda, E. M., 2011, "A Closed-Form, Hierarchical, Multi-Interphase Model for Composites—Derivation, Verification and Application to Nanocomposites," J. Mech. Phys. Solids, **59**(1), pp. 43–63.
[277] Hernández-Pérez, A., and Avilés, F., 2010, "Modeling the Influence of Interphase on the Elastic Properties of Carbon Nanotube Composites," Comput. Mater. Sci., **47**(4), pp. 926–933.
[278] Mahiou, H., and Béakou, A., 1998, "Modelling of Interfacial Effects on the Mechanical Properties of Fibre-Reinforced Composites," Compos. Part A, **29**(9–10), pp. 1035–1048.
[279] Kiritsi, C. C., and Anifantis, N. K., 2001, "Load Carrying Characteristics of Short Fiber Composites Containing a Heterogeneous Interphase Region," Comput. Mater. Sci., **20**(1), pp. 86–97.
[280] You, L. H., You, X. Y., and Zheng, Z. Y., 2006, "Thermomechanical Analysis of Elastic-Plastic Fibrous Composites Comprising an Inhomogeneous Interphase," Comput. Mater. Sci., **36**(4), pp. 440–450.
[281] Yao, Y., Chen, S., and Chen, P., 2013, "The Effect of a Graded Interphase on the Mechanism of Stress Transfer in a Fiber-Reinforced Composite," Mech. Mater., **58**, pp. 35–54.
[282] Sabiston, T., Mohammadi, M., Cherkaoui, M., Lévesque, J., and Inal, K., 2016, "Micromechanics for a Long Fibre Reinforced Composite Model With a Functionally Graded Interphase," Compos. Part B, **84**, pp. 188–199.
[283] Sburlati, R., and Cianci, R., 2015, "Interphase Zone Effect on the Spherically Symmetric Elastic Response of a Composite Material Reinforced by Spherical Inclusions," Int. J. Solids Struct., **71**, pp. 91–98.
[284] Sburlati, R., Cianci, R., and Kashtalyan, M., 2018, "Hashin's Bounds for Elastic Properties of Particle-Reinforced Composites With Graded Interphase," Int. J. Solids Struct., **138**, pp. 224–235.
[285] Rao, Y. N., and Dai, H. L., 2017, "Micromechanics-Based Thermo-Viscoelastic Properties Prediction of Fiber Reinforced Polymers With Graded Interphases and Slightly Weakened Interfaces," Compos. Struct., **168**, pp. 440–455.
[286] Yang, Y., He, Q., Dai, H. L., Pang, J., Yang, L., Li, X. Q., Rao, Y. N., and Dai, T., 2020, "Micromechanics-Based Analyses of Short Fiber-Reinforced Composites With Functionally Graded Interphases," J. Compos. Mater., **54**(8), pp. 1031–1048.
[287] Broutman, L. J., and Agarwal, B. D., 1974, "A Theoretical Study of the Effect of an Interfacial Layer on the Properties of Composites," Polym. Eng. Sci., **14**(8), pp. 581–588.
[288] Agarwal, B. D., and Bansal, R. K., 1979, "Effect of an Interfacial Layer on the Properties of Fibrous Composites: A Theoretical Analysis," Fibre Sci. Technol., **12**(2), pp. 149–158.
[289] Tsai, H. C., Arocho, A. M., and Gause, L. W., 1990, "Prediction of Fiber-Matrix Interphase Properties and Their Influence on Interface Stress, Displacement and Fracture Toughness of Composite Material," Mater. Sci. Eng. A, **126**(1–2), pp. 295–304.
[290] Nassehi, V., Dhillon, J., and Mascia, L., 1993, "Finite Element Simulation of the Micromechanics of Interlayered Polymer/Fiber Composites: A Study of the Interactions Between the Reinforcing Phases," Compos. Sci. Technol., **47**(4), pp. 349–358.
[291] Nassehi, V., Kinsella, M., and Mascia, L., 1993, "Finite Element Modelling of the Stress Distribution in Polymer Composites With Coated Fibre Interlayers," J. Compos. Mater., **27**(2), pp. 195–214.
[292] Wu, Y., and Dong, Z., 1995, "Three-Dimensional Finite Element Analysis of Composites With Coated Spherical Inclusions," Mater. Sci. Eng. A, **203**(1–2), pp. 314–323.
[293] Tsui, C. P., Tang, C. Y., and Lee, T. C., 2001, "Finite Element Analysis of Polymer Composites Filled by Interphase Coated Particles," J. Mater. Process. Technol., **117**(1–2), pp. 105–110.
[294] Al-Ostaz, A., and Jasiuk, I., 1997, "The Influence of Interface and Arrangement of Inclusions on Local Stresses in Composite Materials," Acta Mater., **45**(10), pp. 4131–4143.
[295] Kari, S., Berger, H., Gabbert, U., Guinovart-Dıaz, R., Bravo-Castillero, J., and Rodrıguez-Ramos, R., 2008, "Evaluation of Influence of Interphase Material Parameters on Effective Material Properties of Three Phase Composites," Compos. Sci. Technol., **68**(3–4), pp. 684–691.
[296] Pathan, M. V., Tagarielli, V. L., and Patsias, S., 2017, "Effect of Fibre Shape and Interphase on the Anisotropic Viscoelastic Response of Fibre Composites," Compos. Struct., **162**, pp. 156–163.
[297] Riaño, L., Belec, L., Chailan, J. F., and Joliff, Y., 2018, "Effect of Interphase Region on the Elastic Behavior of Unidirectional Glass-Fiber/Epoxy Composites," Compos. Struct., **198**, pp. 109–116.
[298] Chang, C., Zhang, Y., and Wang, H., 2019, "Micromechanical Modeling of Unidirectional Composites With Random Fiber and Interphase Thickness Distributions," Arch. Appl. Mech., **89**(12), pp. 2563–2575.
[299] Gosz, M., Moran, B., and Achenbach, J. D., 1994, "On the Role of Interphases in the Transverse Failure of Fiber Composites," Int. J. Damage Mech., **3**(4), pp. 357–377.
[300] Gulrajani, S. N., and Mukherjee, S., 1993, "Sensitivities and Optimal Design of Hexagonal Array Fiber Composites With Respect to Interphase Properties," Int. J. Solids Struct., **30**(15), pp. 2009–2026.
[301] Liu, Y. J., Xu, N., and Luo, J. F., 2000, "Modeling of Interphases in Fiber-Reinforced Composites Under Transverse Loading Using the Boundary Element Method," ASME J. Appl. Mech., **67**(1), pp. 41–49.
[302] Chen, T., 2001, "Thermal Conduction of a Circular Inclusion With Variable Interface Parameter," Int. J. Solids Struct., **38**(17), pp. 3081–3097.
[303] Yao, Z., Kong, F., Wang, H., and Wang, P., 2004, "2D Simulation of Composite Materials Using BEM," Eng. Anal. Bound. Elem., **28**(8), pp. 927–935.
[304] Mogilevskaya, S. G., and Crouch, S. L., 2004, "A Galerkin Boundary Integral Method for Multiple Circular Elastic Inclusions With Uniform Interphase Layers," Int. J. Solids Struct., **41**(5–6), pp. 1285–1311.
[305] Ozmusul, M. S., and Picu, R. C., 2002, "Elastic Moduli of Particulate Composites With Graded Filler-Matrix Interfaces," Polym. Compos., **23**(1), pp. 110–119.
[306] Wang, J., Crouch, S. L., and Mogilevskaya, S. G., 2006, "Numerical Modeling of the Elastic Behavior of Fiber-Reinforced Composites With Inhomogeneous Interphases," Compos. Sci. Technol., **66**(1), pp. 1–18.
[307] Lagache, M., Agbossou, A., Pastor, J., and Muller, D., 1994, "Role of Interphase on the Elastic Behavior of Composite Materials: Theoretical and Experimental Analysis," J. Compos. Mater., **28**(12), pp. 1140–1157.
[308] Pan, L., Adams, D. O., and Rizzo, F. J., 1998, "Boundary Element Analysis for Composite Materials and a Library of Green's Functions," Comput. Struct., **66**(5), pp. 685–693.
[309] Hayes, S. A., Lane, R., and Jones, F. R., 2001, "Fibre/Matrix Stress Transfer Through a Discrete Interphase: Part 1—Single-Fibre Model Composites," Compos. Part A, **32**(3–4), pp. 379–389.
[310] Lane, R., Hayes, S. A., and Jones, F. R., 2001, "Fibre/Matrix Stress Transfer Through a Discrete Interphase: 2—High Volume Fraction Systems," Compos. Sci. Technol., **61**(4), pp. 565–578.
[311] Fisher, F. T., and Brinson, L. C., 2001, "Viscoelastic Interphases in Polymer-Matrix Composites: Theoretical Models and Finite-Element Analysis," Compos. Sci. Technol., **61**(5), pp. 731–748.
[312] Wang, X., Zhang, J., Wang, Z., Zhou, S., and Sun, X., 2011, "Effects of Interphase Properties in Unidirectional Fiber Reinforced Composite Materials," Mater. Des., **32**(6), pp. 3486–3492.
[313] Han, F., Azdoud, Y., and Lubineau, G., 2014, "Computational Modeling of Elastic Properties of Carbon Nanotube/Polymer Composites With Interphase Regions: Part I—Micro-Structural Characterization and Geometric Modeling," Comput. Mater. Sci., **81**, pp. 641–651.
[314] Han, F., Azdoud, Y., and Lubineau, G., 2014, "Computational Modeling of Elastic Properties of Carbon Nanotube/Polymer Composites With Interphase Regions: Part II—Mechanical Modeling," Comput. Mater. Sci., **81**, pp. 652–661.
[315] Xu, W., Xu, B., and Guo, F., 2017, "Elastic Properties of Particle-Reinforced Composites Containing Nonspherical Particles of High Packing Density and Interphase: DEM-FEM Simulation and Micromechanical Theory," Comput. Methods Appl. Mech. Eng., **326**, pp. 122–143.
[316] Lee, S. H., Wang, S., Pharr, G. M., and Xu, H., 2007, "Evaluation of Interphase Properties in a Cellulose Fiber-Reinforced Polypropylene Composite by

Nanoindentation and Finite Element Analysis," Compos. Part A, **38**(6), pp. 1517–1524.
[317] Jiang, Y., Guo, W., and Yang, H., 2008, "Numerical Studies on the Effective Shear Modulus of Particle Reinforced Composites With an Inhomogeneous Inter-Phase," Comput. Mater. Sci., **43**(4), pp. 724–731.
[318] Sabiston, T., Mohammadi, M., Cherkaoui, M., Lévesque, J., and Inal, K., 2016, "Micromechanics Based Elasto-Visco-Plastic Response of Long Fibre Composites Using Functionally Graded Interphases at Quasi-Static and Moderate Strain Rates," Compos. Part B, **100**, pp. 31–43.
[319] Sokołowski, D., and Kamiński, M., 2018, "Computational Homogenization of Carbon/Polymer Composites With Stochastic Interface Defects," Compos. Struct., **183**, pp. 434–449.
[320] Sokołowski, D., and Kamiński, M., 2018, "Homogenization of Carbon/Polymer Composites With Anisotropic Distribution of Particles and Stochastic Interface Defects," Acta Mech., **229**(9), pp. 3727–3765.
[321] Sokołowski, D., and Kamiński, M., 2020, "Probabilistic Homogenization of Hyper-Elastic Particulate Composites With Random Interface," Compos. Struct., **241**, p. 112118.
[322] Kamiński, M., and Ostrowski, P., 2021, "Homogenization of Heat Transfer in Fibrous Composite With Stochastic Interface Defects," Compos. Struct., **261**, p. 113555.
[323] Tac, V., and Gürses, E., 2019, "Micromechanical Modelling of Carbon Nanotube Reinforced Composite Materials With a Functionally Graded Interphase," J. Compos. Mater., **53**(28–30), pp. 4337–4348.
[324] Cheng, Y., Cheng, H., Zhang, K., Jones, K. K., Gao, J., Hu, J., Li, H., and Liu, W. K., 2019, "A Sequential Homogenization of Multi-Coated Micromechanical Model for Functionally Graded Interphase Composites," Comput. Mech., **64**(5), pp. 1321–1337.
[325] Huang, J., Wu, Y., and Huang, L., 2021, "Evaluation of the Mechanical Properties of Graphene-Based Nanocomposites Incorporating a Graded Interphase Based on Isoparametric Graded Finite Element Model," Compos. Interfaces, **28**(6), pp. 543–575.
[326] Le, T. T., 2021, "Probabilistic Modeling of Surface Effects in Nano-Reinforced Materials," Comput. Mater. Sci., **186**, p. 109987.
[327] Papanicolaou, G. C., Paipetis, S. A., and Theocaris, P. S., 1978, "The Concept of Boundary Interphase in Composite Mechanics," Colloid Polym. Sci., **256**(7), pp. 625–630.
[328] Papanicolaou, G. C., and Theocaris, P. S., 1979, "Thermal Properties and Volume Fraction of the Boundary Interphase in Metal-Filled Epoxies," Colloid Polym. Sci., **257**(3), pp. 239–246.
[329] Chu, Y. C., and Rokhlin, S. I., 1995, "Determination of Fiber-Matrix Interphase Moduli From Experimental Moduli of Composites With Multi-Layered Fibers," Mech. Mater., **21**(3), pp. 191–215.
[330] Huang, W., and Rokhlin, S. I., 1996, "Generalized Self-Consistent Model for Composites With Functionally Graded and Multilayered Interphases. Transfer Matrix Approach," Mech. Mater., **22**(3), pp. 219–247.
[331] Rokhlin, S. I., and Huang, W., 1998, "Micromechanical Analysis and Ultrasonic Characterization of Interphases and Interphasial Damage in High Temperature Composites," Compos. Part B, **29**(2), pp. 147–157.
[332] Hashin, Z., and Monteiro, P. J. M., 2002, "An Inverse Method to Determine the Elastic Properties of the Interphase Between the Aggregate and the Cement Paste," Cem. Concrete Res., **32**(8), pp. 1291–1300.
[333] Ramesh, G., Sotelino, E. D., and Chen, W. F., 1996, "Effect of Transition Zone on Elastic Moduli of Concrete Materials," Cem. Concrete Res., **26**(4), pp. 611–622.
[334] Meurs, P. F. M., Schreurs, P. J. G., Peijs, T., and Meijer, H. E. H., 1996, "Characterization of Interphase Conditions in Composite Materials," Compos. Part A, **27**(9), pp. 781–786.
[335] Matzenmiller, A., and Gerlach, S., 2005, "Parameter Identification of Elastic Interphase Properties in Fiber Composites," Compos. Part B, **37**(2–3), pp. 117–126. 2006).
[336] Paley, M., and Aboudi, J., 1992, "Micromechanical Analysis of Composites by the Generalized Cells Model," Mech. Mater., **14**(2), pp. 127–139.
[337] Matzenmiller, A., and Gerlach, S., 2004, "Micromechanical Modeling of Viscoelastic Composites With Compliant Fiber-Matrix Bonding," Comput. Mater. Sci., **29**(3), pp. 283–300.
[338] Broutman, L. J., 1966, "Glass-Resin Joint Strength and Their Effect on Failure Mechanisms in Reinforced Plastics," Polym. Eng. Sci., **6**(3), pp. 263–272.
[339] Bowling, J., and Groves, G. W., 1979, "The Debonding and Pull-Out of Ductile Wires From a Brittle Matrix," J. Mater. Sci., **14**(2), pp. 431–442.
[340] Bartoš, P., 1980, "Analysis of Pull-Out Tests on Fibres Embedded in Brittle Matrices," J. Mater. Sci., **15**(12), pp. 3122–3128.
[341] Miller, B., Muri, P., and Rebenfeld, L., 1987, "A Microbond Method for Determination of the Shear Strength of a Fiber/Resin Interface," Compos. Sci. Technol., **28**(1), pp. 17–32.
[342] Drzal, L. T., and Madhukar, M., 1993, "Fibre-Matrix Adhesion and Its Relationship to Composite Mechanical Properties," J. Mater. Sci., **28**(3), pp. 569–610.
[343] Larson, B. K., and Drzal, L. T., 1994, "Glass Fibre Sizing/Matrix Interphase Formation in Liquid Composite Moulding: Effects on Fibre/Matrix Adhesion and Mechanical Properties," Composite, **25**(7), pp. 711–721.
[344] Mäder, E., and Pisanova, E., 2000, "Characterization and Design of Interphases in Glass Fiber Reinforced Polypropylene," Polym. Compos., **21**(3), pp. 361–368.
[345] Pompe, G., and Mäder, E., 2000, "Experimental Detection of a Transcrystalline Interphase in Glass-Fibre/Polypropylene Composites," Compos. Sci. Technol., **60**(11), pp. 2159–2167.
[346] Shodja, H. M., and Sarvestani, A. S., 2001, "Elastic Fields in Double Inhomogeneity by the Equivalent Inclusion Method," ASME J. Appl. Mech., **68**(1), pp. 3–10.
[347] Mandell, J. F., Grande, D. H., Tsiang, T. H., and McGarry, F. J., 1986, "Modified Mircodebonding Test for Direct in Situ Fiber/Matrix Bond Strength Determination in Fiber Composites," Composite Materials: Testing and Design, ASTM International, West Conshohocken, PA.
[348] Ochiai, S., and Osamura, K., 1987, "Computer Simulation of Strength of Metal Matrix Composites With a Reaction Layer at the Interface," Metall. Trans., **18**(4), pp. 673–679A.
[349] Zhu, H., and Achenbach, J. D., 1991, "Radial Matrix Cracking and Interphase Failure in Transversely Loaded Fiber Composites," Mech. Mater., **11**(4), pp. 347–356.
[350] Weitsman, Y., and Zhu, H., 1993, "Multi-Fracture of Ceramic Composites," J. Mech. Phys. Solids, **41**(2), pp. 351–388.
[351] Asp, L. E., Berglund, L. A., and Talreja, R., 1996, "Effects of Fiber and Interphase on Matrix-Initiated Transverse Failure in Polymer Composites," Compos. Sci. Technol., **56**(6), pp. 657–665.
[352] Wu, W., Verpoest, I., and Varna, J., 1998, "An Improved Analysis of the Stresses in a Single-Fibre Fragmentation Test—II: 3-Phase Model," Compos. Sci. Technol., **58**(1), pp. 41–50.
[353] Needleman, A., Borders, T. L., Brinson, L. C., Flores, V. M., and Schadler, L. S., 2010, "Effect of an Interphase Region on Debonding of a CNT Reinforced Polymer Composite," Compos. Sci. Technol., **70**(15), pp. 2207–2215.
[354] Romanowicz, M., 2010, "Progressive Failure Analysis of Unidirectional Fiber-Reinforced Polymers With Inhomogeneous Interphase and Randomly Distributed Fibers Under Transverse Tensile Loading," Compos. Part A, **41**(12), pp. 1829–1838.
[355] Maligno, A. R., Warrior, N. A., and Long, A. C., 2010, "Effects of Interphase Material Properties in Unidirectional Fibre Reinforced Composites," Compos. Sci. Technol., **70**(1), pp. 36–44.
[356] Sanchez-Palencia, E., 1970, "Comportement Limite D'un Probleme de Transmissiona Travers Une Plaque Faiblement Conductrice," C. R. Math. Acad. Sci., **270**, pp. 1026–1028.
[357] Pham Huy, H., and Sanchez-Palencia, E., 1974, "Phénomènes de Transmission à Travers Des Couches Minces de Conductivitéélevée," J. Math. Anal. Appl., **47**(2), pp. 284–309.
[358] Hashin, Z., 1991, "Thermoelastic Properties of Particulate Composites With Imperfect Interface," J. Mech. Phys. Solids, **39**(6), pp. 745–762.
[359] Hashin, Z., 1991, "Composite Materials With Interphase: Thermoelastic and Inelastic Effects," *Inelastic Deformation of Composite Materials*, Springer-Verlag, New York, pp. 3–34.
[360] Hashin, Z., 1990, "Thermoelastic Properties of Fiber Composites With Imperfect Interface," Mech. Mater., **8**(4), pp. 333–348.
[361] Benveniste, Y., and Miloh, T., 2001, "Imperfect Soft and Stiff Interfaces in Two-Dimensional Elasticity," Mech. Mater., **33**(6), pp. 309–323.
[362] Wang, J., Duan, H. L., Zhang, Z., and Huang, Z. P., 2005, "An Anti-Interpenetration Model and Connections Between Interphase and Interface Models in Particle-Reinforced Composites," Int. J. Mech. Sci., **47**(4–5), pp. 701–718.
[363] Daher, N., and Maugin, G. A., 1986, "The Method of Virtual Power in Continuum Mechanics Application to Media Presenting Singular Surfaces and Interfaces," Acta Mech., **60**(3–4), pp. 217–240.
[364] Lipton, R., and Vernescu, B., 1995, "Variational Methods, Size Effects and Extremal Microgeometries for Elastic Composites With Imperfect Interface," Math. Models Methods Appl. Sci., **05**(08), pp. 1139–1173.
[365] Miller, R. E., and Shenoy, V. B., 2000, "Size-Dependent Elastic Properties of Nanosized Structural Elements," Nanotechnology, **11**(3), pp. 139–147.
[366] Barenblatt, G. I., 1959, "The Formation of Equilibrium Cracks During Brittle Fracture. General Ideas and Hypotheses. Axially-Symmetric Cracks," J. Appl. Math. Mech., **23**(3), pp. 622–444.
[367] Barenblatt, G. I., 1962, "The Mathematical Theory of Equilibrium Cracks in Brittle Fracture," Adv. Appl. Mech., **7**, pp. 55–129.
[368] Dugdale, D. S., 1960, "Yielding of Steel Sheets Containing Slits," J. Mech. Phys. Solids, **8**(2), pp. 100–104.
[369] Jones, J. P., and Whittier, J. S., 1967, "Waves at a Flexibly Bonded Interface," ASME J. Appl. Mech., **34**(4), pp. 905–909.
[370] Mal, A. K., and Bose, S. K., 1974, "Dynamic Elastic Moduli of a Suspension of Imperfectly Bonded Spheres," Math. Proc. Cambridge Philos. Soc., **76**(3), pp. 587–600.
[371] Theocaris, P. S., Paipetis, S. A., and Stassinakis, C. A., 1978, "Effect of Geometry and Imperfect Bonding in Composite Systems With Limiting Shear Properties," Fibre Sci. Technol., **11**(5), pp. 335–352.
[372] Benveniste, Y., 1985, "The Effective Mechanical Behaviour of Composite Materials With Imperfect Contact Between the Constituents," Mech. Mater., **4**(2), pp. 197–208.
[373] Benveniste, Y., and Miloh, T., 1986, "The Effective Conductivity of Multiphase Composites With Imperfect Thermal Contact at Constituent Interfaces," Int. J. Eng. Sci., **24**(9), pp. 1537–1552.
[374] Aboudi, J., 1988, "Constitutive Equations for Elastoplastic Composites With Imperfect Bonding," Int. J. Plasticity, **4**(2), pp. 103–125.
[375] Aboudi, J., 1987, "Damage in Composites-Modeling of Imperfect Bonding," Int. J. Eng. Sci., **28**(2), pp. 103–128.
[376] Takahashi, K., and Chou, T. W., 1988, "Transverse Elastic Moduli of Unidirectional Fiber Composites With Interfacial Debonding," Metall. Trans. A, **19**(1), pp. 129–135.

[377] Shan, H. Z., and Chou, T. W., 1995, "Transverse Elastic Moduli of Unidirectional Fiber Composites With Fiber/Matrix Interfacial Debonding," Compos. Sci. Technol., **53**(4), pp. 383–391.
[378] Karihaloo, B. L., and Viswanathan, K., 1988, "A Partially Debonded Ellipsoidal Inclusion in an Elastic Medium: Part I—Stress and Displacement Fields," Mech. Mater., **7**(3), pp. 191–197.
[379] Karihaloo, B. L., and Viswanathan, K., 1988, "A Partially Debonded Ellipsoidal Inclusion in an Elastic Medium: Part II—Stress Intensity Factors and Debond Opening Displacement," Mech. Mater., **7**(3), pp. 199–203.
[380] Hashin, Z., 1992, "Extremum Principles for Elastic Heterogenous Media With Imperfect Interfaces and Their Application to Bounding of Effective Moduli," J. Mech. Phys. Solids, **40**(4), pp. 767–781.
[381] Levy, A. J., 1991, "The Debonding of Elastic Inclusions and Inhomogeneities," J. Mech. Phys. Solids, **39**(4), pp. 477–505.
[382] Levy, A. J., 1996, "The Effective Dilatational Response of Fiber-Reinforced Composites With Nonlinear Interface," ASME J. Appl. Mech., **63**(2), pp. 357–364.
[383] Qu, J., 1993, "Eshelby Tensor for an Elastic Inclusion With Slightly Weakened Interface," ASME J. Appl. Mech., **60**(4), pp. 1048–1050.
[384] Gao, Z., 1995, "Circular Inclusion With Imperfect Interface: Eshelby's Tensor and Related Problems," ASME J. Appl. Mech., **62**(4), pp. 860–866.
[385] Lee, H. K., and Pyo, S. H., 2008, "Multi-Level Modeling of Effective Elastic Behavior and Progressive Weakened Interface in Particulate Composites," Compos. Sci. Technol., **68**(2), pp. 387–397.
[386] Ju, J. W., and Chen, T. M., 1994, "Micromechanics and Effective Elastoplastic Behavior of Two-Phase Metal Matrix Composites," ASME J. Eng. Mater. Technol., **116**(3), pp. 310–318.
[387] Esteva, M., and Spanos, P. D., 2009, "Effective Elastic Properties of Nanotube Reinforced Composites With Slightly Weakened Interfaces," J. Mech. Mater. Struct., **4**(5), pp. 887–900.
[388] Othmani, Y., Delannay, L., and Doghri, I., 2011, "Equivalent Inclusion Solution Adapted to Particle Debonding With a Non-Linear Cohesive Law," Int. J. Solids Struct., **48**(24), pp. 3326–3335.
[389] Xu, B. X., Mueller, R., and Wang, M. Z., 2011, "The Eshelby Property of Sliding Inclusions," Archive Appl. Mech., **81**(1), pp. 19–35.
[390] Yanase, K., and Ju, J. W., 2012, "Effective Elastic Moduli of Spherical Particle Reinforced Composites Containing Imperfect Interfaces," Int. J. Damage Mech., **21**(1), pp. 97–127.
[391] Hosseini Kordkheili, S. A., and Toozandehjani, H., 2014, "Effective Mechanical Properties of Unidirectional Composites in the Presence of Imperfect Interface," Arch. Appl. Mech., **84**(6), pp. 807–819.
[392] Lee, S., Kim, Y., Lee, J., and Ryu, S., 2019, "Applicability of the Interface Spring Model for Micromechanical Analyses With Interfacial Imperfections to Predict the Modified Exterior Eshelby Tensor and Effective Modulus," Math. Mech. Solids, **24**(9), pp. 2944–2960.
[393] Lee, S., Lee, J., and Ryu, S., 2019, "Modified Eshelby Tensor for an Anisotropic Matrix With Interfacial Damage," Math. Mech. Solids, **24**(6), pp. 1749–1762.
[394] Qu, J., 1993, "The Effect of Slightly Weakened Interfaces on the Overall Elastic Properties of Composite Materials," Mech. Mater., **14**(4), pp. 269–281.
[395] Tan, H., Huang, Y., Liu, C., and Geubelle, P. H., 2005, "The Mori-Tanaka Method for Composite Materials With Nonlinear Interface Debonding," Int. J. Plasticity, **21**(10), pp. 1890–1918.
[396] Tan, H., Liu, C., Huang, Y., and Geubelle, P. H., 2005, "The Cohesive Law for the Particle/Matrix Interfaces in High Explosives," J. Mech. Phys. Solids, **53**(8), pp. 1892–1917.
[397] Tan, H., Huang, Y., Liu, C., Ravichandran, G., and Paulino, G. H., 2007, "Constitutive Behaviors of Composites With Interface Debonding: The Extended Mori-Tanaka Method for Uniaxial Tension," Int. J. Fract., **146**(3), pp. 139–148.
[398] Zhao, Y. H., and Weng, G. J., 1997, "Transversely Isotropic Moduli of Two Partially Debonded Composites," Int. J. Solids Struct., **34**(4), pp. 493–507.
[399] Liu, H. T., Sun, L. Z., and Ju, J. W., 2004, "An Interfacial Debonding Model for Particle-Reinforced Composites," Int. J. Damage Mech., **13**(2), pp. 163–185.
[400] Shao, L. H., Luo, R. Y., Bai, S. L., and Wang, J., 2009, "Prediction of Effective Moduli of Carbon Nanotube-Reinforced Composites With Waviness and Debonding," Compos. Struct., **87**(3), pp. 274–281.
[401] Brassart, L., Inglis, H. M., Delannay, L., Doghri, I., and Geubelle, P. H., 2009, "An Extended Mori-Tanaka Homogenization Scheme for Finite Strain Modeling of Debonding in Particle-Reinforced Elastomers," Comput. Mater. Sci., **45**(3), pp. 611–616.
[402] Teng, H., 2010, "Stiffness Properties of Particulate Composites Containing Debonded Particles," Int. J. Solids Struct., **47**(17), pp. 2191–2200.
[403] Koyama, S., Katano, S., Saiki, I., and Iwakuma, T., 2011, "A Modification of the Mori-Tanaka Estimate of Average Elastoplastic Behavior of Composites and Polycrystals With Interfacial Debonding," Mech. Mater., **43**(10), pp. 538–555.
[404] Nafar Dastgerdi, J., Marquis, G., and Salimi, M., 2014, "Micromechanical Modeling of Nanocomposites Considering Debonding and Waviness of Reinforcements," Compos. Struct., **110**, pp. 1–6.
[405] Duan, H. L., Wang, J., Huang, Z. P., and Luo, Z. Y., 2005, "Stress Concentration Tensors of Inhomogeneities With Interface Effects," Mech. Mater., **37**(7), pp. 723–736.
[406] Duan, H. L., Yi, X., Huang, Z. P., and Wang, J., 2007, "A Unified Scheme for Prediction of Effective Moduli of Multiphase Composites With Interface Effects: Part I—Theoretical Framework," Mech. Mater., **39**(1), pp. 81–93.
[407] Duan, H. L., Yi, X., Huang, Z. P., and Wang, J., 2007, "A Unified Scheme for Prediction of Effective Moduli of Multiphase Composites With Interface Effects: Part II-Application and Scaling Laws," Mech. Mater., **39**(1), pp. 94–103.
[408] Shen, H., Schiavone, P., Ru, C. Q., and Mioduchowski, A., 2000, "An Elliptic Inclusion With Imperfect Interface in Anti-Plane Shear H," Int. J. Solids Struct., **37**(33), pp. 4557–4575.
[409] Shen, H., Schiavone, P., Ru, C. Q., and Mioduchowski, A., 2001, "Stress Analysis of an Elliptic Inclusion With Imperfect Interface in Plane Elasticity," J. Elasticity, **62**(1), pp. 25–46.
[410] Ru, C. Q., and Schiavone, P., 1997, "A Circular Inclusion With Circumferentially Inhomogeneous Interface in Antiplane Shear," Proc. R. Soc. A, **453**(1967), pp. 2551–2572.
[411] Sudak, L. J., Ru, C. Q., Schiavone, P., and Mioduchowski, A., 1999, "Circular Inclusion With Inhomogeneously Imperfect Interface in Plane Elasticity," J. Elasticity, **55**(1), pp. 19–41.
[412] Ru, C. Q., 1998, "Interface Design of Neutral Elastic Inclusions," Int. J. Solids Struct., **35**(7–8), pp. 559–572.
[413] Ru, C. Q., 1998, "A Circular Inclusion With Circumferentially Inhomogeneous Sliding Interface in Plane Elastostatics," ASME J. Appl. Mech., **65**(1), pp. 30–38.
[414] Pagano, N. J., and Tandon, G. P., 1990, "Modeling of Imperfect Bonding in Fibre Reinforced Brittle Matrix," Mech. Mater., **9**(1), pp. 49–64.
[415] Tandon, G. P., and Pagano, N. J., 1996, "Effective Thermoelastic Moduli of a Unidirectional Fiber Composite Containing Interracial Arc Microcracks," ASME J. Appl. Mech., **63**(1), pp. 210–217.
[416] Teng, H., 1992, "On Stiffness Reduction of a Fiber-Reinforced Composite Containing Interfacial Cracks Under Longitudinal Shear," Mech. Mater., **13**(2), pp. 175–183.
[417] Sudak, L. J., and Mioduchowski, A., 2002, "A Three-Phase Circular Inhomogeneity With Imperfect Interface Under Thermomechanical Loadings in Plane Elasticity," Acta Mech., **158**(1–2), pp. 43–56.
[418] Sangani, A. S., and Mo, G., 1997, "Elastic Interactions in Particulate Composites With Perfect as Well as Imperfect Interfaces," J. Mech. Phys. Solids, **45**(11–12), pp. 2001–2031.
[419] Bigoni, D., Serkov, S. K., Valentini, M., and Movchan, A. B., 1998, "Asymptotic Models of Dilute Composites With Imperfectly Bonded Inclusions," Int. J. Solids Struct., **35**(24), pp. 3239–3258.
[420] Sabina, F. J., Guinovart-Díaz, R., Rodriguez-Ramos, R., López-Realpozo, J. C., and Bravo-Castillero, J., 2012, "López-Realpozo, Overall Properties in Fibrous Elastic Composite With Imperfect Contact Condition," Int. J. Eng. Sci., **61**, pp. 142–155.
[421] Artioli, E., Bisegna, P., and Maceri, F., 2010, "Effective Longitudinal Shear Moduli of Periodic Fibre-Reinforced Composites With Radially-Graded Fibres," Int. J. Solids Struct., **47**(3–4), pp. 383–397.
[422] Sevostianov, I., Rodriguez-Ramos, R., Guinovart-Diaz, R., Bravo-Castillero, J., and Sabina, F. J., 2012, "Connections Between Different Models Describing Imperfect Interfaces in Periodic Fiber-Reinforced Composites," Int. J. Solids Struct., **49**(13), pp. 1518–1525.
[423] Ghahremani, F., 1980, "Effect of Grain Boundary Sliding on Anelasticity of Polycrystals," Int. J. Solids Struct., **16**(9), pp. 825–845.
[424] Mura, T., Jasiuk, I., and Tsuchida, B., 1985, "The Stress Field of a Sliding Inclusion," Int. J. Solids Struct., **21**(12), pp. 1165–1179.
[425] Jasiuk, I., Tsuchida, E., and Mura, T., 1987, "The Sliding Inclusion Under Shear," Int. J. Solids Struct., **23**(10), pp. 1373–1385.
[426] Mura, T., and Furuhashi, R., 1984, "The Elastic Inclusion With a Sliding Interface," ASME J. Appl. Mech., **51**(2), pp. 308–310.
[427] Zhong, Z., and Meguid, S. A., 1997, "On the Elastic Field of a Spherical Inhomogeneity With an Imperfectly Bonded Interface," J. Elasticity, **46**(2), pp. 91–113.
[428] Furuhashi, R., Huang, J., and Mura, T., 1992, "Sliding Inclusions and Inhomogeneities With Frictional Interfaces," ASME J. Appl. Mech., **59**(4), pp. 783–788.
[429] Huang, J. H., Furuhashi, R., and Mura, T., 1993, "Frictional Sliding Inclusions," J. Mech. Phys. Solids, **41**(2), pp. 247–265.
[430] Lee, M., Jasiuk, I., and Tsuchida, E., 1992, "The Sliding Circular Inclusion in an Elastic Half-Plane," ASME J. Appl. Mech., **59**(2S), pp. S57–S64.
[431] Kouris, D. A., and Mura, T., 1989, "The Elastic Field of a Hemispherical Inhomogeneity at the Free Surface of an Elastic Half Space," J. Mech. Phys. Solids, **37**(3), pp. 365–379.
[432] Benveniste, Y., and Aboudi, J., 1984, "A Continuum Model for Fiber Reinforced Materials With Debonding," Int. J. Solids Struct., **20**(11–12), pp. 935–951.
[433] Shibata, S., Jasiuk, I., Mori, T., and Mura, T., 1990, "Successive Iteration Method Applied to Composites Containing Sliding Inclusions: Effective Modulus and Anelasticity," Mech. Mater., **9**(3), pp. 229–243.
[434] Devries, F., 1991, "Constitutive Equations for Unidirectional Composites With Imperfect Bonding. The Case of Elastic, Viscous or Viscoelastic Slipping," Compos. Eng., **1**(5), pp. 261–276.
[435] Devries, F., 1993, "Bounds on Elastic Moduli of Unidirectional Composites With Imperfect Bonding," Compos. Eng., **3**(4), pp. 349–382.
[436] Jasiuk, I., Chen, J., and Thorpe, M. F., 1992, "Elastic Moduli of Composites With Rigid Sliding Inclusions," J. Mech. Phys. Solids, **40**(2), pp. 373–391.
[437] Jun, S., and Jasiuk, I., 1993, "Elastic Moduli of Two-Dimensional Composites With Sliding Inclusions-A Comparison of Effective Medium Theories," Int. J. Solids Struct., **30**(18), pp. 2501–2523.

[438] Lubarda, V. A., and Markenscoff, X., 1998, "On the Stress Field in Sliding Ellipsoidal Inclusions With Shear Eigenstrain," ASME J. Appl. Mech., **65**(4), pp. 858–862.
[439] Lubarda, V. A., and Markenscoff, X., 1999, "Energies of Circular Inclusions: Sliding Versus Bonded Interfaces By," Proc. R. Soc. A, **455**(1983), pp. 961–974.
[440] Königsberger, M., Pichler, B., and Hellmich, C., 2014, "Micromechanics of ITZ-Aggregate Interaction in Concrete Part I: Stress Concentration," J. Am. Ceram. Soc., **97**(2), pp. 535–542.
[441] Königsberger, M., Pichler, B., and Hellmich, C., 2014, "Micromechanics of ITZ-Aggregate Interaction in Concrete Part II: Strength Upscaling," J. Am. Ceram. Soc., **97**(2), pp. 543–551.
[442] Fritsch, A., Dormieux, L., Hellmich, C., and Sanahuja, J., 2007, "Micromechanics of Crystal Interfaces in Polycrystalline Solid Phases of Porous Media: Fundamentals and Application to Strength of Hydroxyapatite Biomaterials," J. Mater. Sci., **42**(21), pp. 8824–8837.
[443] He, L. H., and Jiang, J., 2003, "Transient Mechanical Response of Laminated Elastic Strips With Viscous Interfaces in Cylindrical Bending," Compos. Sci. Technol., **63**(6), pp. 821–828.
[444] Funn, J. V., and Dutta, I., 1998, "Creep Behavior of Interfaces in Fiber Reinforced Metal-Matrix Composites," Acta Mater., **47**(1), pp. 149–164.
[445] Qu, T., Verma, D., Shahidi, M., Pichler, B., Hellmich, C., and Tomar, V., 2015, "Mechanics of Organic-Inorganic Biointerfaces-Implications for Strength and Creep Properties," MRS Bull., **40**(4), pp. 349–358.
[446] He, L. H., and Liu, Y. L., 2005, "Damping Behavior of Fibrous Composites With Viscous Interface Under Longitudinal Shear Loads," Compos. Sci. Technol., **65**(6), pp. 855–860.
[447] Shahidi, M., Pichler, B., and Hellmich, C., 2014, "Viscous Interfaces as Source for Material Creep: A Continuum Micromechanics Approach," Eur. J. Mech., A/Solids, **45**, pp. 41–58.
[448] Shahidi, M., Pichler, B., and Hellmich, C., 2016, "Interfacial Micromechanics Assessment of Classical Rheological Models: I—Single Interface Size and Viscosity," J. Eng. Mech., **142**(3), p. 04015092.
[449] Shahidi, M., Pichler, B., and Hellmich, C., 2016, "Interfacial Micromechanics Assessment of Classical Rheological Models: II—Multiple Interface Sizes and Viscosities," J. Eng. Mech., **142**(3), p. 04015093.
[450] Shahidi, M., Pichler, B., and Hellmich, C., 2016, "How Interface Size, Density, and Viscosity Affect Creep and Relaxation Functions of Matrix-Interface Composites: A Micromechanical Study," Acta Mech., **227**(1), pp. 229–252.
[451] Eberhardsteiner, L., Hellmich, C., and Scheiner, S., 2014, "Layered Water in Crystal Interfaces as Source for Bone Viscoelasticity: Arguments From a Multiscale Approach," Comput. Methods Biomech. Biomed. Eng., **17**(1), pp. 48–63.
[452] Chaboche, J. L., Feyel, F., and Monerie, Y., 2001, "Interface Debonding Models: A Viscous Regularization With a Limited Rate Dependency," Int. J. Solids Struct., **38**(18), pp. 3127–3160.
[453] Nair, S. V., Jakus, K., and Lardner, T. J., 1991, "The Mechanics of Matrix Cracking in Fiber Reinforced Ceramic Composites Containing a Viscous Interface," Mech. Mater., **12**(3–4), pp. 229–244.
[454] Chen, W. Q., and Lee, K. Y., 2004, "Time-Dependent Behaviors of Angle-Ply Laminates With Viscous Interfaces in Cylindrical Bending," Eur. J. Mech., A/Solids, **23**(2), pp. 235–245.
[455] Owen, D. R. J., and Lyness, J. F., 1972, "Investigation of Bond Failure in Fiber-Reinforced Materials by the Finite Eleent Method," Fibre Sci. Technol., **5**(2), pp. 129–141.
[456] Lene, F., and Leguillon, D., 1982, "Homogenized Constitutive Law for a Partially Cohesive Composite Material," Int. J. Solids Struct., **18**(5), pp. 443–458.
[457] Needleman, A., 1987, "A Continuum Model for Void Nucleation by Inclusion Debonding," ASME J. Appl. Mech., **54**(3), pp. 525–531.
[458] Steif, P. S., and Hoysan, F., 1987, "An Energy Method for Calculating the Stiffness of Aligned Short-Fiber Composites," Mech. Mater., **6**(3), pp. 197–210.
[459] Xu, X. P., and Needleman, A., 1994, "Numerical Simulations of Fast Crack Growth in Brittle Solids," J. Mech. Phys. Solids, **42**(9), pp. 1397–1434.
[460] Bisegna, P., and Luciano, R., 1998, "Bounds on the Overall Properties of Composites With Debonded Frictionless Interfaces," Mech. Mater., **28**(1–4), pp. 23–32.
[461] Wriggers, P., Zavarise, G., and Zohdi, T. I., 1998, "A Computational Study of Interfacial Debonding Damage in Fibrous Composite Materials," Comput. Mater. Sci., **12**(1), pp. 39–56.
[462] Würkner, M., Berger, H., and Gabbert, U., 2014, "Numerical Investigations of Effective Properties of Fiber Reinforced Composites With Parallelogram Arrangements and Imperfect Interface," Compos. Struct., **116**, pp. 388–394.
[463] Würkner, M., Berger, H., and Gabbert, U., 2013, "Numerical Study of Effective Elastic Properties of Fiber Reinforced Composites With Rhombic Cell Arrangements and Imperfect Interface," Int. J. Eng. Sci., **63**, pp. 1–9.
[464] Zheng, S. F., Denda, M., and Weng, G. J., 2000, "Interfacial Partial Debonding and Its Influence on the Elasticity of a Two-Phase Composite," Mech. Mater., **32**(12), pp. 695–709.
[465] Caporale, A., Luciano, R., and Sacco, E., 2006, "Micromechanical Analysis of Interfacial Debonding in Unidirectional Fiber-Reinforced Composites," Comput. Struct., **84**(31–32), pp. 2200–2211.
[466] Achenbach, J. D., and Zhu, H., 1989, "Effect of Interfacial Zone on Mechanical Behavior and Failure of Fiber-Reinforced Composites," J. Mech. Phys. Solids, **37**(3), pp. 381–393.
[467] Achenbach, J. D., and Zhu, H., 1990, "Effect of Interphase on Micro and Macromechanical Behavior of Hexagonal-Array Fiber Composites," ASME J. Appl. Mech., **57**(4), pp. 956–963.
[468] Zhu, Q. Z., Gu, S. T., Yvonnet, J., Shao, J. F., and He, Q. C., 2011, "Three-Dimensional Numerical Modelling by XFEM of Spring-Layer Imperfect Curved Interfaces With Applications to Linearly Elastic Composite Materials," Int. J. Numer. Methods Eng., **88**(4), pp. 307–328.
[469] Fritzen, F., and Leuschner, M., 2015, "Nonlinear Reduced Order Homogenization of Materials Including Cohesive Interfaces," Comput. Mech., **56**(1), pp. 131–151.
[470] Leuschner, M., and Fritzen, F., 2017, "Reduced Order Homogenization for Viscoplastic Composite Materials Including Dissipative Imperfect Interfaces," Mech. Mater., **104**, pp. 121–138.
[471] Koutsawa, Y., 2018, "Overall Properties of Piezoelectric Composites With Spring-Type Imperfect Interfaces Using the Mechanics of Structure Genome," Compos. Part B, **153**, pp. 337–345.
[472] Nairn, J. A., 2007, "Numerical Implementation of Imperfect Interfaces," Comput. Mater. Sci., **40**(4), pp. 525–536.
[473] Yeh, J. R., 1992, "The Effect of Interface on the Transverse Properties of Composites," Int. J. Solids Struct., **29**(20), pp. 2493–2502.
[474] Camacho, G. T., and Ortiz, M., 1996, "Computational Modelling of Impact Damage in Brittle Materials," Int. J. Solids Struct., **33**(20–22), pp. 2899–2938.
[475] De-Andrés, A., Pérez, J. L., and Ortiz, M., 1999, "Elastoplastic Finite Element Analysis of Three-Dimensional Fatigue Crack Growth in Aluminum Shafts Subjected to Axial Loading," Int. J. Solids Struct., **36**(15), pp. 2231–2258.
[476] Ortiz, M., and Pandolfi, A., 1999, "Finite-Deformation Irreversible Cohesive Elements for Three-Dimensional Crack-Propagation Analysis," Int. J. Numer. Methods Eng., **44**(9), pp. 1267–1282.
[477] Alfano, G., and Crisfield, M. A., 2001, "Finite Element Interface Models for the Delamination Analysis of Laminated Composites: Mechanical and Computational Issues," Int. J. Numer. Methods Eng., **50**(7), pp. 1701–1736.
[478] Mi, Y., Crisfield, M. A., Davies, G. A. O., and Hellweg, H. B., 1998, "Progressive Delamination Using Interface Elements," J. Compos. Mater., **32**(14), pp. 1246–1272.
[479] Gasser, T. C., and Holzapfel, G. A., 2003, "Geometrically Non-Linear and Consistently Linearized Embedded Strong Discontinuity Models for 3D Problems With an Application to the Dissection Analysis of Soft Biological Tissues," Comput. Methods Appl. Mech. Eng., **192**(47–48), pp. 5059–5098.
[480] Mergheim, J., and Steinmann, P., 2006, "A Geometrically Nonlinear FE Approach for the Simulation of Strong and Weak Discontinuities," Comput. Methods Appl. Mech. Eng., **195**(37–40), pp. 5037–5052.
[481] Hansbo, A., and Hansbo, P., 2002, "An Unfitted Finite Element Method, Based on Nitsche's Method, for Elliptic Interface Problems," Comput. Methods Appl. Mech. Eng., **191**(47–48), pp. 5537–5552.
[482] Hansbo, A., and Hansbo, P., 2004, "A Finite Element Method for the Simulation of Strong and Weak Discontinuities in Solid Mechanics," Comput. Methods Appl. Mech. Eng., **193**(33–35), pp. 3523–3540.
[483] van den Bosch, M. J., Schreurs, P. J. G., and Geers, M. G. D., 2008, "On the Development of a 3D Cohesive Zone Element in the Presence of Large Deformations," Comput. Mech., **42**(2), pp. 171–180.
[484] van den Bosch, M. J., Schreurs, P. J. G., and Geers, M. G. D., 2006, "An Improved Description of the Exponential Xu and Needleman Cohesive Zone Law for Mixed-Mode Decohesion," Eng. Fract. Mech., **73**(9), pp. 1220–1234.
[485] van den Bosch, M. J., Schreurs, P. J. G., and Geers, M. G. D., 2007, "A Cohesive Zone Model With a Large Displacement Formulation Accounting for Interfacial Fibrilation," Eur. J. Mech., A/Solids, **26**(1), pp. 1–19.
[486] Vossen, B. G., Schreurs, P. J. G., van der Sluis, O., and Geers, M. G. D., 2013, "On the Lack of Rotational Equilibrium in Cohesive Zone Elements," Comput. Methods Appl. Mech. Eng., **254**, pp. 146–153.
[487] Ottosen, N. S., Ristinmaa, M., and Mosler, J., 2015, "Fundamental Physical Principles and Cohesive Zone Models at Finite Displacements—Limitations and Possibilities," Int. J. Solids Struct., **53**, pp. 70–79.
[488] Ottosen, N. S., Ristinmaa, M., and Mosler, J., 2016, "Framework for Non-Coherent Interface Models at Finite Displacement Jumps and Finite Strains," J. Mech. Phys. Solids, **90**, pp. 124–141.
[489] Heitbreder, T., Ottosen, N. S., Ristinmaa, M., and Mosler, J., 2017, "Consistent Elastoplastic Cohesive Zone Model at Finite Deformations—Variational Formulation," Int. J. Solids Struct., **106–107**, pp. 284–293.
[490] Heitbreder, T., Ottosen, N. S., Ristinmaa, M., and Mosler, J., 2018, "On Damage Modeling of Material Interfaces: Numerical Implementation and Computational Homogenization," Comput. Methods Appl. Mech. Eng., **337**, pp. 1–27.
[491] Hillerborg, A., Modéer, M., and Petersson, P. E., 1976, "Analysis of Crack Formation and Crack Growth in Concrete by Means of Fracture Mechanics and Finite Elements," Cem. Concrete Res., **6**(6), pp. 773–781.
[492] Ghosh, S., Ling, Y., Majumdar, B., and Kim, R., 2000, "Interfacial Debonding Analysis in Multiple Fiber Reinforced Composites," Mech. Mater., **32**(10), pp. 561–591.
[493] Wells, G. N., and Sluys, L. J., 2001, "A New Method for Modelling Cohesive Cracks Using Finite Elements," Int. J. Numer. Methods Eng., **50**(12), pp. 2667–2682.
[494] Guo, R., Shi, H. J., and Yao, Z. H., 2003, "Modeling of Interfacial Debonding Crack in Particle Reinforced Composites Using Voronoi Cell Finite Element Method," Comput. Mech., **32**(1–2), pp. 52–59.
[495] Segurado, J., and LLorca, J., 2004, "A New Three-Dimensional Interface Finite Element to Simulate Fracture in Composites," Int. J. Solids Struct., **41**(11–12), pp. 2977–2993.

[496] Aghdam, M. M., and Falahatgar, S. R., 2004, "Micromechanical Modeling of Interface Damage of Metal Matrix Composites Subjected to Transverse Loading," Compos. Struct., **66**(1–4), pp. 415–420.
[497] Raghavan, P., and Ghosh, S., 2005, "A Continuum Damage Mechanics Model for Unidirectional Composites Undergoing Interfacial Debonding," Mech. Mater., **37**, pp. 955–979.
[498] Fagerström, M., and Larsson, R., 2006, "Theory and Numerics for Finite Deformation Fracture Modelling Using Strong Discontinuities," Int. J. Numer. Methods Eng., **66**(6), pp. 911–948.
[499] Charlotte, M., Laverne, J., and Marigo, J. J., 2006, "Initiation of Cracks With Cohesive Force Models: A Variational Approach," Eur. J. Mech., A/Solids, **25**(4), pp. 649–669.
[500] Ghosh, S., Bai, J., and Raghavan, P., 2007, "Concurrent Multi-Level Model for Damage Evolution in Microstructurally Debonding Composites," Mech. Mater., **39**(3), pp. 241–266.
[501] Aymerich, F., Dore, F., and Priolo, P., 2009, "Simulation of Multiple Delaminations in Impacted Cross-Ply Laminates Using a Finite Element Model Based on Cohesive Interface Elements," Compos. Sci. Technol., **69**(11–12), pp. 1699–1709.
[502] Paggi, M., and Wriggers, P., 2011, "A Nonlocal Cohesive Zone Model for Finite Thickness Interfaces—Part I: Mathematical Formulation and Validation With Molecular Dynamics," Comput. Mater. Sci., **50**(5), pp. 1625–1633.
[503] Paggi, M., and Wriggers, P., 2011, "A Nonlocal Cohesive Zone Model for Finite Thickness Interfaces—Part II: FE Implementation and Application to Polycrystalline Materials," Comput. Mater. Sci., **50**(5), pp. 1634–1643.
[504] Bouhala, L., Makradi, A., Belouettar, S., Kiefer-Kamal, H., and Fréres, P., 2013, "Modelling of Failure in Long Fibres Reinforced Composites by X-FEM and Cohesive Zone Model," Compos. Part B, **55**, pp. 352–361.
[505] Wang, X., Zhang, J., Wang, Z., Liang, W., and Zhou, L., 2013, "Finite Element Simulation of the Failure Process of Single Fiber Composites Considering Interface Properties," Compos. Part B, **45**(1), pp. 573–582.
[506] Tu, W., and Pindera, M. J., 2014, "Cohesive Zone-Based Damage Evolution in Periodic Materials Via Finite Volume Homogenization," ASME J. Appl. Mech., **81**(10), p. 101005.
[507] Pike, M. G., and Oskay, C., 2015, "XFEM Modeling of Short Microfiber Reinforced Composites With Cohesive Interfaces," Finite Elem. Anal. Des., **106**, pp. 16–31.
[508] Wu, C., Gowrishankar, S., Huang, R., and Liechti, K. M., 2016, "On Determining Mixed-Mode Traction-Separation Relations for Interfaces," Int. J. Fract., **202**(1), pp. 1–19.
[509] Rezaei, S., Jaworek, D., Mianroodi, J. R., Wulfinghoff, S., and Reese, S., 2019, "Atomistically Motivated Interface Model to Account for Coupled Plasticity and Damage at Grain Boundaries," J. Mech. Phys. Solids, **124**, pp. 325–349.
[510] Rezaei, S., Mianroodi, J. R., Khaledi, K., and Reese, S., 2020, "A Nonlocal Method for Modeling Interfaces: Numerical Simulation of Decohesion and Sliding at Grain Boundaries," Comput. Methods Appl. Mech. Eng., **362**, p. 112836.
[511] Bayat, H. R., Rezaei, S., Brepols, T., and Reese, S., 2020, "Locking-Free Interface Failure Modeling by a Cohesive Discontinuous Galerkin Method for Matching and Nonmatching Meshes," Int. J. Numer. Methods Eng., **121**(8), pp. 1762–1790.
[512] Cammarata, R. C., 1994, "Surface and Interface Stress Effects in Thin Films," Prog. Surf. Sci., **46**(1), pp. 1–38.
[513] Cammarata, R. C., Sieradzki, K., and Spaepen, F., 2000, "Simple Model for Interface Stresses With Application to Misfit Dislocation Generation in Epitaxial Thin Films," J. Appl. Phys., **87**(3), pp. 1227–1234.
[514] Cammarata, R. C., 2009, "Generalized Thermodynamics of Surfaces With Applications to Small Solid Systems," Solid State Phys., **61**, pp. 1–75.
[515] Cammarata, R. C., 1997, "Surface and Interface Stress Effects on Interfacial and Nanostructured Materials," Mater. Sci. Eng. A, **237**(2), pp. 180–184.
[516] Shuttleworth, R., 1950, "The Surface Tension of Solids," Proc. Phys. Soc. A, **63**(5), pp. 444–457.
[517] Chen, T., Chiu, M. S., and Weng, C. N., 2006, "Derivation of the Generalized Young-Laplace Equation of Curved Interfaces in Nanoscaled Solids," J. Appl. Phys., **100**(7), p. 074308.
[518] Povstenko, Y. Z., 1993, "Theoretical Investigation of Phenomena Caused by Heterogeneous Surface Tension in Solids," J. Mech. Phys. Solids, **41**(9), pp. 1499–1514.
[519] Gurtin, M. E., and Murdoch, A. I., 1975, "A Continuum Theory of Elastic Material Surfaces," Arch. Ration. Mech. Anal., **57**(4), pp. 291–323.
[520] Murdoch, A. I., 1976, "A Thermodynamical Theory of Elastic Material Interfaces," Q. J. Mech. Appl. Math., **29**(3), pp. 245–275.
[521] Gurtin, M. E., and Murdoch, A. I., 1978, "Surface Stress in Solids," Int. J. Solids Struct., **14**(6), pp. 431–440.
[522] Cahn, J. W., and Lärché, F., 1982, "Surface Stress and the Chemical Equilibrium of Small Crystals-II. Solid Particles Embedded in a Solid Matrix," Acta Metall., **30**(1), pp. 51–56.
[523] Nix, W. D., and Gao, H., 1998, "An Atomistic Interpretation of Interface Stress," Scr. Mater., **39**(12), pp. 1653–1661.
[524] Gao, X., Huang, Z., Qu, J., and Fang, D., 2014, "A Curvature-Dependent Interfacial Energy-Based Interface Stress Theory and Its Applications to Nano-Structured Materials: (I) General Theory," J. Mech. Phys. Solids, **66**, pp. 59–77.
[525] Gao, X., Huang, Z., and Fang, D., 2017, "Curvature-Dependent Interfacial Energy and Its Effects on the Elastic Properties of Nanomaterials," Int. J. Solids Struct., **113–114**, pp. 100–107.
[526] Caillerie, D., 1978, "Sur le Comportement Limite D'une Inclusion Mince de Grande Rigidite," C. R. L'Acad. Sci. Série 1, **287**, pp. 675–678.
[527] Lemrabet, K., and Lions, J. L. R., 1987, "Le Problème de Ventcel Pour le Système de L'élasticité Dans un Domaine de IR3," Comptes Rendus de L'Académie Des Sciences. Série 1 Mathématique, **304**, pp. 151–154.
[528] Rubin, M. B., and Benveniste, Y., 2004, "A Cosserat Shell Model for Interphases in Elastic Media," J. Mech. Phys. Solids, **52**(5), pp. 1023–1052.
[529] Rizzoni, R., Dumont, S., Lebon, F., and Sacco, E., 2014, "Higher Order Model for Soft and Hard Elastic Interfaces," Int. J. Solids Struct., **51**(23–24), pp. 4137–4148.
[530] Fried, E., and Todres, R. E., 2005, "Mind the Gap: The Shape of the Free Surface of a Rubber-Like Material in Proximity to a Rigid Contactor," J. Elasticity, **80**(1–3), pp. 97–151.
[531] Fried, E., and Gurtin, M. E., 2007, "Thermomechanics of the Interface Between a Body and Its Environment," Contin. Mech. Thermodyn., **19**(5), pp. 253–271.
[532] Dingreville, R., and Qu, J., 2008, "Interfacial Excess Energy, Excess Stress and Excess Strain in Elastic Solids: Planar Interfaces," J. Mech. Phys. Solids, **56**(5), pp. 1944–1954.
[533] Dingreville, R., and Qu, J., 2007, "A Semi-Analytical Method to Compute Surface Elastic Properties," Acta Mater., **55**(1), pp. 141–147.
[534] Dingreville, R., Hallil, A., and Berbenni, S., 2014, "From Coherent to Incoherent Mismatched Interfaces: A Generalized Continuum Formulation of Surface Stresses," J. Mech. Phys. Solids, **72**, pp. 40–60.
[535] Dingreville, R., Qu, J., and Cherkaoui, M., 2005, "Surface Free Energy and Its Effect on the Elastic Behavior of Nano-Sized Particles, Wires and Films," J. Mech. Phys. Solids, **53**(8), pp. 1827–1854.
[536] Dumont, S., Rizzoni, R., Lebon, F., and Sacco, E., 2018, "Soft and Hard Interface Models for Bonded Elements," Compos. Part B, **153**, pp. 480–490.
[537] Sharma, P., Ganti, S., and Bhate, N., 2003, "Effect of Surfaces on the Size-Dependent Elastic State of Nano-Inhomogeneities," Appl. Phys. Lett., **82**(4), pp. 535–537.
[538] Sharma, P., 2004, "Size-Dependent Elastic Fields of Embedded Inclusions in Isotropic Chiral Solids," Int. J. Solids Struct., **41**(22–23), pp. 6317–6333.
[539] Yang, F., 2004, "Size-Dependent Effective Modulus of Elastic Composite Materials: Spherical Nanocavities at Dilute Concentrations," J. Appl. Phys., **95**(7), pp. 3516–3520.
[540] Sun, L., Wu, Y., Huang, Z., and Wang, J., 2004, "Interface Effect on the Effective Bulk Modulus of a Particle-Reinforced Composite," Acta Mech. Sin., **20**, pp. 676–679.
[541] Duan, H. L., Wang, J., Huang, Z. P., and Karihaloo, B. L., 2005, "Eshelby Formalism for Nano-Inhomogeneities," Proc. R. Soc. A, **461**(2062), pp. 3335–3353.
[542] Duan, H. L., Wang, J., Huang, Z. P., and Karihaloo, B. L., 2005, "Size-Dependent Effective Elastic Constants of Solids Containing Nano-Inhomogeneities With Interface Stress," J. Mech. Phys. Solids, **53**(7), pp. 1574–1596.
[543] Duan, H. L., Wang, J., and Karihaloo, B. L., 2009, Theory of Elasticity at the Nanoscale, Vol. 42, Elsevier, Amsterdam, The Netherlands.
[544] Huang, Z. P., and Wang, J., 2006, "A Theory of Hyperelasticity of Multi-Phase Media With Surface/Interface Energy Effect," Acta Mech., **182**(3–4), pp. 195–210.
[545] Monteiro, E., He, Q. C., and Yvonnet, J., 2011, "Hyperelastic Large Deformations of Two-Phase Composites With Membrane-Type Interface," Int. J. Eng. Sci., **49**(9), pp. 985–1000.
[546] Huang, Z. P., and Sun, L., 2007, "Size-Dependent Effective Properties of a Heterogeneous Material With Interface Energy Effect: From Finite Deformation Theory to Infinitesimal Strain Analysis," Acta Mech., **190**(1–4), pp. 151–163.
[547] He, L. H., 2006, "Self-Strain of Solids With Spherical Nanovoids," Appl. Phys. Lett., **88**(15), p. 151909.
[548] Lim, C. W., Li, Z. R., and He, L. H., 2006, "Size Dependent, Non-Uniform Elastic Field Inside a Nano-Scale Spherical Inclusion Due to Interface Stress," Int. J. Solids Struct., **43**(17), pp. 5055–5065.
[549] Chen, T., Dvorak, G. J., and Yu, C. C., 2007, "Size-Dependent Elastic Properties of Unidirectional Nano-Composites With Interface Stresses," Acta Mech., **188**(1–2), pp. 39–54.
[550] Chen, T., Dvorak, G. J., and Yu, C. C., 2007, "Solids Containing Spherical Nano-Inclusions With Interface Stresses: Effective Properties and Thermal-Mechanical Connections," Int. J. Solids Struct., **44**(3–4), pp. 941–955.
[551] Mi, C., and Kouris, D., 2006, "Nanoparticles Under the Influence of Surface/Interface Elasticity," J. Mech. Mater. Struct., **1**(4), pp. 763–791.
[552] Mi, C., and Kouris, D., 2017, "Surface Mechanics Implications for a Nano-voided Metallic Thin-Plate Under Uniform Boundary Loading," Math. Mech. Solids, **22**(3), pp. 401–419.
[553] Mi, C., 2017, "Surface Mechanics Induced Stress Disturbances in an Elastic Half-Space Subjected to Tangential Surface Loads," Eur. J. Mech., A/Solids, **65**, pp. 59–69.
[554] Le Quang, H., and He, Q. C., 2007, "Size-Dependent Effective Thermoelastic Properties of Nanocomposites With Spherically Anisotropic Phases," J. Mech. Phys. Solids, **55**(9), pp. 1899–1931.
[555] Le Quang, H., and He, Q. C., 2008, "Variational Principles and Bounds for Elastic Inhomogeneous Materials With Coherent Imperfect Interfaces," Mech. Mater., **40**(10), pp. 865–884.
[556] Le Quang, H., and He, Q. C., 2009, "Estimation of the Effective Thermoelastic Moduli of Fibrous Nanocomposites With Cylindrically Anisotropic Phases," Archive Appl. Mech., **79**(3), pp. 225–248.

[557] Mogilevskaya, S. G., Crouch, S. L., and Stolarski, H. K., 2008, "Multiple Interacting Circular Nano-Inhomogeneities With Surface/Interface Effects," J. Mech. Phys. Solids, **56**(6), pp. 2298–2327.
[558] Mogilevskaya, S. G., Crouch, S. L., Stolarski, H. K., and Benusiglio, A., 2010, "Equivalent Inhomogeneity Method for Evaluating the Effective Elastic Properties of Unidirectional Multi-Phase Composites With Surface/Interface Effects," Int. J. Solids Struct., **47**(3–4), pp. 407–418.
[559] Mogilevskaya, S. G., Crouch, S. L., La Grotta, A., and Stolarski, H. K., 2010, "The Effects of Surface Elasticity and Surface Tension on the Transverse Overall Elastic Behavior of Unidirectional Nano-Composites," Compos. Sci. Technol., **70**(3), pp. 427–434.
[560] Mogilevskaya, S. G., Stolarski, H. K., and Crouch, S. L., 2012, "On Maxwells Concept of Equivalent Inhomogeneity: When Do the Interactions Matter?," J. Mech. Phys. Solids, **60**(3), pp. 391–417.
[561] Jammes, M., Mogilevskaya, S. G., and Crouch, S. L., 2009, "Multiple Circular Nano-Inhomogeneities and/or Nano-Pores in One of Two Joined Isotropic Elastic Half-Planes," Eng. Anal. Bound. Elem., **33**(2), pp. 233–248.
[562] Kushch, V. I., Mogilevskaya, S. G., Stolarski, H. K., and Crouch, S. L., 2011, "Elastic Interaction of Spherical Nanoinhomogeneities With Gurtin-Murdoch Type Interfaces," J. Mech. Phys. Solids, **59**(9), pp. 1702–1716.
[563] Kushch, V. I., Mogilevskaya, S. G., Stolarski, H. K., and Crouch, S. L., 2013, "Elastic Fields and Effective Moduli of Particulate Nanocomposites With the Gurtin-Murdoch Model of Interfaces," Int. J. Solids Struct., **50**(7–8), pp. 1141–1153.
[564] Kushch, V. I., Sevostianov, I., and Chernobai, V. S., 2014, "Effective Conductivity of Composite With Imperfect Contact Between Elliptic Fibers and Matrix: Maxwell's Homogenization Scheme," Int. J. Eng. Sci., **83**, pp. 146–161.
[565] Muskhelishvili, N. I., 2013, *Some Basic Problems of the Mathematical Theory of Elasticity*, Springer Science & Business Media, Dordrecht, The Netherlands.
[566] Kushch, V. I., and Sevostianov, I., 2016, "The "Rigorous" Maxwell Homogenization Scheme in 2D Elasticity: Effective Stiffness Tensor of Composite With Elliptic Inhomogeneities," Mech. Mater., **103**, pp. 44–54.
[567] Benveniste, Y., and Miloh, T., 2007, "Soft Neutral Elastic Inhomogeneities With Membrane-Type Interface Conditions," J. Elasticity, **88**(2), pp. 87–111.
[568] Dormieux, L., and Kondo, D., 2010, "An Extension of Gurson Model Incorporating Interface Stresses Effects," Int. J. Eng. Sci., **48**(6), pp. 575–581.
[569] Dormieux, L., and Kondo, D., 2013, "Non Linear Homogenization Approach of Strength of Nanoporous Materials With Interface Effects," Int. J. Eng. Sci., **71**, pp. 102–110.
[570] Brach, S., Dormieux, L., Kondo, D., and Vairo, G., 2017, "Strength Properties of Nanoporous Materials: A 3-Layered Based Non-Linear Homogenization Approach With Interface Effects," Int. J. Eng. Sci., **115**, pp. 28–42.
[571] Kushch, V. I., 2018, "Stress Field and Effective Elastic Moduli of Periodic Spheroidal Particle Composite With Gurtin-Murdoch Interface," Int. J. Eng. Sci., **132**, pp. 79–96.
[572] Sharma, P., and Wheeler, L. T., 2007, "Size-Dependent Elastic State of Ellipsoidal Nano-Inclusions Incorporating Surface/Interface Tension," ASME J. Appl. Mech., **74**(3), pp. 447–454.
[573] Yang, F., 2006, "Effect of Interfacial Stresses on the Elastic Behavior of Nanocomposite Materials," J. Appl. Phys., **99**(5), p. 054306.
[574] Chen, T., and Dvorak, G. J., 2006, "Fibrous Nanocomposites With Interface Stress: Hill's and Levin's Connections for Effective Moduli," Appl. Phys. Lett., **88**(21), p. 211912.
[575] Chen, T., 2008, "Exact Size-Dependent Connections Between Effective Moduli of Fibrous Piezoelectric Nanocomposites With Interface Effects," Acta Mech., **196**(3–4), pp. 205–217.
[576] Chen, H., Liu, X., and Hu, G., 2008, "Overall Plasticity of Micropolar Composites With Interface Effect," Mech. Mater., **40**(9), pp. 721–728.
[577] Fischer, F. D., and Svoboda, J., 2010, "Stresses in Hollow Nanoparticles," Int. J. Solids Struct., **47**(20), pp. 2799–2805.
[578] Brisard, S., Dormieux, L., and Kondo, D., 2010, "Hashin-Shtrikman Bounds on the Shear Modulus of a Nanocomposite With Spherical Inclusions and Interface Effects," Comput. Mater. Sci., **50**(2), pp. 403–410.
[579] Li, P., Wang, Q., and Shi, S., 2011, "Differential Scheme for the Effective Elastic Properties of Nano-Particle Composites With Interface Effect," Comput. Mater. Sci., **50**(11), pp. 3230–3237.
[580] Dong, C. Y., 2012, "An Integral Equation Formulation of Two- and Three-Dimensional Nanoscale Inhomogeneities," Comput. Mech., **49**(3), pp. 309–318.
[581] Javili, A., Ottosen, N. S., Ristinmaa, M., and Mosler, J., 2018, "Aspects of Interface Elasticity Theory," Math. Mech. Solids, **23**(7), pp. 1004–1024.
[582] Javili, A., 2012, "Thermomechanics of Solids Accounting for Surfaces and Interfaces," Ph.D. thesis, Erlangen, Germany.
[583] Nazarenko, L., Bargmann, S., and Stolarski, H., 2014, "Influence of Interfaces on Effective Properties of Nanomaterials With Stochastically Distributed Spherical Inclusions," Int. J. Solids Struct., **51**(5), pp. 954–966.
[584] Chatzigeorgiou, G., Chemisky, Y., and Meraghni, F., 2015, "Computational Micro to Macro Transitions for Shape Memory Alloy Composites Using Periodic Homogenization," Smart Mater. Struct., **24**(3), p. 035009.
[585] Nazarenko, L., Stolarski, H., and Altenbach, H., 2016, "Effective Properties of Short-Fiber Composites With Gurtin-Murdoch Model of Interphase," Int. J. Solids Struct., **97–98**, pp. 75–88.
[586] Nazarenko, L., Bargmann, S., and Stolarski, H., 2017, "Closed-Form Formulas for the Effective Properties of Random Particulate Nanocomposites With Complete Gurtin-Murdoch Model of Material Surfaces," Contin. Mech. Thermodyn., **29**(1), pp. 77–96.
[587] Dai, M., Li, M., and Schiavone, P., 2018, "Plane Deformations of an Inhomogeneity-Matrix System Incorporating a Compressible Liquid Inhomogeneity and Complete Gurtin-Murdoch Interface Model," ASME J. Appl. Mech., **85**(2), p. 121010.
[588] Steigmann, D. J., and Ogden, R. W., 1997, "Plane Deformations of Elastic Solids With Intrinsic Boundary Elasticity," Proc. R. Soc. A, **453**(1959), pp. 853–877.
[589] Steigmann, D. J., and Ogden, R. W., 1999, "Elastic Surface - Substrate Interactions," Proc. R. Soc. London A, **455**(1982), pp. 437–474.
[590] Chhapadia, P., Mohammadi, P., and Sharma, P., 2011, "Curvature-Dependent Surface Energy and Implications for Nanostructures," J. Mech. Phys. Solids, **59**(10), pp. 2103–2115.
[591] Zemlyanova, A. Y., and Mogilevskaya, S. G., 2018, "On Spherical Inhomogeneity With Steigmann–Ogden Interface," ASME J. Appl. Mech., **85**(12), p. 121009.
[592] Zemlyanova, A. Y., and Mogilevskaya, S. G., 2018, "Circular Inhomogeneity With Steigmann–Ogden Interface: Local Fields, Neutrality, and Maxwell's Type Approximation Formula," Int. J. Solids Struct., **135**, pp. 85–98.
[593] Han, Z., Mogilevskaya, S. G., and Schillinger, D., 2018, "Local Fields and Overall Transverse Properties of Unidirectional Composite Materials With Multiple Nanofibers and Steigmann–Ogden Interfaces," Int. J. Solids Struct., **147**, pp. 166–182.
[594] Ban, Y., and Mi, C., 2020, "Analytical Solutions of a Spherical Nanoinhomogeneity Under Far-Field Unidirectional Loading Based on Steigmann-Ogden Surface Model," Math. Mech. Solids, **25**(10), pp. 1904–1923.
[595] Le, T. T., 2020, "Probabilistic Investigation of the Effect of Stochastic Imperfect Interfaces in Nanocomposites," Mech. Mater., **151**, p. 103608.
[596] Le, T. T., 2020, "Multiscale Analysis of Elastic Properties of Nano-Reinforced Materials Exhibiting Surface Effects. Application for Determination of Effective Shear Modulus," J. Compos. Sci., **4**(4), p. 172.
[597] Tian, L., and Rajapakse, R. K. N. D., 2007, "Elastic Field of an Isotropic Matrix With a Nanoscale Elliptical Inhomogeneity," Int. J. Solids Struct., **44**(24), pp. 7988–8005.
[598] Tian, L., and Rajapakse, R. K. N. D., 2007, "Analytical Solution for Size-Dependent Elastic Field of a Nanoscale Circular Inhomogeneity," ASME J. Appl. Mech., **74**(3), pp. 568–574.
[599] Yvonnet, J., He, Q. C., and Toulemonde, C., 2008, "Numerical Modelling of the Effective Conductivities of Composites With Arbitrarily Shaped Inclusions and Highly Conducting Interface," Compos. Sci. Technol., **68**(13), pp. 2818–2825.
[600] Dong, C. Y., and Pan, E., 2011, "Boundary Element Analysis of Nanoinhomogeneities of Arbitrary Shapes With Surface and Interface Effects," Eng. Anal. Boundary Elem., **35**(8), pp. 996–1002.
[601] Dai, M., Schiavone, P., and Gao, C. F., 2016, "Prediction of the Stress Field and Effective Shear Modulus of Composites Containing Periodic Inclusions Incorporating Interface Effects in Anti-Plane Shear," J. Elasticity, **125**(2), pp. 217–230.
[602] Javili, A., McBride, A. T., and Steinmann, P., 2013, "Numerical Modelling of Thermomechanical Solids With Highly Conductive Energetic Interfaces," Int. J. Numer. Methods Eng., **93**(5), pp. 551–574.
[603] Javili, A., Chatzigeorgiou, G., McBride, A. T., Steinmann, P., and Linder, C., 2015, "Computational Homogenization of Nano-Materials Accounting for Size Effects Via Surface Elasticity," GAMM Mitteilungen, **38**(2), pp. 285–312.
[604] Javili, A., McBride, A., Steinmann, P., and Reddy, B. D., 2014, "A Unified Computational Framework for Bulk and Surface Elasticity Theory: A Curvilinear-Coordinate-Based Finite Element Methodology," Comput. Mech., **54**(3), pp. 745–762.
[605] Koutsawa, Y., Tiem, S., Yu, W., Addiego, F., and Giunta, G., 2017, "A Micromechanics Approach for Effective Elastic Properties of Nano-Composites With Energetic Surfaces/Interfaces," Compos. Struct., **159**, pp. 278–287.
[606] Chen, Q., Wang, G., and Pindera, M. J., 2018, "Finite Volume Homogenization and Localization of Nanoporous Materials With Cylindrical Voids. Part 1: Theory and Validation," Eur. J. Mech., A/Solids, **70**, pp. 141–155.
[607] Chen, Q., Sun, Y., Wang, G., and Pindera, M. J., 2019, "Finite Volume Homogenization and Localization of Nanoporous Materials With Cylindrical Voids. Part 2: New Results," Eur. J. Mech., A/Solids, **73**, pp. 331–348.
[608] Chen, Q., and Pindera, M. J., 2020, "Homogenization and Localization of Elastic-Plastic Nanoporous Materials With Gurtin-Murdoch Interfaces: An Assessment of Computational Approaches," Int. J. Plasticity, **124**, pp. 42–70.
[609] Dong, C. Y., and Lo, S. H., 2013, "Boundary Element Analysis of an Elastic Half-Plane Containing Nanoinhomogeneities," Comput. Mater. Sci., **73**, pp. 33–40.
[610] Dong, C. Y., and Zhang, G. L., 2013, "Boundary Element Analysis of Three Dimensional Nanoscale Inhomogeneities," Int. J. Solids Struct., **50**(1), pp. 201–208.
[611] Zhao, X., Bordas, S. P. A., and Qu, J., 2013, "A Hybrid Smoothed Extended Finite Element/Level Set Method for Modeling Equilibrium Shapes of Nano-Inhomogeneities," Comput. Mech., **52**(6), pp. 1417–1428.
[612] Gao, W., Yu, S., and Huang, G., 2006, "Finite Element Characterization of the Size-Dependent Mechanical Behaviour in Nanosystems," Nanotechnology, **17**, pp. 1118–1122.
[613] Farsad, M., Vernerey, F. J., and Park, H. S., 2010, "An Extended Finite Element/Level Set Method to Study Surface Effects on the Mechanical Behavior

and Properties of Nanomaterials," Int. J. Numer. Methods Eng., **84**(12), pp. 1466–1489.
[614] Parvanova, S. L., Vasilev, G. P., Dineva, P. S., and Manolis, G. D., 2016, "Dynamic Analysis of Nano-Heterogeneities in a Finite-Sized Solid by Boundary and Finite Element Methods," Int. J. Solids Struct., **80**, pp. 1–18.
[615] Liu, W., Liu, Y., Su, X., and Li, Z., 2014, "Finite Element Analysis of the Interface/Surface Effect on the Elastic Wave Band Structure of Two-Dimensional Nanosized Phononic Crystals," Int. J. Appl. Mech., **06**(01), p. 1450005.
[616] Hashin, Z., 2002, "Thin Interphase/Imperfect Interface in Elasticity With Application to Coated Fiber Composites," J. Mech. Phys. Solids, **50**(12), pp. 2509–2537.
[617] Benveniste, Y., 2006, "A General Interface Model for a Three-Dimensional Curved Thin Anisotropic Interphase Between Two Anisotropic Media," J. Mech. Phys. Solids, **54**(4), pp. 708–734.
[618] Benveniste, Y., 2013, "Models of Thin Interphases With Variable Moduli in Plane-Strain Elasticity," Math. Mech. Solids, **18**(2), pp. 119–134.
[619] Benveniste, Y., 2013, "Models of Thin Interphases and the Effective Medium Approximation in Composite Media With Curvilinearly Anisotropic Coated Inclusions," Int. J. Eng. Sci., **72**, pp. 140–154.
[620] Bövik, P., 1994, "On the Modelling of Thin Interface Layers in Elastic and Acoustic Scattering Problems," Q. J. Mech. Appl. Math., **47**(1), pp. 17–42.
[621] Monchiet, V., and Bonnet, G., 2010, "Interfacial Models in Viscoplastic Composites Materials," Int. J. Eng. Sci., **48**(12), pp. 1762–1768.
[622] Gu, S. T., and He, Q. C., 2011, "Interfacial Discontinuity Relations for Coupled Multifield Phenomena and Their Application to the Modeling of Thin Interphases as Imperfect Interfaces," J. Mech. Phys. Solids, **59**(7), pp. 1413–1426.
[623] Gu, S. T., Monteiro, E., and He, Q. C., 2011, "Coordinate-Free Derivation and Weak Formulation of a General Imperfect Interface Model for Thermal Conduction in Composites," Compos. Sci. Technol., **71**(9), pp. 1209–1216.
[624] Gu, S. T., Liu, J. T., and He, Q. C., 2014, "Size-Dependent Effective Elastic Moduli of Particulate Composites With Interfacial Displacement and Traction Discontinuities," Int. J. Solids Struct., **51**(13), pp. 2283–2296.
[625] Serpilli, M., Rizzoni, R., Lebon, F., and Dumont, S., 2019, "An Asymptotic Derivation of a General Imperfect Interface Law for Linear Multiphysics Composites," Int. J. Solids Struct., **180–181**, pp. 97–107.
[626] Wang, M., and Ye, W., 2020, "Size-Dependent Elastic Field of Nano-Inhomogeneity: From Interface Effect to Interphase Effect," Archive Appl. Mech., **90**(10), pp. 2319–2333.
[627] Xu, Y., He, Q. C., and Gu, S. T., 2016, "Effective Elastic Moduli of Fiber-Reinforced Composites With Interfacial Displacement and Stress Jumps," Int. J. Solids Struct., **80**, pp. 146–157.
[628] Firooz, S., Chatzigeorgiou, G., Meraghni, F., and Javili, A., 2019, "Homogenization Accounting for Size Effects in Particulate Composites Due to General Interfaces," Mech. Mater., **139**, p. 103204.
[629] Firooz, S., Chatzigeorgiou, G., Meraghni, F., and Javili, A., 2020, "Bounds on Size Effects in Composites Via Homogenization Accounting for General Interfaces," Contin. Mech. Thermodyn., **32**(1), pp. 173–206.
[630] Chatzigeorgiou, G., Meraghni, F., and Javili, A., 2017, "Generalized Interfacial Energy and Size Effects in Composites," J. Mech. Phys. Solids, **106**, pp. 257–282.
[631] Gu, S. T., Liu, J. T., and He, Q. C., 2014, "The Strong and Weak Forms of a General Imperfect Interface Model for Linear Coupled Multifield Phenomena," Int. J. Eng. Sci., **85**, pp. 31–46.
[632] Javili, A., Steinmann, P., and Mosler, J., 2017, "Micro-to-Macro Transition Accounting for General Imperfect Interfaces," Comput. Methods Appl. Mech. Eng., **317**, pp. 274–317.
[633] Javili, A., Kaessmair, S., and Steinmann, P., 2014, "General Imperfect Interfaces," Comput. Methods Appl. Mech. Eng., **275**, pp. 76–97.
[634] Kaessmair, S., Javili, A., and Steinmann, P., 2014, "Thermomechanics of Solids With General Imperfect Coherent Interfaces," Archive Appl. Mech., **84**(9–11), pp. 1409–1426.
[635] Javili, A., 2018, "Variational Formulation of Generalized Interfaces for Finite Deformation Elasticity," Math. Mech. Solids, **23**(9), pp. 1303–1322.
[636] Saeb, S., Steinmann, P., and Javili, A., 2019, "Designing Tunable Composites With General Interfaces," Int. J. Solids Struct., **171**, pp. 181–188.
[637] Saeb, S., Steinmann, P., and Javili, A., 2018, "Bounds on Size-Dependent Behaviour of Composites," Philos. Mag., **98**(6), pp. 437–463.
[638] Saeb, S., Steinmann, P., and Javili, A., 2019, "On Effective Behavior of Microstructures Embedding General Interfaces With Damage," Comput. Mech., **64**(6), pp. 1473–1494.
[639] Firooz, S., and Javili, A., 2019, "Understanding the Role of General Interfaces in the Overall Behavior of Composites and Size Effects," Comput. Mater. Sci., **162**, pp. 245–254.
[640] Firooz, S., 2019, "Homogenization of Composites Embedding General Imperfect Interfaces," Master's thesis, Bilkent University, Ankara, Turkey.
[641] Shih, G. C., and Ebert, L. J., 1987, "Theoretical Modelling of the Effect of the Interfacial Shear Strength on the Longitudinal Tensile Strength of Unidirectional Composites," J. Compos. Mater., **21**(3), pp. 207–224.
[642] Tvergaard, V., and Hutchinson, J. W., 1993, "The Influence of Plasticity on Mixed Mode Interface Toughness," J. Mech. Phys. Solids, **41**(6), pp. 1119–1135.
[643] Y., Wei, J. W., and Hutchinson, 1999, "Models of Interface Separation Accompanied by Plastic Dissipation at Multiple Scales," Int. J. Fract., **95**(1/4), pp. 1–17.
[644] Park, K., Paulino, G. H., and Roesler, J. R., 2009, "A Unified Potential-Based Cohesive Model of Mixed-Mode Fracture," J. Mech. Phys. Solids, **57**(6), pp. 891–908.
[645] Chandra, N., 2002, "Evaluation of Interfacial Fracture Toughness Using Cohesive Zone Model," Compos. Part A, **33**(10), pp. 1433–1447.
[646] Li, S., Thouless, M. D., Waas, A. M., Schroeder, J. A., and Zavattieri, P. D., 2005, "Use of mode-I Cohesive-Zone Models to Describe the Fracture of an Adhesively-Bonded Polymer-Matrix Composite," Compos. Sci. Technol., **65**(2), pp. 281–293.
[647] Sun, C. T., and Jin, Z. H., 2006, "Modeling of Composite Fracture Using Cohesive Zone and Bridging Models," Compos. Sci. Technol., **66**(10), pp. 1297–1302.
[648] Park, K., and Paulino, G. H., 2011, "Cohesive Zone Models: A Critical Review of Traction-Separation Relationships Across Fracture Surfaces," ASME Appl. Mech. Rev., **64**(6), p. 060802.
[649] Klarbring, A., 1991, "Derivation of a Model of Adhesively Bonded Joints by the Asymptotic Expansion Method," Int. J. Eng. Sci., **29**(4), pp. 493–512.
[650] Klarbring, A., and Movchan, A. B., 1998, "Asymptotic Modelling of Adhesive Joints," Mech. Mater., **28**(1–4), pp. 137–145.
[651] Geymonat, G., Krasucki, F., and Lenci, S., 1999, "Mathematical Analysis of a Bonded Joint With a Soft Thin Adhesive," Math. Mech. Solids, **4**(2), pp. 201–225.
[652] Xu, C., Siegmund, T., and Ramani, K., 2003, "Rate-Dependent Crack Growth in Adhesives: I. Modeling Approach," Int. J. Adhes. Adhes., **23**(1), pp. 9–13.
[653] Zhang, L., and Wang, J., 2009, "A Generalized Cohesive Zone Model of the Peel Test for Pressure-Sensitive Adhesives," Int. J. Adhes. Adhes., **29**(3), pp. 217–224.
[654] Alfano, M., Furgiuele, F., Leonardi, A., Maletta, C., and Paulino, G. H., 2009, "Mode I Fracture of Adhesive Joints Using Tailored Cohesive Zone Models," Int. J. Fract., **157**(1–2), pp. 193–204.
[655] Mubashar, A., Ashcroft, I. A., Critchlow, G. W., and Crocombe, A. D., 2011, "Strength Prediction of Adhesive Joints After Cyclic Moisture Conditioning Using a Cohesive Zone Model," Eng. Fract. Mech., **78**(16), pp. 2746–2760.
[656] Campilho, R. D. S. G., Banea, M. D., Neto, J. A. B. P., and Da Silva, L. F. M., 2013, "Modelling Adhesive Joints With Cohesive Zone Models: Effect of the Cohesive Law Shape of the Adhesive Layer," Int. J. Adhes. Adhes., **44**, pp. 48–56.
[657] Espinosa, H. D., Dwivedi, S., and Lu, H. C., 2000, "Modeling Impact Induced Delamination of Woven Fiber Reinforced Composites With Contact/Cohesive Laws," Comput. Methods Appl. Mech. Eng., **183**(3–4), pp. 259–290.
[658] Hu, N., Zemba, Y., Okabe, T., Yan, C., Fukunaga, H., and Elmarakbi, A. M., 2008, "A New Cohesive Model for Simulating Delamination Propagation in Composite Laminates Under Transverse Loads," Mech. Mater., **40**(11), pp. 920–935.
[659] Aymerich, F., Dore, F., and Priolo, P., 2008, "Prediction of Impact-Induced Delamination in Cross-Ply Composite Laminates Using Cohesive Interface Elements," Compos. Sci. Technol., **68**(12), pp. 2383–2390.
[660] Liu, P. F., and Islam, M. M., 2013, "A Nonlinear Cohesive Model for Mixed-Mode Delamination of Composite Laminates," Compos. Struct., **106**, pp. 47–56.
[661] Parrinello, F., Marannano, G., and Borino, G., 2016, "A Thermodynamically Consistent Cohesive-Frictional Interface Model for Mixed Mode Delamination," Eng. Fract. Mech., **153**, pp. 61–79.
[662] Reinoso, J., Paggi, M., and Blázquez, A., 2017, "A Nonlinear Finite Thickness Cohesive Interface Element for Modeling Delamination in Fibre-Reinforced Composite Laminates," Compos. Part B, **109**, pp. 116–128.
[663] England, A. H., 1966, "An Arc Around a Circular Elastic Inclusion," ASME J. Appl. Mech., **33**(3), pp. 637–640.
[664] Tvergaard, V., and Hutchinson, J. W., 1996, "Effect of Strain-Dependent Cohesive Zone Model on Predictions of Crack Growth Resistance," Int. J. Solids Struct., **33**(20–22), pp. 3297–3308.
[665] Yang, B., Mall, S., and Ravi-Chandar, K., 2001, "A Cohesive Zone Model for Fatigue Crack Growth in Quasibrittle Materials," Int. J. Solids Struct., **38**(22–23), pp. 3927–3944.
[666] Roe, K. L., and Siegmund, T., 2003, "An Irreversible Cohesive Zone Model for Interface Fatigue Crack Growth Simulation," Eng. Fract. Mech., **70**(2), pp. 209–232.
[667] Bouvard, J. L., Chaboche, J. L., Feyel, F., and Gallerneau, F., 2009, "A Cohesive Zone Model for Fatigue and Creep-Fatigue Crack Growth in Single Crystal Superalloys," Int. J. Fatigue, **31**(5), pp. 868–879.
[668] Kawashita, L. F., and Hallett, S. R., 2012, "A Crack Tip Tracking Algorithm for Cohesive Interface Element Analysis of Fatigue Delamination Propagation in Composite Materials," Int. J. Solids Struct., **49**(21), pp. 2898–2913.
[669] Ingraffea, A. R., Gerstk, W. H., Gergely, P., and Saouma, V., 1984, "Fracture Mechanics of Bond in Reinforced Concrete," J. Struct. Eng., **110**(4), pp. 871–890.
[670] Huang, N. C., and Korobeinik, M. Y., 2001, "Interfacial Debonding of a Spherical Inclusion Embedded in an Infinite Medium Under Remote Stress," Int. J. Fract., **107**(1), pp. 11–30.
[671] Fan, H., and Wang, G. F., 2003, "Screw Dislocation Interacting With Imperfect Interface," Mech. Mater., **35**(10), pp. 943–953.
[672] Mori, T., and Mura, T., 1987, "Blocking Effect of Inclusions on Grain Boundary Sliding; Spherical Grain Approximation," J. Mech. Phys. Solids, **35**(5), pp. 631–641.
[673] Pezzotta, M., Zhang, Z. L., Jensen, M., Grande, T., and Einarsrud, M. A., 2008, "Cohesive Zone Modeling of Grain Boundary Microcracking Induced

by Thermal Anisotropy in Titanium Diboride Ceramics," Comput. Mater. Sci., **43**(3), pp. 440–449.
[674] Wulfinghoff, S., 2017, "A Generalized Cohesive Zone Model and a Grain Boundary Yield Criterion for Gradient Plasticity Derived From Surface- and Interface-Related Arguments," Int. J. Plasticity, **92**, pp. 57–78.
[675] Wei, Y., and Hutchinson, J. W., 1998, "Interface Strength, Work of Adhesion and Plasticity in the Peel Test," *Recent Advances in Fracture Mechanics*, Springer, Dordrecht, The Netherlands, pp. 315–333.
[676] Hashin, Z., 1972, "Theory of Fiber Reinforced Materials," National Aeronautics and Space Administration, Washington, DC, Report No. NASA CR-1974.
[677] Takahashi, K., Ikeda, M., Harakawa, K., Tanaka, K., and Sakai, T., 1978, "Analysis of the Effect of Interfacial Slippage on the Elastic Moduli of a Particle-Filled Polymer," J. Polym. Sci., **16**(3), pp. 415–425.
[678] Asaro, R. J., 1975, "Somigliana Dislocations and Internal Stresses; With Application to Second Phase Hardening," Int. J. Eng. Sci., **13**(3), pp. 271–286.
[679] He, L. H., 2001, "Transient Stress Relaxation Around Spherical Inclusions by Interfacial Diffusion and Sliding," Acta Mech., **149**(1–4), pp. 115–133.
[680] Toya, M., 1974, "A Crack Along the Interface of a Circular Inclusion Embedded in an Infinite Solid," J. Mech. Phys. Solids, **22**(5), pp. 325–348.
[681] Ju, J. W., 1991, "A Micromechanical Damage Model for Uniaxially Reinforced Composites Weakened by Interfacial Arc Microcracks," ASME J. Appl. Mech., **58**(4), pp. 923–930.
[682] Javili, A., 2019, "A Note on Traction Continuity Across an Interface in a Geometrically Non-Linear Framework," Math. Mech. Solids, **24**(8), pp. 2478–2496.
[683] Moeckel, G. P., 1975, "Thermodynamics of an Interface," Arch. Rational Mech. Anal., **57**(3), pp. 255–280.
[684] Dell'isola, F., and Romano, A., 1987, "On the Derivation of Thermodynamical Balance Equations for Continuous Systems With a Nanomaterial Interface," Int. J. Eng. Sci., **25**(11–12), pp. 1459–1468.
[685] Leo, P. H., and Sekerka, R. F., 1989, "The Effect of Surface Stress on Crystal-Melt and Crystal-Crystal Equilibrium," Acta Metall., **37**(12), pp. 3119–3138.
[686] Weissmüller, J., and Cahn, J. W., 1997, "Mean Stresses in Microstructures Due to Interface Stresses: A Generalization of a Capillary Equation for Solids," Acta Mater., **45**(5), pp. 1899–1906.
[687] Exadaktylos, G. E., and Vardoulakis, I., 1998, "Surface Instability in Gradient Elasticity With Surface Energy," Int. J. Solids Struct., **35**(18), pp. 2251–2281.
[688] Exadaktylos, G., 1998, "Gradient Elasticity With Surface Energy: Mode-I Crack Problem," Int. J. Solids Struct., **35**(5–6), pp. 421–456.
[689] Forest, S., and Sievert, R., 2003, "Elastoviscoplastic Constitutive Frameworks for Generalized Continua," Acta Mech., **160**(1–2), pp. 71–111.
[690] Müller, P., and Saúl, A., 2004, "Elastic Effects on Surface Physics," Surf. Sci. Rep., **54**, pp. 157–258.
[691] Wang, Z. Q., Zhao, Y. P., and Huang, Z. P., 2010, "The Effects of Surface Tension on the Elastic Properties of Nano Structures," Int. J. Eng. Sci., **48**(2), pp. 140–150.
[692] Šilhavý, M., 2011, "Equilibrium of Phases With Interfacial Energy: A Variational Approach," J. Elasticity, **105**(1–2), pp. 271–303.
[693] Altenbach, H., and Eremeyev, V. A., 2011, "On the Shell Theory on the Nanoscale With Surface Stresses," Int. J. Eng. Sci., **49**(12), pp. 1294–1301.
[694] Javili, A., Mcbride, A., Mergheim, J., Steinmann, P., and Schmidt, U., 2013, "Micro-to-Macro Transitions for Continua With Surface Structure at the Microscale," Int. J. Solids Struct., **50**(16–17), pp. 2561–2572.
[695] Davydov, D., Javili, A., and Steinmann, P., 2013, "On Molecular Statics and Surface-Enhanced Continuum Modeling of Nano-Structures," Comput. Mater. Sci., **69**, pp. 510–519.
[696] Mi, C., and Kouris, D., 2013, "Stress Concentration Around a Nanovoid Near the Surface of an Elastic Half-Space," Int. J. Solids Struct., **50**(18), pp. 2737–2748.
[697] Zhang, W. X., and Wang, T. J., 2007, "Effect of Surface Energy on the Yield Strength of Nanoporous Materials," Appl. Phys. Lett., **90**(6), p. 063104.
[698] Duan, H. L., Karihaloo, B. L., Wang, J., and Yi, X., 2006, "Effective Conductivities of Heterogeneous Media Containing Multiple Inclusions With Various Spatial Distributions," Phys. Rev. B, **73**(17), p. 174203.
[699] Mogilevskaya, S. G., and Crouch, S. L., 2002, "A Galerkin Boundary Integral Method for Multiple Circular Elastic Inclusions With Homogeneously Imperfect Interfaces," Int. J. Solids Struct., **39**(18), pp. 4723–4746.
[700] Tian, L., and Rajapakse, R. K. N. D., 2007, "Finite Element Modelling of Nanoscale Inhomogeneities in an Elastic Matrix," Comput. Mater. Sci., **41**(1), pp. 44–53.
[701] Nitsche, J., 1971, "Über Ein Variationsprinzip Zur Lösung Von Dirichlet-Problemen Bei Verwendung Von Teilräumen, Die Keinen Randbedingungen Unterworfen Sind," Abhandlungen Aus Dem Mathematischen Seminar Der Universität Hamburg, **36**(1), pp. 9–15.
[702] Mosler, J., and Scheider, I., 2011, "A Thermodynamically and Variationally Consistent Class of Damage-Type Cohesive Models," J. Mech. Phys. Solids, **59**(8), pp. 1647–1668.
[703] Saeb, S., Firooz, S., Steinmann, P., and Javili, A., 2021, "Generalized Interfaces Via Weighted Averages for Application to Graded Interphases at Large Deformations," J. Mech. Phys. Solids, **149**, p. 104234.
[704] Spring, D. W., and Paulino, G. H., 2015, "Computational Homogenization of the Debonding of Particle Reinforced Composites: The Role of Interphases in Interfaces," Comput. Mater. Sci., **109**, pp. 209–224.
[705] Hashemi, R., Spring, D. W., and Paulino, G. H., 2015, "On Small Deformation Interfacial Debonding in Composite Materials Containing Multi-Coated Particles," J. Compos. Mater., **49**(27), pp. 3439–3455.
[706] Gitman, I. M., Askes, H., and Sluys, L. J., 2007, "Representative Volume: Existence and Size Determination," Eng. Fract. Mech., **74**(16), pp. 2518–2534.
[707] Charalambakis, N., Chatzigeorgiou, G., Chemisky, Y., and Meraghni, F., 2018, "Mathematical Homogenization of Inelastic Dissipative Materials: A Survey and Recent Progress," Contin. Mech. Thermodyn., **30**(1), pp. 1–51.
[708] Pindera, M. J., Khatam, H., Drago, A. S., and Bansal, Y., 2009, "Micromechanics of Spatially Uniform Heterogeneous Media: A Critical Review and Emerging Approaches," Compos. Part B, **40**(5), pp. 349–378.
[709] Geers, M. G. D., Kouznetsova, V. G., Matouš, K., and Yvonnet, J., 2017, Homogenization Methods and Multiscale Modeling: Nonlinear Problems, Encyclopedia of Computational Mechanics 2nd ed., Wiley Online Library, pp. 1–34.
[710] Rajagopal, K. R., 2007, "The Elasticity of Elasticity," Z. Angew. Math. Phys., **58**(2), pp. 309–317.
[711] Yvonnet, J., Mitrushchenkov, A., Chambaud, G., and He, Q. C., 2011, "Finite Element Model of Ionic Nanowires With Size-Dependent Mechanical Properties Determined by ab Initio Calculations," Comput. Methods Appl. Mech. Eng., **200**(5–8), pp. 614–625.
[712] Park, H. S., Klein, P. A., and Wagner, G. J., 2006, "A Surface Cauchy-Born Model for Nanoscale Materials," Int. J. Numer. Methods Eng., **68**(10), pp. 1072–1095.
[713] Park, H. S., and Klein, P. A., 2007, "Surface Cauchy-Born Analysis of Surface Stress Effects on Metallic Nanowires," Phys. Rev. B, **75**(8), p. 085408.